DEVELOPMENT OF ANALYTICAL METHODS TO INVESTIGATE THE FORMATION OF OXYLIPINS DURING OXIDATIVE STRESS AND INFLAMMATION

Dissertation

to obtain the academic degree

Doctor rerum naturalium

(Dr. rer. nat.)

Faculty of Mathematics and Natural Sciences

of the

Bergische Universität Wuppertal

by

Katharina M. Rund

Landau (Pfalz)

- 2019 -

Erster Gutachter: ..... Prof. Dr. Nils Helge Schebb

Zweiter Gutachter: .....Prof. Dr. Julia Bornhorst

Tag der mündlichen Prüfung: 21.11.2019

Für meine Familie

The PhD thesis can be quoted as follows:

urn:nbn:de:hbz:468-20201113-112756-1
[http://nbn-resolving.de/urn/resolver.pl?urn=urn%3Anbn%3Ade%3Ahbz%3A468-20201113-112756-1]

DOI: 10.25926/3ktm-wk43
[https://doi.org/10.25926/3ktm-wk43]

Die Umsonst-Erfahrung der Vergeblichkeit wird zur Umsonst-Erfahrung der Freude. Auch wenn oftmals unsere Arbeit umsonst, vergeblich ist, gibt es die zweite Chance, umsonst, gratis, ohne Bedingung außer der, dass wir es versuchen. Die Freude, dass es gelingen kann, ist einen weiteren Versuch wert.

D. Haite

Table of Contents

Chapter 1

Introduction and Scope

A variety of physiological functions in the body is mediated by oxygenated polyunsaturated fatty acids (PUFA) including regulation of blood pressure, endothelial function, blood coagulation and kidney function. These eicosanoids (in the case of formation from 20-carbon PUFA) and other oxylipins are formed endogenously by oxygenation of n6- and n3-PUFA in the arachidonic acid (ARA) cascade *via* three main enzymatic pathways or autoxidation resulting in a multitude of structurally distinct products [1, 2]. Enzymatic conversion of PUFA by cyclooxygenases (COX), lipoxygenases (LOX) or cytochrome P450 monooxygenases (CYP) leads to the generation of regio- and stereospecifically oxygenated products, such as prostanoids, hydroxy-PUFA or epoxy-PUFA. In contrast, PUFA autoxidation underlies a radical mechanism and gives rise to a complex mixture of oxidative products with similar structure but diverse regio- and stereochemistry.

Formation of oxylipins in the body is strictly controlled and a dysregulation of oxylipin formation contributes to the pathogenesis of diseases. Therefore, investigation of the oxylipin profile has gained increasing interest as valuable marker to assess the (patho)physiological state and may also provide information about the oxidative stress status of the organism.

Under normal physiological conditions, PUFA which are predominantly esterified in phospholipids of plasma membranes or in blood lipoproteins, are released upon stimulation by lipases, e.g. phospholipase A_2 or lipoprotein lipase [3, 4], to make them accessible for enzymatic conversion by COX, LOX or CYP [5]. Conversion of PUFA by COX forms intermediately unstable cyclic

endoperoxides (PGG, PGH) which are rapidly transformed to thromboxanes and prostanoids with varying ring structures depending on the presence of distinct prostanoid synthases [6]. Activity of LOX initially results – depending on the involved isoform (5-LOX, 12-LOX, 15-LOX) – in formation of stereo- and regioselective hydroperoxy-PUFA which can be reduced to respective hydroxy-PUFA or further processed by sequential conversion with the same or different isoforms to dihydroxy- or trihydroxy-PUFA and other oxylipins including leukotrienes, lipoxins, resolvins, protectins and maresins [7-10]. Different CYP isoforms catalyze the formation of hydroxy-PUFA or *cis*-epoxy-PUFA (*R,S*- and *S,R*-enantiomers), respectively, whereby the latter are hydrolyzed by soluble epoxide hydrolase (sEH) forming the corresponding vicinal dihydroxy-PUFA [11, 12]. While almost all PUFA-converting enzymes require free (i.e. non-esterified) PUFA substrates, 15-LOX (encoded by the gene *ALOX15*), e.g. present in distinct blood cells (eosinophils, reticulocytes, stimulated monocytes), is also able to oxygenate esterified PUFA, thus forming directly hydroxy-PUFA esterified in phospholipids or complex lipids [13-15]. Furthermore, following their acute formation several free oxylipins are also readily incorporated in membrane lipids thereby contributing to the esterified portion of oxylipins [16-18].

Besides enzymatic conversion, due to their pentadiene structure PUFA are prone to non-enzymatic autoxidation, which is particularly relevant during oxidative stress. In this free radical-mediated process oxidation of PUFA is initiated by abstraction of a bisallylic hydrogen radical, followed by addition of molecular oxygen, thus leading to racemic hydroperoxy-PUFA radicals which comprise multiple regioisomers. Further conversion during chain oxidation reactions yields a complex mixture of secondary oxidation products carrying hydro(pero)xy, epoxy, keto or cyclic functional groups within their structure [19]. One class of cyclic autoxidation products which is predominantly formed esterified in phospholipids comprises prostaglandin-like structures, so-called isoprostanes (IsoP), of which F-ring-IsoP, particularly the ARA derived 15*(R,S)*-15-F_{2t}-IsoP were evaluated as promising oxidative stress markers *in vivo* [20, 21].

In order to assess the physiological or pathophysiological role of oxylipins, their potential use as biomarkers for diseases and oxidative stress, or their modulation by the diet, powerful analytical techniques are required [22]. In the past years targeted LC-MS/MS methods have been increasingly applied for the selective and sensitive detection of oxylipins allowing parallel analysis of numerous oxylipins derived from different formation pathways [1]. Initially, most methods were focused on ARA derived eicosanoids or oxylipins from single pathways (COX, LOX, CYP). Based on the observation that the different formation branches are linked and a modulation of single enzyme activities results in a shift towards other pathways, it is now widely acknowledged that the overall physiological response is rather mediated by the whole profile than by the presence and concentration of individual oxylipins [1]. For this reason a comprehensive oxylipin profile covering oxylipins from all major biologically relevant n6- and n3-PUFA derived from all pathways needs to be determined. However, comprehensive methods analyzing both, enzymatically and non-enzymatically formed oxylipins in parallel are limited. Regarding autoxidatively formed IsoP, existing LC-MS/MS methods are mainly focused on ARA derived products or IsoP from individual PUFA which limits their applicability with respect to the varying fatty acid composition of different tissues and specimen. Furthermore, with regard to the vast number of potentially formed isomers these methods are restricted in terms of their analyte coverage (Fig. 1.1). In **chapter 2**, an LC-ESI(-)-MS/MS method for the analysis of IsoP and isofuran (IsoF) isomers is described covering a wide range of these stable prostaglandin-like autoxidation products from all biologically relevant PUFA. Considering the multitude of potential isomers, a focus is set on the selection of specific fragments for selected reaction monitoring (SRM) of individual regioisomers and the chromatographic separation of diastereomers which have identical fragmentation behavior to allow their selective quantification. The combination of this method with a targeted oxylipin method for the analysis of enzymatically formed oxylipins forms the basis for the comprehensive investigation of the overall oxylipin pattern.

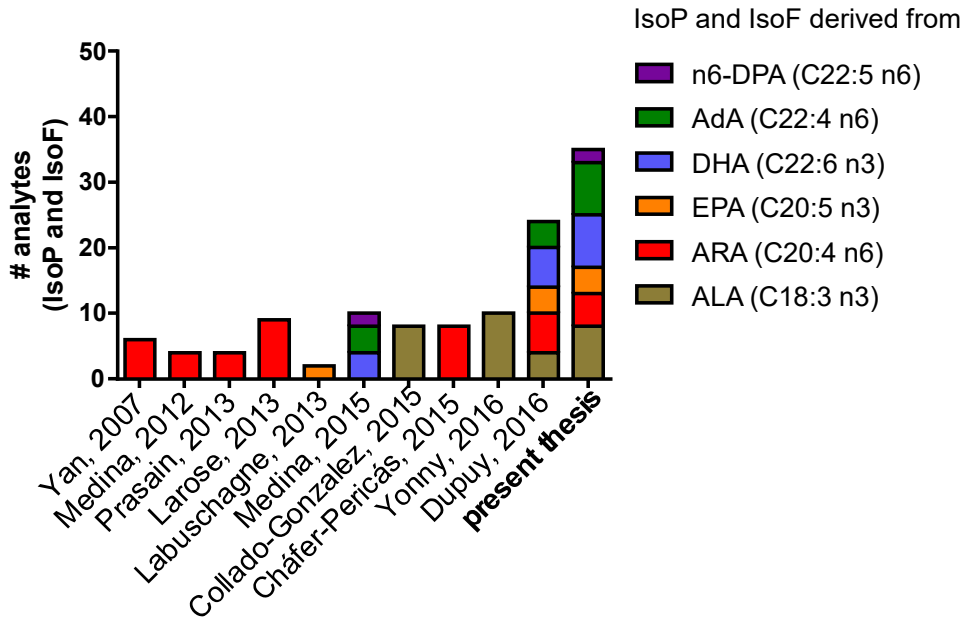

Fig. 1.1: Comparison of the analyte coverage of current LC-MS/MS methods for the analysis of isoprostanes (IsoP) and isofurans (IsoF) derived from different PUFA [23-32].

A major concern in the analysis of oxylipins in biological samples is their susceptibility to *ex vivo* oxidation which may result from autoxidative processes as well as residual enzymatic activity in the samples. Thus, the endogenous oxylipin pattern may be altered between sample collection and analysis. Particularly samples from biobanks or clinical studies collected in the clinical routine are handled under conditions which are hard to control. These samples oftentimes originate from severely diseased patients and are particularly valuable to characterize the (patho)physiological role of oxylipins or to contribute to the discovery of new disease biomarkers. However, changes in the levels of distinct oxylipins due to pre-analytical variations may impair the validity and significance of the analyzed oxylipin profile and thus may contribute to misleading interpretation. **Chapter 3** examines the impact of whole blood storage or transport within a large hospital prior to further processing on the oxylipin profile. As blood is the most commonly analyzed specimen in clinical studies, providing information about the systemic state of the donor, differences of oxylipins in plasma and serum are evaluated. Furthermore, accounting for the occurrence of oxylipins in blood as free mediators as well as esterified to lipids

within lipoproteins, the effects on the free as well as the total (i.e. sum of free and esterified) oxylipin profile are investigated. The studies allow gaining information about the reliability and applicability of clinical blood samples and the stability of oxylipins.

An important class of oxylipins comprises epoxy-PUFA which act vasodilatory, anti-inflammatory and analgesic and are of high interest in the context of several diseases ranging from hypertension [33] and diabetes [34, 35] to cancer [36, 37]. In the body each of the double bonds of the PUFA can be transformed by the epoxygenase activity of CYP resulting in the generation of respective *cis*-epoxy-PUFA (*R,S*- and *S,R*-enantiomers) regioisomers. Using LC-MS/MS the different epoxy-PUFA regioisomers are selectively analyzed based on their specific SRM transitions. When investigating biological samples, however, for each regioisomer a second peak is frequently detected eluting slightly later than the authentic *cis*-epoxy-PUFA standard and showing an identical product ion spectrum. During the analysis of red blood cells (RBC) a similar peak pattern was observed and characterization of the structure of these later eluting peaks identified them as the respective *trans*-epoxy-PUFA isomers (*S,S*- and *R,R*-enantiomers) [38, 39]. Though they also have been shown to possess biological activity, particularly vasoregulatory properties (e.g. relaxing pre-constricted arteries, acting anti-aggregatory), these *trans*-epoxy-PUFA are rarely considered when epoxy-PUFA are investigated. Based on the observations that their levels increase after incubation of RBC with *tert*-butyl hydroperoxide [39], which is an inducer of oxidative stress, and that these peaks are also detected in aged PUFA stocks (Fig. 1.2), their formation is assumed to be related to autoxidative processes. In **chapter 4** the formation of *trans*-epoxy-PUFA in the context of oxidative stress is thoroughly characterized in various models including several different cell lines as well as the *in vivo* model organism *Caenorhabditis elegans* and an *in vivo* model of murine renal ischemia reperfusion injury. The significance of their generation in response to oxidative stress and their potential suitability as alternative oxidative stress markers is further evaluated by their correlation with the levels of IsoP, which are commonly used as biomarkers of oxidative stress *in vivo*.

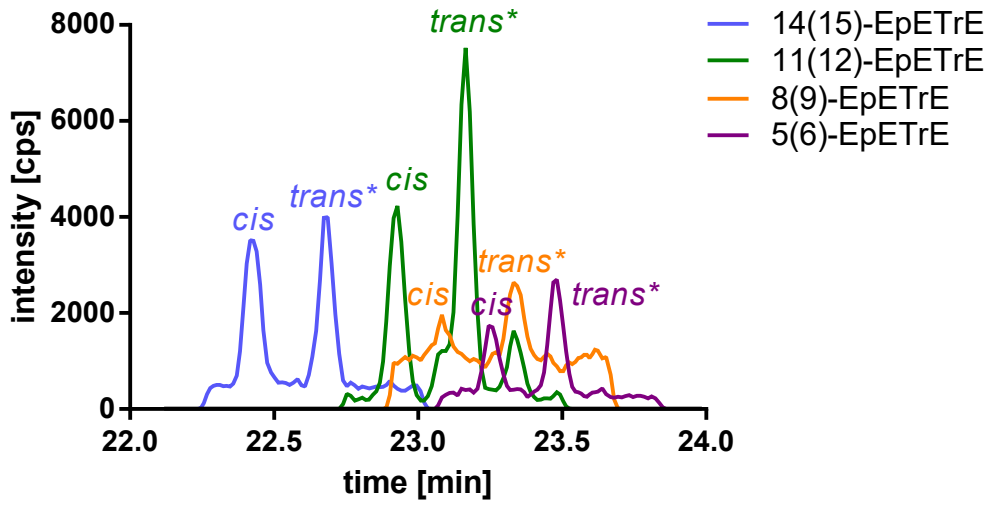

Fig. 1.2: Chromatographic separation of ARA derived *cis*- and tentatively identified (*) *trans*-epoxy-PUFA (EpETrE) regioisomers in an aged ARA stock solution stored at −80 °C.

Besides formation *via* enzymatic and non-enzymatic pathways, the overall oxylipin pattern is considerably affected by the PUFA status. With regard to epoxy-PUFA, terminal n3-derived *cis*-epoxy-PUFA (17(18)-EpETE and 19(20)-EpDPE) are suggested as appropriate indicators for the endogenous n3-PUFA status based on a preferred epoxygenation of the n3-double bond by CYP [40, 41]. Considering varying physiological activities and properties of respective products from different precursor PUFA, the analysis of a broad spectrum of oxylipins is essential when studying their physiological role. In **chapter 5** the developed targeted LC-MS/MS method enabling the parallel analysis of enzymatically and non-enzymatically formed oxylipins from the major n6- and n3-PUFA is applied to study the effects of an anti-inflammatory treatment by dietary n3-PUFA supplementation in a murine model of oxidative stress and inflammation in the kidney. Renal ischemia reperfusion injury (IRI) resulting from temporal interruption of renal blood flow and subsequent reperfusion is linked to pro-oxidative processes and the release of pro-inflammatory cytokines. n3-PUFA are associated with anti-inflammatory effects which are on the one hand attributed to their direct action by modifying the membrane composition, or by binding to transcription factors such as NF-κB or PPARγ hereby altering the transcription of pro-inflammatory or anti-inflammatory genes [42]. On the other hand, n3-PUFA act as alternative

substrates in the ARA cascade and give rise to oxylipins with less potency compared to ARA derived prostanoids or leukotrienes. Moreover, they also lead to the generation of oxylipins with anti-inflammatory properties or may even form so-called specialized pro-resolving mediators which are considered to be actively involved in inflammation resolution. In order to evaluate the role of n3-PUFA in renal IRI, changes in the PUFA and the oxylipin pattern are analyzed in parallel with renal function parameters as well as inflammatory markers.

Overall, this thesis aims to contribute to a better understanding of the functional role of oxylipins by using a comprehensive oxylipin profile to provide information about oxidative stress and (patho)physiology as well as the nutritional n3-PUFA status.

1.1 References

1. Gladine C., Ostermann A. I., Newman J. W. and Schebb N. H. (2019) MS-based targeted metabolomics of eicosanoids and other oxylipins: Analytical and inter-individual variabilities. *Free Radic Biol Med*. 144, pp. 72-89; doi: 10.1016/j.freeradbiomed.2019.05.012.
2. Gabbs M., Leng S., Devassy J. G., Monirujjaman M. and Aukema H. M. (2015) Advances in our understanding of oxylipins derived from dietary PUFAs. *Adv Nutr*. 6(5), pp. 513-540; doi: 10.3945/an.114.007732.
3. Dennis E. A., Cao J., Hsu Y.-H., Magrioti V. and Kokotos G. (2011) Phospholipase A2 enzymes: Physical structure, biological function, disease implication, chemical inhibition, and therapeutic intervention. *Chem Rev*. 111(10), pp. 6130-6185; doi: 10.1021/cr200085w.
4. Shearer G. C. and Newman J. W. (2008) Lipoprotein lipase releases esterified oxylipins from very low-density lipoproteins. *Prostaglandins Leukot Essent Fatty Acids*. 79(6), pp. 215-222; doi: 10.1016/j.plefa.2008.09.023.
5. Buczynski M. W., Dumlao D. S. and Dennis E. A. (2009) Thematic review series: Proteomics - An integrated omics analysis of eicosanoid biology. *J Lipid Res*. 50(6), pp. 1015-1038; doi: 10.1194/jlr.R900004-JLR200.
6. Smith W. L., Urade Y. and Jakobsson P.-J. (2011) Enzymes of the cyclooxygenase pathways of prostanoid biosynthesis. *Chem Rev*. 111(10), pp. 5821-5865; doi: 10.1021/cr2002992.
7. Haeggstrom J. Z. and Funk C. D. (2011) Lipoxygenase and leukotriene pathways: Biochemistry, biology, and roles in disease. *Chem Rev*. 111(10), pp. 5866-5898; doi: 10.1021/cr200246d.
8. Kutzner L., Goloshchapova K., Heydeck D., Stehling S., Kuhn H. and Schebb N. H. (2017) Mammalian ALOX15 orthologs exhibit pronounced dual positional specificity

with docosahexaenoic acid. *Biochim Biophys Acta*. 1862(7), pp. 666-675; doi: 10.1016/j.bbalip.2017.04.001.

9. Serhan C. N. and Petasis N. A. (2011) Resolvins and protectins in inflammation resolution. *Chem Rev*. 111(10), pp. 5922-5943; doi: 10.1021/cr100396c.
10. Kutzner L., Rund K. M., Ostermann A. I., Hartung N. M., Galano J.-M., Balas L., Durand T., Balzer M. S., David S. and Schebb N. H. (2019) Development of an optimized LC-MS method for the detection of specialized pro-resolving mediators in biological samples. *Front Pharmacol*. 10:169; doi: 10.3389/fphar.2019.00169.
11. Westphal C., Konkel A. and Schunck W.-H. (2015) Cytochrome P450 enzymes in the bioactivation of polyunsaturated fatty acids and their role in cardiovascular disease. In: *Monooxygenase, Peroxidase and Peroxygenase Properties and Mechanisms of Cytochrome P450*. E. G. Hrycay and S. M. Bandiera (eds.), Springer International Publishing, Cham, pp. 151-187; doi: 10.1007/978-3-319-16009-2_6.
12. Morisseau C. and Hammock B. D. (2013) Impact of soluble epoxide hydrolase and epoxyeicosanoids on human health. *Annu Rev Pharmacol Toxicol*. 53(1), pp. 37-58; doi: 10.1146/annurev-pharmtox-011112-140244.
13. Brinckmann R., Schnurr K., Heydeck D., Rosenbach T., Kolde G. and Kühn H. (1998) Membrane translocation of 15-lipoxygenase in hematopoietic cells is calcium-dependent and activates the oxygenase activity of the enzyme. *Blood*. 91(1), pp. 64-74; doi: 10.1182/blood.V91.1.64.
14. Belkner J., Stender H. and Kühn H. (1998) The rabbit 15-lipoxygenase preferentially oxygenates LDL cholesterol esters, and this reaction does not require vitamin E. *J Biol Chem*. 273(36), pp. 23225-23232; doi: 10.1074/jbc.273.36.23225.
15. Maskrey B. H., Bermúdez-Fajardo A., Morgan A. H., Stewart-Jones E., Dioszeghy V., Taylor G. W., Baker P. R. S., Coles B., Coffey M. J., Kühn H. and O'Donnell V. B. (2007) Activated platelets and monocytes generate four hydroxyphosphatidylethanolamines via lipoxygenase. *J Biol Chem*. 282(28), pp. 20151-20163; doi: 10.1074/jbc.M611776200.
16. Karara A., Dishman E., Falck J. R. and Capdevila J. H. (1991) Endogenous epoxyeicosatrienoyl-phospholipids - A novel class of cellular glycerolipids containing epoxidized arachidonate moieties. *J Biol Chem*. 266(12), pp. 7561-7569.
17. Klett E. L., Chen S., Yechoor A., Lih F. B. and Coleman R. A. (2017) Long-chain acyl-CoA synthetase isoforms differ in preferences for eicosanoid species and long-chain fatty acids. *J Lipid Res*. 58(5), pp. 884-894; doi: 10.1194/jlr.M072512.
18. Hammond V. J. and O'Donnell V. B. (2012) Esterified eicosanoids: Generation, characterization and function. *Biochim Biophys Acta*. 1818(10), pp. 2403-2412; doi: 10.1016/j.bbamem.2011.12.013.
19. Yin H., Xu L. and Porter N. A. (2011) Free radical lipid peroxidation: Mechanisms and analysis. *Chem Rev*. 111(10), pp. 5944-5972; doi: 10.1021/cr200084z.
20. Morrow J. D., Awad J. A., Boss H. J., Blair I. A. and Roberts II L. J. (1992) Non-cyclooxygenase-derived prostanoids (F2-isoprostanes) are formed in situ on phospholipids. *Proc Natl Acad Sci U S A*. 89(22), pp. 10721-10725; doi: 10.1073/pnas.89.22.10721.
21. Kadiiska M. B., Gladen B. C., Baird D. D., Germolec D., Graham L. B., Parker C. E., Nyska A., Wachsman J. T., Ames B. N., Basu S., Brot N., Fitzgerald G. A., Floyd R. A., George M., Heinecke J. W., Hatch G. E., Hensley K., Lawson J. A., Marnett L. J., Morrow J. D., Murray D. M., Plastaras J., Roberts II L. J., Rokach J., Shigenaga M. K., Sohal R. S., Sun J., Tice R. R., Van Thiel D. H., Wellner D., Walter P. B., Tomer K. B., Mason R. P. and Barrett J. C. (2005) Biomarkers of oxidative stress study II. Are oxidation products of lipids, proteins, and DNA markers of CCl4 poisoning? *Free Radic Biol Med*. 38(6), pp. 698-710; doi: 10.1016/j.freeradbiomed.2004.09.017.

22. Liakh I., Pakiet A., Sledzinski T. and Mika A. (2019) Modern methods of sample preparation for the analysis of oxylipins in biological samples. *Molecules*. 24(8):1639; doi: 10.3390/molecules24081639.
23. Yan W., Byrd G. D. and Ogden M. W. (2007) Quantitation of isoprostane isomers in human urine from smokers and nonsmokers by LC-MS/MS. *J Lipid Res*. 48(7), pp. 1607-1617; doi: 10.1194/jlr.M700097-JLR200.
24. Medina S., Dominguez-Perles R., Gil J. I., Ferreres F., Garcia-Viguera C., Martinez-Sanz J. M. and Gil-Izquierdo A. (2012) A ultra-pressure liquid chromatography/triple quadrupole tandem mass spectrometry method for the analysis of 13 eicosanoids in human urine and quantitative 24 hour values in healthy volunteers in a controlled constant diet. *Rapid Commun Mass Spectrom*. 26(10), pp. 1249-1257; doi: 10.1002/rcm.6224.
25. Prasain J. K., Arabshahi A., Taub P. R., Sweeney S., Moore R., Sharer J. D. and Barnes S. (2013) Simultaneous quantification of F2-isoprostanes and prostaglandins in human urine by liquid chromatography tandem-mass spectrometry. *J Chromatogr B Analyt Technol Biomed Life Sci*. 913–914, pp. 161-168; doi: 10.1016/j.jchromb.2012.12.009.
26. Larose J., Julien P. and Bilodeau J. F. (2013) Analysis of F2-isoprostanes in plasma of pregnant women by HPLC-MS/MS using a column packed with core-shell particles. *J Lipid Res*. 54(5), pp. 1505-1511; doi: 10.1194/jlr.D034553.
27. Labuschagne C. F., Stigter E. C., Hendriks M. M., Berger R., Rokach J., Korswagen H. C. and Brenkman A. B. (2013) Quantification of in vivo oxidative damage in Caenorhabditis elegans during aging by endogenous F3-isoprostane measurement. *Aging Cell*. 12(2), pp. 214-223; doi: 10.1111/acel.12043.
28. Medina S., Miguel-Elizaga I. D., Oger C., Galano J. M., Durand T., Martinez-Villanueva M., Castillo M. L., Villegas-Martinez I., Ferreres F., Martinez-Hernandez P. and Gil-Izquierdo A. (2015) Dihomo-isoprostanes - nonenzymatic metabolites of AdA - are higher in epileptic patients compared to healthy individuals by a new ultrahigh pressure liquid chromatography-triple quadrupole-tandem mass spectrometry method. *Free Radic Biol Med*. 79, pp. 154-163; doi: 10.1016/j.freeradbiomed.2014.11.005.
29. Collado-Gonzalez J., Medina S., Durand T., Guy A., Galano J. M., Torrecillas A., Ferreres F. and Gil-Izquierdo A. (2015) New UHPLC-QqQ-MS/MS method for quantitative and qualitative determination of free phytoprostanes in foodstuffs of commercial olive and sunflower oils. *Food Chem*. 178, pp. 212-220; doi: 10.1016/j.foodchem.2015.01.097.
30. Chafer-Pericas C., Rahkonen L., Sanchez-Illana A., Kuligowski J., Torres-Cuevas I., Cernada M., Cubells E., Nunez-Ramiro A., Andersson S., Vento M. and Escobar J. (2015) Ultra high performance liquid chromatography coupled to tandem mass spectrometry determination of lipid peroxidation biomarkers in newborn serum samples. *Anal Chim Acta*. 886, pp. 214-220; doi: 10.1016/j.aca.2015.06.028.
31. Yonny M. E., Rodríguez Torresi A., Cuyamendous C., Réversat G., Oger C., Galano J.-M., Durand T., Vigor C. and Nazareno M. A. (2016) Thermal stress in melon plants: Phytoprostanes and phytofurans as oxidative stress biomarkers and the effect of antioxidant supplementation. *J Agric Food Chem*. 64(44), pp. 8296-8304; doi: 10.1021/acs.jafc.6b03011.
32. Dupuy A., Le Faouder P., Vigor C., Oger C., Galano J. M., Dray C., Lee J. C.-Y., Valet P., Gladine C., Durand T. and Bertrand-Michel J. (2016) Simultaneous quantitative profiling of 20 isoprostanoids from omega-3 and omega-6 polyunsaturated fatty acids by LC-MS/MS in various biological samples. *Anal Chim Acta*. 921, pp. 46-58; doi: 10.1016/j.aca.2016.03.024.

33. Ulu A., Harris T. R., Morisseau C., Miyabe C., Inoue H., Schuster G., Dong H., Iosif A.-M., Liu J.-Y., Weiss R. H., Chiamvimonvat N., Imig J. D. and Hammock B. D. (2013) Anti-inflammatory effects of ω-3 polyunsaturated fatty acids and soluble epoxide hydrolase inhibitors in angiotensin-II-dependent hypertension. *Journal of cardiovascular pharmacology*. 62(3), pp. 285-297; doi: 10.1097/FJC.0b013e318298e460.

34. Luria A., Bettaieb A., Xi Y., Shieh G.-J., Liu H.-C., Inoue H., Tsai H.-J., Imig J. D., Haj F. G. and Hammock B. D. (2011) Soluble epoxide hydrolase deficiency alters pancreatic islet size and improves glucose homeostasis in a model of insulin resistance. *Proc Natl Acad Sci U S A*. 108(22), pp. 9038-9043; doi: 10.1073/pnas.1103482108.

35. Inceoglu B., Wagner K. M., Yang J., Bettaieb A., Schebb N. H., Hwang S. H., Morisseau C., Haj F. G. and Hammock B. D. (2012) Acute augmentation of epoxygenated fatty acid levels rapidly reduces pain-related behavior in a rat model of type I diabetes. *Proc Natl Acad Sci U S A*. 109(28), pp. 11390-11395; doi: 10.1073/pnas.1208708109.

36. Panigrahy D., Edin M. L., Lee C. R., Huang S., Bielenberg D. R., Butterfield C. E., Barnés C. M., Mammoto A., Mammoto T., Luria A., Benny O., Chaponis D. M., Dudley A. C., Greene E. R., Vergilio J.-A., Pietramaggiori G., Scherer-Pietramaggiori S. S., Short S. M., Seth M., Lih F. B., Tomer K. B., Yang J., Schwendener R. A., Hammock B. D., Falck J. R., Manthati V. L., Ingber D. E., Kaipainen A., D'Amore P. A., Kieran M. W. and Zeldin D. C. (2012) Epoxyeicosanoids stimulate multiorgan metastasis and tumor dormancy escape in mice. *J Clin Invest*. 122(1), pp. 178-191; doi: 10.1172/JCI58128.

37. Zhang G., Panigrahy D., Mahakian L. M., Yang J., Liu J.-Y., Stephen Lee K. S., Wettersten H. I., Ulu A., Hu X., Tam S., Hwang S. H., Ingham E. S., Kieran M. W., Weiss R. H., Ferrara K. W. and Hammock B. D. (2013) Epoxy metabolites of docosahexaenoic acid (DHA) inhibit angiogenesis, tumor growth, and metastasis. *Proc Natl Acad Sci U S A*. 110(16), pp. 6530-6535; doi: 10.1073/pnas.1304321110.

38. Jiang H., McGiff J. C., Quilley J., Sacerdoti D., Reddy L. M., Falck J. R., Zhang F., Lerea K. M. and Wong P. Y. (2004) Identification of 5,6-trans-epoxyeicosatrienoic acid in the phospholipids of red blood cells. *J Biol Chem*. 279(35), pp. 36412-36418; doi: 10.1074/jbc.M403962200.

39. Jiang H., Quilley J., Reddy L. M., Falck J. R., Wong P. Y. and McGiff J. C. (2005) Red blood cells: Reservoirs of cis- and trans-epoxyeicosatrienoic acids. *Prostaglandins Other Lipid Mediat*. 75(1-4), pp. 65-78; doi: 10.1016/j.prostaglandins.2004.10.003.

40. Fischer R., Konkel A., Mehling H., Blossey K., Gapelyuk A., Wessel N., von Schacky C., Dechend R., Muller D. N., Rothe M., Luft F. C., Weylandt K. and Schunck W. H. (2014) Dietary omega-3 fatty acids modulate the eicosanoid profile in man primarily via the CYP-epoxygenase pathway. *J Lipid Res*. 55(6), pp. 1150-1164; doi: 10.1194/jlr.M047357.

41. Murphy R. C. (2015) Specialized pro-resolving mediators: Do they circulate in plasma? *J Lipid Res*. 56(9), pp. 1641-1642; doi: 10.1194/jlr.C062356.

42. Calder P. C. (2015) Marine omega-3 fatty acids and inflammatory processes: Effects, mechanisms and clinical relevance. *Biochim Biophys Acta*. 1851(4), pp. 469-484; doi: 10.1016/j.bbalip.2014.08.010.

Chapter 2

Development of an LC-ESI(-)-MS/MS method for the simultaneous quantification of 35 isoprostanes and isofurans derived from the major n3- and n6-PUFAs*

Misregulation of oxidative and antioxidative processes in the organism – oxidative stress – contributes to the pathogenesis of different diseases, e.g. inflammatory or neurodegenerative diseases. Oxidative stress leads to autoxidation of polyunsaturated fatty acids giving rise to prostaglandin-like isoprostanes (IsoP) and isofurans (IsoF). On the one hand they could serve as biomarker of oxidative stress and on the other hand may act as lipid mediators, similarly as the enzymatically formed oxylipins. In the present paper we describe the development of an LC-ESI(-)-MS/MS method allowing the parallel quantification of 27 IsoP and 8 IsoF derived from 6 different PUFA (ALA, ARA, EPA, AdA, n6-DPA, DHA) within 12 minutes. The chromatographic separation was carried out on an RP-C18 column (2.1 x 150 mm, 1.8 µm) yielding narrow peaks with an average width at half maximum of 3.3 to 4.2 sec. Detection was carried out on a triple quadrupole mass spectrometer operating in selected reaction monitoring mode allowing the selective detection of regioisomers. The limit of detection ranged between 0.1 and 1 nM allowing in combination with solid phase extraction the detection of IsoP and IsoF at subnanomolar concentrations in biological samples. The method was validated for human plasma showing high accuracy and precision. Application of the approach on the investigation of oxidative stress in cultured cells indicated a distinct pattern of IsoP and IsoF in response to reactive oxygen species which warrants further investigation. The described method is not only the most comprehensive approach for the simultaneous quantification of IsoP and IsoF, but it was also integrated in a targeted metabolomics method (Ostermann et al. (2015) Anal Bioanal Chem) allowing the quantification of in total 164 oxylipins formed enzymatically and non-enzymatically within 30.5 min.

* Reprinted from *Analytica Chimica Acta,* Vol. 1037, Rund K. M., Ostermann A. I., Kutzner L., Galano J.-M., Oger C., Vigor C., Wecklein S., Seiwert N., Durand T., Schebb N. H., Development of an LC-ESI(-)-MS/MS method for the simultaneous quantification of 35 isoprostanes and isofurans derived from the major n3- and n6-PUFAs, pp. 63-74, Copyright (2018), with permission from Elsevier. doi: 10.1016/j.aca.2017.11.002.

Author contributions: KR designed research, performed experiments and wrote the manuscript; AO, LK performed experiments and wrote the manuscript; JMG, CO, CV, TD provided standard substances and contributed to manuscript writing; SW, NS performed experiments; NHS designed research and wrote the manuscript.

2.1 Introduction

Oxidative stress results from misregulation of oxidative and antioxidative mechanisms in the organism and is characterized by increased formation of reactive oxygen and nitrogen species (RONS) [1-3]. These highly reactive molecules attack biomolecules, thereby e.g. modifying proteins as well as DNA and causing mutations [4]. Oxidative degradation of membrane lipids alters the function of membranes and gives rise to a multitude of reactive and stable products [5, 6]. Oxidative stress, and thus autoxidation, is associated with the pathophysiology of several diseases including inflammatory, cardiovascular, respiratory and neurodegenerative diseases.

In order to evaluate oxidative stress in health and disease, several biomolecules affected by autoxidation (i.e. proteins, DNA, lipids), their degradation products (e.g. malondialdehyde (MDA)) or endogenous antioxidants (e.g. glutathione (GSH), glutathione disulfide (GSSG)) are used as common biomarkers [7].

In a multi-laboratory comparison of different oxidative stress markers the measurement of 15-F_{2t}-IsoP, an isoprostane derived from arachidonic acid (C20:4 n6, ARA) was found to be promising for the evaluation of the oxidative stress status *in vivo* [8]. Isoprostanes (IsoP) are prostaglandin-like autoxidation products formed from free PUFA and under physiological conditions dominantly from PUFA esterified in phospholipids [9]. During non-enzymatic, free radical mediated autoxidation, PUFA are initially converted *via* radical abstraction of a bisallylic hydrogen and subsequent addition of molecular oxygen to hydroperoxy fatty acid radicals (Fig. 2.1). Depending on the position of the initial radical abstraction, different regioisomeric hydroperoxy radicals are formed. The primary formed hydroperoxy intermediates further undergo secondary reactions leading to a diverse product spectrum. For instance, a sequence of two 5-*exo*-cyclization steps of the hydroperoxy radicals followed by addition of molecular oxygen and reduction of the side chain hydroperoxide leads to prostaglandin-H-like bicyclic endoperoxide intermediates. These are under physiological

conditions unstable and react in the presence of reducing agents like GSH to stable F-ring isoprostanes or – when reducing cellular agents are depleted – undergo isomerization to D- or E-ring isomers (Fig. 2.1) [10].

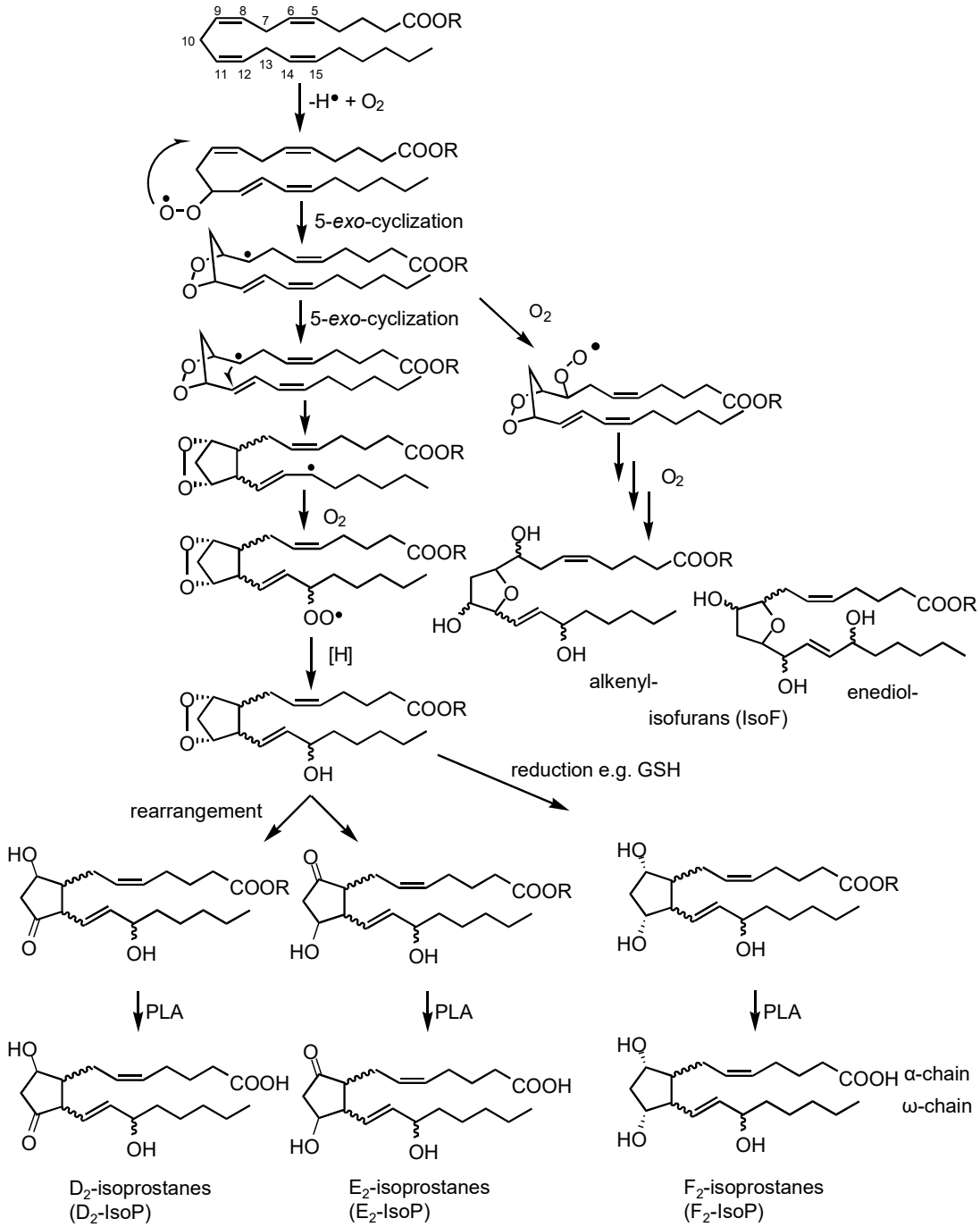

Fig. 2.1: Simplified mechanism of isoprostane (IsoP) and isofuran (IsoF) formation from arachidonic acid bound in phospholipids (R) depending on O_2 concentration. The bicyclic endoperoxide intermediate is under physiological conditions unstable and in the presence of reducing agents like GSH reduced to stable F-ring isoprostanes. When reducing cellular agents are depleted it undergoes isomerization to D- or E-ring isomers. Finally, the esterified oxylipins can be released by phospholipase (PLA).

From ARA, 4 regioisomeric F_2-IsoP can be formed each comprising 8 racemic diastereomers leading to a total of 64 possible isomers. However, the regioisomers are formed at different rates with the terminal 5- and 15-F_2-IsoP being more abundant compared to the 8- and 12-F_2-IsoP isomers [11, 12]. Also, other PUFA can be converted by an analogous mechanism leading to F_1-PhytoP from α-linolenic acid (C18:3 n3, ALA) and F_3-IsoP from eicosapentaenoic acid (C20:5 n3, EPA). Adrenic acid (C22:4 n6, AdA) gives rise to F_2-dihomo-IsoP, docosahexaenoic acid (C22:6 n3, DHA) and docosapentaenoic acid (C22:5 n6, n6-DPA) to F_4-NeuroP and F_3-NeuroP_{n6}, respectively.

The product spectrum during autoxidation is directed by the oxygen content: With increasing oxygen concentration (i.e. partial pressure) the levels of IsoP increase. However, above 21% no further increase of IsoP occurs while the formation of another class of cyclic PUFA derivatives, the tetrahydrofuran substituted isofurans (IsoF), is significantly elevated *in vitro* [13]. Based on two proposed formation mechanisms – the cyclic peroxide cleavage pathway and the epoxide hydrolysis pathway – 8 regioisomeric isofurans comprising 32 stereoisomers are formed from ARA resulting in a total of 256 possible isomers [13]. Conversion of other PUFA by an analogous mechanism leads to PhytoF [14, 15], dihomo-IsoF and NeuroF from ALA, AdA and DHA, respectively.

Moreover, depending on the tissue fatty acid composition a characteristic pattern of the formed isoprostanes results. For example, DHA and AdA are both found in the brain, however AdA is predominantly enriched in myelin which is part of the white matter, whereas DHA is enriched in neurons present in the grey matter [16]. Consequently, F_2-dihomo-IsoP are associated with oxidative stress of the white matter, whereas F_4-NeuroP are related to oxidative damage of the grey matter *in vitro* [17].

The analysis of isoprostanes in biological matrices is challenging because of their low concentration and the multitude of possible isomers formed from different PUFA. Several methods using gas chromatography (GC) and liquid

chromatography (LC) coupled to mass-spectrometry (MS) as well as immunoassays are described for the analysis [18-38]. Immunoassays like ELISA which only allow the analysis of single isomers are easy to handle and enable high sample throughput. However, due to the multitude of structurally similar isoprostanes, ELISAs are susceptible to cross-reactivity leading to an overestimation compared to LC-MS and GC-MS methods [37, 38]. In contrast, chromatographic methods coupled to MS allow the selective and sensitive parallel quantification of multiple isomers derived from a single as well as different PUFA. In addition to sample preparation steps, including extraction and purification, GC-MS requires derivatization of the analytes to volatile derivatives. Since this is more laborious, LC-MS has been predominantly used in the past years [26-34, 39, 40]. Most LC-MS methods cover only ARA derived F_2-IsoP, especially the prominent 15-F_{2t}-IsoP isomer [26-29, 32, 40] or are focused on IsoP derived from a single PUFA [31, 34, 39]. Only few methods have been described enabling the parallel quantification of IsoP derived from different PUFA [30, 33, 41].

However, keeping the tissue specific PUFA pattern in mind, the simultaneous analysis of a comprehensive set of IsoP and IsoF from all biologically relevant PUFA is crucial for the evaluation of oxidative stress *in vivo* independent of the origin of the analyzed biological specimen. Therefore, we developed in the present study a new, sensitive LC-ESI(-)-MS/MS method covering a comprehensive set of IsoP and IsoF from 6 biologically relevant PUFA that was integrated in an established method covering enzymatically formed oxylipins. The mass-spectrometric and chromatographic parameters were optimized and the method performance was thoroughly characterized. Finally, the method was applied on the investigation of the formation of IsoP and IsoF in response to *tert*-butyl hydroperoxide (*t*-BOOH) induced oxidative stress in HCT-116 cells.

2.2 Experimental

2.2.1 Chemicals

The isoprostane standard 15-F_{2t}-IsoP as well as the deuterated internal standards (IS) $^{2}H_4$-15-F_{2t}-IsoP ($^{2}H_4$-8-*iso*-$PGF_{2\alpha}$) and $^{2}H_{11}$-5(*R,S*)-5-F_{2t}-IsoP ($^{2}H_{11}$-(±)5-$iPF_{2\alpha}$-VI) were purchased from Cayman Chemicals (local distributor: Biomol, Hamburg, Germany). All other IsoP and IsoF standards, i.e. ARA derived 5-F_{2t}-IsoP, 5-*epi*-5-F_{2t}-IsoP, 2,3-dinor-15-F_{2t}-IsoP, 15-*epi*-2,3-dinor-15-F_{2t}-IsoP, EPA derived 5-F_{3t}-IsoP, 5-*epi*-5-F_{3t}-IsoP, 8-F_{3t}-IsoP, 8-*epi*-8-F_{3t}-IsoP, DHA derived 4(*R,S*)-4-F_{4t}-NeuroP, 10-F_{4t}-NeuroP, 10-*epi*-10-F_{4t}-NeuroP, 14(*R,S*)-14-F_{4t}-NeuroP, 4(*R,S*)-ST-Δ^5-8-NeuroF, AdA derived 17(*R,S*)-17-F_{2t}-dihomo-IsoP, *ent*-7(*R,S*)-7-F_{2t}-dihomo-IsoP, 17(*R,S*)-10-*epi*-SC-Δ^{15}-11-dihomo-IsoF, 7(*R,S*)-ST-Δ^8-11-dihomo-IsoF, n6-DPA derived 4-F_{3t}-$NeuroP_{n6}$, 4-*epi*-4-F_{3t}-$NeuroP_{n6}$, and ALA derived *ent*-9-F_{1t}-PhytoP, *ent*-9-*epi*-9-F_{1t}-PhytoP, *ent*-16-F_{1t}-PhytoP, *ent*-16-*epi*-16-F_{1t}-PhytoP, 16-B_1-PhytoP, 9-L_1-PhytoP, *ent*-16(*R,S*)-13-*epi*-ST-Δ^{14}-9-PhytoF as well as the unlabeled odd-chain IS C19-17-*epi*-17-F_{1t}-PhytoP and C21-15-F_{2t}-IsoP were synthesized, using our last strategy as described [14, 42, 43]. 4(*R,S*)-4-F_{4t}-NeuroP, 14(*R,S*)-14-F_{4t}-NeuroP, 4(*R,S*)-ST-Δ^5-8-NeuroF, 17(*R,S*)-17-F_{2t}-dihomo-IsoP, *ent*-7(*R,S*)-7-F_{2t}-dihomo-IsoP, 17(*R,S*)-10-*epi*-SC-Δ^{15}-11-dihomo-IsoF, 7(*R,S*)-ST-Δ^8-11-dihomo-IsoF, *ent*-16(*R,S*)-13-*epi*-ST-Δ^{14}-9-PhytoF were only available as epimeric mixtures. LC-MS-grade methanol (MeOH), acetonitrile (ACN) and acetic acid were purchased from Fisher Scientific (Schwerte, Germany). *n*-Hexane (HPLC Grade) was obtained from Carl Roth (Karlsruhe, Germany). All other chemicals were purchased from Sigma Aldrich (Schnelldorf, Germany). Pooled human EDTA-plasma was generated by centrifugation (10 min, 4 °C, 20,000 × g) of EDTA-blood, followed by mixing plasma from six healthy male and female volunteers aged between 25 and 38 years and immediately stored at −80 °C until analysis. All volunteers gave their written informed consent and all procedures were conducted according to the guidelines laid down in the

Declaration of Helsinki and approved by the ethic committee at the Medical Association of Lower Saxony (Hannover, Germany).

2.2.2 Calibration and quantification of IsoP

For calibration, stock solutions of the individual analytes (in MeOH) were mixed and diluted in glass volumetric flasks (5–100 mL) with MeOH at 10 concentration levels (0.1, 0.25, 0.5, 1, 2, 5, 10, 20, 100 and 500 nM), each with 20 nM of the four internal standards. Calibration curves were calculated using linear least square regression (weighting: $1/x^2$). Analyte quantification was carried out based on the analyte to corresponding IS (Tab. 2.1) area ratio using the obtained calibration curves.

2.2.3 In vitro assay

HCT-116 human colorectal carcinoma cells were grown in 10 cm dishes (5×10^6 cells/dish) and incubated after 24 h with 50 µM and 200 µM of *t*-BOOH (Sigma Aldrich, Schnelldorf, Germany) for 30 min, 1 h and 2 h. The cells were then detached using trypsin and harvested by centrifugation (5 min, 4 °C, 300 × g). After a washing step in cold PBS, the cells were centrifuged again (5 min, 4 °C, 300 × g) and the supernatant was discarded. The remaining cell pellet was snap-frozen in liquid nitrogen and stored at −80 °C until analysis. The cytotoxicity of the used *t*-BOOH concentrations was assessed using the MTS assay, which is based on the reduction of the tetrazolium salt MTS (3-(4,5-dimethylthiazol-2-yl)-5-(3-carboxymethoxyphenyl)-2-(4-sulfophenyl)-2H-tetrazolium) by viable cells. To this end, HCT-116 cells were seeded at a density of 2×10^4 per well and grown overnight. Cells were then incubated with 50 µM and 200 µM *t*-BOOH for 2 h and the viability was assessed as described [44].

2.2.4 Sample extraction

Human plasma was extracted using anion exchange Bond Elut Certify II SPE cartridges (200 mg, 3 mL, Agilent, Waldbronn, Germany) [45]. In brief, 10 µL of IS solution (containing 100 nM of $^{2}H_{4}$-15-F_{2t}-IsoP, $^{2}H_{11}$-5(*R,S*)-5-F_{2t}-IsoP, C19-17-*epi*-17-F_{1t}-PhytoP, C21-15-F_{2t}-IsoP and 13 isotope labeled internal standards used in the targeted metabolomics method [45], appendix Tab. 8.1) and 10 µL of antioxidant solution (0.2 mg/mL BHT and EDTA, 100 µM indomethacin, 100 µM of the soluble epoxide hydrolase inhibitor *trans*-4-[4-(3-adamantan-1-yl-ureido)-cyclohexyloxy]-benzoic acid (*t*-AUCB) [46] in MeOH/water (50/50, *v/v*)) were added to 500 µL freshly thawed human plasma.

The proteins were precipitated by addition of 1400 µL ice cold MeOH and storage at −80 °C for at least 30 min. After centrifugation (10 min, 4 °C, 20,000 × g) the supernatant was evaporated under a N_2-stream to a volume less than 1 mL and diluted with 2 mL of 0.1 M disodium hydrogen phosphate buffer adjusted to pH 5.5 with acetic acid, thus yielding a MeOH content of < 17% (pH = 6).

The SPE cartridge was preconditioned with one column volume of each, ethyl acetate/*n*-hexane (75/25, *v/v*) containing 1% acetic acid, MeOH, and 0.1 M disodium hydrogen phosphate adjusted to pH 6.0 with acetic acid in water/MeOH (95/5, *v/v*). After loading onto the preconditioned cartridge, the sample was washed with 3 mL water and 3 mL water/MeOH (50/50, *v/v*) and dried with excess pressure of N_2 for 1 min. The analytes were eluted with 2 mL of 75/25 *(v/v)* ethyl acetate/*n*-hexane with 1% acetic acid in tubes containing 6 µL of 30% glycerol in MeOH as trap solution for the analytes, and evaporated until only the glycerol plug remained using a vacuum concentrator (1 mbar, 30 °C, 45–60 min; Christ, Osterode am Harz, Germany). The residue was resuspended in 50 µL MeOH containing 40 nM of 1-(1-(ethylsulfonyl)piperidin-4-yl)-3-(4-(trifluoromethoxy)phenyl)urea as IS2 for the calculation of the extraction efficiency of the IS, centrifuged (10 min, 4 °C, 20,000 × g) and analyzed by LC-MS/MS.

For the analysis of isoprostanes formed in cell incubations, 10 µL of the antioxidant solution, 50 µL water and 300 µL MeOH were added to the cell pellets which contained about 1×10^7 cells. After homogenization in a ball mill (MM 400, Retsch, Haan, Germany) using two 3 mm stainless steel beads (10 min, 25 Hz), 600 µL MTBE was added and the homogenate was vigorously mixed. For separation of the aqueous and the organic layers 300 µL 0.15 M ammonium acetate solution was added. Following mixing and centrifugation (5 min, 4 °C, 3500 × g), the upper organic layer was transferred to another tube and the aqueous phase was washed with 300 µL MTBE. The combined organic layers were evaporated using a vacuum concentrator (1 mbar, 30 °C, 90–120 min). To the residue 10 µL IS solution (100 nM, see above), 500 µL water/MeOH (50/50, *v/v*) and 300 µL 10 M NaOH were added and lipids were hydrolyzed for 30 min at 60 °C. After hydrolysis, the sample was immediately cooled, neutralized using acetic acid (50%) and mixed with 1900 µL 0.1 M disodium hydrogen phosphate buffer (pH = 6). SPE was conducted as described above.

2.2.5 Method characterization

The method was characterized and validated regarding linearity, sensitivity (limit of detection (LOD) and lower limit of quantification (LLOQ)), extraction efficiency, intra- and interday accuracy and precision based on criteria of the guideline on bioanalytical method validation of the European Medicines Agency [47]. Linearity was assessed using standard solutions covering a concentration range from 0.1 to 500 nM. The LOD was determined as the concentration yielding a signal to noise ratio (S/N) ≥ 3. The concentration with a S/N ≥ 5 and an accuracy and precision within the calibration curve of ± 20% was defined as LLOQ and set as the lowest concentration of the calibration curve.

The extraction efficiency at three different level of plasma volumes (200, 500 and 1000 µL human plasma) was determined as the recovery of the IS spiked

to the sample prior extraction calculated using a calibration curve normalized to IS2 which is added in the last step of the analysis.

Intraday accuracy and precision (relative standard deviation, RSD) were evaluated in plasma samples spiked at four concentration levels (3 nM, 10 nM, 30 nM, 100 nM in vial) with IsoP and IsoF prior extraction. Four replicates of each level as well as unspiked plasma were analyzed. For interday accuracy and precision the samples were analyzed on 3 days. The accuracy was calculated by comparing the determined concentration with the added concentration. For IsoP isomers detected in unspiked plasma samples this concentration was substracted from the determined concentration following spiking.

2.2.6 LC-ESI(-)-MS/MS analysis

Samples (5 µL) were injected into the LC-MS system using a HTS xt-PAL autosampler (CTC Analytics, Switzerland, local distributor: Axel Semrau, Sprockhövel, Germany) equipped with a 100 µL syringe and a 20 µL sample loop. The sample rack was kept at 4 °C.

Liquid chromatography was performed using a 1290 Infinity LC System (Agilent, Waldbronn, Germany) composed of a binary pump and a column oven. Separation of the analytes was carried out on a Zorbax Eclipse Plus C18 reversed-phase column (2.1 x 150 mm, particle size 1.8 µm; Agilent, Waldbronn, Germany) at 40 °C equipped upstream with an inline filter (3 µm, 1290 infinity II in-line filter, Agilent, Waldbronn, Germany) and a SecurityGuard Ultra C18 cartridge as precolumn (2.1 x 2 mm, Phenomenex, Aschaffenburg, Germany). The mobile phase consisted of 0.1% acetic acid as solvent A and 800/150/1 (*v/v/v*) ACN/MeOH/acetic acid as solvent B. The chromatographic separation was achieved using the following binary gradient with a flow rate of 0.3 mL/min: 0–1.0 min isocratic 25% B, 1.0–1.5 min linear from 25% B to 30% B, 1.5–10.0 min linear from 35% B to 53% B, 10.0–19.5 min linear from

53% B to 68% B, 19.5–24.5 min linear from 68% B to 95% B, 24.5–27.0 min isocratic 95% B, 27.0–27.10 min linear from 95% B to 25% B followed by reconditioning for 3.4 min. During the first 2 min and the last 6 min of each run the LC flow was directed to waste using the 2-position-6-port valve integrated in the MS. Detection was carried out on a 6500 QTRAP mass-spectrometer (Sciex, Darmstadt, Germany) following negative electrospray ionization (ESI(-)) with the following source settings: ion-spray voltage: −4500 V, curtain gas (N_2): 35 psi, nebulizer gas (gas 1, zero air): 60 psi generated with a zero air generator (UHP-300-ZA-S-E, Parker, Kaarst, Germany) and drying gas (gas 2, zero air): 60 psi at a temperature of 475 °C. The offset of the sprayer was 0.250 cm for the vertical axis and 0.550 cm for the horizontal axis, the electrode protrusion was approx. 1 mm.

The analytes were detected in scheduled selected reaction monitoring mode (SRM) using nitrogen as collision gas (set to “high”, 12 psi) with a detection window of ± 22.5 sec around the expected retention time and a cycle time of 0.4 sec. The compound specific parameters were optimized for each analyte and are summarized in Tab. 2.1. The LC-MS analysis of isoprostanes and related analytes from other PUFA was combined with an established multimethod for oxylipins [45, 48, 49]. A list of all covered analytes and their mass spectrometric parameters can be found in the appendix (Tab. 8.2). For data acquisition and instrument control Analyst Software (version 1.6.2, Sciex) and for integration and quantification Multiquant (version 2.1.1, Sciex) was used.

2.3 Results and Discussion

For selective and sensitive LC-MS analysis of the isoprostanes and related analytes the mass spectrometric parameters were optimized for each compound individually and the chromatographic conditions were adjusted in order to yield good and rapid separation of the isobaric isomers.

2.3.1 Mass spectrometric detection

Isoprostanes are autoxidative derivatives of fatty acids containing a carboxylic moiety, thus ionization was carried out in ESI(-) mode leading to the formation of $[M-H]^-$ ions, whose dominating formation was confirmed in MS full scan experiments. For each compound the declustering potential (DP) was optimized in single ion monitoring (SIM) mode of the $[M-H]^-$ ion to achieve an effective transmission of the ionized analytes from the source to the entrance of the vacuum chamber with minimal in-source fragmentation. For selective detection of regioisomers specific fragment ions for selected reaction monitoring (SRM) were chosen from the product ion spectra (appendix Fig. 8.1) and the collision energy (CE) was optimized. The optimized MS parameters are shown in Tab. 2.1. The structure of F-IsoP is characterized by a prostanoid-like F-ring with two hydroxyl groups and one further hydroxyl group in one of the two side chains, either the α-chain (carboxy terminus) or the ω-chain (methyl terminus) (Fig. 2.1). Accordingly, for different regioisomers identical abundant fragments resulting from unspecific loss of H_2O or CO_2 as well as combinations of CO_2 and up to 3-fold H_2O loss were observed (Fig. 2.2 A and B). Thus, for selective MS detection of different regioisomers the choice of specific fragment ions is crucial. Specific fragments result from backbone fragmentation and can be attributed to α-cleavage adjacent to the hydroxyl group in the side chain which is referred to as “α-hydroxy-β-ene-rearrangement”, a common fragmentation for unsaturated hydroxy-fatty acids [50]. For the investigated F-IsoP the observed α-fragments comprise the carboxy-terminus with or without subsequent loss of CO_2 and/or H_2O. Depending on the side chain where the hydroxyl group is located, the predominantly observed α-fragments can be assigned to distinct cleavage sites relative to the hydroxyl group: F-IsoP with the hydroxyl group in the α-chain, e.g. *ent*-9-F_{1t}-PhytoP (Fig. 2.2 A), showed an α-fragmentation which could be attributed to the cleavage on the methyl side of the hydroxyl group leading to a specific fragment containing the carboxyl- and the hydroxyl-moiety (*m/z* 170.9 for *ent*-9-F_{1t}-PhytoP). By contrast, the dominantly observed fragments of F-IsoP with the hydroxyl group in the ω-chain, e.g. *ent*-16-F_{1t}-

PhytoP (Fig. 2.2 B), could be assigned to the cleavage on the carboxyl side relative to the hydroxyl group and thus to a fragmentation segment carrying the carboxyl-moiety (*m/z* 269.1 for *ent*-16-F_{1t}-PhytoP). Interestingly, the DHA derived 10(*R,S*)-10-F_{4t}-NeuroP with the hydroxyl group in the α-chain and the 14(*R,S*)-14-F_{4t}-NeuroP with the hydroxyl group in the ω-chain are exceptions, showing a reverse fragmentation behavior compared to the observed pattern for the other F-IsoP described above, i.e. forming predominantly charged fragments which can be assigned to the reverse α-cleavage site relative to the hydroxyl group (appendix Fig. 8.1 D(ii) and (iii)). The selected fragment ions are consistent with the transitions used in other SRM methods for almost all F-IsoP with exception of 16(*R,S*)-16-F_{1t}-PhytoP [31], 8(*R,S*)-8-F_{3t}-IsoP [32, 33] and 17(*R,S*)-17-F_{2t}-dihomo-IsoP [30, 33, 43]. For those analytes different transitions compared to existing methods were selected which, however, could be ascribed to specific α-cleavages of the backbone of the molecule.

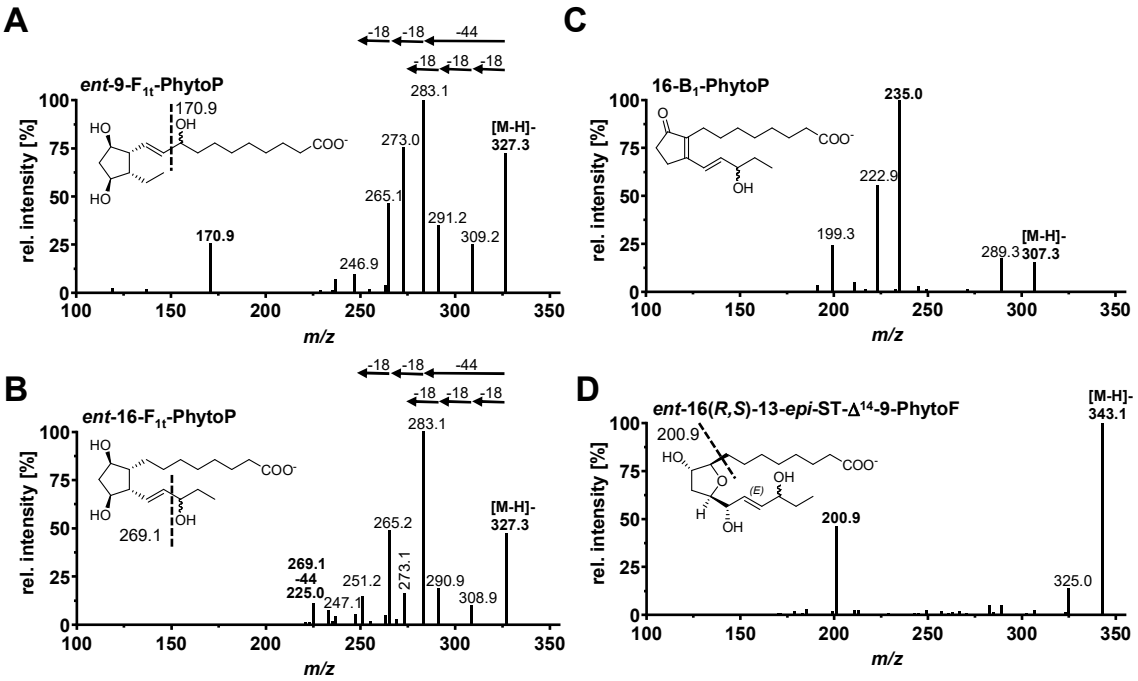

Fig. 2.2: Collision-induced dissociation (CID) product ion spectra of [M-H]$^-$ ions of α-linolenic acid derived PhytoP and PhytoF. **(A)** *ent*-9-F_{1t}-PhytoP (F-ring-PhytoP carrying the hydroxyl group in the α-chain) **(B)** *ent*-16-F_{1t}-PhytoP (F-ring-PhytoP carrying the hydroxyl group in the ω-chain) **(C)** 16-B_1-PhytoP (cyclopentenone with B-ring structure) **(D)** *ent*-16(*R,S*)-13-*epi*-ST-Δ^{14}-9-PhytoF (enediol-furan).

The investigated cyclopentenone PhytoP with B- (Fig. 2.2 C) and L-ring structure (appendix, Fig. 8.1 A(iv)) only gave rise to few abundant fragment ions. Based on this fragmentation pattern no suggestion for the site of fragmentation could be made. For structural elucidation of the formed fragments, further studies, e.g. using isotopically labeled standards are necessary. Nevertheless, the selected transitions were specific for these PhytoP and have been reported previously for their quantification [31, 34].

The isofurans are structurally characterized by a furan-like 5-membered oxygen containing ring carrying a hydroxyl group and additionally two hydroxyl groups in the side chains located either in the same side chain as it is the case for enediol furans or in different side chains like in alkenyl furans (Fig. 2.1). For each of the investigated IsoF the fragmentation behavior is distinct: Compared to F-IsoP unspecific loss of H_2O and CO_2 is less pronounced and specific fragments resulting from backbone cleavage might be attributed either to fragmentation next to the furan ring (Fig. 2.2 D) or adjacent to one of the side chain hydroxyl groups (as e.g. for 7(*R,S*)-ST-Δ^8-11-dihomo-IsoF, appendix Fig. 8.1 E(iii)). However, 4(*R,S*)-ST-Δ^5-8-NeuroF and 17(*R,S*)-10-*epi*-SC-Δ^8-11-dihomo-IsoF show a different fragmentation pattern (appendix Fig. 8.1 D(iv) and E(iv)) and suggestions for the structure of the fragments and fragmentation sites cannot be made based on the data. For 17(*R,S*)-10-*epi*-SC-Δ^8-11-dihomo-IsoF the transition reported previously corresponding to the fragment with the highest abundance was selected [43]. Regarding 4(*R,S*)-ST-Δ^5-8-NeuroF the fragment used in previous methods (*m/z* 123) [51] showed poor intensity, thus the fragment (*m/z* 187) with the highest abundance was selected (appendix Fig. 8.1 D(iv)).

Tab. 2.1: Parameters of the LC-ESI(-)-MS/MS method for the quantification of isoprostanes and isofurans. Shown are the mass transitions for quantification in scheduled SRM mode, electronical MS parameters (declustering potential (DP), entrance potential (EP), collision energy (CE), collision cell exit potential (CXP)), the assigned internal standards (IS), retention time (t_R), full peak width at half maximum (FWHM), limit of detection (LOD), the calibration range (lower limit of quantification (LLOQ), upper limit of quantification (ULOQ)), correlation coefficient (r) and the normalized slope of the calibration curve.

Analyte	Mass transition		MS parameters [1]				IS	t_R [2] [min]	FWHM [3] [sec]	LOD [4]		Calibration range LLOQ [5] ULOQ [6] [nM]		r [7]	slope [8]
	Q1	Q3	DP	EP	CE	CXP				[nM]	[pg on column]				
ent-16(*R,S*)-13-*epi*-ST-Δ^{14}-9-PhytoF 1 *)	343.1	200.9	-80	-10	-33	-8	C19-17-*epi*-17-F_{1t}-PhytoP	4.19	3.4	0.12	0.20	0.24	235	0.9993	0.91
ent-16(*R,S*)-13-*epi*-ST-Δ^{14}-9-PhytoF 2 *)	343.1	200.9	-80	-10	-33	-8	C19-17-*epi*-17-F_{1t}-PhytoP	4.30	3.4	0.13	0.23	0.26	265	0.9995	1.02
ent-16-*epi*-F_{1t}-PhytoP	327.3	225.0	-70	-10	-34	-8	C19-17-*epi*-17-F_{1t}-PhytoP	4.72	3.3	0.25	0.41	0.50	500	0.9983	0.78
ent-16-F_{1t}-PhytoP	327.3	225.0	-70	-10	-34	-8	C19-17-*epi*-17-F_{1t}-PhytoP	4.89	3.4	0.25	0.41	0.50	500	0.9997	0.73
ent-9-F_{1t}-PhytoP	327.3	170.9	-40	-10	-31	-8	C19-17-*epi*-17-F_{1t}-PhytoP	4.81	3.3	0.10	0.16	0.25	500	0.9991	1.44
ent-9-*epi*-F_{1t}-PhytoP	327.3	170.9	-40	-10	-31	-8	C19-17-*epi*-17-F_{1t}-PhytoP	4.98	3.3	0.25	0.41	0.50	500	0.9990	1.12
15(*R,S*)-2,3-dinor-15-F_{2t}-IsoP	325.2	237.0	-40	-10	-18	-8	C19-17-*epi*-17-F_{1t}-PhytoP	5.41	3.3	0.25	0.41	0.50	500	0.9995	1.79
8-F_{3t}-IsoP	351.1	155.0	-60	-10	-27	-8	C19-17-*epi*-17-F_{1t}-PhytoP	6.15	3.6	0.50	0.88	1.0	500	0.9980	0.70
8-*epi*-8-F_{3t}-IsoP	351.1	155.0	-60	-10	-27	-8	C19-17-*epi*-17-F_{1t}-PhytoP	6.51	3.3	0.50	0.88	1.0	500	0.9992	0.60
5(*R,S*)-5-F_{3t}-IsoP	351.2	114.9	-50	-10	-27	-8	C19-17-*epi*-17-F_{1t}-PhytoP	6.53	3.4	1.0	1.8	2.0	500	0.9962	0.07
15-F_{2t}-IsoP (8-*iso*-$PGF_{2\alpha}$)	353.1	193.1	-70	-6	-33	-8	$^2H_4$-15-F_{2t}-IsoP	7.56	3.7	0.25	0.44	0.50	500	0.9989	0.98
10-F_{4t}-NeuroP	377.2	153.0	-40	-10	-25	-8	$^2H_4$-15-F_{2t}-IsoP	8.04	3.3	0.25	0.47	0.50	500	0.9989	1.81
10-*epi*-10-F_{4t}-NeuroP	377.2	153.0	-40	-10	-25	-8	$^2H_4$-15-F_{2t}-IsoP	8.37	3.5	0.50	0.95	1.0	500	0.9990	0.88
5(*R,S*)-5-F_{2t}-IsoP	353.2	114.8	-60	-10	-26	-8	$^2H_{11}$-5(*R,S*)-5-F_{2t}-IsoP	8.07	3.5	0.25	0.44	0.50	500	0.9959	0.52
16-B_1-PhytoP	307.3	235.0	-60	-10	-27	-8	$^2H_{11}$-5(*R,S*)-5-F_{2t}-IsoP	8.26	3.7	0.10	0.15	0.25	500	0.9994	3.00
9-L_1-PhytoP	307.3	185.1	-60	-10	-27	-8	$^2H_{11}$-5(*R,S*)-5-F_{2t}-IsoP	8.33	3.7	0.10	0.15	0.25	500	0.9986	3.07
14(*R,S*)-14-F_{4t}-NeuroP	377.2	205.1	-50	-10	-27	-8	C21-15-F_{2t}-IsoP	8.62	6.5	10	19	20	500	0.9998	0.09
4(*R,S*)-4-F_{4t}-NeuroP	377.1	101.3	-60	-10	-26	-8	C21-15-F_{2t}-IsoP	9.35	3.6	0.50	0.95	1.0	500	0.9982	0.23
4(*R,S*)-ST-Δ^5-8-NeuroF	393.3	187.2	-40	-10	-29	-8	C21-15-F_{2t}-IsoP	9.59	4.2	20	39	40	500	0.9941	0.02
17(*R,S*)-17-F_{2t}-dihomo-IsoP 1 *)	381.3	263.2	-90	-10	-31	-8	C21-15-F_{2t}-IsoP	9.78	3.6	0.63	1.2	1.3	314	0.9967	0.31
17(*R,S*)-17-F_{2t}-dihomo-IsoP 2 *)	381.3	263.2	-90	-10	-31	-8	C21-15-F_{2t}-IsoP	9.95	3.2	0.37	0.71	0.75	186	0.9980	0.19
7(*R,S*)-ST-Δ^8-11-dihomo-IsoF	397.3	245.1	-50	-10	-31	-8	C21-15-F_{2t}-IsoP	9.81	8.9 [#]	1.0	2.0	2.0	500	0.9993	0.42
ent-7(*R,S*)-7-F_{2t}-dihomo-IsoP	381.3	143.0	-50	-10	-31	-8	C21-15-F_{2t}-IsoP	9.86	5.7	0.25	0.48	0.50	500	0.9972	1.87
4(*R,S*)-4-F_{3t}-$NeuroP_{n6}$	379.2	101.0	-50	-10	-29	-8	C21-15-F_{2t}-IsoP	11.03	4.1	0.50	0.95	1.0	500	0.9971	0.59
17(*R,S*)-10-*epi*-SC-Δ^{15}-11-dihomo-IsoF 1 *)	397.1	221.0	-90	-10	-31	-8	C21-15-F_{2t}-IsoP	11.26	3.7	0.52	1.0	1.0	260	0.9992	0.41
17(*R,S*)-10-*epi*-SC-Δ^{15}-11-dihomo-IsoF 2 *)	397.1	221.0	-90	-10	-31	-8	C21-15-F_{2t}-IsoP	11.44	3.7	0.48	0.96	0.96	240	0.9982	0.38
C19-17-*epi*-17-F_{1t}-PhytoP	341.3	239.0	-70	-10	-35	-8	IS	6.02	3.3						
$^2H_4$-15-F_{2t}-IsoP	357.2	196.8	-50	-6	-33	-8	IS	7.54	3.6						
$^2H_{11}$-5(*R,S*)-5-F_{2t}-IsoP	364.3	115.2	-40	-10	-29	-10	IS	7.97	4.5						
C21-15-F_{2t}-IsoP	367.2	193.1	-60	-10	-35	-8	IS	9.18	3.8						

1) The collision cell exit potential (CXP) was for all analytes -8 V. **2)** Relative standard deviation of t_R within one batch was ≤ 0.18% (< 0.01 min). **3)** Full peak width at half maximum (FWHM) was determined as mean width of standards with the concentrations LLOQ–100 nM, for 14(*R,S*)-14-F_{4t}-NeuroP and 4(*R,S*)-ST-Δ^5-8-NeuroF concentrations LLOQ–500 nM were used; [#] for 7(*R,S*)-ST-Δ^8-11-dihomo-IsoF (incompletely separated) the FWHM was determined at the half maximal height of the smaller peak (see Fig. 2.3 B(V))]. **4)** LOD was set to the lowest concentration yielding a signal to noise ratio ≥ 3. **5)** LLOQ was set to the lowest calibration standard injected yielding a signal to noise ratio ≥ 5 and an accuracy in the calibration curve within ± 20%. **6)** ULOQ concentration does not represent the end of the dynamic range, but is the highest calibration standard injected. **7)** Calibration was performed as linear weighted least square regression using $1/x^2$ weighting. **8)** Slope of the calibration curve normalized for all analytes to 15-F_{2t}-IsoP × 10. *) Isomers were provided as mixture of two diastereomers which were chromatographically separated; 1 and 2 indicate the two isomers (see Fig. 2.3). The individual concentration of each isomer was calculated based on the ratio in SIM.

2.3.2 Chromatographic separation

The chromatographic separation was optimized in order to obtain an efficient separation of the isobaric isomers in a reasonable time. The method covers 25 F-ring IsoP comprising 12 diastereomeric (epimeric) pairs and one single stereoisomer derived from ALA, ARA, EPA, n6-DPA, DHA and AdA, one B- and one L-ring PhytoP and 4 epimeric pairs of IsoF derived from ALA, DHA and AdA. Using a C18 column with sub 2 µm particles and an optimized gradient of acidified water and ACN as well as MeOH, separation of the analytes could be achieved within 12 minutes (Fig. 2.3 A). The ALA derived PhytoF and F_{1t}-PhytoP elute first, followed by the polar β-oxidation metabolites 15(*R,S*)-2,3-dinor-15-F_{2t}-IsoP from ARA and the IsoP from EPA and ARA. B- and L-ring PhytoP and DHA derived F_{4t}-NeuroP and NeuroF elute in the middle part of the chromatogram followed by AdA derived F_{2t}-dihomo-IsoP and dihomo-IsoF as well as n6-DPA derived 4(*R,S*)-4-F_{3t}-$NeuroP_{n6}$ (Fig. 2.3).

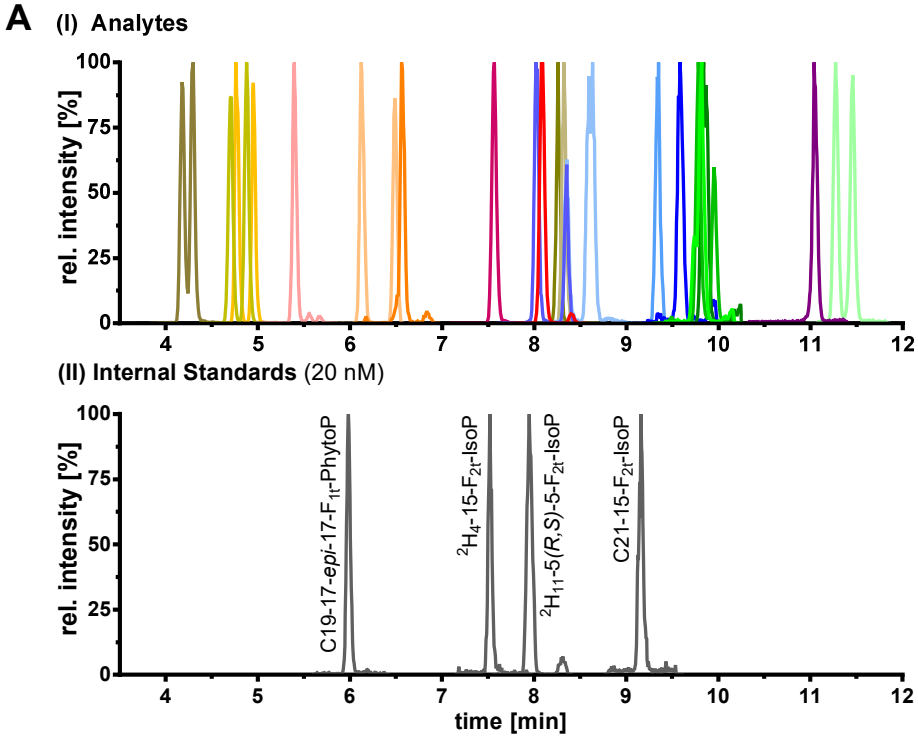

Fig. 2.3: (A) Chromatographic separation of **(I)** 27 isoprostanes and 8 isofurans derived from 6 different PUFA. Shown are the SRM signals used for quantification following injection of a multianalyte standard (100 nM; except 14(*R,S*)-14-F_{4t}-NeuroP, 4(*R,S*)-ST-Δ^5-8-NeuroF, *ent*-7(*R,S*)-7-F_{2t}-dihomo-IsoP, 17(*R,S*)-17-F_{2t}-dihomo-IsoP each 500 nM). **(II)** For the quantification 4 internal standards (20 nM) are used: 2 deuterated IS and 2 odd-chain IS.

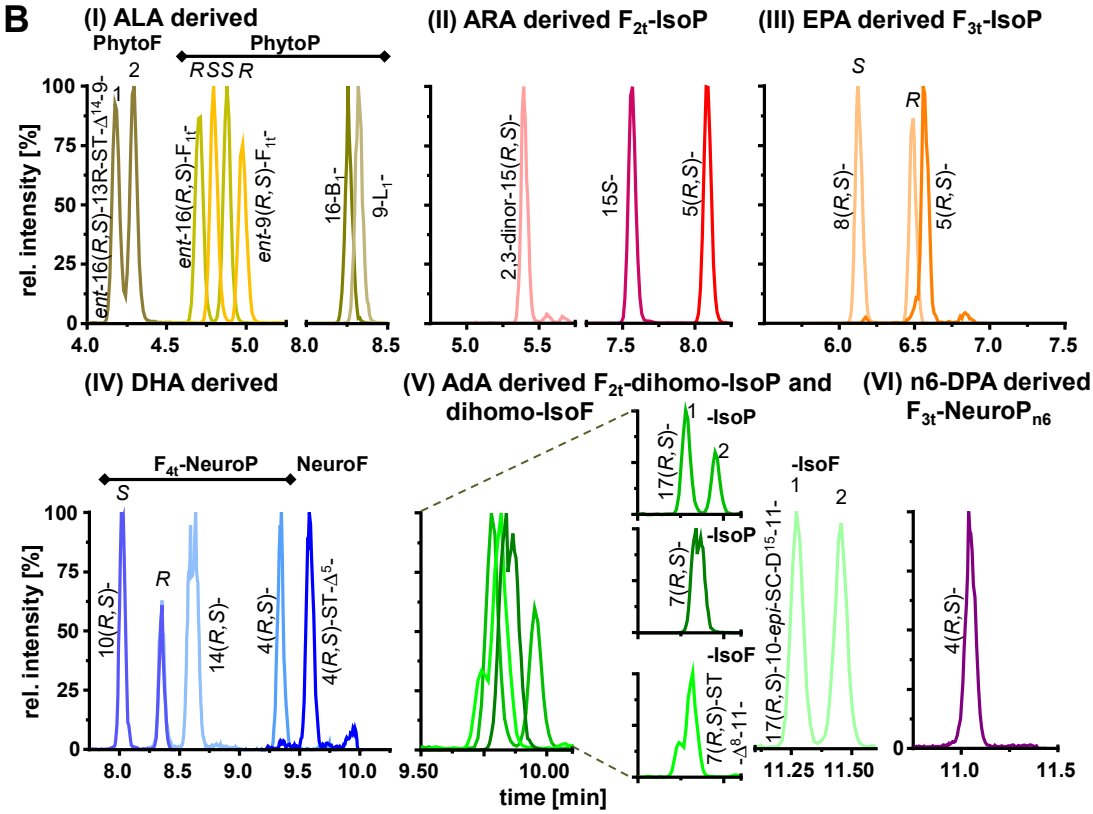

Fig. 2.3: (B) Chromatographic separation efficiency of isoprostanoids covered by the method grouped by their precursor PUFA. Shown are the SRM signals used for quantification of **(I)** α-linolenic acid (C18:3 n3, ALA) derived *ent*-16(*R,S*)-13-*epi*-ST-Δ^{14}-9-PhytoF, *ent*-16-F_{1t}-PhytoP, *ent*-16-*epi*-16-F_{1t}-PhytoP, *ent*-9-F_{1t}-PhytoP, *ent*-9-*epi*-F_{1t}-PhytoP, 16-B_1-PhytoP, 9-L_1-PhytoP; **(II)** arachidonic acid (C20:4 n6, ARA) derived 15(*R,S*)-2,3-dinor-15-F_{2t}-IsoP, 15-F_{2t}-IsoP (= 8-*iso*-$PGF_{2\alpha}$), 5(*R,S*)-5-F_{2t}-IsoP; **(III)** eicosapentaenoic acid (C20:5 n3, EPA) derived 8-F_{3t}-IsoP, 8-*epi*-8-F_{3t}-IsoP, 5(*R,S*)-5-F_{3t}-IsoP; **(IV)** docosahexaenoic acid (C22:6 n3, DHA) derived 10-F_{4t}-NeuroP, 10-*epi*-10-F_{4t}-NeuroP, 14(*R,S*)-14-F_{4t}-NeuroP, 4(*R,S*)-4-F_{4t}-NeuroP, 4(*R,S*)-ST-Δ^5-8-NeuroF; **(V)** adrenic acid (C22:4 n6, AdA) derived 7(*R,S*)-ST-Δ^8-11-dihomo-IsoF, *ent*-7(*R,S*)-7-F_{2t}-dihomo-IsoP, 17(*R,S*)-17-F_{2t}-dihomo-IsoP, 17(*R,S*)-10-*epi*-SC-Δ^5-11-dihomo-IsoF; **(VI)** docosapentaenoic acid (C22:5 n6, n6-DPA) derived 4(*R,S*)-4-F_{3t}-$NeuroP_{n6}$.

The initial gradient conditions were adjusted in order to achieve separation from the void volume (1.5 min), i.e. sufficient retention of the early eluting analytes, which is characterized by a retention factor k of at least 2. The first analytes (PhytoF) elute at 4.19 and 4.30 min (after more than two void volumes), which corresponds to a retention factor of k ≥ 1.8, showing a sufficient separation from the unretained void volume. The slope of the gradient was optimized in order to yield a high separation efficiency of most epimeric pairs.

A short isocratic step (1 min) with 25% organic at the beginning of the gradient was included to focus the analytes at the front end of the column. This led to

narrow peaks over the whole separation time (exemplary shown in Fig. 2.4) characterized by a full width at half maximum (FWHM) of about 3.3–4.2 seconds for almost all analytes (Tab. 2.1). Some epimeric pairs, e.g. 14(*R,S*)-14-F_{4t}-NeuroP and *ent*-7(*R,S*)-7-F_{2t}-dihomo-IsoP (Tab. 2.1, Fig. 2.3 B), showed a broader FWHM due to incomplete separation of the epimers.

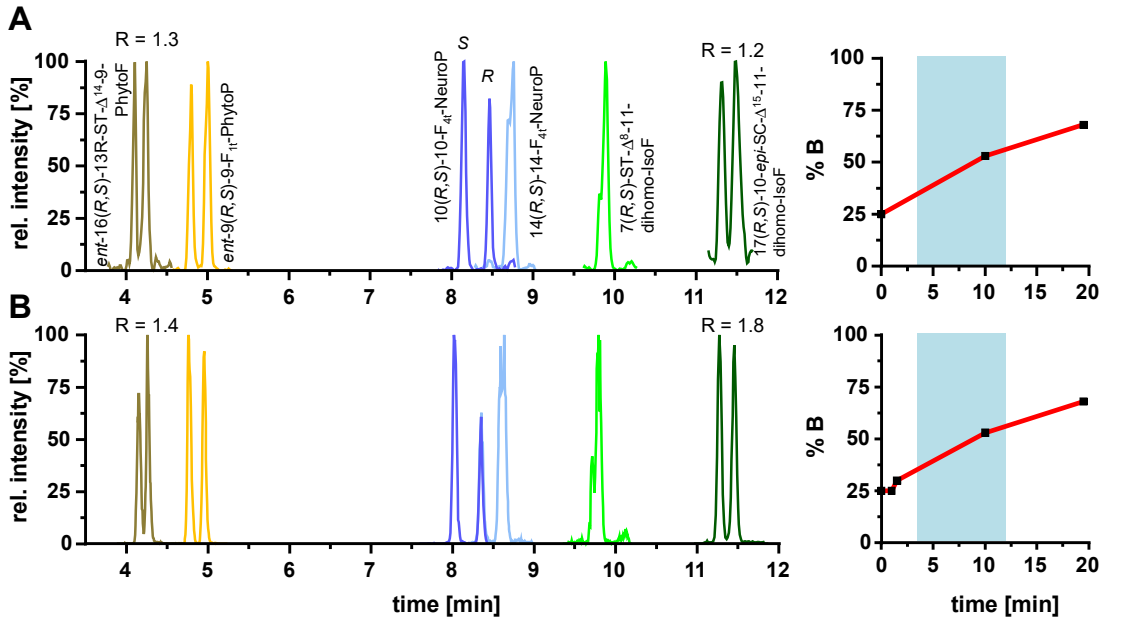

Fig. 2.4: Chromatographic separation efficiency of selected epimeric pairs using a gradient starting with 25% organic **(A)** without and **(B)** with inclusion of a short isocratic step (1 min) at the beginning of the gradient. The resolution (R) is indicated for selected epimeric pairs.

The chromatographic separation showed a high stability regarding retention time with an interbatch RSD of ≤ 0.25%, i.e. < 0.02 min (n = 360) or < 0.01 min within one batch (n = 50).

The gradient allows an efficient separation of 7 critical epimeric pairs of IsoP and IsoF characterized by a resolution of R > 1.5. With exception of *ent*-16(*R,S*)-13-*epi*-ST-Δ^{14}-9-PhytoF, which is the first eluting epimeric pair showing a resolution of R = 1.4, the resolution of the other separated epimers is R ≥ 1.7. However, 3 epimeric pairs (14(*R,S*)-14-F_{4t}-NeuroP, *ent*-7(*R,S*)-7-F_{2t}-dihomo-IsoP and 7(*R,S*)-ST-Δ^{8}-11-dihomo-IsoF) show an incomplete separation and 6 epimeric pairs coelute (Fig. 2.3 B). The use of a shallower gradient with an increase of 0.5% B/min instead of 2.7% B/min or isocratic separation (data not

shown) only slightly improved the separation of the incompletely separated and coeluting stereoisomers while further prolonging the analysis time. Thus, only the use of a different column or mobile phase thereby changing the selectivity of the chromatographic system could solve this separation problem. However, we regarded these parameters as fixed during method development because the analytical procedure should be integrated in an existing method, already established in our laboratory, for the analysis of enzymatically formed oxylipins [45, 48, 49]. This combination enables to determine 129 oxylipins in addition to the covered IsoP and IsoF, thus allowing the detection of a total of 164 oxylipins formed enzymatically and *via* autoxidation together with 17 IS within 30.5 min. The mass spectrometric and chromatographic performance parameters for all analytes are summarized in the appendix Tab. 8.2.

2.3.3 Method performance

Quantification of the analytes was carried out based on the analyte to corresponding IS area ratio using the calibration curves. For the IsoP and IsoF two deuterated IsoP ($^{2}H_{11}$-5(*R,S*)-5-F_{2t}-IsoP and $^{2}H_{4}$-15-F_{2t}-IsoP) and two odd-chain unlabeled IsoP (C19-17-*epi*-17-F_{1t}-PhytoP and C21-15-F_{2t}-IsoP) that are eluted over the analytical time (Fig. 2.3 A) were used as IS. For 5(*R,S*)-5-F_{2t}-IsoP and 15-F_{2t}-IsoP their respective isotopologs were used as IS. For the other analytes the assignment of the IS was based on retention time (Tab. 2.1).

Characterization of the method performance was oriented on the guideline on bioanalytical method validation of the European Medicines Agency [47]. The sensitivity of the method was assessed by determining the LOD and the LLOQ based on the signal to noise ratio (Tab. 2.1). The concentration leading to an S/N ≥ 3 was defined as LOD (exemplary shown for 2,3-dinor-15-F_{2t}-IsoP, Fig. 2.5). Almost all analytes showed a comparable LOD ranging from 0.15–2 pg on column. However, 14(*R,S*)-14-F_{4t}-NeuroP and 4(*R,S*)-ST-Δ^{5}-8-NeuroF showed a considerably higher LOD with 19 pg and 39 pg on column, respectively. Since the same differences in the signal intensity were observed in

SIM mode (data not shown), these higher LOD could either be explained by different ionization behavior of the compounds or by impure standard stock solutions of these two compounds. Similar to the LOD, the LLOQ (i.e. the concentration with a S/N ≥ 5 and an accuracy of 80–120% within the calibration curve) ranged from 0.25 to 2 nM for almost all IsoP and IsoF except 14(*R,S*)-14-F_{4t}-NeuroP and 4(*R,S*)-ST-Δ^5-8-NeuroF.

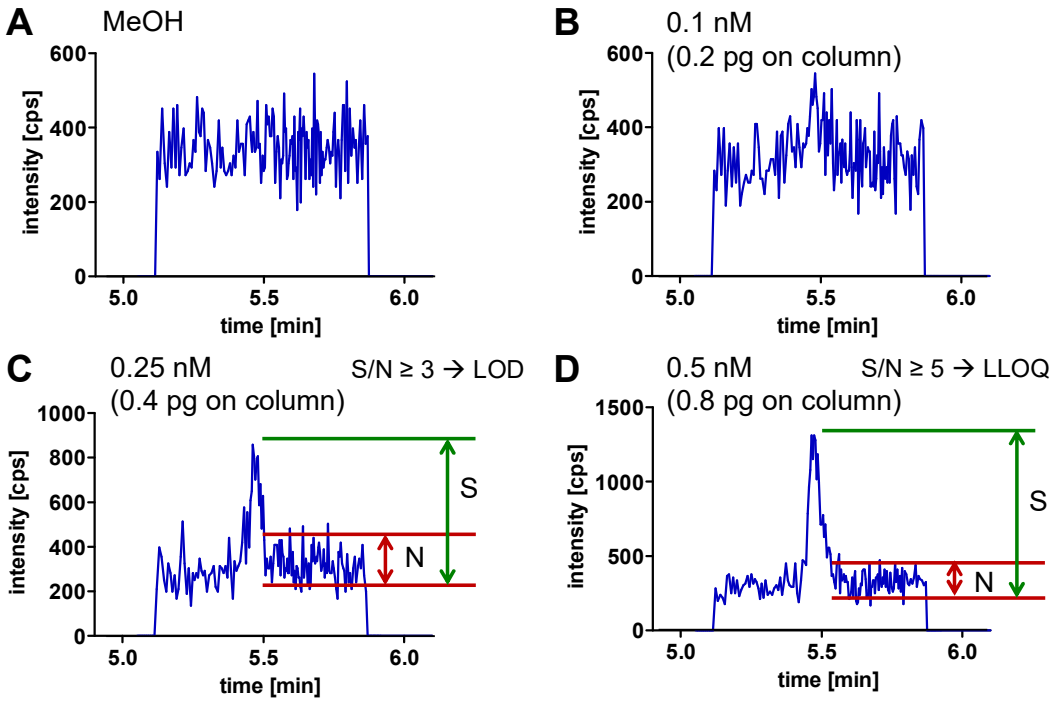

Fig. 2.5: Determination of the limit of detection (LOD) and lower limit of quantification (LLOQ) for 2,3-dinor-15-F_{2t}-IsoP based on the signal to noise ratio (S/N). Starting from **(A)** blank (MeOH), successive standards **(B), (C), (D)** with increasing concentration of the analyte were injected. **(C)** The concentration yielding a S/N ≥ 3 was set as LOD. **(D)** The concentration with a S/N ≥ 5 and an accuracy within the calibration curve of ± 20% was defined as LLOQ.

The sensitivity was also reflected by the slope of the calibration curves. Comparing the slopes of all covered IsoP and IsoF normalized to the same IS revealed that 14(*R,S*)-14-F_{4t}-NeuroP and 4(*R,S*)-ST-Δ^5-8-NeuroF showed remarkably lower slopes compared to the other analytes (factor 10 and 50 lower, respectively, compared to the mean of normalized slopes) which is consistent with the observed higher LLOQ and LOD (Tab. 2.1). Interestingly this higher LLOQ for 14(*R,S*)-14-F_{4t}-NeuroP was also observed previously [33]. Remarkably, 5(*R,S*)-5-F_{3t}-IsoP with an LLOQ of 2 nM, showed a comparatively

low slope. Compared to other IsoP, a slightly higher LLOQ for 5(*R,S*)-5-F_{3t}-IsoP was also reported previously [33].

The obtained LOD and LLOQ are in a similar range as reported previously for other oxylipins [45], and in comparison with previous reports for isoprostanes the obtained sensitivity was comparable or slightly better [30, 33]. Noteworthy, two methods which were focused only on F_{2t}-IsoP [40] and PhytoP and PhytoF [34] reported LLOQs one to two orders of magnitude lower despite using a comparable triple quadrupole mass spectrometer. This may be in part explained by the high injection volume of 50 µL as well as the use of a micro-HPLC instrumentation [34, 40]. In our method, using a higher injection volume led to peak splitting and inacceptable peak shape (Fig. 2.6). This is caused by the high elution power of the methanol which is used to reconstitute the samples after SPE. Using a more polar solvent leads to an insufficient solution of less polar hydroxy- and epoxy-fatty acids which are also covered by our method and thus the amount of sample injected cannot be further increased. Nevertheless, our approach is still one of the three most sensitive methods described so far for the detection of IsoP. Moreover, it is the most comprehensive approach for the simultaneous quantification of prostanoid-like autoxidation products and covers more analytes than all previous methods.

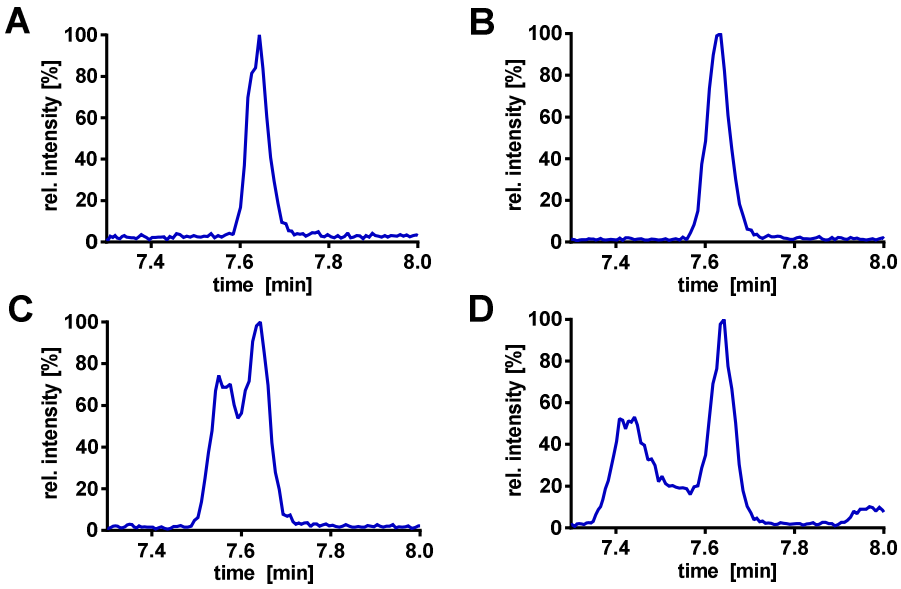

Fig. 2.6: Peak shape of 15-F_{2t}-IsoP (10 nM in methanol) with increasing injection volume. **(A)** 5 µL, **(B)** 10 µL, **(C)** 15 µL, **(D)** 20 µL.

Matching between method sensitivity and expected concentration in biological samples one should take into account that the baseline levels of IsoP and IsoF are very low, e.g. the commonly analyzed 15(*R,S*)-15-F_{2t}-IsoP is in the range of 40–170 pg/mL human plasma of healthy subjects (total, i.e. free and esterified level) [52], corresponding to 0.1–0.5 nM. Sufficient sample preparation including a pre-concentration step as carried out in the presented method by an optimized SPE procedure is therefore needed to determine these compounds in biological samples.

For quantification, calibration curves at 10 concentration levels covering a concentration range from 0.1–500 nM for each analyte were prepared. With linear least square regression based on $1/x^2$ weighting correlation coefficients ≥ 0.994 were achieved for all analytes indicating linearity for the covered concentration range (Tab. 2.1). The highest calibration level was set as upper limit of quantification (ULOQ), however does not represent the end of the linear detector response. Taking the low physiological concentration of IsoP and IsoF into account the calibration of higher concentrations as carried out in other methods [30-33] was for the intended application not necessary.

2.3.4 Extraction efficiency

The extraction efficiency from biological samples was characterized based on the recovery of IS spiked to the sample prior extraction. For the evaluation of the extraction efficiency of the used sample preparation procedure different volumes (200 µL, 500 µL, 1000 µL) of plasma from healthy volunteers were extracted by SPE. As shown in Fig. 2.7, recoveries in the range of 80–100% for all IS regardless of the used plasma volume indicate a sufficient extraction for quantitative determination.

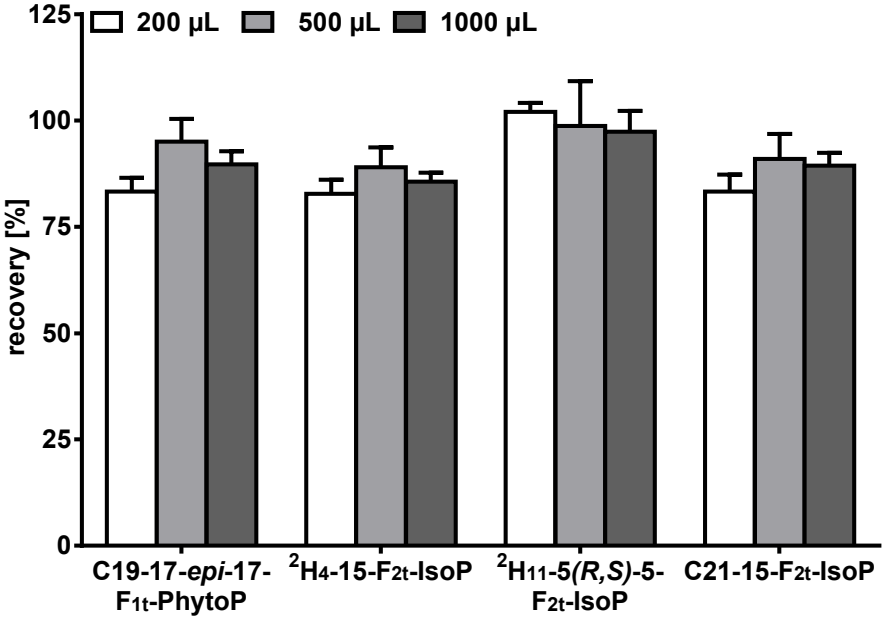

Fig. 2.7: Recovery of internal standards added to 200 µL, 500 µL and 1000 µL human plasma at the beginning of sample preparation followed by protein precipitation with MeOH and solid phase extraction. Shown are mean ± SD (n = 4).

Regarding all IsoP and IsoF covered by the method, no IsoF and only ARA derived F_{2t}-IsoP were detected in the analyzed human plasma from healthy subjects. The most abundant regioisomer was 5(*R,S*)-5-F_{2t}-IsoP with comparable concentration for all investigated volumes (128 ± 13 pM, 138 ± 6 pM and 132 ± 6 pM for 200 µL, 500 µL and 1000 µL, respectively) indicating a good accuracy and precision regardless of the amount of sample/matrix injected. For 15-F_{2t}-IsoP, which is the most studied regioisomer, lower levels were detected (48 ± 1 pM and 38 ± 1 pM for 500 µL and 1000 µL, respectively). This is consistent with previous findings reporting concentrations for 15(*R,S*)-15-F_{2t}-IsoP in the range of 16–48 pg/mL (45–135 pM) [19] and 3–25 pg/mL (8–71 pM) [53] in human plasma of healthy subjects.

2.3.5 Intra- and interday accuracy and precision

Intra- and interday accuracy and precision were characterized oriented on the guideline on bioanalytical method validation of the European Medicines Agency. In order to evaluate the accuracy and precision of the analytical procedure, human plasma samples spiked at four concentration levels prior extraction were analyzed in four replicates. The intraday accuracy ranged for all analytes from 77 to 121% indicating low interference of plasma matrix and good extraction efficiency of the analytes using the presented SPE procedure. Intraday precision calculated as RSD was < 15% for almost all analytes at all spiking levels with few exceptions being, however, below 22% (Tab. 2.2). Interday precision was better, below 11% for 10, 30 and 100 nM spiking levels, thus indicating a stable method which allows the analysis of large sample batches. However, at the low concentration level (3 nM), which is close to LLOQ, RSDs showed a trend towards higher values, but were still < 22% for almost all analytes, except 7(*R,S*)-ST-Δ^8-11-dihomo-IsoF (LLOQ of 2 nM, RSD = 32%, Tab. 2.2).

Tab. 2.2: Intra- and interday accuracy (acc.) as well as precision (prec.) of the extraction of all IsoP and IsoF comprised by the method from human plasma (500 µL). For the determination of accuracy and precision, IsoP and IsoF were spiked in four concentration levels to the plasma samples (3, 10, 30, 100 nM) at the beginning of the sample preparation. Accuracy was determined from the calculated concentration following SPE in comparison to the spiking standard solution and precision was calculated as relative standard deviation of the sample sets (n = 4 for intra- and n = 3 for interday). *) For IsoP and IsoF which were available as isomeric mixtures, the spiking level correspond to the sum concentration of both isomers in the mixture and individual spiking level were calculated based on the isomeric ratio of the substances.

	Analyte	conc [nM]	INTRADAY acc.[%]	INTRADAY prec.[%]	INTERDAY acc.[%]	INTERDAY prec.[%]
ALA	*ent*-9-F_{1t}-PhytoP	3	103	6	111	4
		10	96	4	98	6
		30	96	3	96	2
		100	99	7	93	1
	ent-9-*epi*-9-F_{1t}-PhytoP	3	98	8	109	2
		10	93	2	85	7
		30	93	4	91	4
		100	94	3	87	2
	ent-16-*epi*-16-F_{1t}-PhytoP	3	112	6	115	9
		10	99	2	100	4
		30	98	3	102	2
		100	100	6	96	5

	Analyte	conc [nM]	INTRADAY acc.[%]	INTRADAY prec.[%]	INTERDAY acc.[%]	INTERDAY prec.[%]
	ent-16-F_{1t}-PhytoP	3	121	4	125	2
		10	99	2	99	4
		30	96	4	101	3
		100	100	6	96	8
	9-L_1-PhytoP	3	99	13	93	1
		10	98	10	91	3
		30	103	18	124	1
		100	95	6	94	5
	16-B_1-PhytoP	3	101	13	127	8
		10	102	10	100	3
		30	108	16	133	1
		100	100	5	99	1
	ent-16(*R,S*)-13-*epi*-ST-Δ^{14}-9-PhytoF 1 ***)**	1.4	89	9	94	4
		4.7	89	6	88	3
		14	91	2	92	1
		47	93	6	86	1
	ent-16(*R,S*)-13-*epi*-ST-Δ^{14}-9-PhytoF 2 ***)**	1.6	104	6	100	4
		5.3	91	2	92	4
		16	94	4	97	2
		53	97	7	93	5
ARA	5(*R,S*)-5-F_{2t}-IsoP	3	91	4	91	4
		10	84	6	81	3
		30	82	3	78	4
		100	87	8	83	3
	15-F_{2t}-IsoP (8-*iso*-$PGF_{2\alpha}$)	3	102	4	108	7
		10	94	1	94	3
		30	101	6	93	2
		100	97	7	95	0
	15(*R,S*)-2,3-dinor-15-F_{2t}-IsoP	3	88	4	101	7
		10	89	7	93	2
		30	87	7	80	2
		100	96	7	90	3
EPA	5(*R,S*)-5-F_{3t}-IsoP	3	110	11	150	2
		10	104	3	102	7
		30	96	6	92	2
		100	103	5	89	0
	8-F_{3t}-IsoP	3	103	5	97	3
		10	97	3	94	4
		30	96	4	94	3
		100	99	8	93	3
	8-*epi*-8-F_{3t}-IsoP	3	98	5	107	1
		10	91	3	96	3
		30	88	4	86	2
		100	95	5	91	4
DHA	4(*R,S*)-4-F_{4t}-NeuroP	3	92	16	114	5
		10	83	7	98	3
		30	85	16	74	9
		100	95	15	84	3
	10-F_{4t}-NeuroP	3	113	4	124	3
		10	109	2	112	3
		30	119	8	108	2
		100	113	12	103	1

	Analyte	conc [nM]	INTRADAY acc.[%]	INTRADAY prec.[%]	INTERDAY acc.[%]	INTERDAY prec.[%]
	10-*epi*-10-F_{4t}-NeuroP	3	105	9	118	12
		10	99	5	100	2
		30	106	10	87	3
		100	102	10	97	4
	14(*R,S*)-14-F_{4t}-NeuroP	3	< LLOQ		< LLOQ	
		10	< LLOQ		< LLOQ	
		30	103	5	100	12
		100	101	7	97	17
	4(*R,S*)-ST-Δ^5-8-NeuroF	3	< LLOQ		< LLOQ	
		10	< LLOQ		< LLOQ	
		30	< LLOQ		< LLOQ	
		100	93	22	78	6
AdA	*ent*-7(*R,S*)-7-F_{2t}-dihomo-IsoP	3	95	12	105	3
		10	80	7	103	4
		30	92	9	91	6
		100	96	13	90	8
	17(*R,S*)-17-F_{2t}-dihomo-IsoP 1 *)	1.9	100	10	119	19
		6.3	100	7	116	2
		19	98	4	100	6
		63	102	12	94	6
	17(*R,S*)-17-F_{2t}-dihomo-IsoP 2 *)	1.1	106	14	65	15
		3.7	77	5	97	21
		11	85	15	77	8
		37	97	14	89	7
	7(*R,S*)-ST-Δ^8-11-dihomo-IsoF	3	93	13	92	32
		10	97	10	104	11
		30	99	9	101	2
		100	100	12	96	7
	17(*R,S*)-10-*epi*-SC-Δ^{15}-11-dihomo-IsoF 1 *)	1.6	109	7	90	15
		5.2	93	7	103	2
		16	107	9	122	8
		52	105	8	97	9
	17(*R,S*)-10-*epi*-SC-Δ^{15}-11-dihomo-IsoF 2 *)	1.4	96	6	96	13
		4.8	96	6	108	1
		14	103	11	124	10
		48	101	9	97	10
n6-DPA	4(*R,S*)-4-F_{3t}-$NeuroP_{n6}$	3	93	11	105	22
		10	77	13	94	1
		30	78	22	63	9
		100	84	17	79	11

2.3.6 Formation of IsoP in cell culture

The developed method was applied to investigate the formation of IsoP and IsoF in HCT-116 cells during oxidative stress caused by *t*-BOOH. First, the viability of HCT-116 cells treated with increasing doses of *t*-BOOH for 2 h was

determined with the MTS assay, revealing no effects at a dose of 50 µM and a moderate reduction of the viability to 84% in cells incubated with 200 µM *t*-BOOH (appendix Fig. 8.6 A). Following incubation a large number of IsoP were detected in the cells, i.e. 5(*R,S*)-5-F_{2t}-IsoP, 15-F_{2t}-IsoP, *ent*-7(*R,S*)-7-F_{2t}-dihomo-IsoP, 17(*R,S*)-17-F_{2t}-dihomo-IsoP 2, 5(*R,S*)-5-F_{3t}-IsoP, 4(*R,S*)-4-F_{4t}-NeuroP, 10-F_{4t}-NeuroP, 10-*epi*-10-F_{4t}-IsoP (Tab. 2.3, Fig. 2.8). In control incubations the levels of the detected IsoP were low or below the LLOQ (Tab. 2.3, Fig. 2.8), with EPA derived 5(*R,S*)-5-F_{3t}-IsoP being most abundant.

Tab. 2.3: Total (i.e. free and esterified) concentrations of IsoP in HCT-116 cells following incubation with 50 µM and 200 µM *t*-butyl hydroperoxide for 30 min, 1 h and 2 h. Shown are the mean ± SD (n = 3). For analytes below the limit of quantification the LLOQ is given.

	analyte [fmol/10^6 cells]	**incubation time**	**control**	**50 µM**	**200 µM**
			Mean ± SD	**Mean ± SD**	**Mean ± SD**
ARA	5(*R,S*)-5-F_{2t}-IsoP	30 min	12 ± 3	47 ± 5	123 ± 16
		1h	11 ± 2	47 ± 8	165 ± 19
		2 h	15 ± 7	43 ± 13	232 ± 115
	15-F_{2t}-IsoP (8-*iso*-$PGF_{2\alpha}$)	30 min	< 5.0	15 ± 2	34 ± 3
		1h	< 5.0	14 ± 2	44 ± 2
		2 h	< 5.0	12 ± 3	54 ± 25
EPA	5(*R,S*)-5-F_{3t}-IsoP	30 min	40 ± 11	167 ± 39	424 ± 17
		1h	39 ± 4	155 ± 30	625 ± 113
		2 h	44 ± 19	133 ± 46	737 ± 300
DHA	4(*R,S*)-4-F_{4t}-NeuroP	30 min	5.4 ± 0.6	26 ± 5	69 ± 6
		1h	5.9 ± 1.4	24 ± 5	89 ± 13
		2 h	6.7 ± 2.2	22 ± 3	105 ± 48
	10-F_{4t}-NeuroP	30 min	< 2.5	< 2.5	5.8 ± 0.6
		1h	< 2.5	< 2.5	7.1 ± 0.8
		2 h	< 2.5	< 2.5	8.9 ± 4.2
	10-*epi*-10-F_{4t}-NeuroP	30 min	< 5.0	5.9 ± 0.4	13 ± 2
		1h	< 5.0	5.4 ± 0.7	16 ± 2
		2 h	< 5.0	5.7 ± 0.9	20 ± 9
AdA	*ent*-7(*R,S*)-7-F_{2t}-dihomo-IsoP	30 min	< 2.5	3.8 ± 0.2	8.6 ± 1.0
		1h	< 2.5	3.6 ± 0.6	14 ± 3
		2 h	< 2.5	3.7 ± 0.9	18 ± 10
	17(*R,S*)-17-F_{2t}-dihomo-IsoP 2	30 min	< 3.7	< 3.7	4.0 ± 0.4
		1h	< 3.7	< 3.7	4.7 ± 1.4
		2 h	< 3.7	< 3.7	4.6 ± 1.0

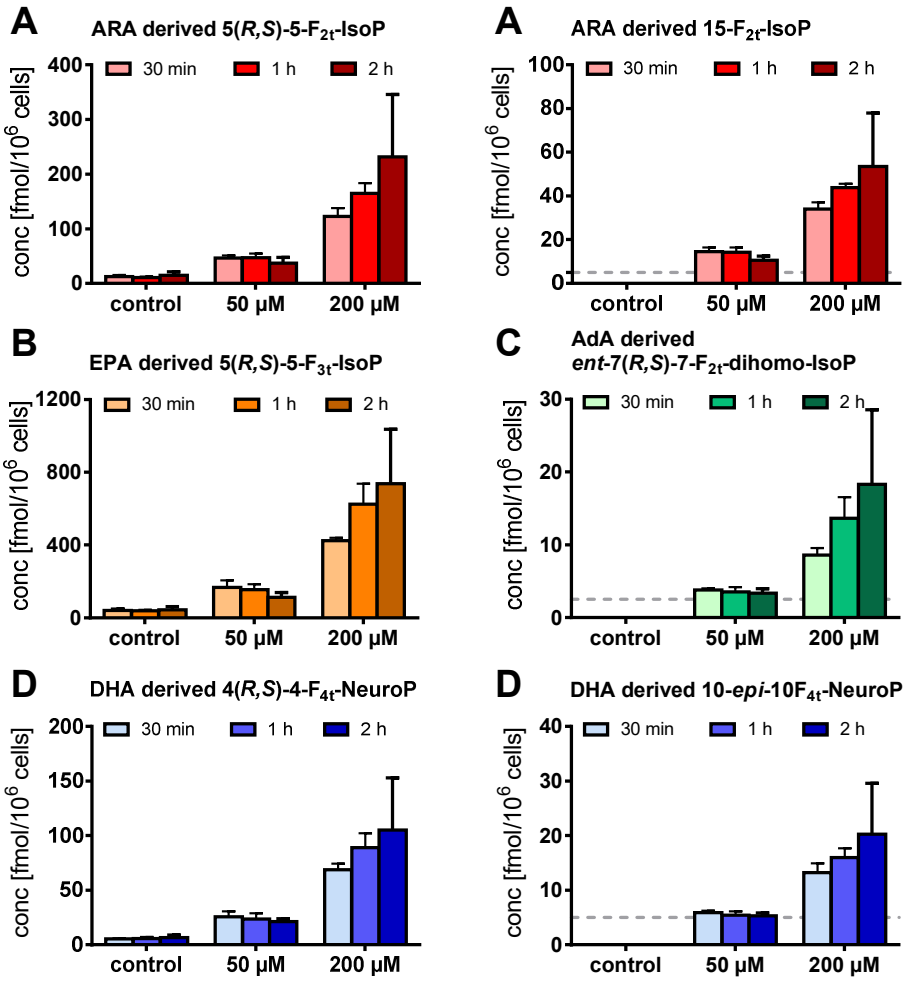

Fig. 2.8: Application of the method on the analysis of HTC-116 cells. IsoP were quantified following incubation with 50 µM and 200 µM *t*-butyl hydroperoxide for 30 min, 1 h and 2 h. Shown are representative IsoP derived from **(A)** ARA, **(B)** EPA, **(C)** AdA, **(D)** DHA. All results are shown as mean ± SD (n = 3) and the grey dashed line indicates the lower limit of quantification (LLOQ).

Regarding distribution of the different IsoP, a dominant formation of regioisomers carrying the side chain hydroxyl group in proximity to the carboxy terminus was observed for the IsoP formed from all different PUFA: 5(*R,S*)-5-F_{2t}-IsoP, 5(*R,S*)-5-F_{3t}-IsoP, *ent*-7(*R,S*)-7-F_{2t}-dihomo-IsoP and 4(*R,S*)-4-F_{4t}-NeuroP. At high concentrations of *t*-BOOH also other regiosomers were formed and the IsoP concentration increased dose dependently with the *t*-BOOH concentration. IsoP levels after 30 min with 200 µM were generally higher than after 2 h of incubation with 50 µM *t*-BOOH. Moreover, with 200 µM *t*-BOOH, even if not statistically significant, a trend towards higher levels of IsoP with

increasing incubation time was observed while in incubations with 50 µM *t*-BOOH similar concentrations of IsoP were found for the different time points. This may indicate a cellular defense mechanism against ROS and thus IsoP levels do not further increase. It is also remarkable that with higher *t*-BOOH concentration the regioisomers with the side chain hydroxyl group in proximity to the carboxy terminus were stronger elevated than other regiosomers (Tab. 2.3, Fig. 2.8), which may indicate not only differences in formation but also in the metabolism rates of the different regioisomers. This becomes particularly evident for the ARA derived IsoP. Here, 3–4-fold higher levels of 5(*R,S*)-5-F_{2t}-IsoP were found compared to 15-F_{2t}-IsoP while in livers of CCl_4 exposed rats a ratio of 1.5:1 was found [12]. However, it should be noted that these differences might also indicate species specific formation and metabolism rates of different regioisomers. The metabolism of the F_2-IsoP, particularly 15-F_{2t}-IsoP has been well described [54, 55]. By contrast, the metabolism of the NeuroP is yet not well understood, except an earlier investigation reported by Lawson *et al.* who showed that 7-F_{4t}-NeuroP is readily beta-oxidized to 5-F_{3t}-IsoP (an isoprostanoid metabolite from EPA oxidation) and excreted [56] whereas certain NeuroP like 4-F_{4t}-NeuroP are probably more stable due to the presence of the side chain hydroxyl group at C4, which can limit access of the enzymes involved in beta-oxidation as it is the case for 5-hydroxy eicosanoids [57].

These results indicate that either the cellular formation is cell specific or the products are metabolized at different rates. The cellular formation of IsoP in response to oxidative stress and especially the resulting IsoP pattern warrants further investigation. In particular, application of different cell types and cell lines, e.g. deficient in different ROS defense mechanisms, should be used to understand the intracellular formation and the metabolic fate of IsoP. This investigation will allow gaining more insights into the role of IsoP in biology and help to identify specific biomarkers for distinct physiological states. With the developed method described herein, we provide the ideal tool to comprehensively quantify IsoP derived from all biologically relevant PUFA.

2.4 References

1. Weidinger A. and Kozlov A. (2015) Biological activities of reactive oxygen and nitrogen species: Oxidative stress versus signal transduction. *Biomolecules*. 5(2), pp. 472-484; doi: 10.3390/biom5020472.
2. Sies H. (1985) 1 - Oxidative Stress: Introductory Remarks. In: *Oxidative Stress*. H. Sies (ed.), Academic Press, London, pp. 1-8; doi: 10.1016/B978-0-12-642760-8.50005-3.
3. Jones D. P. and Sies H. (2015) The redox code. *Antioxid Redox Signal*. 23(9), pp. 734-746; doi: 10.1089/ars.2015.6247.
4. Sies H. (1986) Biochemistry of oxidative stress. *Angew Chem Int Ed Engl*. 25(12), pp. 1058-1071; doi: 10.1002/anie.198610581.
5. Stark G. (2005) Functional consequences of oxidative membrane damage. *J Membr Biol*. 205(1), pp. 1-16; doi: 10.1007/s00232-005-0753-8.
6. Yin H., Xu L. and Porter N. A. (2011) Free radical lipid peroxidation: Mechanisms and analysis. *Chem Rev*. 111(10), pp. 5944-5972; doi: 10.1021/cr200084z.
7. Giustarini D., Dalle-Donne I., Tsikas D. and Rossi R. (2009) Oxidative stress and human diseases: Origin, link, measurement, mechanisms, and biomarkers. *Crit Rev Clin Lab Sci*. 46(5-6), pp. 241-281; doi: 10.3109/10408360903142326.
8. Kadiiska M. B., Gladen B. C., Baird D. D., Germolec D., Graham L. B., Parker C. E., Nyska A., Wachsman J. T., Ames B. N., Basu S., Brot N., Fitzgerald G. A., Floyd R. A., George M., Heinecke J. W., Hatch G. E., Hensley K., Lawson J. A., Marnett L. J., Morrow J. D., Murray D. M., Plastaras J., Roberts II L. J., Rokach J., Shigenaga M. K., Sohal R. S., Sun J., Tice R. R., Van Thiel D. H., Wellner D., Walter P. B., Tomer K. B., Mason R. P. and Barrett J. C. (2005) Biomarkers of oxidative stress study II. Are oxidation products of lipids, proteins, and DNA markers of CCl4 poisoning? *Free Radic Biol Med*. 38(6), pp. 698-710; doi: 10.1016/j.freeradbiomed.2004.09.017.
9. Morrow J. D., Awad J. A., Boss H. J., Blair I. A. and Roberts II L. J. (1992) Non-cyclooxygenase-derived prostanoids (F2-isoprostanes) are formed in situ on phospholipids. *Proc Natl Acad Sci U S A*. 89(22), pp. 10721-10725; doi: 10.1073/pnas.89.22.10721.
10. Morrow J. D., Roberts II L. J., Daniel V. C., Awad J. A., Mirochnitchenko O., Swift L. L. and Burk R. F. (1998) Comparison of formation of D2/E2-isoprostanes and F2-isoprostanes in vitro and in vivo - Effects of oxygen tension and glutathione. *Arch Biochem Biophys*. 353(1), pp. 160-171; doi: 10.1006/abbi.1998.0645.
11. Waugh R. J. and Murphy R. C. (1996) Mass spectrometric analysis of four regioisomers of F2-isoprostanes formed by free radical oxidation of arachidonic acid. *J Am Soc Mass Spectrom*. 7(5), pp. 490-499; doi: 10.1016/1044-0305(95)00709-1.
12. Waugh R. J., Morrow J. D., Roberts II L. J. and Murphy R. C. (1997) Identification and relative quantitation of F2-isoprostane regioisomers formed in vivo in the rat. *Free Radic Biol Med*. 23(6), pp. 943-954; doi: 10.1016/S0891-5849(97)00133-0.
13. Fessel J. P., Porter N. A., Moore K. P., Sheller J. R. and Roberts II L. J. (2002) Discovery of lipid peroxidation products formed in vivo with a substituted tetrahydrofuran ring (isofurans) that are favored by increased oxygen tension. *Proc Natl Acad Sci U S A*. 99(26), pp. 16713-16718; doi: 10.1073/pnas.252649099.
14. Cuyamendous C., Leung K. S., Durand T., Lee J. C.-Y., Oger C. and Galano J. M. (2015) Synthesis and discovery of phytofurans: Metabolites of α-linolenic acid peroxidation. *Chem Commun (Camb)*. 51(86), pp. 15696-15699; doi: 10.1039/c5cc05736a.

15. Cuyamendous C., Leung K. S., Bultel-Poncé V., Guy A., Durand T., Galano J.-M., Lee J. C.-Y. and Oger C. (2017) Total synthesis and in vivo quantitation of phytofurans derived from α-linolenic acid. *Eur J Org Chem*. 2017(17), pp. 2486-2490; doi: 10.1002/ejoc.201700270.
16. Skinner E. R., Watt C., Besson J. A. and Best P. V. (1993) Differences in the fatty acid composition of the grey and white matter of different regions of the brains of patients with Alzheimer's disease and control subjects. *Brain*. 116(3), pp. 717-725; doi: 10.1093/brain/116.3.717.
17. VanRollins M., Woltjer R. L., Yin H., Morrow J. D. and Montine T. J. (2008) F2-Dihomo-isoprostanes arise from free radical attack on adrenic acid. *J Lipid Res*. 49(5), pp. 995-1005; doi: 10.1194/jlr.M700503-JLR200.
18. Schweer H., Watzer B., Seyberth H. W. and Nüsing R. M. (1997) Improved quantification of 8-epi-prostaglandin F2α and F2-isoprostanes by gas chromatography/triple-stage quadrupole mass spectrometry: Partial cyclooxygenase-dependent formation of 8-epi-prostaglandin F2α in humans. *J Mass Spectrom*. 32(12), pp. 1362-1370; doi: 10.1002/(SICI)1096-9888(199712)32:12<1362::AID-JMS606>3.0.CO;2-N.
19. Signorini C., Comporti M. and Giorgi G. (2003) Ion trap tandem mass spectrometric determination of F2-isoprostanes. *J Mass Spectrom*. 38(10), pp. 1067-1074; doi: 10.1002/jms.520.
20. Musiek E. S., Cha J. K., Yin H., Zackert W. E., Terry E. S., Porter N. A., Montine T. J. and Morrow J. D. (2004) Quantification of F-ring isoprostane-like compounds (F4-neuroprostanes) derived from docosahexaenoic acid in vivo in humans by a stable isotope dilution mass spectrometric assay. *J Chromatogr B Analyt Technol Biomed Life Sci*. 799(1), pp. 95-102; doi: 10.1016/j.jchromb.2003.10.036.
21. Lee J. C.-Y., Jenner A. M. and Halliwell B. (2004) Rapid preparation of human urine and plasma samples for analysis of F2-isoprostanes by gas chromatography-mass spectrometry. *Biochem Biophys Res Commun*. 320(3), pp. 696-702; doi: 10.1016/j.bbrc.2004.06.015.
22. Lee J. C.-Y., Huang S. H., Jenner A. M. and Halliwell B. (2008) Measurement of F2-isoprostanes, hydroxyeicosatetraenoic products, and oxysterols from a single plasma sample. *Free Radic Biol Med*. 44(7), pp. 1314-1322; doi: 10.1016/j.freeradbiomed.2007.12.026.
23. Signorini C., Ciccoli L., Leoncini S., Carloni S., Perrone S., Comporti M., Balduini W. and Buonocore G. (2009) Free iron, total F2-isoprostanes and total F4-neuroprostanes in a model of neonatal hypoxic-ischemic encephalopathy: Neuroprotective effect of melatonin. *J Pineal Res*. 46(2), pp. 148-154; doi: 10.1111/j.1600-079X.2008.00639.x.
24. Milne G. L., Gao B., Terry E. S., Zackert W. E. and Sanchez S. C. (2013) Measurement of F2-isoprostanes and isofurans using gas chromatography–mass spectrometry. *Free Radic Biol Med*. 59, pp. 36-44; doi: 10.1016/j.freeradbiomed.2012.09.030.
25. Briskey D. R., Wilson G. R., Fassett R. G. and Coombes J. S. (2014) Optimized method for quantification of total F2-isoprostanes using gas chromatography–tandem mass spectrometry. *J Pharm Biomed Anal*. 90, pp. 161-166; doi: 10.1016/j.jpba.2013.11.028.
26. Yan W., Byrd G. D. and Ogden M. W. (2007) Quantitation of isoprostane isomers in human urine from smokers and nonsmokers by LC-MS/MS. *J Lipid Res*. 48(7), pp. 1607-1617; doi: 10.1194/jlr.M700097-JLR200.
27. Medina S., Dominguez-Perles R., Gil J. I., Ferreres F., Garcia-Viguera C., Martinez-Sanz J. M. and Gil-Izquierdo A. (2012) A ultra-pressure liquid chromatography/triple quadrupole tandem mass spectrometry method for the analysis of 13 eicosanoids in

human urine and quantitative 24 hour values in healthy volunteers in a controlled constant diet. *Rapid Commun Mass Spectrom*. 26(10), pp. 1249-1257; doi: 10.1002/rcm.6224.

28. Prasain J. K., Arabshahi A., Taub P. R., Sweeney S., Moore R., Sharer J. D. and Barnes S. (2013) Simultaneous quantification of F2-isoprostanes and prostaglandins in human urine by liquid chromatography tandem-mass spectrometry. *J Chromatogr B Analyt Technol Biomed Life Sci*. 913–914, pp. 161-168; doi: 10.1016/j.jchromb.2012.12.009.
29. Larose J., Julien P. and Bilodeau J. F. (2013) Analysis of F2-isoprostanes in plasma of pregnant women by HPLC-MS/MS using a column packed with core-shell particles. *J Lipid Res*. 54(5), pp. 1505-1511; doi: 10.1194/jlr.D034553.
30. Medina S., Miguel-Elizaga I. D., Oger C., Galano J. M., Durand T., Martinez-Villanueva M., Castillo M. L., Villegas-Martinez I., Ferreres F., Martinez-Hernandez P. and Gil-Izquierdo A. (2015) Dihomo-isoprostanes - nonenzymatic metabolites of AdA - are higher in epileptic patients compared to healthy individuals by a new ultrahigh pressure liquid chromatography-triple quadrupole-tandem mass spectrometry method. *Free Radic Biol Med*. 79, pp. 154-163; doi: 10.1016/j.freeradbiomed.2014.11.005.
31. Collado-Gonzalez J., Medina S., Durand T., Guy A., Galano J. M., Torrecillas A., Ferreres F. and Gil-Izquierdo A. (2015) New UHPLC-QqQ-MS/MS method for quantitative and qualitative determination of free phytoprostanes in foodstuffs of commercial olive and sunflower oils. *Food Chem*. 178, pp. 212-220; doi: 10.1016/j.foodchem.2015.01.097.
32. Chafer-Pericas C., Rahkonen L., Sanchez-Illana A., Kuligowski J., Torres-Cuevas I., Cernada M., Cubells E., Nunez-Ramiro A., Andersson S., Vento M. and Escobar J. (2015) Ultra high performance liquid chromatography coupled to tandem mass spectrometry determination of lipid peroxidation biomarkers in newborn serum samples. *Anal Chim Acta*. 886, pp. 214-220; doi: 10.1016/j.aca.2015.06.028.
33. Dupuy A., Le Faouder P., Vigor C., Oger C., Galano J. M., Dray C., Lee J. C.-Y., Valet P., Gladine C., Durand T. and Bertrand-Michel J. (2016) Simultaneous quantitative profiling of 20 isoprostanoids from omega-3 and omega-6 polyunsaturated fatty acids by LC-MS/MS in various biological samples. *Anal Chim Acta*. 921, pp. 46-58; doi: 10.1016/j.aca.2016.03.024.
34. Yonny M. E., Rodríguez Torresi A., Cuyamendous C., Réversat G., Oger C., Galano J.-M., Durand T., Vigor C. and Nazareno M. A. (2016) Thermal stress in melon plants: Phytoprostanes and phytofurans as oxidative stress biomarkers and the effect of antioxidant supplementation. *J Agric Food Chem*. 64(44), pp. 8296-8304; doi: 10.1021/acs.jafc.6b03011.
35. Wang Z., Ciabattoni G., Creminon C., Lawson J., Fitzgerald G. A., Patrono C. and Maclouf J. (1995) Immunological characterization of urinary 8-epi-prostaglandin F2α excretion in man. *J Pharmacol Exp Ther*. 275(1), pp. 94-100.
36. Basu S. (1998) Radioimmunoassay of 8-iso-prostaglandin F2α: An index for oxidative injury via free radical catalysed lipid peroxidation. *Prostaglandins Leukot Essent Fatty Acids*. 58(4), pp. 319-325; doi: 10.1016/S0952-3278(98)90042-4.
37. Il'yasova D., Morrow J. D., Ivanova A. and Wagenknecht L. E. (2004) Epidemiological marker for oxidant status: Comparison of the ELISA and the gas chromatography/mass spectrometry assay for urine 2,3-dinor-5,6-dihydro-15-F2t-isoprostane. *Ann Epidemiol*. 14(10), pp. 793-797; doi: 10.1016/j.annepidem.2004.03.003.
38. Klawitter J., Haschke M., Shokati T., Klawitter J. and Christians U. (2011) Quantification of 15-F2t-isoprostane in human plasma and urine: Results from enzyme-linked immunoassay and liquid chromatography/tandem mass spectrometry

cannot be compared. *Rapid Commun Mass Spectrom*. 25(4), pp. 463-468; doi: 10.1002/rcm.4871.

39. Labuschagne C. F., Stigter E. C., Hendriks M. M., Berger R., Rokach J., Korswagen H. C. and Brenkman A. B. (2013) Quantification of in vivo oxidative damage in Caenorhabditis elegans during aging by endogenous F3-isoprostane measurement. *Aging Cell*. 12(2), pp. 214-223; doi: 10.1111/acel.12043.
40. Aszyk J., Kot J., Tkachenko Y., Woźniak M., Bogucka-Kocka A. and Kot-Wasik A. (2017) Novel liquid chromatography method based on linear weighted regression for the fast determination of isoprostane isomers in plasma samples using sensitive tandem mass spectrometry detection. *J Chromatogr B Analyt Technol Biomed Life Sci*. 1051, pp. 17-23; doi: 10.1016/j.jchromb.2017.02.021.
41. Chung M. L. S., Lee K. Y. E. and Lee C.-Y. J. (2013) Profiling of oxidized lipid products of marine fish under acute oxidative stress. *Food Chem Toxicol*. 53, pp. 205-213; doi: 10.1016/j.fct.2012.11.047.
42. Oger C., Brinkmann Y., Bouazzaoui S., Durand T. and Galano J. M. (2008) Stereocontrolled access to isoprostanes via a bicyclo[3.3.0]octene framework. *Org Lett*. 10(21), pp. 5087-5090; doi: 10.1021/ol802104z.
43. de la Torre A., Lee Y. Y., Oger C., Sangild P. T., Durand T., Lee J. C.-Y. and Galano J.-M. (2014) Synthesis, discovery, and quantitation of dihomo-isofurans: Biomarkers for in vivo adrenic acid peroxidation. *Angew Chem Int Ed Engl*. 53(24), pp. 6249-6252; doi: 10.1002/anie.201402440.
44. Mimmler M., Peter S., Kraus A., Stroh S., Nikolova T., Seiwert N., Hasselwander S., Neitzel C., Haub J., Monien B. H., Nicken P., Steinberg P., Shay J. W., Kaina B. and Fahrer J. (2016) DNA damage response curtails detrimental replication stress and chromosomal instability induced by the dietary carcinogen PhIP. *Nucleic Acids Res*. 44(21), pp. 10259-10276; doi: 10.1093/nar/gkw791.
45. Ostermann A. I., Willenberg I. and Schebb N. H. (2015) Comparison of sample preparation methods for the quantitative analysis of eicosanoids and other oxylipins in plasma by means of LC-MS/MS. *Anal Bioanal Chem*. 407(5), pp. 1403-1414; doi: 10.1007/s00216-014-8377-4.
46. Hwang S. H., Tsai H.-J., Liu J.-Y., Morisseau C. and Hammock B. D. (2007) Orally bioavailable potent soluble epoxide hydrolase inhibitors. *J Med Chem*. 50(16), pp. 3825-3840; doi: 10.1021/jm070270t.
47. European Medicines Agency (2011) Guideline on bioanalytical method validation. EMEA/CHMP/EWP/192217/2009 Rev. 1 Corr. 2**. Commitee for Medicinal Products for Human Use (CHMP), 21 July 2011.
48. Willenberg I., Meschede A. K., Gueler F., Jang M. S., Shushakova N. and Schebb N. H. (2015) Food polyphenols fail to cause a biologically relevant reduction of COX-2 activity. *PLoS One*. 10(10):e0139147; doi: 10.1371/journal.pone.0139147.
49. Willenberg I., Rund K., Rong S., Shushakova N., Gueler F. and Schebb N. H. (2016) Characterization of changes in plasma and tissue oxylipin levels in LPS and CLP induced murine sepsis. *Inflamm Res*. 65(2), pp. 133-142; doi: 10.1007/s00011-015-0897-7.
50. Murphy R. C., Barkley R. M., Zemski Berry K., Hankin J., Harrison K., Johnson C., Krank J., McAnoy A., Uhlson C. and Zarini S. (2005) Electrospray ionization and tandem mass spectrometry of eicosanoids. *Anal Biochem*. 346(1), pp. 1-42; doi: 10.1016/j.ab.2005.04.042.
51. de la Torre A., Lee Y. Y., Mazzoni A., Guy A., Bultel-Poncé V., Durand T., Oger C., Lee J. C.-Y. and Galano J.-M. (2015) Total syntheses and in vivo quantitation of novel neurofuran and dihomo-isofuran derived from docosahexaenoic acid and adrenic acid. *Chemistry*. 21(6), pp. 2442-2446; doi: 10.1002/chem.201405497.

52. Bastani N. E., Gundersen T. E. and Blomhoff R. (2009) Determination of 8-epi PGF2α concentrations as a biomarker of oxidative stress using triple-stage liquid chromatography/tandem mass spectrometry. *Rapid Commun Mass Spectrom*. 23(18), pp. 2885-2890; doi: 10.1002/rcm.4197.
53. Haschke M., Zhang Y. L., Kahle C., Klawitter J., Korecka M., Shaw L. M. and Christians U. (2007) HPLC-atmospheric pressure chemical ionization MS/MS for quantification of 15-F2t-isoprostane in human urine and plasma. *Clin Chem*. 53(3), pp. 489-497; doi: 10.1373/clinchem.2006.078972.
54. Chiabrando C., Valagussa A., Rivalta C., Durand T., Guy A., Zuccato E., Villa P., Rossi J.-C. and Fanelli R. (1999) Identification and measurement of endogenous β-oxidation metabolites of 8-epi-prostaglandin F2α. *J Biol Chem*. 274(3), pp. 1313-1319; doi: 10.1074/jbc.274.3.1313.
55. Roberts II L. J., Moore K. P., Zackert W. E., Oates J. A. and Morrow J. D. (1996) Identification of the major urinary metabolite of the F2-isoprostane 8-iso-prostaglandin F2α in humans. *J Biol Chem*. 271(34), pp. 20617-20620; doi: 10.1074/jbc.271.34.20617.
56. Lawson J. A., Kim S., Powell W. S., FitzGerald G. A. and Rokach J. (2006) Oxidized derivatives of ω-3 fatty acids: Identification of IPF3α-VI in human urine. *J Lipid Res*. 47(11), pp. 2515-2524; doi: 10.1194/jlr.M600327-JLR200.
57. Stene D. O. and Murphy R. C. (1988) Metabolism of leukotriene E4 in isolated rat hepatocytes - Identification of β-oxidation products of sulfidopeptide leukotrienes. *J Biol Chem*. 263(6), pp. 2773-2778.

Chapter 3

Clinical blood sampling for oxylipin analysis – Effect of storage and pneumatic tube transport of blood on free and total oxylipin profile in human plasma and serum*

Quantitative analysis of oxylipins is of increasing interest in clinical studies. Most commonly blood samples are analyzed to investigate (patho)physiological changes in the oxylipin pattern. However, storage after sampling and transport of blood might induce artificial changes in the apparent oxylipin profile due to ex-vivo formation/degradation by autoxidation or enzymatic activity.

In the present study we investigated the stability of free (i.e. non-esterified) and total oxylipins in EDTA-plasma and serum generated under clinical conditions assessing the influence of delays in blood processing and automated transportation:

Free cytochrome P450 monooxygenase and 5-lipoxygenase (LOX) formed oxylipins as well as autoxidation products were marginally affected by storage of whole blood up to 4 h at 4 °C, while total (i.e. sum of free and esterified) levels of these oxylipins were stable up to 24 h and following transport. Cyclooxygenase (COX) products (TxB_2, 12-HHT) and 12-LOX derived hydroxy-fatty acids were prone for storage and transport induced changes due to platelet activation. Total oxylipin patterns were generally more stable than the concentration of free oxylipins. In serum, coagulation induced higher levels of COX and 12-LOX products showing a high inter-individual variability.

Overall, our results indicate that total EDTA-plasma oxylipins are the most stable blood oxylipin marker for clinical samples. Here, storage of blood before further processing is acceptable for a period up to 24 hours at 4 °C. However, levels of platelet derived oxylipins should be interpreted with caution regarding potential ex-vivo formation.

* Preprint. Adapted from *Analyst*, 145, Rund K. M., Nolte F., Doricic J., Greite R., Schott S., Lichtinghagen R., Gueler F., Schebb N. H., Clinical blood sampling for oxylipin analysis – Effect of storage and pneumatic tube transport of blood on free and total oxylipin profile in human plasma and serum, pp. 2378-2388, (2020) – Published by The Royal Society of Chemistry. doi: 10.1039/C9AN01880H.

Author contributions: KR designed research, performed experiments and wrote the manuscript; FN performed experiments as student research assistant under the supervision of KR; JD, RG, SS, RL performed experiments; FG, NHS designed research and wrote the manuscript.

3.1 Introduction

Oxygenated polyunsaturated fatty acids (PUFA), i.e. eicosanoids and other oxylipins, are highly potent endogenous mediators of physiological and pathophysiological processes including regulation of endothelial function, blood pressure, thrombosis and inflammation [1-4].

Oxylipins are formed endogenously by conversion of PUFA within the arachidonic acid (ARA, C20:4 n6) cascade *via* three major enzymatic pathways as well as non-enzymatic autoxidation leading to a multitude of oxygenated products from different PUFA precursors: (I) Conversion by cyclooxygenases (COX) results in formation of prostanoids and thromboxanes; (II) lipoxygenases (LOX) convert PUFA to regio- and stereoselective hydroperoxy-PUFA which can be reduced to hydroxy-PUFA or further converted to leukotrienes or multiple hydroxylated PUFA; and (III) action of cytochrome P450 monooxygenases (CYP) leads to formation of hydroxylated PUFA and epoxy-PUFA whereby the latter can be further hydrolyzed to vicinal dihydroxy-PUFA by soluble epoxide hydrolases [1, 5, 6]. Besides regio- and stereoselective conversion by these enzymes, non-enzymatic radical mediated autoxidation gives rise to structurally similar oxygenated products with diverse regio- and stereochemistry such as isoprostanoids (IsoP), hydroxy-PUFA and epoxy-PUFA which also possess biological activity [7-10].

Dysregulation of oxylipin formation is implicated among others in cardiovascular, immune or metabolic diseases [11, 12] and several pharmaceuticals act by modulating the oxylipin profile (e.g. non-steroidal anti-inflammatory drugs, anti-thrombotic drugs, the asthma drug zileuton) [13-15]. Considering the multitude and diversity of oxylipins as well as the different pathways involved in oxylipin formation the overall physiological effect might result rather from the general profile than from the levels of a single oxylipin [16, 17]. Therefore, comprehensive and reliable quantification of the oxylipin pattern may be valuable to evaluate the disease state or monitor the action of drugs.

For clinical diagnostics blood specimen, i.e. plasma or serum, are the most widely used biofluids reflecting the systemic condition of the donor. In blood, oxylipins occur in their free form, are associated with proteins, such as albumin [18, 19], however the major part (> 90%) – particularly hydroxy- and epoxy-PUFA as well as isoprostanoids – is esterified in cellular lipids (i.e. in blood cells) and in lipoproteins [20-22].

Endogenous factors, such as sex [23], age [24], physical exercise [25, 26], health status [27], intake of drugs [13, 15, 28] or diet [17, 29] as well as variation in expression or genetic polymorphisms in enzymes [30-33] impact the oxylipin profile of an individuum. Moreover exogenous, pre-analytical factors relevant during collection, processing and storage of samples until analysis affect the oxylipin pattern [5], thus complicating its reliable interpretation.

In hospitals clinical blood samples are usually collected on a ward or in the emergency unit and are afterwards transported from the phlebotomy site to the clinical chemistry laboratory *via* transport systems such as pneumatic tube system transport (PTS) where centrifugation and generation of plasma or serum takes place.

The oxylipin pattern and its information about the physiological status of the patient strongly depends upon the choice for serum or plasma during blood withdrawal. During serum generation the blood coagulation cascade is triggered which includes activation of platelets resulting in a massive increase of platelet derived oxylipins such as 12-LOX metabolites and thromboxanes [34, 35]. For plasma different anticoagulants during blood collection, such as EDTA, heparin or citrate are used. The type of anticoagulant affects the formation of oxylipins, particularly hydroxy-PUFA and platelet derived oxylipins (12-LOX and COX derived products) [34, 36]. Therefore, blood sampling, i.e. choice of the blood specimen, has to be carefully considered in clinical studies with respect to the analytes of interest, and standardized within studies.

Following blood withdrawal, temperature and transitory storage time as well as transport to the clinical chemistry laboratory such as pneumatic tube system transport (PTS), are relevant pre-analytical factors which are hard to control in a clinical setting. Few studies investigated the influence of duration and temperature during whole blood storage prior to further processing and revealed changes for some free, i.e. non-esterified oxylipins in the generated plasma especially after longer times (> 30 min) at elevated temperatures (room temperature, RT) [16, 34]. However, no data about the influence of typical sample handling in the clinic on the oxylipin pattern exists. This is especially necessary to evaluate the suitability and reliability of the oxylipin pattern in blood samples from clinical studies, as well as in samples collected from patients in emergency or intensive care units or from biobanks. Moreover, this data is an essential prerequisite to deduce the physiological role of a changed oxylipin pattern in clinical studies as well as its suitability as biomarker for disease.

In the present study we therefore investigated the impact of storage of blood samples after collection for different periods of time at 4 °C as well as the transfer from the ward to the clinical chemistry laboratory within a large hospital using PTS until the removal of cells (plasma or serum generation). For all conditions, levels of both, free and total oxylipins, i.e. after alkaline hydrolysis, were determined in EDTA-plasma and serum to evaluate if free or total oxylipins are more stable in plasma or serum. In order to deduce pathway specific effects a comprehensive set of oxylipins covering representative analytes derived from ARA, eicosapentaenoic acid (EPA) and docosahexaenoic acid (DHA) from COX, LOX, CYP as well as non-enzymatic conversion was analyzed.

3.2 Experimental

3.2.1 Chemicals

Oxylipin and deuterated oxylipin standards were purchased from Cayman Chemicals (local distributor: Biomol, Hamburg, Germany). LC-MS-grade methanol (MeOH), LC-MS-grade acetonitrile (ACN), LC-MS-grade isopropanol, and LC-MS-grade acetic acid were obtained from Fisher Scientific (Schwerte, Germany). Sodium acetate trihydrate, sodium hydrogen phosphate and *n*-hexane (HPLC grade) were obtained from Carl Roth (Karlsruhe, Germany) and potassium hydroxide (KOH, 85%) from Gruessing GmbH (Filsum, Germany). 2-(1-thienyl)ethyl 3,4-dihydroxybenzylidenecyanoacetate (2-TEDC) was obtained from Santa Cruz. Ethyl acetate, phenyl methyl sulfonyl fluoride (PMSF) and all other chemicals were purchased from Sigma Aldrich (Schnelldorf, Germany).

3.2.2 Blood sampling and pre-analytical procedures

Venous blood samples were collected from 6 individual volunteers (4 females and 2 males, 23–56 years) by venipuncture in EDTA-monovettes (Sarstedt, Nümbrecht, Germany) and serum monovettes (Sarstedt, Nümbrecht Germany). Blood was collected at 10 am and no dietary restrictions were given. Each individual had breakfast before the blood sampling.

From each individual plasma and serum samples were generated by centrifugation (20 min, 4 °C, 5000 rpm, Thermo Scientific, Heraeus, Multifuge 3SR+) at 4 time points as described below: immediate, after 4 hours at 4 °C, after 24 hours at 4 °C and after pneumatic tube system transport (PTS) from the hospital ward to the clinical chemistry laboratory. For basal levels (t0) one plasma and serum monovette from each individual was centrifuged about 15 min after blood sampling. The supernatant, i.e. plasma or serum, was transferred to a cryotube and stored at −80 °C until analysis. To investigate the

influence of storage on oxylipins, blood samples were maintained for about 30 min at room temperature reflecting the time blood sampling takes on a hospital ward. Afterwards monovettes from each individual were stored at 4 °C in the fridge for 4 hours or 24 hours until further processing to generate plasma or serum as described above. After 30 min of storage at room temperature an additional monovette was transferred by the PTS to the clinical chemistry laboratory where plasma and serum were generated in an analogous manner.

All procedures were conducted according to the guidelines laid down in the Declaration of Helsinki and approved by the ethic committee of the Hannover Medical School (MHH ethical approval 6895) and all volunteers gave their written informed consent.

3.2.3 Extraction and quantification of oxylipins

Free oxylipins as well as total, i.e. free and esterified oxylipins were extracted from individual plasma and serum samples using anion exchange Bond Elut Certify II SPE cartridges (200 mg, 3 mL, Agilent, Waldbronn, Germany) as described with modifications [37].

Analysis of free oxylipins was carried out as described [38]. In brief, to 500 µL plasma or serum 10 µL antioxidant solution (0.2 mg/mL BHT and EDTA, 100 µM of the cyclooxygenase inhibitor indomethacin, 100 µM of the soluble epoxide hydrolase inhibitor *trans*-4-[4-(3-adamantan-1-yl-ureido)-cyclohexyl-oxy]-benzoic acid (*t*-AUCB) in MeOH/water (50/50, *v/v*)), 10 µL of 250 mM protease inhibitor PMSF in isopropanol, 10 µL of 100 µM LOX inhibitor 2-TEDC in MeOH and 10 µL of an internal standard (IS) solution (containing 100 nM of $^{2}H_4$-6-keto-$PGF_{1\alpha}$, $^{2}H_4$-15-F_{2t}-IsoP, $^{2}H_{11}$-5(*R,S*)-5-F_{2t}-IsoP, $^{2}H_4$-PGE_2, $^{2}H_4$-PGD_2, $^{2}H_4$-TxB_2, $^{2}H_4$-LTB_4, $^{2}H_4$-9,10-DiHOME, $^{2}H_{11}$-14,15-DiHETrE, $^{2}H_4$-9-HODE, $^{2}H_8$-5-HETE, $^{2}H_8$-12-HETE, $^{2}H_6$-20-HETE, $^{2}H_4$-9(10)-EpOME, $^{2}H_{11}$-14(15)-EpETrE) were added. Samples were diluted with 1 mL 1 M sodium acetate (pH 6.0, water/MeOH 95/5, *v/v*) and loaded on the preconditioned SPE cartridge.

Total, i.e. free and esterified oxylipins were extracted from 100 µL plasma or serum as described with slight modifications [39]. After addition of 10 µL antioxidant solution and 10 µL IS solution, 400 µL isopropanol was added and samples were stored for 30 min at −80 °C for protein precipitation. After centrifugation the supernatant was hydrolyzed (300 µL 1.5 M KOH (75/25, MeOH/water, *v/v*), immediately neutralized with acetic acid, diluted with 2 mL sodium phosphate buffer (pH 5.5) and extracted by SPE.

The extracts were analyzed in scheduled selected reaction monitoring mode following negative electrospray ionization by LC-MS/MS (QTRAP, Sciex, Darmstadt, Germany) [37, 40]. In parallel to the samples aliquots of pooled human quality control plasma (QC) were extracted using the same sample preparation procedure for free (n = 6) and total oxylipins (n = 7), respectively.

3.2.4 Data analysis

Oxylipins were quantified based on the analyte to corresponding IS area ratio using external calibration with linear least square regression ($1/x^2$ weighting) as described [37].

In order to evaluate the influence of storage or transport of blood on oxylipin levels in plasma and serum %differences *vs* t0 (immediate sample processing) were calculated for each time point (tx) for each individual using the following formula: $100 \times (conc_{tx} - conc_{t0}) / conc_{t0}$. The relevance of change in the analyte concentration was evaluated by comparison with the acceptable change limit (ACL) calculated using $ACL = 2.77 \times RSD_{QC}$ according to DIN ISO 5725-6 [41]. The factor 2.77 is based on $1.96 \times \sqrt{2}$, where 1.96 is used to cover the 95% confidence interval for bi-directional changes and $\sqrt{2}$ is used as the difference of two values is compared (at tx and t0). The relative standard deviation (RSD) was based on the RSD of quality control plasma samples (n = 6–7) analyzed in parallel with the samples (Tab. 3.1).

Data evaluation was carried out using GraphPad Prism version 6.01 for Windows (GraphPad Software, La Jolla California USA, www.graphpad.com).

3.3 Results

Oxylipins were analyzed by LC-MS/MS in plasma and serum of 6 individuals generated at four time points after blood collection in EDTA- and serum-tubes, respectively: i) immediately; after storage at 4 °C for ii) 4 hours or iii) 24 hours; or iv) after transfer *via* the pneumatic tube transport system (PTS) to the clinical chemistry laboratory. At all conditions oxylipins were determined as free mediators (Fig. 3.1, appendix Fig. 8.2, Fig. 8.3) as well as after alkaline hydrolysis comprising both free and esterified oxylipins (Fig. 3.2, appendix Fig. 8.4, Fig. 8.5). For the major formation pathways of the arachidonic acid cascade (COX, 5-LOX, 12-LOX, 15-LOX, CYP and non-enzymatic) selected ARA derived oxylipins (Fig. 3.1, Fig. 3.2) were evaluated together with their EPA derived and DHA derived counterparts (appendix Fig. 8.2, Fig. 8.3, Fig. 8.4, Fig. 8.5) to investigate pathway specific effects in the changes.

3.3.1 Levels of oxylipins in plasma and serum after immediate processing

Comparing free oxylipins levels in plasma and serum after immediate processing (Fig. 3.1, appendix Fig. 8.2, Fig. 8.3) revealed 2–3 orders of magnitude higher concentrations of COX-derived PGE_2, TxB_2 and 12-HHT in serum compared to plasma (21–125-; 128–948-; 68–500-fold, respectively). Similarly, also 12-LOX derived 12-HETE, 12-HEPE and 14-HDHA were massively increased (13–103-; 2–73-; 2–47-fold, respectively) in serum, while 15-LOX derived 15-HETE, 15-HEPE and 17-HDHA were elevated to a lesser extent (1–26-; 1–6-; 1–6-fold, respectively) and 5-LOX derived 5-HETE, 5-HEPE and 4-HDHA and 7-HDHA were unchanged or only slightly elevated (1–5-; 1–2-; 1–2-fold, respectively) in serum. In contrast, concentrations of CYP

derived epoxy- and dihydroxy-PUFA were almost similar in plasma and serum consistent for ARA, EPA and DHA derived products. Levels of non-enzymatically formed ARA derived 5(*R,S*)-5-F_{2t}-IsoP were comparable in plasma and serum.

Regarding concentrations after immediate processing following alkaline hydrolysis (Fig. 3.2, appendix Fig. 8.4, Fig. 8.5), levels of total oxylipins showed the same trend as their free counterparts when comparing plasma and serum: Levels of epoxy- and dihydroxy-PUFA, as well as 5(*R,S*)-5-F_{2t}-IsoP were comparable in plasma and serum. Serum levels of total 12-HHT were elevated to a similar extent (51–441-fold) compared to free 12-HHT. For hydroxy-PUFA differences between plasma and serum were moderate: Levels of 12-LOX derived 12-HETE, 12-HEPE, 14-HDHA were clearly elevated (5–50-; 2–14-; 2–16-fold, respectively) while 15-LOX derived 15-HETE, 15-HEPE, 17-HDHA (1–3-; 1–2-; 1–3-fold, respectively) were same or only slightly higher in serum, and levels of 5-LOX derived 5-HETE, 5-HEPE and 4-HDHA and 7-HDHA were similar in plasma and serum after hydrolysis.

Comparing levels of free and total oxylipins revealed similar concentrations for dihydroxy-PUFA while levels of hydroxy-PUFA, epoxy-PUFA and 5(*R,S*)-5-F_{2t}-IsoP were massively higher after hydrolysis.

3.3.2 Analytical variability of oxylipins in plasma and serum

Stability of oxylipins in the differently stored and transported blood samples before processing to plasma and serum was evaluated based on changes in the apparent oxylipin levels in comparison to immediate processing and the “acceptable change limit” (ACL). The ACL covers the analytical variance including sample preparation and is based on the relative standard deviation of quality control plasma samples analyzed in parallel with the samples with similar concentrations (Tab. 3.1). For free oxylipins the ACL was below 35% for most analytes, except for PGE_2 and 7-HDHA with concentrations near the

LLOQ (48% and 58%, respectively), and for 12-LOX products (42–51%). Similarly, for total oxylipins the ACL was below 40% for most analytes, except for epoxy-PUFA (48–60%) and DHA derived hydroxy-PUFA (43–49%).

Tab. 3.1: Levels of representative free and total oxylipins quantified in quality control plasma analyzed in parallel with the samples (n = 6–7), their lower limit of quantification, their relative standard deviation (RSD) and the acceptable change limit (ACL) calculated using ACL = 2.77 × RSD_{QC}.

	free oxylipins					total, i.e. free and esterified oxylipins				
Analyte	**LLOQ**	**Mean ± SD**		**RSD [%]**	**ACL**	**LLOQ**	**Mean ± SD**		**RSD [%]**	**ACL**
PGE_2	0.025	0.03 ± 0.004		17	**48**	*				
TxB_2	0.125	0.52 ± 0.06		12	**32**	*				
12-HHT	0.05	0.53 ± 0.07		14	**39**	0.25	1.25 ± 0.13		9	**26**
12-HETE	0.050	5.63 ± 0.89		16	**44**	0.25	8.48 ± 0.90		11	**30**
12-HEPE	0.063	1.51 ± 0.28		18	**51**	0.313	1.14 ± 0.10		9	**25**
14-HDHA	0.10	3.63 ± 0.55		15	**42**	0.5	2.98 ± 0.53		18	**49**
15-HETE	0.125	1.14 ± 0.10		8	**23**	0.625	10.42 ± 1.50		14	**40**
15-HEPE	0.125	0.20 ± 0.03		14	**39**	0.625	1.05 ± 0.15		14	**39**
17-HDHA	0.20	0.89 ± 0.12		13	**36**	1	4.54 ± 0.75		17	**46**
5-HETE	0.05	0.86 ± 0.09		11	**29**	0.25	17.77 ± 1.55		9	**24**
5-HEPE	0.05	0.26 ± 0.03		13	**36**	0.25	2.69 ± 0.16		6	**16**
4-HDHA	0.025	0.35 ± 0.03		7	**21**	0.125	3.62 ± 0.45		12	**34**
7-HDHA	0.10	0.11 ± 0.02		21	**58**	0.5	2.47 ± 0.39		16	**43**
14(15)-EpETrE	0.05	0.10 ± 0.01		9	**24**	0.25	54.46 ± 11.78		22	**60**
17(18)-EpETE	0.10	< LLOQ				0.5	5.11 ± 0.88		17	**48**
19(20)-EpDPE	0.05	0.31 ± 0.03		9	**26**	0.25	11.60 ± 2.06		18	**49**
14,15-DiHETrE	0.01	0.64 ± 0.04		6	**16**	0.05	1.53 ± 0.16		11	**29**
17,18-DiHETE	0.025	0.55 ± 0.06		11	**31**	0.125	0.80 ± 0.07		9	**25**
19,20-DiHDPE	0.05	3.09 ± 0.17		5	**15**	0.25	3.77 ± 0.16		4	**12**
5(*R,S*)-5-F_{2t}-IsoP	0.05	0.11 ± 0.01		10	**28**	0.25	0.47 ± 0.05		11	**31**
11-HETE	0.05	0.31 ± 0.02		7	**20**	0.25	6.42 ± 0.74		11	**32**
9-HETE	0.25	< LLOQ				1.25	6.37 ± 0.77		12	**34**
18-HEPE	0.10	0.42 ± 0.02		4	**10**	0.5	1.30 ± 0.15		12	**33**

* PGE_2 and TxB_2 are degraded during alkaline hydrolysis

3.3.3 Stability of free oxylipins in plasma and serum

Regarding changes of free oxylipins in plasma after storage or PTS of blood samples, levels of 5(*R,S*)-5-F_{2t}-IsoP, terminal dihydroxy-PUFA and epoxy-PUFA as well as 5-LOX products were almost stable at all investigated conditions with slight deviations for 5-LOX products in samples from a single individuum and for epoxy-PUFA in samples stored 24 h at 4 °C before processing. Changes of PGE_2, TxB_2 and 12-HHT were within the ACL for most samples after 4 h storage at 4 °C, while in samples stored for 24 h levels were clearly increased and after PTS further elevated with high inter-individual variance. 12-LOX metabolites showed a similar pattern with massive increases after PTS. With respect to 15-LOX metabolites, changes of 15-HETE and 17-HDHA were within the ACL in 4 h stored samples, clearly higher in 24 h stored samples, but only slightly elevated in PTS samples, while interestingly changes of 15-HEPE were within the ACL at all investigated conditions.

In serum overall storage/transport-induced changes of free oxylipins were more pronounced. PGE_2, TxB_2 and 12-HHT showed a similar pattern in all stored and transported samples with high inter-individual variance being within the ACL for samples from 2–3 individuals, but massively higher for 2–4 individuals. For 12-LOX and 15-LOX metabolites changes were higher compared to plasma, though similar in 4 h and 24 h stored samples, but massively higher in PTS samples with high inter-individual variance. 5-LOX metabolites were almost stable in 4 h stored samples, but exceeded the ACL in 24 h stored and PTS samples. While dihydroxy-PUFA were stable in all conditions, changes of epoxy-PUFA and 5(*R,S*)-5-F_{2t}-IsoP were within the ACL in almost all samples stored 4 h and after PTS, but were slightly higher than the ACL in 24 h stored blood samples.

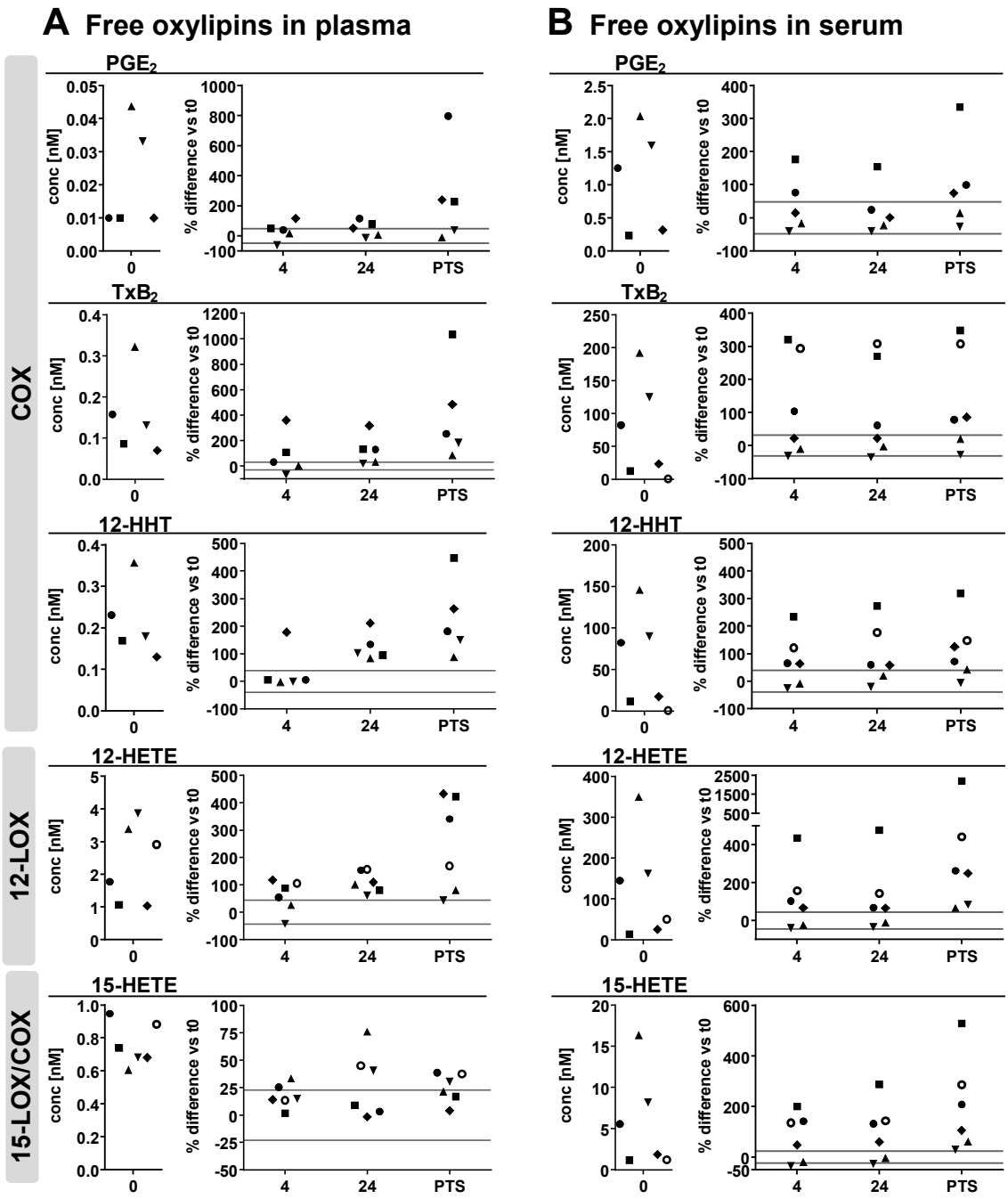

Fig. 3.1: ARA derived free oxylipins in **(A)** plasma and **(B)** serum. Shown are individual concentrations (n = 6) of selected oxylipins from major formation pathways at t0 (immediate processing) and %difference *vs* t0 after 4 hours and 24 hours at 4 °C or after pneumatic tube transport (PTS) prior to centrifugation to generate plasma or serum. The different symbols represent samples from different individual human subjects. The grey lines indicate the acceptable change limits calculated based on relative standard deviation of quality control plasma (summarized in Tab. 3.1). **Figure is continued on page 58.**

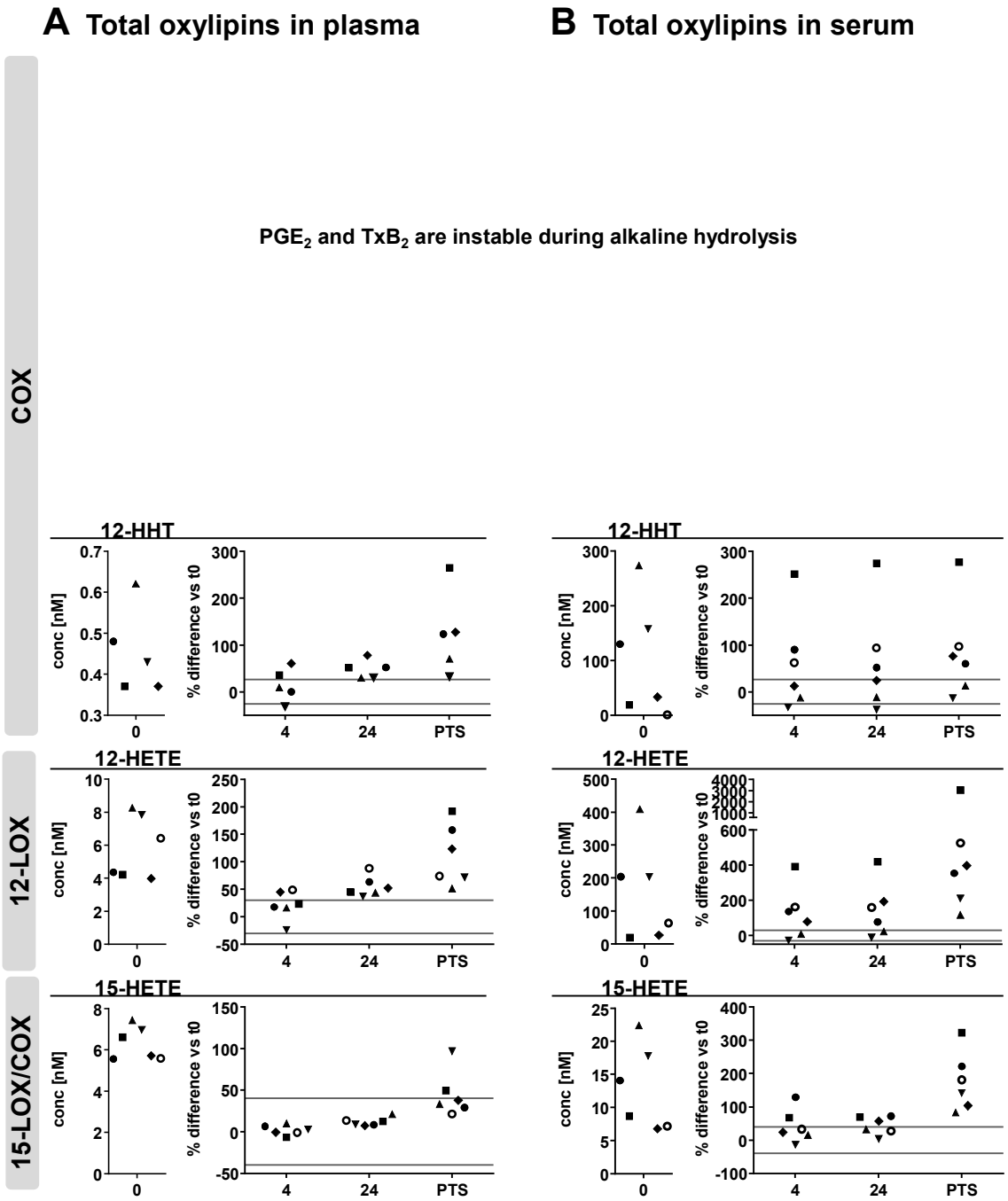

Fig. 3.2: ARA derived total (i.e. sum of free and esterified) oxylipins in **(A)** plasma and **(B)** serum. Shown are individual concentrations (n = 6) of selected oxylipins from major formation pathways at t0 (immediate processing) and %difference *vs* t0 after 4 hours and 24 hours at 4 °C or after pneumatic tube transport (PTS) prior to centrifugation to generate plasma or serum. The different symbols represent samples from different individual human subjects. The grey lines indicate the acceptable change limits calculated based on relative standard devivation of quality control plasma (summarized in Tab. 3.1). **Figure is continued on page 59.**

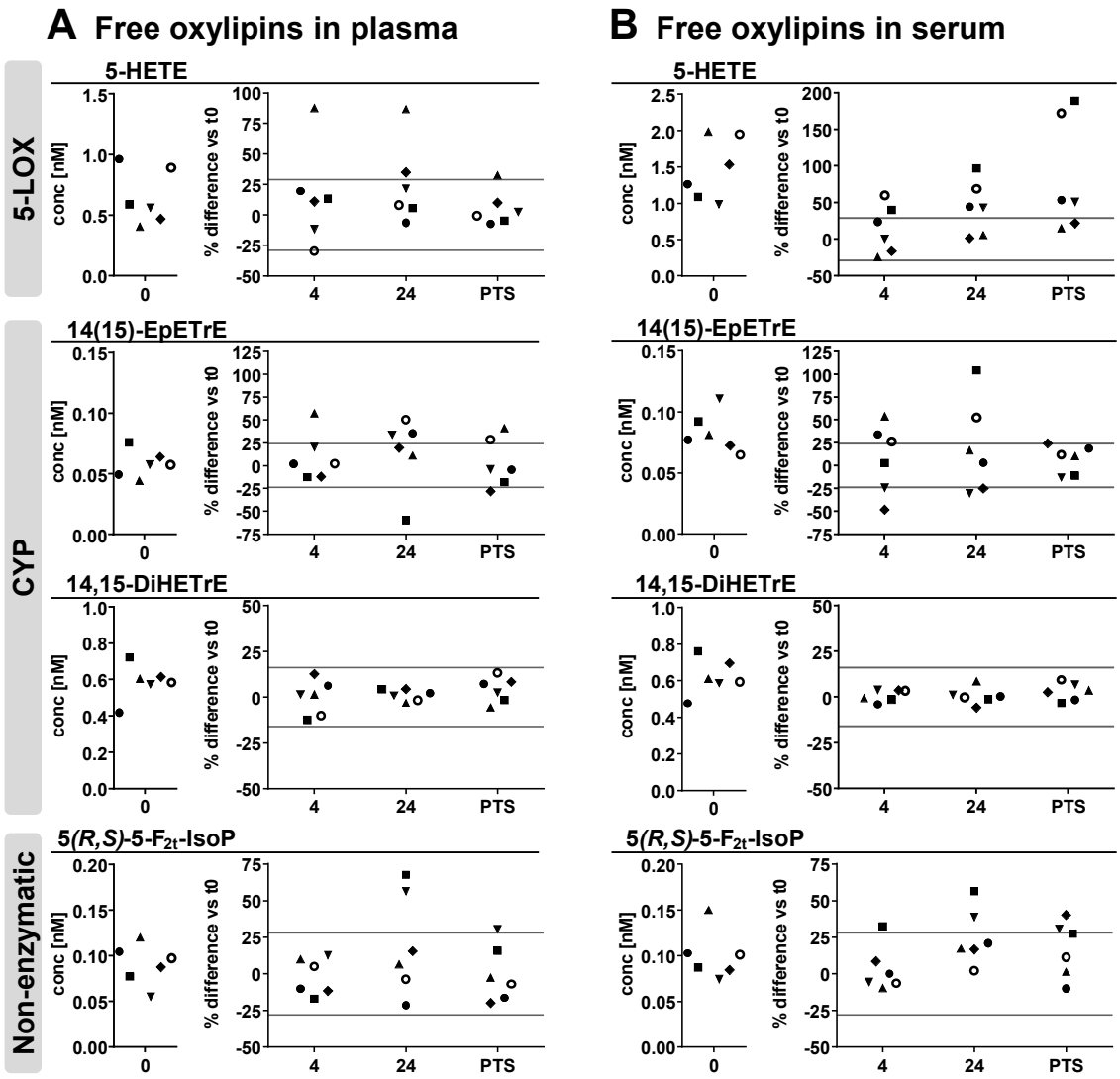

Fig. 3.1: Continued from page 56. ARA derived free oxylipins in **(A)** plasma and **(B)** serum.

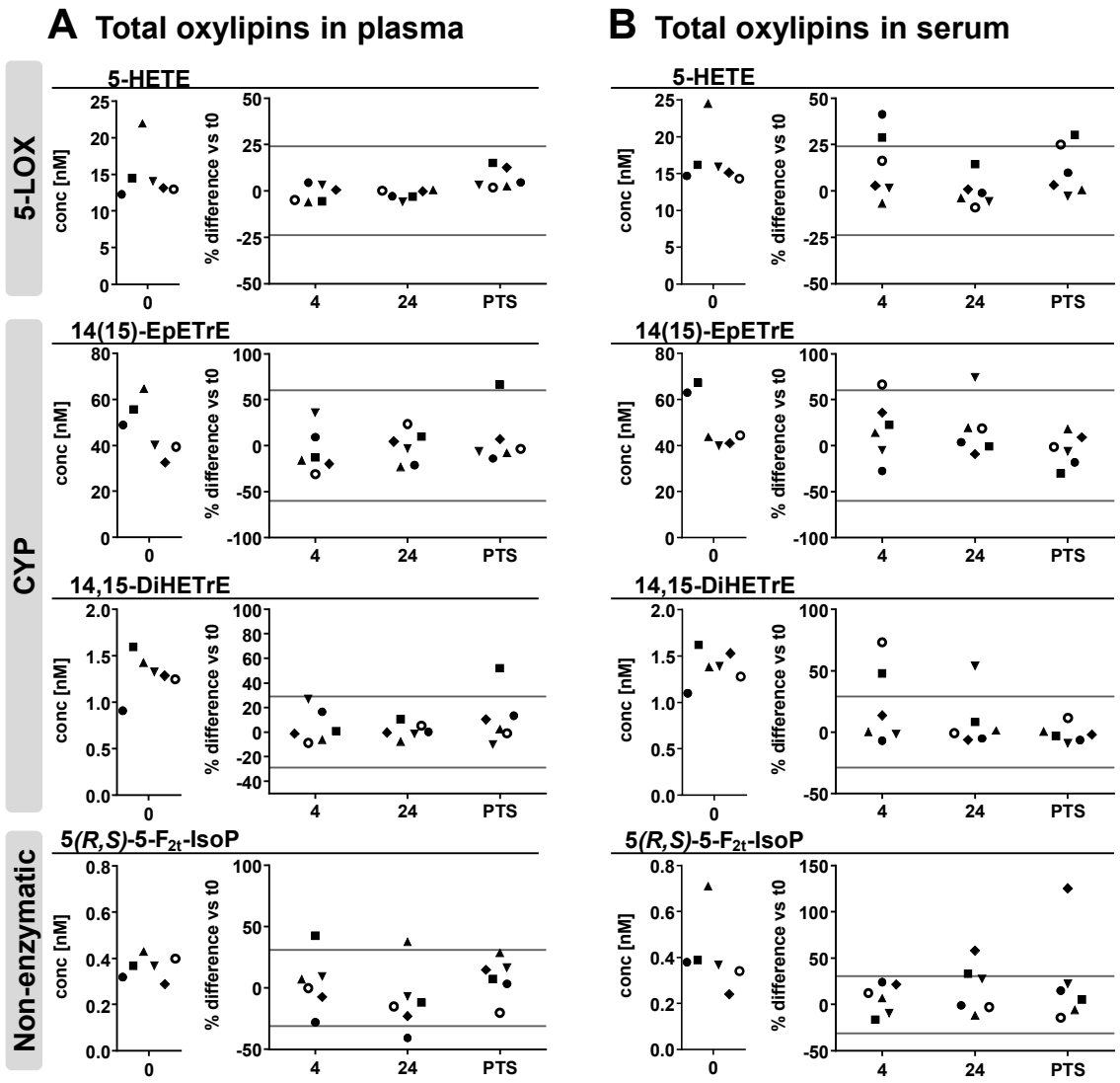

Fig. 3.2: Continued from page 57. ARA derived total oxylipins in **(A)** plasma and **(B)** serum.

3.3.4 Stability of total oxylipins in plasma and serum

Similar to free oxylipins, storage/transport-induced lower changes of total oxylipins in plasma compared to serum. However, the overall impact of sample handling was less pronounced for total levels compared to free oxylipins. In plasma and serum for all conditions changes of total 5-LOX metabolites, dihydroxy-PUFA, epoxy-PUFA as well as 5(*R,S*)-5-F_{2t}-IsoP were within the respective ACL for almost all individual samples. 15-LOX-metabolites were stable in plasma of 4 h and 24 h stored blood samples, while in PTS samples slight increases were observed being most pronounced for DHA derived 17-HDHA. Deviations in serum were higher, slightly exceeding the ACL in 4 h and 24 h stored samples, while being massively elevated in PTS samples, with high inter-individual variance. The strongest influence of pre-processing handling was observed for 12-LOX metabolites, being more pronounced in serum than in plasma. While 12-LOX metabolites in plasma were stable in 4 h stored samples and slightly elevated in 24 h stored samples, in serum they were clearly increased, already exceeding the ACL in almost all 4 h and 24 h stored samples. Changes in PTS samples were considerably higher than the ACL for plasma and serum, being however massively higher in serum with higher inter-individual variance. For total 12-HHT the extent and pattern of changes was similar to free 12-HHT.

3.4 Discussion

Targeted oxylipin metabolomics of clinical samples is increasingly becoming valuable in the evaluation of the disease state or for the discovery of disease biomarkers [5]. However, blood sampling in clinical routine is often accompanied with uncontrolled transitory time intervals during collection and processing until further analysis and standardized handling of samples is hard to attain in the clinical setting. Efficient transport systems are established in large hospitals, such as pneumatic tube system transport (PTS), to achieve fast sample delivery to the clinical chemistry laboratory. The influence of these “real

life" blood sample handling has been previously described for hemolysis and clinical chemistry parameters [42, 43], however no information is available on its impact on the oxylipin pattern. Because of the oxidation-prone structure of oxylipins as well as the residual enzymatic activity in blood samples related to PUFA converting enzymes in blood cells, artificial formation and degradation of oxylipins during the pre-analytical workflow including collection, transport, processing, storage and preparation of samples cannot be excluded and may impact reliable interpretation of the analyzed oxylipin pattern. Therefore, we evaluated in the present study the effect of storage of whole blood samples at 4 °C for 4 h and 24 h as well as of the transport *via* the PTS prior to centrifugation on the levels of a comprehensive set of free and total oxylipins in EDTA-plasma and serum covering oxylipins from all major formation pathways.

Serum generation is associated with massive increase of free and total platelet derived oxylipins

In direct comparison of free oxylipin levels in directly processed plasma and serum we observed a massive increase of COX and 12-LOX derived products by 1–3 orders of magnitude in serum. Levels of 15-LOX products were also elevated however to a lesser extent, while 5-LOX derived metabolites were only slightly higher in serum, and CYP derived epoxy- and dihydroxy-PUFA were almost similar in plasma and serum. This is consistent with previous studies observing massive higher levels of free TxB_2, 12-HHT and 12-HETE in serum compared to plasma [34, 35, 44]. The observed increase in these eicosanoids is attributable to the intrinsic activation of the clotting cascade triggered by the contact of the contact system factor FXII which circulates in the blood with the negatively charged surfaces in the vacutainer used to generate serum during blood collection [45]. Activation of this protease cascade ultimately leads to the activation of platelets and their main PUFA converting enzymes COX-1 and 12-LOX and subsequently to the formation of TxA_2, 12-HHT (*via* COX-1) and 12-HETE (12-LOX) during coagulation [46, 47]. The observed increase in 15-HETE could also – besides synthesis *via* 12/15-LOX which is under homeostatic conditions predominantly present in eosinophils [48] – related to

activated platelets *via* COX-1 which have been shown to produce 15-HETE (predominantly the *S*-enantiomer) and 11-HETE [49]. Consistently, 11-HETE showed a similar pattern (Fig. 3.3). The slight elevation of 5-HETE levels in serum is also consistent with previous reports [34, 35] and the prevailing proportion of 5(*S*)-HETE [35] suggests contribution of enzymatic formation *via* 5-LOX expressed in various leukocytes [50] which have been implicated in the regulation of thrombosis [51].

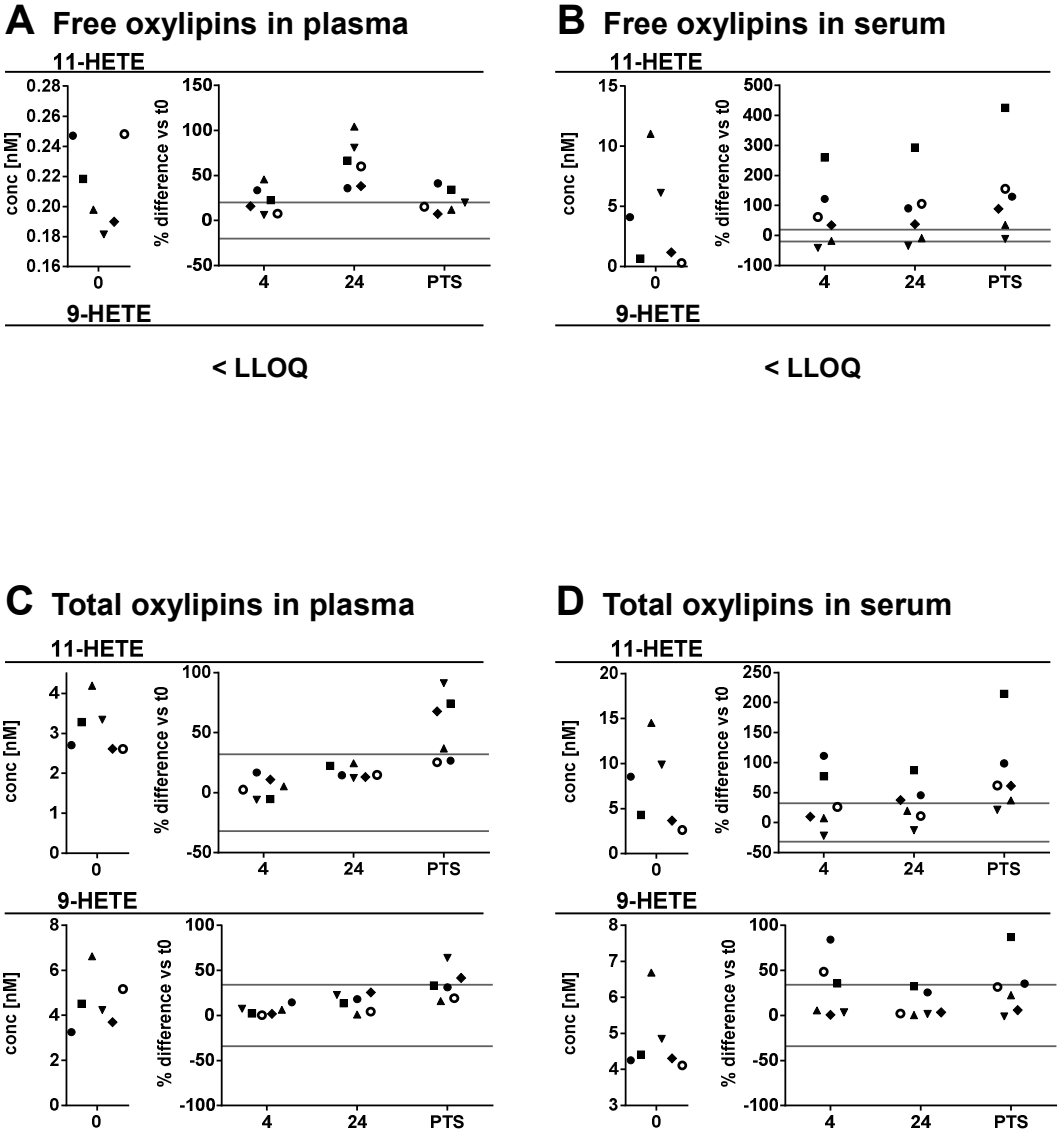

Fig. 3.3: ARA derived 11-HETE and 9-HETE in **(A+C)** plasma and **(B+D)** serum. Shown are individual concentration (n = 6) of **(A+B)** free or **(C+D)** total (comprising free and esterified) mediators at t0 (immediate processing) and %difference *vs* t0 after storage for 4 hours and 24 hours at 4 °C and after pneumatic tube transport prior to centrifugation to generate plasma or serum. The different symbols represent samples from different individual human subjects. The grey lines indicate acceptable change limits calculated based on relative standard deviation of quality control plasma (summarized in Tab. 3.1).

Respective hydroxy-PUFA derived from EPA and DHA, showed the same pattern as their ARA derived counterparts supporting the contribution of these enzymatic pathways to their formation during serum generation (appendix Fig. 8.2, Fig. 8.3, Fig. 8.4**,** Fig. 8.5). However, these metabolites were elevated to a lesser extent reflecting the low levels of EPA and DHA in blood competing with ARA for their enzymatic conversion, as human 12/15-LOX and 12-LOX enzymes have been shown to prefer DHA and EPA over ARA [52]. The observation that levels of non-enzymatically formed 5(*R,S*)-5-F_{2t}-IsoP were almost similar in plasma and serum suggests that autoxidative processes do not play a major role in freshly prepared serum. Similar only marginal alterations were seen for 9-HETE (Fig. 3.3), which is discussed as autoxidation product.

The major portion of hydroxy- and epoxy-PUFA, as well as 5(*R,S*)-5-F_{2t}-IsoP was found esterified in plasma and serum, because massive higher concentrations were observed after alkaline hydrolysis, consistent with earlier reports [20-22]. Dihydroxy-PUFA were only present non-esterified with same apparent concentration for free and total oxylipins. Since under alkaline conditions thromboxanes as well as β-hydroxy-keto-prostanoids, e.g. PGE_2 and PGD_2, are degraded [53], we used formation of 12-HHT as a surrogate for COX activity [46]. The levels of 12-HHT were similar with and without hydrolysis and massively increased in serum. Thus, also the total oxylipin pattern based on 12-HHT, reflects increased COX activity due to platelet activation during serum generation.

Serum generation was also accompanied by an increase in total hydroxy-PUFA levels which was however less pronounced compared to the respective free hydroxy-PUFA. Even though it has been shown that eosinophilic 12/15-LOX directly form esterified 15-HETE in phospholipids [48], and platelet 12-LOX derived hydroxy-PUFA are readily esterified contributing to the esterified pool [54], only a minor increase of 12- and 15-HETE (and respective EPA and DHA products) was observed in total oxylipins in comparison to their free levels.

Esterified oxylipins in the cell free fraction of blood (i.e. serum and plasma) is thus hardly influenced by the activation of the coagulation cascade.

Plasma oxylipin profile is more stable than serum and total oxylipins are more stable than free oxylipins

The extended transitory storage of whole blood prior to further processing to plasma or serum can cause formation and degradation of several oxylipins due to prolonged *ex vivo* contact with blood cells, i.e. erythrocytes, leukocytes or platelets, exhibiting enzymatic activity *versus* PUFA and oxylipins. In order to evaluate the impact of the transitory storage or PTS transport we used the ACL based on the methodological RSD obtained from quality control plasma samples analyzed in parallel [41] which was in a similar range as previously reported for both, free [34, 55] and total oxylipins [39].

Free oxylipins in plasma from whole blood stored at 4 °C for 4 h remained almost stable with exception of samples from a few individuals showing higher deviations for 12-LOX and COX-1 derived products. After 24 h at 4 °C besides considerable increase in platelet-derived oxylipins also 15-LOX products were clearly increased. Though these results are consistent with a previous study reporting that free oxylipins in EDTA-whole blood are stable up to 2 h at 4 °C [34], another study showed a clear decrease of some prostanoids (PGE_2, $PGF_{2\alpha}$), hydroxy-PUFA (11- and 15-HETE) and epoxy-PUFA (14(15)- and 11(12)-EpETrE) in EDTA-whole blood already after 1 h on ice [16].

In contrast to plasma, free oxylipins in serum of stored clotted whole blood were largely unstable. Especially platelet-derived (COX and 12-LOX) as well as 15-LOX products showed a strong increase with high inter-individual variance similar for 4 h and 24 h at 4 °C. 5-LOX derived products were stronger elevated after longer storage (24 h *vs* 4 h). Consistently, La Frano *et al* reported that a “freezing delay” of clotted whole blood dramatically elevated hydroxy-PUFA attributed to ongoing enzymatic processes in cooled whole blood [56].

Apparent total oxylipin patterns were considerably more stable towards transitory storage of whole blood. However, the observed changes revealed a similar pattern as for free oxylipins: Total plasma oxylipins were stable for 4 h at 4 °C and showed only elevation of platelet derived oxylipins after 24 h. In serum similarly to free oxylipins platelet derived oxylipins were massively increased after 4 h and 24 h, however increase in 15-LOX products was less pronounced and absent for 5-LOX products. These results suggest that transitory storage at 4 °C without removal of the blood cells or/and the blood clot led to enzymatic activity resulting from *ex-vivo* activation of platelets. This leads to considerable artificial *ex-vivo* formation of COX and 12-LOX products. While in plasma this can be ascribed to continuing enzymatic conversion related to the duration of storage, the high inter-individual variances in platelet-derived metabolites in serum which are similar at 4 h and 24 h indicate that these changes result rather from individual differences in the platelets and enzymatic activity of the blood coagulation cascade. One should note, that under all conditions the levels of free as well as total oxylipins of CYP derived dihydroxy-PUFA were stable and free levels of epoxy-PUFA showed only slight increases after 24 h. Moreover, the almost unchanged 5(*R,S*)-5-F_{2t}-IsoP and 9-HETE levels indicate that only minor autoxidation takes place during the delay in sample processing.

Non-controlled blood transport amplifies formation of platelet derived (COX-1, 12-LOX) oxylipins

Automated pneumatic tube transport of blood caused in all samples a massive increase in 12-LOX and COX products with high inter-individual variances. While 15-LOX metabolites were only slightly and 5-LOX products barely affected in plasma, in serum PTS transport also led to a clear elevation of these hydroxy-PUFA. Again, these changes were more pronounced for free oxylipins. Consistent with previous studies observing decreased clotting time after PTS transport [57, 58] these observations suggest that during PTS transport platelets might be activated, e.g. due to shear stress or hemolysis induced by physical forces (shaking, rapid acceleration). Even though the used PTS has not been evaluated with regard to its impact on platelet function and different

PTS might have varying effects, the observed increase in platelet derived COX and 12-LOX metabolites after PTS are likely attributable to enhanced platelet activation during PTS.

3.5 Conclusion

In the present study we investigated the impact of transitory storage as well as PTS transport of whole blood samples on the pattern of free and total oxylipins in plasma and serum with the aim to evaluate if free or total oxylipins are more stable in plasma or serum after whole blood handling in a clinical setting. Based on parallel analysis of oxylipins derived from ARA, EPA and DHA from all major formation pathways including COX, LOX, CYP as well as non-enzymatic conversion we could show: 1.) Free oxylipins in plasma are stable up to 4 h at 4 °C and prolonged storage as well as sample transport led to increased levels of COX and 12-LOX products. 2.) The total oxylipin pattern in plasma and serum is less affected by transitory storage and transport. 3.) Blood coagulation, i.e. serum generation, leads to massively higher levels of free and total COX and 12-LOX derived oxylipins due to *ex-vivo* platelet activation. 4.) Serum samples showed higher storage and transport induced variability and inter-individual differences were more pronounced. Thus, with respect to clinical studies – where blood sampling cannot be tightly controlled – total plasma oxylipins seem to be the best analytical marker for the blood oxylipin pattern. While great caution with respect to artifact formation in interpretation of 12-LOX and COX metabolites is required, total levels of 5-LOX, CYP as well as the autoxidation product 5(*R,S*)-5-F_{2t}-IsoP are almost stable with respect to blood handling conditions.

3.6 References

1. Gabbs M., Leng S., Devassy J. G., Monirujjaman M. and Aukema H. M. (2015) Advances in our understanding of oxylipins derived from dietary PUFAs. *Adv Nutr*. 6(5), pp. 513-540; doi: 10.3945/an.114.007732.
2. Konkel A. and Schunck W.-H. (2011) Role of cytochrome P450 enzymes in the bioactivation of polyunsaturated fatty acids. *Biochim Biophys Acta*. 1814(1), pp. 210-222; doi: 10.1016/j.bbapap.2010.09.009.
3. Yeung J., Hawley M. and Holinstat M. (2017) The expansive role of oxylipins on platelet biology. *J Mol Med (Berl)*. 95(6), pp. 575-588; doi: 10.1007/s00109-017-1542-4.
4. Dennis E. A. and Norris P. C. (2015) Eicosanoid storm in infection and inflammation. *Nat Rev Immunol*. 15(8), pp. 511-523; doi: 10.1038/nri3859.
5. Gladine C., Ostermann A. I., Newman J. W. and Schebb N. H. (2019) MS-based targeted metabolomics of eicosanoids and other oxylipins: Analytical and inter-individual variabilities. *Free Radic Biol Med*. 144, pp. 72-89; doi: 10.1016/j.freeradbiomed.2019.05.012.
6. Buczynski M. W., Dumlao D. S. and Dennis E. A. (2009) Thematic review series: Proteomics - An integrated omics analysis of eicosanoid biology. *J Lipid Res*. 50(6), pp. 1015-1038; doi: 10.1194/jlr.R900004-JLR200.
7. Milne G. L., Dai Q. and Roberts II L. J. (2015) The isoprostanes - 25 years later. *Biochim Biophys Acta*. 1851(4), pp. 433-445; doi: 10.1016/j.bbalip.2014.10.007.
8. Yin H., Xu L. and Porter N. A. (2011) Free radical lipid peroxidation: Mechanisms and analysis. *Chem Rev*. 111(10), pp. 5944-5972; doi: 10.1021/cr200084z.
9. Rund K. M., Heylmann D., Seiwert N., Wecklein S., Oger C., Galano J.-M., Durand T., Chen R., Gueler F., Fahrer J., Bornhorst J. and Schebb N. H. (2019) Formation of trans-epoxy fatty acids correlates with formation of isoprostanes and could serve as biomarker of oxidative stress. *Prostaglandins Other Lipid Mediat*. 144:106334; doi: 10.1016/j.prostaglandins.2019.04.004.
10. Jiang H., McGiff J. C., Quilley J., Sacerdoti D., Reddy L. M., Falck J. R., Zhang F., Lerea K. M. and Wong P. Y. (2004) Identification of 5,6-trans-epoxyeicosatrienoic acid in the phospholipids of red blood cells. *J Biol Chem*. 279(35), pp. 36412-36418; doi: 10.1074/jbc.M403962200.
11. Capra V., Bäck M., Barbieri S. S., Camera M., Tremoli E. and Rovati G. E. (2013) Eicosanoids and their drugs in cardiovascular diseases: Focus on atherosclerosis and stroke. *Med Res Rev*. 33(2), pp. 364-438; doi: 10.1002/med.21251.
12. Hardwick J. P., Eckman K., Lee Y. K., Abdelmegeed M. A., Esterle A., Chilian W. M., Chiang J. Y. and Song B. J. (2013) Eicosanoids in metabolic syndrome. *Adv Pharmacol*. 66, pp. 157-266; doi: 10.1016/B978-0-12-404717-4.00005-6.
13. Brune K. and Patrignani P. (2015) New insights into the use of currently available non-steroidal anti-inflammatory drugs. *Journal of pain research*. 8, pp. 105-118; doi: 10.2147/JPR.S75160.
14. Crescente M., Menke L., Chan M. V., Armstrong P. C. and Warner T. D. (2019) Eicosanoids in platelets and the effect of their modulation by aspirin in the cardiovascular system (and beyond). *British journal of pharmacology*. 176(8), pp. 988-999; doi: 10.1111/bph.14196.
15. Song J., Liu X., Rao T. S., Chang L., Meehan M. J., Blevitt J. M., Wu J., Dorrestein P. C. and Milla M. E. (2015) Phenotyping drug polypharmacology via eicosanoid profiling of blood. *J Lipid Res*. 56(8), pp. 1492-1500; doi: 10.1194/jlr.M058677.

16. Willenberg I., Ostermann A. I. and Schebb N. H. (2015) Targeted metabolomics of the arachidonic acid cascade: Current state and challenges of LC-MS analysis of oxylipins. *Anal Bioanal Chem*. 407(10), pp. 2675-2683; doi: 10.1007/s00216-014-8369-4.
17. Ostermann A. I. and Schebb N. H. (2017) Effects of omega-3 fatty acid supplementation on the pattern of oxylipins: A short review about the modulation of hydroxy-, dihydroxy-, and epoxy-fatty acids. *Food Funct*. 8(7), pp. 2355-2367; doi: 10.1039/c7fo00403f.
18. Ek-Von Mentzer B. A., Zhang F. and Hamilton J. A. (2001) Binding of 13-HODE and 15-HETE to phospholipid bilayers, albumin, and intracellular fatty acid binding proteins - Implications for transmembrane and intracellular transport and for protection from lipid peroxidation. *J Biol Chem*. 276(19), pp. 15575-15580; doi: 10.1074/jbc.M011623200.
19. Brock T. G. (2008) Capturing proteins that bind polyunsaturated fatty acids: Demonstration using arachidonic acid and eicosanoids. *Lipids*. 43(2), pp. 161-169; doi: 10.1007/s11745-007-3136-3.
20. Shearer G. C. and Newman J. W. (2008) Lipoprotein lipase releases esterified oxylipins from very low-density lipoproteins. *Prostaglandins Leukot Essent Fatty Acids*. 79(6), pp. 215-222; doi: 10.1016/j.plefa.2008.09.023.
21. Schebb N. H., Ostermann A. I., Yang J., Hammock B. D., Hahn A. and Schuchardt J. P. (2014) Comparison of the effects of long-chain omega-3 fatty acid supplementation on plasma levels of free and esterified oxylipins. *Prostaglandins Other Lipid Mediat*. 113-115, pp. 21-29; doi: 10.1016/j.prostaglandins.2014.05.002.
22. Morrow J. D., Awad J. A., Boss H. J., Blair I. A. and Roberts II L. J. (1992) Non-cyclooxygenase-derived prostanoids (F2-isoprostanes) are formed in situ on phospholipids. *Proc Natl Acad Sci U S A*. 89(22), pp. 10721-10725; doi: 10.1073/pnas.89.22.10721.
23. Pace S., Sautebin L. and Werz O. (2017) Sex-biased eicosanoid biology: Impact for sex differences in inflammation and consequences for pharmacotherapy. *Biochem Pharmacol*. 145, pp. 1-11; doi: 10.1016/j.bcp.2017.06.128.
24. Caligiuri S. P. B., Parikh M., Stamenkovic A., Pierce G. N. and Aukema H. M. (2017) Dietary modulation of oxylipins in cardiovascular disease and aging. *Am J Physiol Heart Circ Physiol*. 313(5), pp. H903-H918; doi: 10.1152/ajpheart.00201.2017.
25. Giordano R. M., Newman J. W., Pedersen T. L., Ramos M. I. and Stebbins C. L. (2011) Effects of dynamic exercise on plasma arachidonic acid epoxides and diols in human volunteers. *Int J Sport Nutr Exerc Metab*. 21(6), pp. 471-479; doi: 10.1123/ijsnem.21.6.471.
26. Capo X., Martorell M., Sureda A., Tur J. A. and Pons A. (2016) Effects of dietary docosahexaenoic, training and acute exercise on lipid mediators. *J Int Soc Sports Nutr*. 13:16; doi: 10.1186/s12970-016-0126-y.
27. Zivkovic A. M., Yang J., Georgi K., Hegedus C., Nording M. L., O'Sullivan A., German J. B., Hogg R. J., Weiss R. H., Bay C. and Hammock B. D. (2012) Serum oxylipin profiles in IgA nephropathy patients reflect kidney functional alterations. *Metabolomics*. 8(6), pp. 1102-1113; doi: 10.1007/s11306-012-0417-5.
28. Gottschall H., Schmöcker C., Hartmann D., Rohwer N., Rund K., Kutzner L., Nolte F., Ostermann A. I., Schebb N. H. and Weylandt K. H. (2018) Aspirin alone and combined with a statin suppresses eicosanoid formation in human colon tissue. *J Lipid Res*. 59(5), pp. 864-871; doi: 10.1194/jlr.M078725.
29. Schramm D. D., Wang J. F., Holt R. R., Ensunsa J. L., Gonsalves J. L., Lazarus S. A., Schmitz H. H., German J. B. and Keen C. L. (2001) Chocolate procyanidins decrease the leukotriene-prostacyclin ratio in humans and human aortic endothelial cells. *Am J Clin Nutr*. 73(1), pp. 36-40; doi: 10.1093/ajcn/73.1.36.

30. Berthelot C. C., Kamita S. G., Sacchi R., Yang J., Nording M. L., Georgi K., Hegedus Karbowski C., German J. B., Weiss R. H., Hogg R. J., Hammock B. D. and Zivkovic A. M. (2015) Changes in PTGS1 and ALOX12 gene expression in peripheral blood mononuclear cells are associated with changes in arachidonic acid, oxylipins, and oxylipin/fatty acid ratios in response to omega-3 fatty acid supplementation. *PLoS One*. 10(12):e0144996; doi: 10.1371/journal.pone.0144996.
31. Ross S., Eikelboom J., Anand S. S., Eriksson N., Gerstein H. C., Mehta S., Connolly S. J., Rose L., Ridker P. M., Wallentin L., Chasman D. I., Yusuf S. and Pare G. (2014) Association of cyclooxygenase-2 genetic variant with cardiovascular disease. *Eur Heart J*. 35(33), pp. 2242-2248; doi: 10.1093/eurheartj/ehu168.
32. Stephensen C. B., Armstrong P., Newman J. W., Pedersen T. L., Legault J., Schuster G. U., Kelley D., Vikman S., Hartiala J., Nassir R., Seldin M. F. and Allayee H. (2011) ALOX5 gene variants affect eicosanoid production and response to fish oil supplementation. *J Lipid Res*. 52(5), pp. 991-1003; doi: 10.1194/jlr.P012864.
33. Zordoky B. N. and El-Kadi A. O. (2010) Effect of cytochrome P450 polymorphism on arachidonic acid metabolism and their impact on cardiovascular diseases. *Pharmacol Ther*. 125(3), pp. 446-463; doi: 10.1016/j.pharmthera.2009.12.002.
34. Dorow J., Becker S., Kortz L., Thiery J., Hauschildt S. and Ceglarek U. (2016) Preanalytical investigation of polyunsaturated fatty acids and eicosanoids in human plasma by liquid chromatography-tandem mass spectrometry. *Biopreserv Biobank*. 14(2), pp. 107-113; doi: 10.1089/bio.2015.0005.
35. Mazaleuskaya L. L., Salamatipour A., Sarantopoulou D., Weng L., FitzGerald G. A., Blair I. A. and Mesaros C. (2018) Analysis of HETEs in human whole blood by chiral UHPLC-ECAPCI/HRMS. *J Lipid Res*. 59(3), pp. 564-575; doi: 10.1194/jlr.D081414.
36. Jonasdottir H. S., Brouwers H., Toes R. E. M., Ioan-Facsinay A. and Giera M. (2018) Effects of anticoagulants and storage conditions on clinical oxylipid levels in human plasma. *Biochim Biophys Acta*. 1863(12), pp. 1511-1522; doi: 10.1016/j.bbalip.2018.10.003.
37. Rund K. M., Ostermann A. I., Kutzner L., Galano J.-M., Oger C., Vigor C., Wecklein S., Seiwert N., Durand T. and Schebb N. H. (2018) Development of an LC-ESI(-)-MS/MS method for the simultaneous quantification of 35 isoprostanes and isofurans derived from the major n3- and n6-PUFAs. *Anal Chim Acta*. 1037, pp. 63-74; doi: 10.1016/j.aca.2017.11.002.
38. Greupner T., Kutzner L., Nolte F., Strangmann A., Kohrs H., Hahn A., Schebb N. H. and Schuchardt J. P. (2018) Effects of a 12-week high-α-linolenic acid intervention on EPA and DHA concentrations in red blood cells and plasma oxylipin pattern in subjects with a low EPA and DHA status. *Food Funct*. 9(3), pp. 1587-1600; doi: 10.1039/c7fo01809f.
39. Ostermann A. I., Koch E., Rund K. M., Kutzner L., Mainka M. and Schebb N. H. (2020) Targeting esterified oxylipins by LC-MS – Effect of sample preparation on oxylipin pattern. *Prostaglandins Other Lipid Mediat*. 146:106384; doi: 10.1016/j.prostaglandins.2019.106384.
40. Kutzner L., Rund K. M., Ostermann A. I., Hartung N. M., Galano J.-M., Balas L., Durand T., Balzer M. S., David S. and Schebb N. H. (2019) Development of an optimized LC-MS method for the detection of specialized pro-resolving mediators in biological samples. *Front Pharmacol*. 10:169; doi: 10.3389/fphar.2019.00169.
41. DIN ISO 5725-6:2002-08, Accuracy (trueness and precision) of measurement methods and results — Part 6: Use in practice of accuracy values (ISO 5725-6:1994 including Technical Corrigendum 1:2001).
42. Sodi R., Darn S. M. and Stott A. (2004) Pneumatic tube system induced haemolysis: Assessing sample type susceptibility to haemolysis. *Ann Clin Biochem*. 41(3), pp. 237-240; doi: 10.1258/000456304323019631.

43. Koessler J., Kobsar Anna L., Brunner K., Stolz H., Dossler B., Walter U. and Steigerwald U. (2011) The preanalytical influence of two different mechanical transport systems on laboratory analysis. *Clin Chem Lab Med*. 49(8), pp. 1379-1382; doi: 10.1515/CCLM.2011.198.
44. Ishikawa M., Tajima Y., Murayama M., Senoo Y., Maekawa K. and Saito Y. (2013) Plasma and serum from nonfasting men and women differ in their lipidomic profiles. *Biol Pharm Bull*. 36(4), pp. 682-685; doi: 10.1248/bpb.b12-00799.
45. Maas C., Oschatz C. and Renné T. (2011) The plasma contact system 2.0. *Semin Thromb Hemost*. 37(4), pp. 375-381; doi: 10.1055/s-0031-1276586.
46. Matsunobu T., Okuno T., Yokoyama C. and Yokomizo T. (2013) Thromboxane A synthase-independent production of 12-hydroxyheptadecatrienoic acid, a BLT2 ligand. *J Lipid Res*. 54(11), pp. 2979-2987; doi: 10.1194/jlr.M037754.
47. O'Donnell Valerie B., Murphy Robert C. and Watson Steve P. (2014) Platelet lipidomics: Modern day perspective on lipid discovery and characterization in platelets. *Circ Res*. 114(7), pp. 1185-1203; doi: 10.1161/CIRCRESAHA.114.301597.
48. Uderhardt S., Ackermann J. A., Fillep T., Hammond V. J., Willeit J., Santer P., Mayr M., Biburger M., Miller M., Zellner K. R., Stark K., Zarbock A., Rossaint J., Schubert I., Mielenz D., Dietel B., Raaz-Schrauder D., Ay C., Gremmel T., Thaler J., Heim C., Herrmann M., Collins P. W., Schabbauer G., Mackman N., Voehringer D., Nadler J. L., Lee J. J., Massberg S., Rauh M., Kiechl S., Schett G., O'Donnell V. B. and Krönke G. (2017) Enzymatic lipid oxidation by eosinophils propagates coagulation, hemostasis, and thrombotic disease. *J Exp Med*. 214(7), pp. 2121-2138; doi: 10.1084/jem.20161070.
49. Rauzi F., Kirkby N. S., Edin M. L., Whiteford J., Zeldin D. C., Mitchell J. A. and Warner T. D. (2016) Aspirin inhibits the production of proangiogenic 15(S)-HETE by platelet cyclooxygenase-1. *FASEB J*. 30(12), pp. 4256-4266; doi: 10.1096/fj.201600530R.
50. Haeggstrom J. Z. and Funk C. D. (2011) Lipoxygenase and leukotriene pathways: Biochemistry, biology, and roles in disease. *Chem Rev*. 111(10), pp. 5866-5898; doi: 10.1021/cr200246d.
51. Swystun L. L. and Liaw P. C. (2016) The role of leukocytes in thrombosis. *Blood*. 128(6), pp. 753-762; doi: 10.1182/blood-2016-05-718114.
52. Kutzner L., Goloshchapova K., Heydeck D., Stehling S., Kuhn H. and Schebb N. H. (2017) Mammalian ALOX15 orthologs exhibit pronounced dual positional specificity with docosahexaenoic acid. *Biochim Biophys Acta*. 1862(7), pp. 666-675; doi: 10.1016/j.bbalip.2017.04.001.
53. Gladine C., Newman J. W., Durand T., Pedersen T. L., Galano J.-M., Demougeot C., Berdeaux O., Pujos-Guillot E., Mazur A. and Comte B. (2014) Lipid profiling following intake of the omega 3 fatty acid DHA identifies the peroxidized metabolites F4-neuroprostanes as the best predictors of atherosclerosis prevention. *PLoS One*. 9(2):e89393; doi: 10.1371/journal.pone.0089393.
54. Hammond V. J. and O'Donnell V. B. (2012) Esterified eicosanoids: Generation, characterization and function. *Biochim Biophys Acta*. 1818(10), pp. 2403-2412; doi: 10.1016/j.bbamem.2011.12.013.
55. Ostermann A. I., Greupner T., Kutzner L., Hartung N. M., Hahn A., Schuchardt J. P. and Schebb N. H. (2018) Intra-individual variance of the human plasma oxylipin pattern: Low inter-day variability in fasting blood samples versus high variability during the day. *Anal Methods*. 10(40), pp. 4935-4944; doi: 10.1039/C8AY01753K.
56. La Frano M. R., Carmichael S. L., Ma C., Hardley M., Shen T., Wong R., Rosales L., Borkowski K., Pedersen T. L., Shaw G. M., Stevenson D. K., Fiehn O. and Newman J. W. (2018) Impact of post-collection freezing delay on the reliability of serum

metabolomics in samples reflecting the California mid-term pregnancy biobank. *Metabolomics*. 14:151; doi: 10.1007/s11306-018-1450-9.

57. Thalén S., Forsling I., Eintrei J., Söderblom L. and Antovic J. P. (2013) Pneumatic tube transport affects platelet function measured by multiplate electrode aggregometry. *Thromb Res*. 132(1), pp. 77-80; doi: 10.1016/j.thromres.2013.04.020.
58. Wallin O., Soderberg J., Grankvist K., Jonsson P. A. and Hultdin J. (2008) Preanalytical effects of pneumatic tube transport on routine haematology, coagulation parameters, platelet function and global coagulation. *Clin Chem Lab Med*. 46(10), pp. 1443-1449; doi: 10.1515/CCLM.2008.288.

Chapter 4

Formation of *trans*-epoxy fatty acids correlates with formation of isoprostanes and could serve as biomarker of oxidative stress*

In mammals, epoxy-polyunsaturated fatty acids (epoxy-PUFA) are enzymatically formed from naturally occurring all-cis PUFA by cytochrome P450 monooxygenases leading to the generation of cis-epoxy-PUFA (mixture of R,S- and S,R-enantiomers). In addition, also non-enzymatic chemical peroxidation gives rise to epoxy-PUFA leading to both, cis- and trans-epoxy-PUFA (mixture of R,R- and S,S-enantiomers). Here, we investigated for the first time trans-epoxy-PUFA and the trans/cis-epoxy-PUFA ratio as potential new biomarker of lipid peroxidation. Their formation was analyzed in correlation with the formation of isoprostanes (IsoP), which are commonly used as biomarkers of oxidative stress. Five oxidative stress models were investigated including incubations of three human cell lines as well as the in vivo model Caenorhabditis elegans with tert-butyl hydroperoxide (t-BOOH) and analysis of murine kidney tissue after renal ischemia reperfusion injury (IRI). A comprehensive set of IsoP and epoxy-PUFA derived from biologically relevant PUFA (ARA, EPA and DHA) was simultaneously quantified by LC-ESI(-)-MS/MS. Following renal IRI only a moderate increase in the kidney levels of IsoP and no relevant change in the trans/cis-epoxy-PUFA ratio was observed. In all investigated cell lines (HCT-116, HepG2 and Caki-2) as well as C. elegans a dose dependent increase of both, IsoP and the trans/cis-epoxy-PUFA ratio in response to the applied t-BOOH was observed. The different cell lines showed a distinct time dependent pattern consistent for both classes of autoxidatively formed oxylipins. Clear and highly significant correlations of the trans/cis-epoxy-PUFA ratios with the IsoP levels were found in all investigated cell lines and C. elegans. Based on this, we suggest the trans/cis-epoxy-PUFA ratio as potential new biomarker of oxidative stress, which warrants further investigation.

* Reprinted from *Prostaglandins & Other Lipid Mediators,* Vol. 144*,* Rund K. M., Heylmann D., Seiwert N., Wecklein S., Oger C., Galano J.-M., Durand T., Chen R., Gueler F., Fahrer J., Bornhorst J., Schebb N. H., Formation of *trans*-epoxy fatty acids correlates with formation of isoprostanes and could serve as biomarker of oxidative stress, 106334, Copyright (2019), with permission from Elsevier. doi: 10.1016/j.prostaglandins.2019.04.004.

Author contributions: KR designed research, performed experiments and wrote the manuscript; DH performed experiments and contributed to manuscript writing; NS, SW performed experiments; CO, JMG, TD provided standard substances and contributed to manuscript writing; RC performed experiments; FG, JF, NHS designed research, wrote the manuscript.

4.1 Introduction

Oxidative stress, i.e. the imbalance of antioxidative and oxidative mechanisms is associated with the pathophysiology of several diseases. It is characterized by an impairment of redox signaling and control in the organism, ambivalently caused and/or resulting by the disease state [1]. Various diseases are linked to oxidative stress including inflammatory, cardiovascular, respiratory and neurological diseases [2].

Elevated levels of reactive oxygen and nitrogen species (RONS) formed in the course of oxidative stress oxidatively modify biomolecules including lipids, proteins, DNA, thereby altering their biological properties and function. Polyunsaturated fatty acids (PUFA) which are essential constituents in membrane phospholipids are susceptible to free radical mediated autoxidation [3]. During this lipid peroxidation radical abstraction of a bisallylic hydrogen and subsequent addition of molecular oxygen results initially in conversion of PUFA to hydroperoxy fatty acid radicals which are further converted in chain oxidation reactions giving rise to a multitude of reactive and stable secondary oxidation products which *inter alia* bear hydro(pero)xy, epoxy and cyclic moieties [4]. Several of these products arising during non-enzymatic autoxidation are structurally similar to products formed by enzymatic conversion. However, enzymatic conversion of PUFA by cyclooxygenase (COX) results in regio- and stereospecific formation of prostaglandins (PG), whereas non-enzymatic lipid peroxidation leads to a complex mixture of regio- and stereoisomeric prostaglandin-like products, referred to as isoprostanes (IsoP), comprising in the case of arachidonic acid (ARA, C20:4 n6) 64 different F_2-IsoP isomers [5, 6]. While only free, i.e. non-esterified PUFA are enzymatically converted by COX, IsoP are formed from PUFA esterified in phospholipids and are released upon stimuli [7]. PG, like PGE_2, are known to be potent mediators of inflammation and for selected IsoP also biological activity have been shown, e.g. 15-F_{2t}-IsoP acting as renal vasoconstrictor [8]. ARA derived F_2-IsoP, especially 15-F_{2t}-IsoP (8-*iso*-$PGF_{2\alpha}$), were assessed to be valuable for the

evaluation of oxidative stress *in vivo* and the latter is commonly used as biomarker in diseases and environmental exposures implicated with oxidative stress [9-11]. However, in recent years the validity of the sole measurement of 15-F_{2t}-IsoP as biomarker of oxidative stress is regarded controversial as it besides non-enzymatic autoxidation may also arise from enzymatic conversion by COX [12, 13]. To account for the contribution of both pathways to the detected 15-F_{2t}-IsoP level, determination of the 15-F_{2t}-IsoP/$PGF_{2\alpha}$ ratio may be used to differentiate between non-enzymatic and enzymatic formation and enable accurately evaluating the underlying oxidative stress [14, 15]. Moreover, the parallel analysis of different IsoP isomers from individual as well as multiple biological relevant PUFA – as carried out in the present study – allows drawing comprehensive conclusions on the oxidative stress status independent from the origin of the analyzed specimen.

In addition to IsoP a multitude of autoxidative PUFA products is generated during lipid peroxidation. This includes products with epoxy moieties resulting from hydroperoxides *via* intramolecular homolytic substitution of the peroxide bond by an adjacent carbon radical [4]. Epoxy-PUFA are well characterized highly potent lipid mediators which possess important biological properties, e.g. acting anti-inflammatory and vasodilatory [16] and are present in body fluids and tissues (e.g. plasma, red blood cells, liver, kidney, lung, heart) [17, 18]. In mammals they are generated from enzymatic conversion of the naturally occurring all-*cis* PUFA by cytochrome P450 monooxygenases (CYP) leading to regioisomeric *cis*-epoxy-PUFA (*R,S*- and *S,R*-enantiomers, Fig. 4.1) for each of the double bonds with distinct stereo- and regioselectivity depending on the respective involved CYP isoform [19, 20]. Similarly to COX only the free, non-esterified PUFA are enzymatically converted by CYP, whereas in contrast to PG, epoxy-PUFA are mainly incorporated in lipids [21], e.g. predominantly the *sn*-2 position of phospholipids [22].

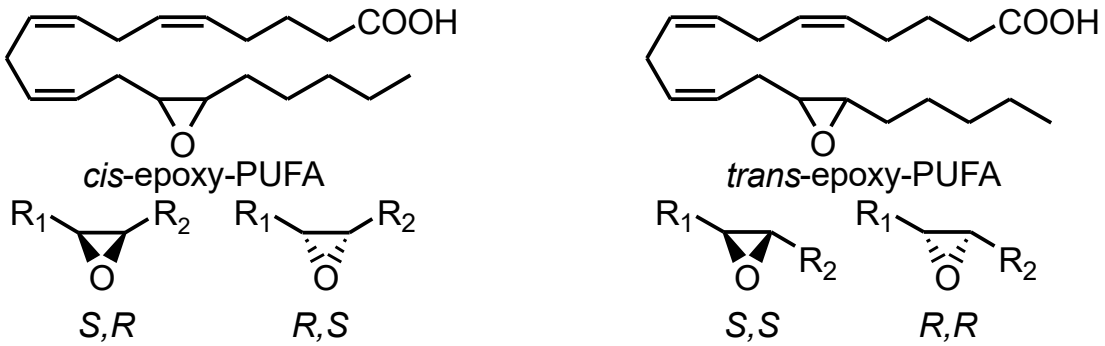

Fig. 4.1: Stereochemistry of epoxy-PUFA. Each of the four double bonds can be epoxygenated resulting in the formation of four regioisomeric epoxy-PUFA from ARA each comprising two diastereoisomers, i.e. *cis*- and *trans*-epoxy-PUFA isomers with two enantiomers (with *S,R* and *R,S* or *S,S* and *R,R* configuration, respectively).

Apart from the CYP derived *cis*-epoxy-PUFA also *trans*-epoxy-PUFA (*S,S*- and *R,R*-enantiomers, Fig. 4.1) have been detected in red blood cells (RBC) [23] and heart tissue from untreated healthy animals [24]. Exposure of RBC with the oxidative stress causing agent *tert*-butyl hydroperoxide (*t*-BOOH) led to an increase of ARA derived epoxy-PUFA compared to control [25, 26]. Regarding stereochemistry in response to *t*-BOOH treatment both diastereomers (i.e. *cis* and *trans*) increased in RBC, though a greater increase of *trans*-epoxy-ARA was observed [26]. A favored formation of *trans*- over *cis*-epoxy-ARA was also observed after exposing ARA to radical starter in benzene and liposomes [24]. However, so far no information about the time course of *trans*-epoxy-PUFA formation in biological settings and its correlation to the extent of oxidative stress is available.

In the present study we examined the formation of IsoP and epoxy-PUFA following oxidative stress to investigate the potential use of *trans*-epoxy-PUFA and the *trans/cis*-epoxy-PUFA ratio as marker of oxidative stress. For this purpose, we extended an established LC-ESI(-)-MS/MS method covering enzymatically and non-enzymatically formed oxylipins to enable the separation and parallel quantification of *cis*- and *trans*-epoxy-PUFA. The concentration and time dependent generation of the oxidative lipid metabolites was examined in three cell lines from different human tissues and the model organism *Caenorhabditis elegans (C. elegans)* causing oxidative stress by treatment with

t-BOOH, and in murine kidney tissue after renal ischemia reperfusion injury (IRI). The parallel assessment of both, IsoP – known biomarker of oxidative stress – and epoxy-PUFA allowed us to demonstrate the applicability of the *trans/cis*-epoxy-PUFA ratio as oxidative stress marker.

4.2 Experimental

4.2.1 Chemicals

Standards of regioisomeric *cis*-epoxy-PUFA (mixture of *R,S*- and *S,R*-enantiomers), isoprostane 15-F_{2t}-IsoP and the deuterated internal standards (IS) $^{2}H_{4}$-15-F_{2t}-IsoP ($^{2}H_{4}$-8-*iso*-$PGF_{2\alpha}$), $^{2}H_{11}$-5(*R,S*)-5-F_{2t}-IsoP ($^{2}H_{11}$-(±)5-$iPF_{2\alpha}$-VI), $^{2}H_{4}$-9(10)-EpOME, $^{2}H_{11}$-14(15)-EpETrE were purchased from Cayman Chemicals (local distributor: Biomol, Hamburg, Germany). Other IsoP and IsoF standards from the biologically relevant PUFA α-linolenic acid (18:3 n3, ALA), ARA, eicosapentaenoic acid (20:5 n3, EPA), adrenic acid (22:4 n6, AdA), docosapentaenoic acid (22:5 n6, n6-DPA), docosahexaenoic acid (22:6 n3, DHA) [27] were synthesized according to our chemical strategies already described in the literature [28-32]. LC-MS-grade methanol (MeOH), LC-MS-grade acetonitrile (ACN), LC-MS-grade isopropanol and LC-MS-grade acetic acid were purchased from Fisher Scientific (Schwerte, Germany). Disodium hydrogen phosphate dihydrate and *n*-hexane (HPLC Grade) were obtained from Carl Roth (Karlsruhe, Germany). Potassium hydroxide (85%) was obtained from Gruessing GmbH (Filsum, Germany). All other chemicals were purchased from Sigma Aldrich (Schnelldorf, Germany).

4.2.2 Cell culture assay

HCT-116 human colorectal carcinoma cells, Caki-2 human kidney carcinoma cells and HepG2 human liver carcinoma cells were grown in 10 cm dishes and incubated with 50 µM and 200 µM of *t*-BOOH (Sigma Aldrich, Schnelldorf,

Germany) for 30 min, 1 h and 2 h. The cells were harvested using trypsin as described and the cell pellets were stored at −80 °C until analysis [27]. Cell pellets typically contained 5×10^6 (HCT-116), 4×10^6 (Caki-2) and 20×10^6 (HepG2) cells. Cytotoxicity was assessed by the MTS assay (3-(4,5-dimethylthiazol-2-yl)-5-(3-carboxymethoxyphenyl)-2-(4-sulfophenyl)-2H-tetrazolium) as described [27, 33]. The used *t*-BOOH concentration showed no relevant effect on cell viability (> 84%) (appendix Fig. 8.6, [27]).

4.2.3 C. elegans treatment

The N2 Bristol strain, provided by the Caenorhabditis Genetics Center (CGC; University of Minnesota), was propagated at 20 °C on Nematode Growth Medium (NGM) plates spotted with the *Escherichia coli* strain OP50-1 [34]. Age-synchronized L4 stage worms were obtained by treating worms with an alkaline bleach solution (1% NaClO and 0.25 M NaOH) and growing the hatched L1 larvae on OP50-1-seeded NGM plates for approximately 48 h. Treatment was performed using 12,000 L4 stage worms. Therefore, the nematodes were exposed to 0 mM (control) and 2.5 mM *t*-BOOH for 60 min, or 6.5 mM *t*-BOOH for 15, 30, 45 or 60 min in 85 mM NaCl containing 0.01% Tween (6.5 mM represents the lethal dose 50% (LD50) following 1 h exposure (data not shown)). Worms were then pelleted by centrifugation at 1600 rpm for 2 min and washed four times in 85 mM NaCl containing 0.01% Tween. The remaining nematode pellet was snap-frozen in liquid nitrogen and stored at −80 °C until analysis.

4.2.4 Renal ischemia reperfusion injury in mice

C57BL/6J$^{ham\text{-}ztm}$ male mice (12–13 weeks of age) were purchased from the institute of laboratory animal science (Hannover Medical School, Germany). Animals were cared for in accordance with the institution's guidelines for experimental animal welfare and with the guidelines of the American Physiological Society. The animal protection committee of the local authorities

(Lower Saxony State Department for Food Safety and Animal Welfare, LAVES) approved all experiments (approval 33.14-42502-04-14/1657). Mice were housed under conventional conditions with a 12 h light/dark cycle and had free access to food (Altromin 1324 standard mouse diet) and domestic quality drinking water *ad libitum.*

Surgery to induce renal IRI was done in general isoflurane anesthesia (5% induction, 2% maintenance) in combination with iv analgetic treatment with butorphanol. IRI was induced by transient unilateral renal pedicle clamping for 35 min using a non-traumatic vascular clamp [35]. Mice were sacrificed 2 h, 4 h and 24 h after reperfusion by deep general anesthesia and total body perfusion with ice cold PBS. Kidneys were collected, immediately shock frozen and stored at −80 °C until oxylipin analysis.

4.2.5 Quantification of oxylipins

For the analysis of total, i.e. free and esterified oxylipins formed under different treatment conditions cell pellets (comprising 5 × 10^6 HCT-116, 4 × 10^6 Caki-2 or 20 × 10^6 HepG2 cells) and nematode pellets as well as kidney tissue samples (25 ± 3 mg) were extracted following alkaline hydrolysis using anion exchange Bond Elut Certify II SPE cartridges (Agilent, Waldbronn, Germany) as described [27, 36].

In brief, to cell pellets (HCT-116, HepG2, Caki-2), *C. elegans* pellets and kidney tissue samples 10 µL of IS solution (100 nM of $^2H_4$-15-F_{2t}-IsoP, $^2H_{11}$-5(*R,S*)-5-F_{2t}-IsoP, C19-17-*epi*-17-F_{1t}-PhytoP, C21-15-F_{2t}-IsoP, $^2H_4$-6-keto-$PGF_{1\alpha}$, $^2H_4$-PGE_2, $^2H_4$-PGD_2, $^2H_4$-TxB_2, $^2H_4$-LTB_4, $^2H_4$-9-HODE, $^2H_8$-5-HETE, $^2H_8$-12-HETE, $^2H_6$-20-HETE, $^2H_{11}$-14,15-DiHETrE, $^2H_{11}$-14(15)-EpETrE, $^2H_4$-9(10)-EpOME and $^2H_4$-9,10-DiHOME), 10 µL of antioxidant solution (0.2 mg/mL BHT and EDTA, 100 µM indomethacin, 100 µM of the soluble epoxide hydrolase inhibitor ***t**rans*-4-[4-(3-**a**damantan-1-yl-**u**reido)-**c**yclohexyloxy]-**b**enzoic acid (*t*-AUCB) [37] in MeOH/water (50/50, *v/v*)) and 50 µL water were added. The samples were

homogenized after addition of 400 µL isopropanol with a vibration ball mill (MM 400, Retsch, Haan, Germany) using two stainless steel beads (3 mm, 10 min, 25 Hz). After hydrolysis (300 µL 1.5 M KOH (25/75, H_2O/MeOH, *v/v*) for 30 min at 60 °C) the samples were immediately cooled, neutralized using acetic acid (50%) and mixed with 2000 µL 0.1 M disodium hydrogen phosphate buffer (pH = 6.0) followed by SPE. After sample loading, the cartridges were washed with one column volume of each water and MeOH/water (50/50, *v/v*) and dried. The analytes were eluted with 2 mL of 75/25 *(v/v)* ethylacetate/*n*-hexane with 1% acetic acid, evaporated and the residue was resuspended in 50 µL MeOH (containing 40 nM of 1-(1-(ethylsulfonyl)piperidin-4-yl)-3-(4-(trifluoromethoxy)-phenyl)urea as IS2 for the calculation of the extraction efficiency of the IS). After centrifugation (10 min, 4 °C, 20,000 × g) the samples were analyzed by RP-LC-MS/MS (6500 QTRAP, Sciex, Darmstadt, Germany) in scheduled selected reaction monitoring mode following negative electrospray ionization as described [27].

4.2.6 Data analysis

Oxylipin concentrations were quantified using external calibration with authentic standards (linear fitting with $1/x^2$ weighting) based on the analyte to corresponding IS area ratio as described [27]. For each epoxy-fatty acid regioisomer both *cis*- and *trans*-epoxy-PUFA isomers were quantified using the calibration curve of corresponding *cis*-epoxy-PUFA (identified with authentic standards). Based on that, the *trans/cis*-epoxy-PUFA ratios were calculated. For 7(8)-EpDPE and 5(6)-EpETE due to absence of accurate quantitative standards only the *trans/cis*-epoxy-PUFA ratio could be determined. *Trans*-epoxy-PUFA isomers eluting 0.14–0.3 min after their corresponding *cis*-isomers (Fig. 4.2) were identified based on retention time and identical MS-fragmentation pattern as described [23, 24, 26].

Data evaluation and statistical analyses were performed as indicated using GraphPad Prism version 6.01 for Windows (GraphPad Software, La Jolla California USA, www.graphpad.com).

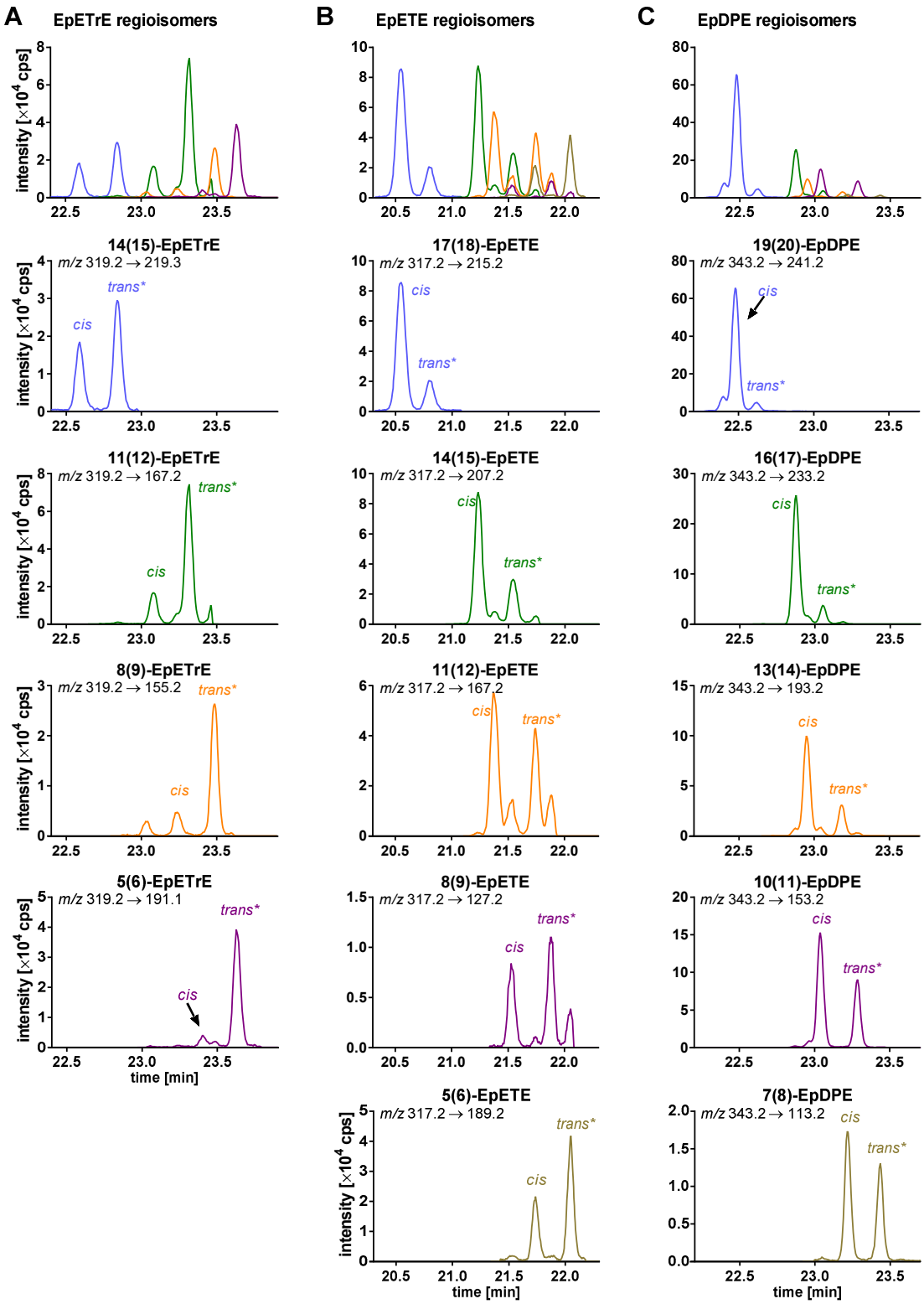

Fig. 4.2: Chromatographic separation of epoxy-PUFA regioisomers. **(A)** ARA derived EpETrE in HCT-116 cells following incubation with 200 µM *t*-BOOH for 2 h. **(B)** EPA derived EpETE in *C. elegans* following incubation with 6.5 mM *t*-BOOH for 1 h and **(C)** DHA derived EpDPE in kidney tissue after unilateral IRI for 35 min and 2 h after reperfusion. Shown are mass transitions used for quantification and determination of *trans/cis*-ratio of individual epoxy-PUFA regioisomers.

4.3 Results

In the present study using a comprehensive LC-MS/MS method total, i.e. free and esterified, levels of IsoP as well as *cis*- and *trans*-epoxy-PUFA derived from different precursor PUFA were simultaneously quantified in cell pellets and *C. elegans* incubated with oxidative stress generating *t*-BOOH, and in murine kidney tissue after renal ischemia reperfusion injury.

4.3.1 Formation of IsoP

IsoP in cells following treatment with t-BOOH

In cell pellets from colorectal (HCT-116), renal (Caki-2) and hepatic (HepG2) origin 6 IsoP regioisomers derived from 4 precursor PUFA (ARA, EPA, DHA, AdA) were quantified. Regarding detected isomers the regioisomers carrying the hydroxyl group in proximity to the carboxy function, i.e. ARA derived 5(*R,S*)-5-F_{2t}-IsoP, EPA derived 5(*R,S*)-5-F_{3t}-IsoP, DHA derived 4(*R,S*)-4-F_{4t}-NeuroP and AdA derived *ent*-7(*R,S*)-7-F_{2t}-dihomo-IsoP showed higher concentration than other regioisomers from the same PUFA or were the only regioisomers detected as it is the case for AdA derived F_{2t}-dihomo-IsoP. Under basal conditions in HCT-116 cells only 5(*R,S*)-5-F_{2t}-IsoP, 5(*R,S*)-5-F_{3t}-IsoP and 4(*R,S*)-4-F_{4t}-NeuroP were detected, while in Caki-2 and HepG2 cells additionally other regioisomers (15-F_{2t}-IsoP and 10(*R,S*)-10-F_{4t}-NeuroP) were found. Interestingly, basal levels of detected IsoP in Caki-2 cells were 2–7-fold higher than in HepG2 and 6–20-fold higher than in HCT-116 cells. In all cell lines incubation with *t*-BOOH led to an increase in IsoP formation, however the dose and time dependent pattern showed considerable differences between the cell types, though being similar for all regioisomers within the individual cell types (Fig. 4.3).

Fig. 4.3 (right, page 83): Total levels of representative **(A)** IsoP and **(B)** epoxy-PUFA derived from ARA, EPA and DHA following incubation of **(I)** HCT-116, **(II)** HepG2 and **(III)** Caki-2 cells with 50 µM and 200 µM *tert*-butyl hydroperoxide (*t*-BOOH) for 0.5 h, 1 h and 2 h. Shown are mean ± SD (HCT-116: n = 4, HepG2: n = 3, Caki-2: n = 4). For epoxy-PUFA the *trans/cis*-epoxy-PUFA-ratio (*trans/cis*) is indicated above the corresponding bars.

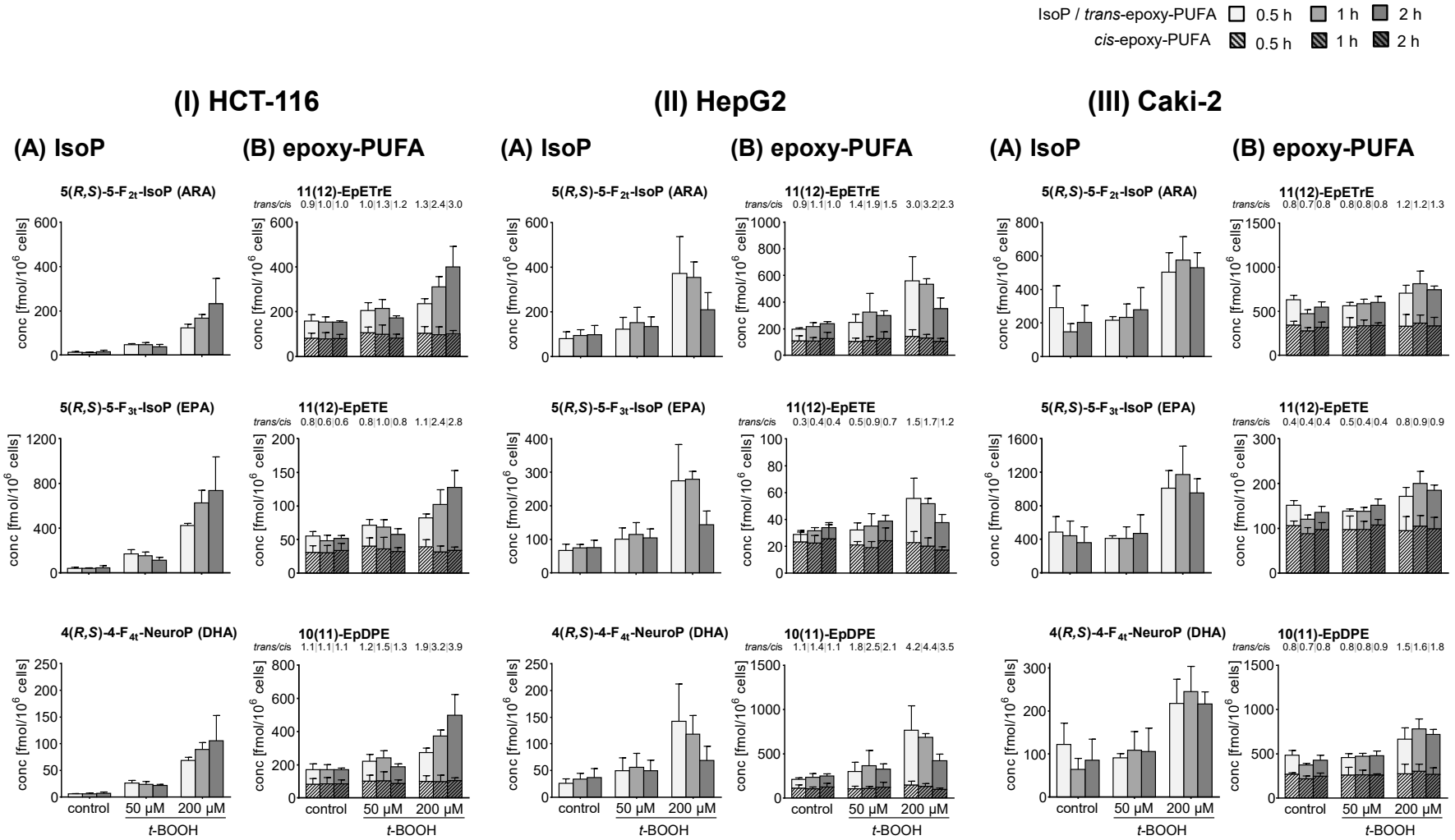
IsoP / trans-epoxy-PUFA 0.5 h 1 h 2 h
cis-epoxy-PUFA 0.5 h 1 h 2 h
(I) HCT-116
(II) HepG2
(III) Caki-2
(A) IsoP
(B) epoxy-PUFA
5(R,S)-5-F2t-IsoP (ARA)
11(12)-EpETrE
5(R,S)-5-F3t-IsoP (EPA)
11(12)-EpETE
4(R,S)-4-F4t-NeuroP (DHA)
10(11)-EpDPE
conc [fmol/10^6 cells]
trans/cis
control
50 µM
200 µM
t-BOOH

In HCT-116 cells a dose dependent increase of IsoP levels was observed leading to 3–5-fold and 10–17-fold higher IsoP concentrations compared to control with 50 µM and 200 µM *t*-BOOH, respectively (Fig. 4.3 (I) A). While with 50 µM *t*-BOOH no effect of the incubation time (0.5 h – 2 h) was observed, 200 µM *t*-BOOH induced a trend towards higher IsoP levels with longer incubation time. In HepG2 cells only 200 µM of *t*-BOOH led to an increase of IsoP levels compared to control (Fig. 4.3 (II) A). Interestingly, with longer incubation time a decrease in IsoP concentrations was observed leading at 2 h to almost same concentrations as with 50 µM *t*-BOOH. In Caki-2 cells only incubation with 200 µM *t*-BOOH led to a slight increase of IsoP concentrations, however here no time dependent change of IsoP levels was observed (Fig. 4.3 (III) A).

IsoP in C. elegans following treatment with t-BOOH

In nematode pellets of wildtype N2 *C. elegans* only EPA derived 5(*R,S*)-5-F_{3t}-IsoP were detected in the control group. Incubation with *t*-BOOH led to an increase and additional formation of EPA derived 8(*R,S*)-8-F_{3t}-IsoP as well as ARA derived 15-F_{2t}-IsoP and 5(*R,S*)-5-F_{2t}-IsoP. A dose dependent increase in IsoP levels was observed with the applied *t*-BOOH concentration leading to 4–6-fold higher IsoP levels for 6.5 mM compared to 2.5 mM *t*-BOOH after 60 min incubation (Fig. 4.4 (I) A). Also, longer incubation time led to a gradual increase resulting in 4–6-fold higher IsoP levels for 60 min compared to 15 min incubation with 6.5 mM *t*-BOOH (Fig. 4.4 (II) A).

Fig. 4.4 (right, page 85): Total levels of **(A)** IsoP and **(B)** epoxy-PUFA derived from ARA and EPA in *C. elegans* incubated for **(I)** 60 min with 2.5 mM and 6.5 mM *t*-BOOH and for **(II)** 15, 30, 45 and 60 min with 6.5 mM *t*-BOOH. Shown are mean ± SD (n = 2–6). In case the levels do not exceed the lower limit of quantification (LLOQ) in one treatment group, the LLOQ is indicated as a dashed line. For epoxy-PUFA the *trans/cis*-epoxy-PUFA-ratio (*trans/cis*) is indicated above the corresponding bars. Statistical differences between control and the treatment groups were evaluated by one-way ANOVA followed by Tukey post-test. For dose dependent formation of 5(*R,S*)-5-F_{2t}-IsoP unpaired t-test was used. For time dependent formation only differences between control and treatment groups are shown, results for differences between all treatments groups are summarized in appendix Tab. 8.3 (* $p < 0.05$, ** $p < 0.01$, *** $p < 0.001$).

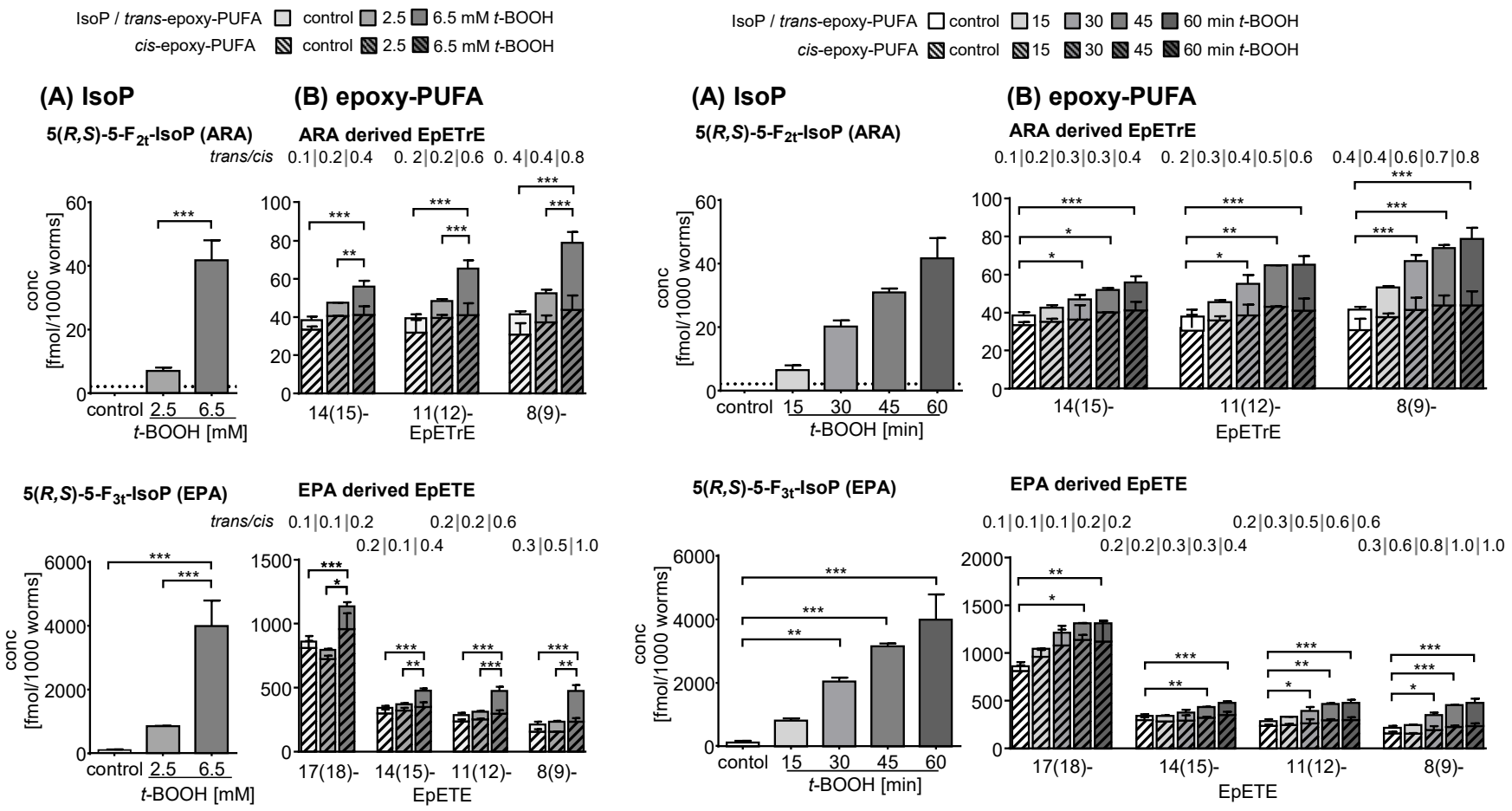
(I) Dose dependent formation after 60 min
IsoP / trans-epoxy-PUFA control 2.5 6.5 mM t-BOOH
cis-epoxy-PUFA control 2.5 6.5 mM t-BOOH
(A) IsoP
(B) epoxy-PUFA
5(R,S)-5-F2t-IsoP (ARA)
ARA derived EpETrE
trans/cis 0.1|0.2|0.4 0. 2|0.2|0.6 0. 4|0.4|0.8
conc [fmol/1000 worms]
control 2.5 6.5
t-BOOH [mM]
14(15)-
11(12)-
8(9)-
EpETrE
5(R,S)-5-F3t-IsoP (EPA)
EPA derived EpETE
trans/cis 0.1|0.1|0.2 0.2|0.2|0.6
0.2|0.1|0.4 0.3|0.5|1.0
17(18)-
14(15)-
11(12)-
8(9)-
EpETE
(II) Time dependent formation at 6.5 mM t-BOOH
IsoP / trans-epoxy-PUFA control 15 30 45 60 min t-BOOH
cis-epoxy-PUFA control 15 30 45 60 min t-BOOH
(A) IsoP
(B) epoxy-PUFA
5(R,S)-5-F2t-IsoP (ARA)
ARA derived EpETrE
0.1|0.2|0.3|0.3|0.4 0. 2|0.3|0.4|0.5|0.6 0.4|0.4|0.6|0.7|0.8
conc [fmol/1000 worms]
control 15 30 45 60
t-BOOH [min]
14(15)-
11(12)-
8(9)-
EpETrE
5(R,S)-5-F3t-IsoP (EPA)
EPA derived EpETE
0.1|0.1|0.1|0.2|0.2 0.2|0.3|0.5|0.6|0.6
0.2|0.2|0.3|0.3|0.4 0.3|0.6|0.8|1.0|1.0
contol 15 30 45 60
17(18)-
14(15)-
11(12)-
8(9)-
EpETE

IsoP in murine kidneys after ischemia reperfusion injury

In murine kidney tissue ARA derived 5(*R,S*)-5-F_{2t}-IsoP and 15-F_{2t}-IsoP and DHA derived 4(*R,S*)-4-F_{4t}-NeuroP and 10(*R,S*)-10-F_{4t}-NeuroP were detected with higher levels of the regioisomers carrying the hydroxyl group in proximity to the carboxy function. While in IRI tissue 2 h after reperfusion higher levels of ARA derived IsoP were observed compared to unclamped contralateral kidney tissue, DHA derived NeuroP remain almost unchanged. 4 h after reperfusion higher levels for both, ARA and DHA derived IsoP were observed in IRI tissue compared to unclamped control. Interestingly, 24 h after unilateral IRI lower levels of DHA derived NeuroP were observed in the IRI kidney compared to the contralateral unclamped kidney, while levels of ARA derived IsoP were similar in the IRI and unclamped kidney (Fig. 4.5 A).

4.3.2 Formation of epoxy-PUFA

Epoxy-PUFA in cells following treatment with t-BOOH

In cell pellets from colorectal (HCT-116), renal (Caki-2) and hepatic (HepG2) origin for all epoxy-PUFA derived from ARA (i.e. EpETrE), EPA (i.e. EpETE) and DHA (i.e. EpDPE) *cis*- and *trans*-isomers could be determined. However as a result of chromatographic interference in HCT-116 cells *cis*-19(20)-EpDPE and in HepG2 cells *cis*-8(9)-EpETE were not evaluable.

In control incubations the *trans/cis*-epoxy-PUFA ratios of the respective regioisomers were similar between the different cell types, however differed between the individual regioisomers. While for most regioisomers levels of *cis*-isomers were higher than of *trans*-isomers, for regioisomers carrying the epoxy moiety in the middle or front part of the carbon chain (i.e. 8(9)-EpETrE, 11(12)-EpETrE, 5(6)-EpETE, 7(8)-EpDPE and 10(11)-EpDPE) the ratios of *trans/cis*-isomers were approximately equal (0.7–1.4) or higher as for 5(6)-EpETrE (*trans/cis*-ratio > 1.5).

Incubation with *t*-BOOH led in all cell lines to an increase of *trans*-epoxy-PUFA levels, while levels of respective *cis*-isomers remained almost constant, resulting in an increase of the *trans/cis*-epoxy-PUFA ratios. However, dose and time dependent formation of *trans*-epoxy-PUFA differed between the investigated cell lines with the individual regioisomers showing the same pattern within the particular cell types irrespective of the precursor PUFA (Fig. 4.3). In HCT-116 cells with 50 µM *t*-BOOH *trans*-epoxy-PUFA remained almost constant, whereas 200 µM *t*-BOOH led to 1.7–6.6-fold higher levels of *trans*-isomers compared to control. Regarding incubation time, only with 200 µM *t*-BOOH a trend towards higher levels of *trans*-epoxy-PUFA with longer incubation was observed, leading to a 1.7–2.7-fold increase of the *trans/cis*-ratios for 1 h and 2 h compared to 0.5 h incubation (Fig. 4.3 (I) B). In HepG2 cells 50 µM *t*-BOOH led only to a slight increase of the *trans/cis*-ratios (1.5–1.8-fold), while with 200 µM *t*-BOOH *trans/cis*-ratios were 2.0–5.2-fold higher compared to control. Similar to HCT-116 cells with 50 µM *t*-BOOH *cis*- and *trans*-isomer levels remained almost unchanged with longer incubation time. In contrast, with 200 µM *t*-BOOH levels of *trans*-epoxy-PUFA increased after 0.5 h and remain similar after 1 h, however after 2 h of incubation a trend towards lower levels of *cis*- and *trans*-epoxy-PUFA was observed (Fig. 4.3 (II) B). In Caki-2 cells only with 200 µM *t*-BOOH a slight trend towards higher levels of *trans*-epoxy-PUFA was observed, however neither 50 µM nor 200 µM *t*-BOOH led to a time dependent change of epoxy-PUFA levels (Fig. 4.3 (III) B).

Epoxy-PUFA in C. elegans following treatment with t-BOOH

In non-exposed wildtype N2 *C. elegans cis*- and *trans*-isomers of all analyzed epoxy-PUFA regioisomers derived from ARA and EPA were detected. Levels of EPA derived epoxy-PUFA were markedly higher than ARA derived epoxy-PUFA. Interestingly, levels of the terminal regioisomers, i.e. 14(15)-EpETrE and 17(18)-EpETE, were different compared to the other regioisomers. While levels of all ARA derived regioisomers were in the same range, 17(18)-EpETE showed 2.7–5.2-fold higher basal levels than the other EPA derived regioisomers. Incubation with *t*-BOOH led to a dose and time dependent increase in epoxy-

PUFA levels. With 2.5 mM *t*-BOOH for 60 min both, *cis*- and *trans*-isomers showed a slight but similar trend towards higher levels compared to control resulting in unchanged *trans/cis*-ratios. Further increasing the applied *t*-BOOH concentration to 6.5 mM led to a favored formation of *trans*- over *cis*-isomers, leading to a 2.3–2.9-fold increase in *trans/cis*-ratios compared to control (Fig. 4.4 (I) B). A similar pattern was also observed regarding incubation time with 6.5 mM *t*-BOOH. While after 15 min *cis*- and *trans*-isomers increased only slightly though to a similar extent, longer incubation (30–60 min) resulted in a favored formation of *trans*- over *cis*-isomers. Consequentially *trans/cis*-ratios increased gradually with longer incubation time resulting in 1.7–2.4-fold higher *trans/cis*-ratios for 60 min compared to 15 min incubation (Fig. 4.4 (II) B).

Epoxy-PUFA in murine kidney after ischemia reperfusion injury

In murine kidney tissue only for ARA and DHA derived epoxy-PUFA regioisomers *cis*- and *trans*-isomers were detected. For both precursor PUFA basal levels of individual epoxy-PUFA regioisomers showed a distinct distribution of *trans*- and *cis*-isomers depending on the position of the epoxy-moiety relative to the carboxy-function: the closer the epoxy-moiety to the carboxy terminus the higher the observed *trans/cis*-ratio (appendix Fig. 8.7). Following unilateral IRI, 2 h after reperfusion levels of epoxy-PUFA remained almost unchanged, while 4 h after reperfusion both *cis*- and *trans*-epoxy-PUFA showed a slight increase compared to unclamped kidney resulting in almost unchanged *trans/cis*-ratios. 24 h after reperfusion levels of ARA derived epoxy-PUFA were similar in IRI and unclamped kidney tissue. While in contrast for DHA derived epoxy-PUFA a decrease of *cis*-isomers was observed in IRI compared to unclamped kidney tissue with almost unchanged *trans*-epoxy-PUFA levels. Interestingly, this decrease was more pronounced for terminal isomers, i.e. 19(20)- and 16(17)-EpDPE compared to 13(14)- and 10(11)-EpDPE (Fig. 4.5 B, appendix Fig. 8.7).

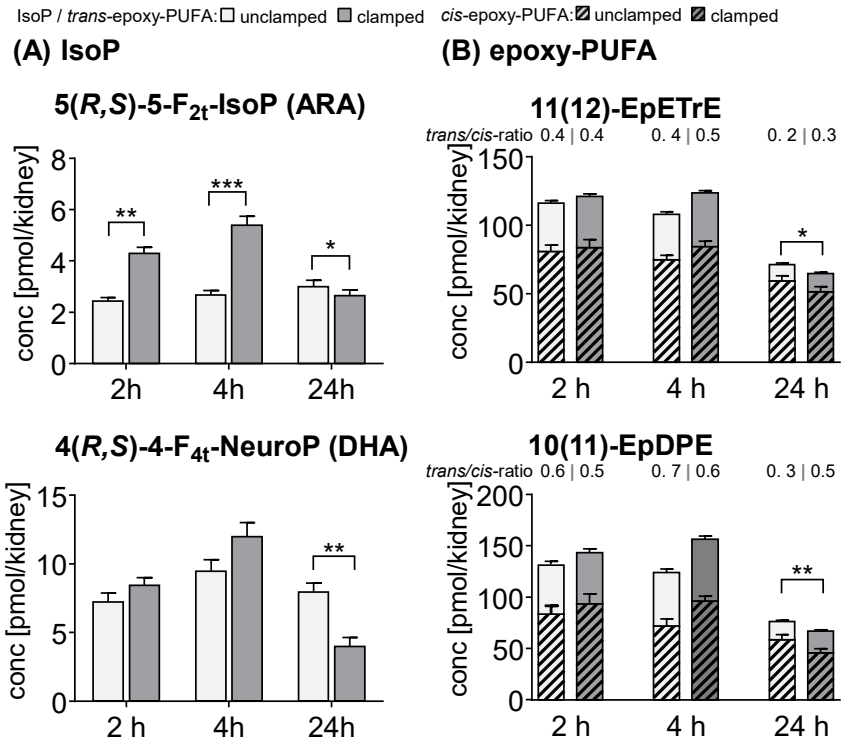

Fig. 4.5: Total levels of **(A)** IsoP and **(B)** epoxy-PUFA derived from ARA and DHA in murine kidney tissue following unilateral IRI for 35 min. Shown are mean ± SEM (n = 6) in the unclamped and IRI kidneys 2 h, 4 h and 24 h after reperfusion. For epoxy-PUFA the *trans/cis*-epoxy-PUFA-ratio (*trans/cis*-ratio) is indicated above the corresponding bars. Statistical differences between the unclamped and IRI kidneys were evaluated by paired t-test for 5(*R,S*)-5-F_{2t}-IsoP, 4(*R,S*)-4-F_{4t}-NeuroP and the *trans/cis*-epoxy-PUFA ratios (* $p < 0.05$, ** $p < 0.01$, *** $p < 0.001$).

4.3.3 Correlation of IsoP

In cell lines as well as in *C. elegans* following incubation with *t*-BOOH a clear correlation between IsoP formation and the *trans/cis*-epoxy-PUFA ratio was found (Fig. 4.6, Tab. 4.1). Pearson correlations between the levels of IsoP regioisomers carrying the hydroxyl group in proximity to the carboxy-function and the ratio of *trans/cis*-epoxy-PUFA regioisomers from the corresponding PUFA were determined (Tab. 4.1): ARA derived 5(*R,S*)-5-F_{2t}-IsoP was correlated with EpETrE regioisomers, EPA derived 5(*R,S*)-5-F_{3t}-IsoP with EpETE regioisomers and DHA derived 4(*R,S*)-4-F_{4t}-NeuroP with EpDPE regioisomers. For all epoxy-PUFA regioisomers positive and highly significant correlations with IsoP levels were obtained in the three cell lines and *C. elegans* (Fig. 4.6, Tab. 4.1). As no significant increase in the *trans/cis*-ratio was found in

murine renal IRI (Fig. 4.5, appendix Fig. 8.7) consequently no correlation of IsoP levels and *trans/cis*-epoxy-PUFA ratios resulted.

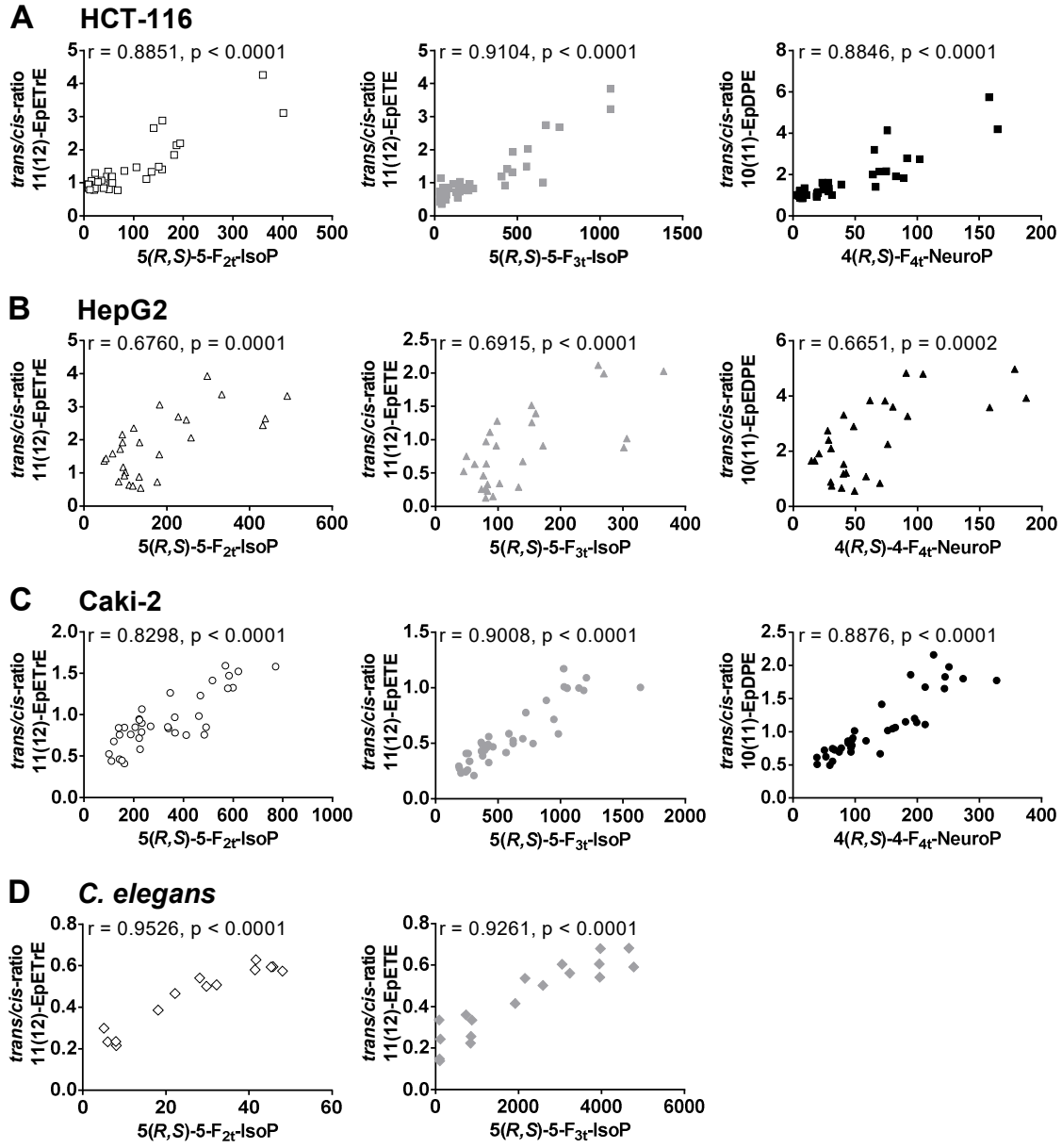

Fig. 4.6: Correlation between the *trans/cis*-ratio of individual epoxy-PUFA regioisomers (i.e. for ARA 11(12)-EpETrE, for EPA 11(12)-EpETE, for DHA 10(11)-EpDPE) and the most abundant IsoP isomer derived from the same precursor PUFA (i.e. for ARA 5(*R,S*)-5-F_{2t}-IsoP, for EPA 5(*R,S*)-5-F_{3t}-IsoP, for DHA 4(*R,S*)-4-F_{4t}-NeuroP). Shown are pearson correlation coefficients r and respective p-values for ARA, EPA and DHA derived oxidative metabolites in **(A)** HCT-116, **(B)** HepG2 and **(C)** Caki-2 cells, as well as in **(D)** *C. elegans* incubated with *t*-BOOH.

Tab. 4.1: Pearson correlations between the *trans/cis*-ratio of individual epoxy-PUFA regioisomers and the most abundant IsoP isomer derived from the same precursor PUFA (i.e. for ARA 5(*R,S*)-5-F_{2t}-IsoP, for EPA 5(*R,S*)-5-F_{3t}-IsoP, for DHA 4(*R,S*)-4-F_{4t}-NeuroP). Shown are pearson correlation coefficients r for ARA, EPA and DHA derived oxidative metabolites in HCT-116, HepG2 and Caki-2 cells, as well as in *C. elegans* incubated with *t*-BOOH, and the respective p-values. * not evaluable due to chromatographic interference.

ARA derived	**5(*R,S*)-5-F_{2t}-IsoP**			
EpETrE	**HCT-116**	**HepG2**	**Caki-2**	***C. elegans***
14(15)-	r = 0.9231 p < 0.0001	r = 0.7177 p < 0.0001	r = 0.8764 p < 0.0001	r = 0.9121 p < 0.0001
11(12)-	r = 0.8851 p < 0.0001	r = 0.6760 p = 0.0001	r = 0.8298 p < 0.0001	r = 0.9526 p < 0.0001
8(9)-	r = 0.9085 p < 0.0001	r = 0.6261 p = 0.0005	r = 0.848 p < 0.0001	r = 0.9150 p < 0.0001
5(6)-	r = 0.8952 p < 0.0001	r = 0.6906 p < 0.0001	r = 0.7978 p < 0.0001	r = 0.8950 p < 0.0001
EPA derived	**5(*R,S*)-5-F_{3t}-IsoP**			
EpETE	**HCT-116**	**HepG2**	**Caki-2**	***C. elegans***
17(18)-	r = 0.8207 p < 0.0001	r = 0.8231 p < 0.0001	r = 0.7832 p < 0.0001	r = 0.9379 p < 0.0001
14(15)-	r = 0.8610 p < 0.0001	r = 0.7929 p < 0.0001	r = 0.8303 p < 0.0001	r = 0.9015 p < 0.0001
11(12)-	r = 0.9104 p < 0.0001	r = 0.6915 p < 0.0001	r = 0.9008 p < 0.0001	r = 0.9261 p < 0.0001
8(9)-	r = 0.8649 p < 0.0001	*	r = 0.7839 p < 0.0001	r = 0.9535 p < 0.0001
5(6)-	r = 0.8335 p < 0.0001	r = 0.6162 p =0.0006	r = 0.8749 p < 0.0001	r = 0.9675 p < 0.0001
DHA derived	**4(*R,S*)-4-F_{4t}-NeuroP**			
EpDPE	**HCT-116**	**HepG2**	**Caki-2**	
19(20)-	*	r = 0.7461 p < 0.0001	r = 0.7327 p < 0.0001	
16(17)-	r = 0.8621 p < 0.0001	r = 0.6950 p < 0.0001	r = 0.8899 p < 0.0001	
13(14)-	r = 0.8342 p < 0.0001	r = 0.7489 p < 0.0001	r = 0.8942 p < 0.0001	
10(11)-	r = 0.8846 p < 0.0001	r = 0.6651 p = 0.0002	r = 0.8876 p < 0.0001	
7(8)-	r = 0.9006 p <0.0001	r = 0.5821 p = 0.0014	r = 0.9042 p < 0.0001	

4.4 Discussion

In the present study total levels of IsoP and *cis*- and *trans*-epoxy-PUFA were simultaneously quantified. Based on that, the correlation between these autoxidatively formed oxylipins during oxidative stress was evaluated in three models: (i) *t*-BOOH induced stress in three cultured cell lines and in (ii) *C. elegans* and (iii) following ischemic reperfusion injury in the kidney in mice.

ARA derived F_2-IsoP are well established marker of oxidative damage formed during lipid peroxidation *in vivo.* Particularly 15-F_{2t}-IsoP (8-*iso*-$PGF_{2\alpha}$) is commonly used as biomarker in diseases and environmental exposures related to oxidative stress [8, 9, 11]. In line we found a strong increase of IsoP in response to *t*-BOOH in all cell lines as well as in *C. elegans* (Fig. 4.3, Fig. 4.4). The modulation of IsoP was markedly different between the cell lines regarding both, dose and time dependency: While in HCT-116 cells already 50 µM *t*-BOOH led to an increase in IsoP levels, in HepG2 and Caki-2 cells a trend towards higher IsoP levels was only observed in incubations with 200 µM *t*-BOOH (Fig. 4.3). This could result from different intracellular RONS detoxifying mechanisms between the cell types, breaking down *t*-BOOH generated radicals and preventing oxidative damage. It seems that only if a threshold in intracellular ROS burden is reached, an increased IsoP formation results. For HCT-116 cells this level seems to be reached at *t*-BOOH concentrations above 50 µM, while for Caki-2 cells only at a high concentration of 200 µM *t*-BOOH IsoP levels are elevated. A threshold of oxidative stress inducing noxae for the formation of IsoP depending on the concentration of oxidative stress inducer was also observed previously in HepG2 cells treated with the redoxcycler paraquat [38]. Here only incubation with concentrations equal or above 100 µM led to an increase in IsoP formation compared to control.

Noteworthy, with high concentration of *t*-BOOH (200 µM) for all detected regioisomers, IsoP levels showed a distinct time dependent pattern in the different cell lines. In HCT-116 cells a trend towards higher IsoP levels with

longer incubation time was observed (Fig. 4.3 (I)). Consistently, a similar time dependent increase of IsoP was previously reported for copper induced peroxidation of ARA and EPA containing phospholipids or of cell lysates [38, 39]. In contrast, in HepG2 cells levels of IsoP showed a decreasing trend with longer incubation and remained unaffected by the incubation time in Caki-2 cells (Fig. 4.3). A decrease in total IsoP levels as observed in HepG2 cells might result from metabolic degradation of the formed oxylipins. As formation of IsoP occurs *in situ* on phospholipids [7] hydrolysis of IsoP containing phospholipids by phospholipase A_2 seems likely to be involved in the observed decrease of total IsoP levels. Indeed, the intracellular type II platelet-factor-acetyl hydrolase exhibiting negligible phospholipase activity against long-chain-PUFA containing membrane phospholipids [40, 41] hydrolyses F_2-IsoP containing phospholipids [42] and was shown to translocate from the cytosol to the membrane upon oxidative stress stimulus [43]. Furthermore, a time course similar to the one observed in HepG2 cells was also observed following CCl_4 induced peroxidation in the rat [7]. Here, total IsoP levels in the liver increased rapidly after CCl_4 was applied with a peak after 2 h, followed by a decrease over time leading to almost restored levels after 24 h. Correspondingly, plasma level of free IsoP arising from release of esterified IsoP showed a similar, however delayed time course, further supporting the hypothesis of phospholipase contribution.

Among the multitude of different IsoP regio- and stereoisomers that can be formed during lipid peroxidation (e.g. for ARA a total of 64 different F_2-isomers) [5], we observed a favored formation of selected regioisomers in all investigated cell lines, *C. elegans* as well as kidney tissue. Regarding IsoP isomers covered in our analysis, regioisomers carrying the side chain hydroxyl group in proximity to the carboxy group, i.e. ARA derived 5(*R,S*)-5-F_{2t}-IsoP, EPA derived 5(*R,S*)-5-F_{3t}-IsoP, DHA derived 4(*R,S*)-4-F_{4t}-NeuroP and AdA derived *ent*-7(*R,S*)-7-F_{2t}-dihomo-IsoP, were observed in higher abundance than its regioisomers. This is consistent with previous studies where a preferred formation of particular regioisomers was observed. Similarly to our results for ARA the 5- and 15-F_{2t}-

IsoP, for EPA the 5- and 18-F_{3t}-IsoP [44] and for DHA the 4- and 20-F_{4t}-NeuroP [45] regioisomers were observed in greater abundance. This may be explained by further oxidative conversion of the precursors involved in the formation of other IsoP regioisomers during autoxidation. One could also expect, that the regioisomers bearing the hydroxyl-group at C4 or C5 position are also more stable towards β-oxidation which could contribute to higher levels of these regioisomers, as has been previously observed for other 5-hydroxy eicosanoids (e.g. leukotrienes) [46, 47].

Remarkably, in all cell lines, levels of these regioisomers were in a similar range for ARA, EPA and DHA derived IsoP (Fig. 4.3), while in *C. elegans* concentration of EPA derived 5(*R,S*)-5-F_{3t}-IsoP was considerably higher than the corresponding ARA derived regioisomer (Fig. 4.4). As PUFA serve as substrates for IsoP formation, the fatty acid composition and PUFA pattern affect the levels of respective formed IsoP. Consistently, the observed high level of EPA derived F_3-IsoP in *C. elegans* is in agreement with the predominant relative EPA content compared to ARA [48].

Regarding formation of epoxy-PUFA, the *trans/cis*-epoxy-PUFA ratio increased with the applied *t*-BOOH concentration in all cell lines and *C. elegans* and showed a distinct time dependent pattern in the different cell lines (Fig. 4.3, Fig. 4.4). The similar pattern in comparison with the observed IsoP levels suggests the contribution of related mechanisms (discussed above). Overall the increase in the *trans/cis*-epoxy-PUFA ratio was mainly caused by a favored formation of *trans*- compared to *cis*-isomers during *t*-BOOH induced oxidative stress. This supports previous findings demonstrating formation of epoxy-PUFA during autoxidation, as has been shown for ARA derived EpETrE in RBC incubated with *t*-BOOH [25, 26]. Consistently, both, free radical induced peroxidation in benzene and liposomes, as well as exposure of RBC to *t*-BOOH led to a favored formation of *trans*- over *cis*-epoxy-ARA [24, 26]. As double bonds in naturally occurring PUFA are oriented all-*cis* a possible mechanism leading to the formation of both, *cis*- and *trans*-epoxy-PUFA could involve PUFA

carbon centered radicals with an adjacent peroxyl group. These are formed at the position of the double bond in the PUFA molecule during the radical chain reaction. These carbon radicals allow for free rotation of the σ-bond prior to intramolecular attack of the peroxyl bond by the reactive carbon radical which leads *via* homolytic substitution to the formation of an epoxy-moiety oriented either *cis* or *trans* [4, 24].

Irrespective of the precursor PUFA the observed increase in the *trans/cis*-epoxy-PUFA ratio following *t*-BOOH induced oxidative stress was similar for all regioisomers, though being slightly higher for 5(6)-EpETE. However, this has to be regarded with caution as 5(6)-EpETE, like 5(6)-EpETrE might rapidly degrade forming a six-membered δ-lacton [49]. Additionally, also high basal levels of *cis*-epoxy-PUFA derived from CYP as observed for the preferred formation of the ω3-epoxygenation product 17(18)-EpETE compared to its other regioisomers in *C. elegans* (Fig. 4.4) might hamper the suitability of the respective *trans/cis*-ratio reflecting the oxidative damage.

Here, we tested for the first time if the *trans/cis*-epoxy-PUFA ratio can reflect oxidative stress. For this purpose we correlated the *trans/cis*-epoxy-PUFA ratio with the level of IsoP, which are established biomarkers of lipid peroxidation. Considering the consistent time and *t*-BOOH concentration dependent pattern, quite clear, positive, highly significant correlations of IsoP levels with the *trans/cis*-epoxy-PUFA ratio were observed for all epoxy-PUFA regioisomers in *t*-BOOH induced oxidative stress in all three cell lines and *C. elegans* (Fig. 4.6, Tab. 4.1). Thus, we suggest that the *trans/cis*-epoxy-PUFA ratio might serve as alternative oxidative stress marker.

However, in the evaluated *in vivo* model of murine renal IRI, the moderate increase of IsoP was not accompanied by an increase in the *trans/cis*-epoxy-PUFA ratio (Fig. 4.5, appendix Fig. 8.7). Thus, here the applicability of the *trans/cis*-epoxy-PUFA ratio as oxidative stress marker cannot be evaluated based on comparison with IsoP levels. Even though IRI is linked to excess ROS formation [50, 51] and an increase of oxidative damage derived IsoP following

renal IRI has been observed in rat models [52, 53], there are various factors influencing measured IsoP levels in this model. These include clamping time, since longer clamping seems to lead to higher IsoP levels [52], as well as the time point of sampling following reperfusion, and the specimen analyzed, e.g. plasma, interstitial fluid, urine or tissue. Consistently to our observation of an increase in total 5(*R,S*)-5-F_{2t}-IsoP levels in the kidney 4 h after reperfusion and a decrease after 24 h (Fig. 4.5), in a rat model of unilateral IRI an increase of oxidized phosphatidylcholine species containing IsoP was observed 6 h after reperfusion which decreased after 24 h [53]. A similar time course of IsoP level was also observed in the liver of CCl_4 treated rats (see above) [7]. These studies show that the time point of measuring oxidative damage for the evaluation of oxidative stress based on IsoP and likewise probably also epoxy-PUFA is crucial [54]. Interestingly, while showing the same time dependent trend, ARA and DHA derived 5(*R,S*)-5-F_{2t}-IsoP and 4(*R,S*)-4-F_{4t}-NeuroP, respectively, were modulated to a different extent in the time course of IRI in mice (Fig. 4.5). Also species specific differences might result in different time courses or extent of changes. Taken together, probably the ischemia reperfusion injury induced oxidative stress does not cause strong lipid oxidation in the investigated model and at the investigated time points. Therefore, other oxidative stress models, e.g. CCl_4 induced liver toxicity [8, 9, 55] or paraquat induced lung toxicity [56, 57] should be used to evaluate the biological significance of the modulated *trans/cis*-epoxy-PUFA ratio during oxidative stress as seen for the *t*-BOOH induced oxidative stress models.

4.5 Conclusion

Based on the presented results, we suggest a potential new biomarker of oxidative damage: the *trans/cis*-epoxy-PUFA ratio. In the investigated human cell lines from hepatic, colorectal and renal origin, as well as in the model organism *C. elegans* an increase in the *trans/cis*-epoxy-PUFA ratio with *t*-BOOH induced oxidative stress was observed. The *trans/cis*-epoxy-PUFA

ratio correlates perfectly with common marker of oxidative stress, i.e. IsoP. However, in the investigated *in vivo* model of murine renal ischemia reperfusion injury an effect on the *trans/cis*-epoxy-PUFA ratio was absent, underlining the need for further investigations especially regarding different oxidative stress agents with different modes of inducing oxidative stress to validate its suitability. This analysis could also pave the way to a mechanistically understanding of *trans*-epoxy-PUFA formation and understanding of their biological role.

4.6 References

1. Sies H., Berndt C. and Jones D. P. (2017) Oxidative stress. *Annu Rev Biochem*. 86(1), pp. 715-748; doi: 10.1146/annurev-biochem-061516-045037.
2. Giustarini D., Dalle-Donne I., Tsikas D. and Rossi R. (2009) Oxidative stress and human diseases: Origin, link, measurement, mechanisms, and biomarkers. *Crit Rev Clin Lab Sci*. 46(5-6), pp. 241-281; doi: 10.3109/10408360903142326.
3. Xu L., Davis T. A. and Porter N. A. (2009) Rate constants for peroxidation of polyunsaturated fatty acids and sterols in solution and in liposomes. *J Am Chem Soc*. 131(36), pp. 13037-13044; doi: 10.1021/ja9029076.
4. Yin H., Xu L. and Porter N. A. (2011) Free radical lipid peroxidation: Mechanisms and analysis. *Chem Rev*. 111(10), pp. 5944-5972; doi: 10.1021/cr200084z.
5. Morrow J. D., Harris T. M. and Roberts II L. J. (1990) Noncyclooxygenase oxidative formation of a series of novel prostaglandins: Analytical ramifications for measurement of eicosanoids. *Anal Biochem*. 184(1), pp. 1-10; doi: 10.1016/0003-2697(90)90002-Q.
6. Jahn U., Galano J. M. and Durand T. (2008) Beyond prostaglandins - Chemistry and biology of cyclic oxygenated metabolites formed by free-radical pathways from polyunsaturated fatty acids. *Angew Chem Int Ed Engl*. 47(32), pp. 5894-5955; doi: 10.1002/anie.200705122.
7. Morrow J. D., Awad J. A., Boss H. J., Blair I. A. and Roberts II L. J. (1992) Non-cyclooxygenase-derived prostanoids (F2-isoprostanes) are formed in situ on phospholipids. *Proc Natl Acad Sci U S A*. 89(22), pp. 10721-10725; doi: 10.1073/pnas.89.22.10721.
8. Morrow J. D., Hill K. E., Burk R. F., Nammour T. M., Badr K. F. and Roberts II L. J. (1990) A series of prostaglandin F2-like compounds are produced in vivo in humans by a non-cyclooxygenase, free radical-catalyzed mechanism. *Proc Natl Acad Sci U S A*. 87(23), pp. 9383-9387; doi: 10.1073/pnas.87.23.9383.
9. Kadiiska M. B., Gladen B. C., Baird D. D., Germolec D., Graham L. B., Parker C. E., Nyska A., Wachsman J. T., Ames B. N., Basu S., Brot N., Fitzgerald G. A., Floyd R. A., George M., Heinecke J. W., Hatch G. E., Hensley K., Lawson J. A., Marnett L. J., Morrow J. D., Murray D. M., Plastaras J., Roberts II L. J., Rokach J., Shigenaga M. K., Sohal R. S., Sun J., Tice R. R., Van Thiel D. H., Wellner D., Walter P. B., Tomer K. B., Mason R. P. and Barrett J. C. (2005) Biomarkers of oxidative stress study II. Are oxidation products of lipids, proteins, and DNA markers of CCl4 poisoning? *Free Radic Biol Med*. 38(6), pp. 698-710; doi: 10.1016/j.freeradbiomed.2004.09.017.
10. Milne G. L., Dai Q. and Roberts II L. J. (2015) The isoprostanes - 25 years later. *Biochim Biophys Acta*. 1851(4), pp. 433-445; doi: 10.1016/j.bbalip.2014.10.007.
11. van't Erve T. J., Kadiiska M. B., London S. J. and Mason R. P. (2017) Classifying oxidative stress by F2-isoprostane levels across human diseases: A meta-analysis. *Redox Biol*. 12, pp. 582-599; doi: 10.1016/j.redox.2017.03.024.
12. Hecker M., Ullrich V., Fischer C. and Meese C. O. (1987) Identification of novel arachidonic acid metabolites formed by prostaglandin H synthase. *Eur J Biochem*. 169(1), pp. 113-123; doi:10.1111/j.1432-1033.1987.tb13587.x.
13. Klein T., Reutter F., Schweer H., Seyberth H. W. and Nüsing R. M. (1997) Generation of the isoprostane 8-epi-prostaglandin $F_{2\alpha}$ *in vitro* and *in vivo via* the cyclooxygenases. *J Pharmacol Exp Ther*. 282(3), pp. 1658-1665.
14. van‘t Erve T. J., Lih F. B., Kadiiska M. B., Deterding L. J., Eling T. E. and Mason R. P. (2015) Reinterpreting the best biomarker of oxidative stress: The 8-iso-PGF2α/PGF2α ratio distinguishes chemical from enzymatic lipid peroxidation. *Free Radic Biol Med*. 83, pp. 245-251; doi: 10.1016/j.freeradbiomed.2015.03.004.

15. van't Erve T. J., Lih F. B., Jelsema C., Deterding L. J., Eling T. E., Mason R. P. and Kadiiska M. B. (2016) Reinterpreting the best biomarker of oxidative stress: The 8-iso-prostaglandin F2α/prostaglandin F2α ratio shows complex origins of lipid peroxidation biomarkers in animal models. *Free Radic Biol Med*. 95, pp. 65-73; doi: 10.1016/j.freeradbiomed.2016.03.001.
16. Morisseau C. and Hammock B. D. (2013) Impact of soluble epoxide hydrolase and epoxyeicosanoids on human health. *Annu Rev Pharmacol Toxicol*. 53(1), pp. 37-58; doi: 10.1146/annurev-pharmtox-011112-140244.
17. Konkel A. and Schunck W.-H. (2011) Role of cytochrome P450 enzymes in the bioactivation of polyunsaturated fatty acids. *Biochim Biophys Acta*. 1814(1), pp. 210-222; doi: 10.1016/j.bbapap.2010.09.009.
18. Westphal C., Konkel A. and Schunck W.-H. (2015) Cytochrome P450 enzymes in the bioactivation of polyunsaturated fatty acids and their role in cardiovascular disease. In: *Monooxygenase, Peroxidase and Peroxygenase Properties and Mechanisms of Cytochrome P450*. E. G. Hrycay and S. M. Bandiera (eds.), Springer International Publishing, Cham, pp. 151-187; doi: 10.1007/978-3-319-16009-2_6.
19. Capdevila J. H., Falck J. R. and Harris R. C. (2000) Cytochrome P450 and arachidonic acid bioactivation: Molecular and functional properties of the arachidonate monooxygenase. *J Lipid Res*. 41(2), pp. 163-181.
20. Capdevila J. H., Karara A., Waxman D. J., Martin M. V., Falck J. R. and Guengerich F. P. (1990) Cytochrome P-450 enzyme-specific control of the regio- and enantiofacial selectivity of the microsomal arachidonic acid epoxygenase. *J Biol Chem*. 265(19), pp. 10865-10871.
21. Willenberg I., Ostermann A. I. and Schebb N. H. (2015) Targeted metabolomics of the arachidonic acid cascade: Current state and challenges of LC-MS analysis of oxylipins. *Anal Bioanal Chem*. 407(10), pp. 2675-2683; doi: 10.1007/s00216-014-8369-4.
22. Bernstrom K., Kayganich K., Murphy R. C. and Fitzpatrick F. A. (1992) Incorporation and distribution of epoxyeicosatrienoic acids into cellular phospholipids. *J Biol Chem*. 267(6), pp. 3686-3690.
23. Jiang H., McGiff J. C., Quilley J., Sacerdoti D., Reddy L. M., Falck J. R., Zhang F., Lerea K. M. and Wong P. Y. (2004) Identification of 5,6-trans-epoxyeicosatrienoic acid in the phospholipids of red blood cells. *J Biol Chem*. 279(35), pp. 36412-36418; doi: 10.1074/jbc.M403962200.
24. Aliwarga T., Raccor B. S., Lemaitre R. N., Sotoodehnia N., Gharib S. A., Xu L. and Totah R. A. (2017) Enzymatic and free radical formation of cis- and trans-epoxyeicosatrienoic acids in vitro and in vivo. *Free Radic Biol Med*. 112, pp. 131-140; doi: 10.1016/j.freeradbiomed.2017.07.015.
25. Nakamura T., Bratton D. L. and Murphy R. C. (1997) Analysis of epoxyeicosatrienoic and monohydroxyeicosatetraenoic acids esterified to phospholipids in human red blood cells by electrospray tandem mass spectrometry. *J Mass Spectrom*. 32(8), pp. 888-896; doi: 10.1002/(SICI)1096-9888(199708)32:8<888::AID-JMS548>3.0.CO;2-W.
26. Jiang H., Quilley J., Reddy L. M., Falck J. R., Wong P. Y. and McGiff J. C. (2005) Red blood cells: Reservoirs of cis- and trans-epoxyeicosatrienoic acids. *Prostaglandins Other Lipid Mediat*. 75(1-4), pp. 65-78; doi: 10.1016/j.prostaglandins.2004.10.003.
27. Rund K. M., Ostermann A. I., Kutzner L., Galano J.-M., Oger C., Vigor C., Wecklein S., Seiwert N., Durand T. and Schebb N. H. (2018) Development of an LC-ESI(-)-MS/MS method for the simultaneous quantification of 35 isoprostanes and isofurans derived from the major n3- and n6-PUFAs. *Anal Chim Acta*. 1037, pp. 63-74; doi: 10.1016/j.aca.2017.11.002.

28. Oger C., Brinkmann Y., Bouazzaoui S., Durand T. and Galano J. M. (2008) Stereocontrolled access to isoprostanes via a bicyclo[3.3.0]octene framework. *Org Lett*. 10(21), pp. 5087-5090; doi: 10.1021/ol802104z.
29. Cuyamendous C., Leung K. S., Durand T., Lee J. C.-Y., Oger C. and Galano J. M. (2015) Synthesis and discovery of phytofurans: Metabolites of α-linolenic acid peroxidation. *Chem Commun (Camb)*. 51(86), pp. 15696-15699; doi: 10.1039/c5cc05736a.
30. de la Torre A., Lee Y. Y., Mazzoni A., Guy A., Bultel-Poncé V., Durand T., Oger C., Lee J. C.-Y. and Galano J.-M. (2015) Total syntheses and in vivo quantitation of novel neurofuran and dihomo-isofuran derived from docosahexaenoic acid and adrenic acid. *Chemistry*. 21(6), pp. 2442-2446; doi: 10.1002/chem.201405497.
31. Oger C., Bultel-Poncé V., Guy A., Durand T. and Galano J.-M. (2012) Total synthesis of isoprostanes derived from adrenic acid and EPA. *Eur J Org Chem*. 2012(13), pp. 2621-2634; doi: 10.1002/ejoc.201200070.
32. Guy A., Oger C., Heppekausen J., Signorini C., De Felice C., Fürstner A., Durand T. and Galano J.-M. (2014) Oxygenated metabolites of n-3 polyunsaturated fatty acids as potential oxidative stress biomarkers: Total synthesis of 8-F3t-IsoP, 10-F4t-NeuroP and [D4]-10-F4t-NeuroP. *Chemistry*. 20(21), pp. 6374-6380; doi: 10.1002/chem.201400380.
33. Mimmler M., Peter S., Kraus A., Stroh S., Nikolova T., Seiwert N., Hasselwander S., Neitzel C., Haub J., Monien B. H., Nicken P., Steinberg P., Shay J. W., Kaina B. and Fahrer J. (2016) DNA damage response curtails detrimental replication stress and chromosomal instability induced by the dietary carcinogen PhIP. *Nucleic Acids Res*. 44(21), pp. 10259-10276; doi: 10.1093/nar/gkw791.
34. Brenner S. (1974) The genetics of *Caenorhabditis elegans*. *Genetics*. 77(1), pp. 71-94.
35. Thorenz A., Derlin K., Schröder C., Dressler L., Vijayan V., Pradhan P., Immenschuh S., Jörns A., Echtermeyer F., Herzog C., Chen R., Rong S., Bräsen J. H., van Kooten C., Kirsch T., Klemann C., Meier M., Klos A., Haller H., Hensen B. and Gueler F. (2018) Enhanced activation of interleukin-10, heme oxygenase-1, and AKT in C5aR2-deficient mice is associated with protection from ischemia reperfusion injury–induced inflammation and fibrosis. *Kidney Int*. 94(4), pp. 741-755; doi: 10.1016/j.kint.2018.04.005.
36. Ostermann A. I., Willenberg I. and Schebb N. H. (2015) Comparison of sample preparation methods for the quantitative analysis of eicosanoids and other oxylipins in plasma by means of LC-MS/MS. *Anal Bioanal Chem*. 407(5), pp. 1403-1414; doi: 10.1007/s00216-014-8377-4.
37. Hwang S. H., Tsai H.-J., Liu J.-Y., Morisseau C. and Hammock B. D. (2007) Orally bioavailable potent soluble epoxide hydrolase inhibitors. *J Med Chem*. 50(16), pp. 3825-3840; doi: 10.1021/jm070270t.
38. Labuschagne C. F., van den Broek N. J., Postma P., Berger R. and Brenkman A. B. (2013) A protocol for quantifying lipid peroxidation in cellular systems by F2-isoprostane analysis. *PLoS One*. 8(11):e80935; doi: 10.1371/journal.pone.0080935.
39. Labuschagne C. F., Stigter E. C., Hendriks M. M., Berger R., Rokach J., Korswagen H. C. and Brenkman A. B. (2013) Quantification of in vivo oxidative damage in Caenorhabditis elegans during aging by endogenous F3-isoprostane measurement. *Aging Cell*. 12(2), pp. 214-223; doi: 10.1111/acel.12043.
40. Hattori M., Arai H. and Inoue K. (1993) Purification and characterization of bovine brain platelet-activating factor acetylhydrolase. *J Biol Chem*. 268(25), pp. 18748-18753.
41. McIntyre T. M., Prescott S. M. and Stafforini D. M. (2009) The emerging roles of PAF acetylhydrolase. *J Lipid Res*. 50(Suppl), pp. S255-S259; doi: 10.1194/jlr.R800024-JLR200.

42. Stafforini D. M., Sheller J. R., Blackwell T. S., Sapirstein A., Yull F. E., McIntyre T. M., Bonventre J. V., Prescott S. M. and Roberts II L. J. (2006) Release of free F2-isoprostanes from esterified phospholipids is catalyzed by intracellular and plasma platelet-activating factor acetylhydrolases. *J Biol Chem*. 281(8), pp. 4616-4623; doi: 10.1074/jbc.M507340200.
43. Matsuzawa A., Hattori K., Aoki J., Arai H. and Inoue K. (1997) Protection against oxidative stress-induced cell death by intracellular platelet-activating factor-acetylhydrolase II. *J Biol Chem*. 272(51), pp. 32315-32320; doi: 10.1074/jbc.272.51.32315.
44. Yin H., Brooks J. D., Gao L., Porter N. A. and Morrow J. D. (2007) Identification of novel autoxidation products of the ω-3 fatty acid eicosapentaenoic acid in vitro and in vivo. *J Biol Chem*. 282(41), pp. 29890-29901; doi: 10.1074/jbc.M703108200.
45. Yin H., Musiek E. S., Gao L., Porter N. A. and Morrow J. D. (2005) Regiochemistry of neuroprostanes generated from the peroxidation of docosahexaenoic acid in vitro and in vivo. *J Biol Chem*. 280(28), pp. 26600-26611; doi: 10.1074/jbc.M503088200.
46. Stene D. O. and Murphy R. C. (1988) Metabolism of leukotriene E4 in isolated rat hepatocytes - Identification of β-oxidation products of sulfidopeptide leukotrienes. *J Biol Chem*. 263(6), pp. 2773-2778.
47. Lawson J. A., Kim S., Powell W. S., FitzGerald G. A. and Rokach J. (2006) Oxidized derivatives of ω-3 fatty acids: Identification of IPF3α-VI in human urine. *J Lipid Res*. 47(11), pp. 2515-2524; doi: 10.1194/jlr.M600327-JLR200.
48. Watts J. L. and Browse J. (2002) Genetic dissection of polyunsaturated fatty acid synthesis in *Caenorhabditis elegans*. *Proc Natl Acad Sci U S A*. 99(9), pp. 5854-5859; doi: 10.1073/pnas.092064799.
49. Fulton D., Falck J. R., McGiff J. C., Carroll M. A. and Quilley J. (1998) A method for the determination of 5,6-EET using the lactone as an intermediate in the formation of the diol. *J Lipid Res*. 39(8), pp. 1713-1721.
50. Granger D. N. and Kvietys P. R. (2015) Reperfusion injury and reactive oxygen species: The evolution of a concept. *Redox Biol*. 6, pp. 524-551; doi: 10.1016/j.redox.2015.08.020.
51. Kadkhodaee M., Hanson G. R., Towner R. A. and Endre Z. H. (1996) Detection of hydroxyl and carbon-centred radicals by EPR spectroscopy after ischaemia and reperfusion of the rat kidney. *Free Radic Res*. 25(1), pp. 31-42; doi: 10.3109/10715769609145654.
52. Wang Z., Colli J. L., Keel C., Bailey K., Grossman L., Majid D. and Lee B. R. (2012) Isoprostane: Quantitation of renal ischemia and reperfusion injury after renal artery clamping in an animal model. *J Endourol*. 26(1), pp. 21-25; doi: 10.1089/end.2011.0188.
53. Solati Z., Edel A. L., Shang Y., O K. and Ravandi A. (2018) Oxidized phosphatidylcholines are produced in renal ischemia reperfusion injury. *PLoS One*. 13(4):e0195172; doi: 10.1371/journal.pone.0195172.
54. Halliwell B. and Lee C. Y. (2010) Using isoprostanes as biomarkers of oxidative stress: Some rarely considered issues. *Antioxid Redox Signal*. 13(2), pp. 145-156; doi: 10.1089/ars.2009.2934.
55. Albano E., Lott K. A., Slater T. F., Stier A., Symons M. C. and Tomasi A. (1982) Spin-trapping studies on the free-radical products formed by metabolic activation of carbon tetrachloride in rat liver microsomal fractions isolated hepatocytes and in vivo in the rat. *Biochem J*. 204(2), pp. 593-603; doi: 10.1042/bj2040593

56. Dinis-Oliveira R. J., Duarte J. A., Sánchez-Navarro A., Remião F., Bastos M. L. and Carvalho F. (2008) Paraquat poisonings: Mechanisms of lung toxicity, clinical features, and treatment. *Crit Rev Toxicol*. 38(1), pp. 13-71; doi: 10.1080/10408440701669959.
57. Harrison F. E., Best J. L., Meredith M. E., Gamlin C. R., Borza D.-B. and May J. M. (2012) Increased expression of SVCT2 in a new mouse model raises ascorbic acid in tissues and protects against paraquat-induced oxidative damage in lung. *PLoS One*. 7(4):e35623; doi: 10.1371/journal.pone.0035623.

Chapter 5

Dietary omega-3 PUFA improved tubular function after ischemia induced acute kidney injury in mice but did not attenuate impairment of renal function*

***Background:** Acute kidney injury (AKI) is an important complication after major surgery and solid organ transplantation. Here, we present a dietary omega-3 polyunsaturated fatty acid (n3-PUFA) supplementation study to investigate whether pre-treatment can reduce ischemia induced AKI in mice.*

***Methods:** Male 12–14 week old C57BL/6J mice received a linoleic acid rich sunflower oil based standard diet containing 10% fat (STD) or the same diet enriched with n3-PUFA (containing 1% EPA and 1% DHA) (STD+n3). After 14 days of feeding bilateral 30 min renal ischemia reperfusion injury (IRI) was conducted to induce AKI and mice were sacrificed at 24 h. Serum creatinine and blood urea nitrogen (BUN) as well as liver enzyme elevation were measured. Kidney damage was analyzed by histology and immunohistochemistry. Furthermore, pro-inflammatory cytokines (IL-6, MCP-1) were determined by qPCR. FA and oxylipin pattern were quantified in blood and kidneys by GC-FID and LC-MS/MS, respectively.*

***Results:** n3-PUFA supplementation prior to renal IRI increased systemic and renal levels of n3-PUFA. Consistently, eicosanoids and other oxylipins derived from n3-PUFA including precursors of specialized pro-resolving mediators were elevated while n6-PUFA derived mediators such as pro-inflammatory prostaglandins were decreased. Feeding of n3-PUFA did not attenuate renal function impairment, morphological renal damage and inflammation characterized by IL-6 and MCP-1 elevation or neutrophil infiltration. However, the tubular transport marker alpha-1 microglobulin (A1M) was significantly higher expressed in proximal tubular epithelial cells of STD+n3 compared to STD fed mice. This indicates a better integrity of proximal tubular epithelial cells and thus significant protection of tubular function. In addition, heme oxygenase-1 (HO-1) which protects tubular function was also up-regulated in the treatment group receiving n3-PUFA supplemented chow.*

***Discussion:** We showed that n3-PUFA pre-treatment did not affect overall renal function or renal inflammation in a mouse model of moderate ischemia induced AKI, but tubular transport was improved. In conclusion, dietary n3-PUFA supplementation altered the oxylipin levels significantly but did not protect from renal function deterioration or attenuate ischemia induced renal inflammation.*

* Reprinted from *Prostaglandins & Other Lipid Mediators*, Vol. 146, Rund K. M., Peng S., Greite R., Claaßen C., Nolte F., Oger C., Galano J.-M., Balas L., Durand T., Chen R., Gueler F., Schebb N. H., Dietary omega-3 PUFA improved tubular function after ischemia induced acute kidney injury in mice but did not attenuate impairment of renal function, 106386, Copyright (2020), with permission from Elsevier. doi :10.1016/j.prostaglandins.2019.106386.

Author contributions: KR designed research, performed experiments and wrote the manuscript; SP performed animal experiments and contributed to manuscript writing; RG evaluated animal experiment data and wrote the manuscript; CC performed experiments as part of his master thesis under the supervision of KR; FN performed experiments as student research assistant under the supervision of KR; CO, JMG, LB, TD provided standard substances and contributed to manuscript writing; RC performed animal experiments; FG, NHS designed research and wrote the manuscript.

5.1 Introduction

Acute kidney injury (AKI) is a frequent complication after major cardiac surgery, solid organ transplantation and also after trauma surgery. Onset of AKI increases morbidity and mortality of the patients and is characterized by an increase in serum creatinine and/or reduction of the glomerular filtration rate (GFR) [1]. In a review of 25,182 trauma patients post-traumatic AKI was as high as 24% and these patients had a 3.4-fold higher risk of death compared to non-AKI patients [2]. Also, after myocardial infarction mortality was 3-fold increased in patients with AKI and incidence of major adverse cardiac events (MACE) was with 26% higher than in non-AKI patients during the three-year follow-up [3]. It has been shown that AKI is not only an acute event but also increases the risk for chronic kidney disease (CKD) [4]. Even if the serum creatinine elevation returns to normal levels shortly after AKI a significant proportion of patients will develop CKD or will even proceed to end stage renal disease with the need of renal replacement therapy [5].

Renal ischemia reperfusion injury (IRI) due to hypotension, major bleeding and hypoxia causes intrarenal vasoconstriction with activation of pro-oxidative mechanisms, release of pro-inflammatory cytokines and subsequent leukocyte invasion [6-9]. The severity of AKI correlates with the long-term outcome and progression to CKD [5].

Established strategies to prevent or attenuate AKI even in scheduled surgeries such as cardiac valve replacement are lacking. Several studies discussed a beneficial role of omega-3 polyunsaturated fatty acids (n3-PUFA) in the context of kidney diseases [10-19]. For the prevention of cardiovascular diseases the nutritional status of n3-PUFA is a well-established risk factor [20, 21]. The higher the incorporation of n3-PUFA, determined by the relative content of EPA and DHA in the cells, typically red blood cells [20, 22], the lower the risk for cardiovascular diseases and mortality [23]. It has to be noted that n3-PUFA are essential constituents of the human diet and that the nutritional status and not the intake of n3-PUFA supplements is related to their physiological effects.

Thus, if only the intake of n3-PUFA by supplementation is correlated to the risk for cardiovascular diseases the outcome is less clear [24, 25].

In the context of renal diseases effects of n3-PUFA supplementation on the outcome in kidney transplantation are inconsistent [26]. However, in some experimental AKI models the administration of n3-PUFA correlated with an improved kidney function [10-15].

The molecular mechanisms underlying beneficial effects of n3-PUFA include direct actions, e.g. binding to ion channels or transcription factors, e.g. NFκB or PPARγ, thereby reducing the expression of pro-inflammatory and activating the expression of anti-inflammatory genes, respectively. As constituents of membranes, e.g. predominantly in phospholipids, n3-PUFA also impact membrane structure and fluidity [27]. However, it is beyond doubt that a relevant part of the physiological effects of n3-PUFA are mediated by their oxygenated products, i.e. eicosanoids and other oxylipins [27-29]. In the so-called arachidonic acid (ARA) cascade PUFA serve as substrates for enzymatic and non-enzymatic conversion resulting in a multitude of lipid mediators from both n6- and n3-PUFA (Fig. 5.1) [27, 28, 30]. Enzymatic conversion of PUFA in the ARA cascade comprises three major pathways: (I) cyclooxygenases (COX) lead to the formation of prostanoids and thromboxanes, (II) cytochrome P450 monooxygenases (CYP) give rise to epoxy-PUFA and terminal hydroxy-PUFA and (III) lipoxygenases lead *via* hydroperoxy-PUFA to hydroxy-PUFA and leukotrienes [31]. Structurally similar to these enzymatically formed products, oxidized PUFA also arise during non-enzymatic autoxidation, e.g. isoprostanes, which also have been shown to possess biological activity [32, 33]. In the kidney oxylipins have important functions in (patho)physiology, e.g. regulation of renal blood flow, glomerular filtration rate and tubular transport function [34-37]. As n3-PUFA compete with ARA for conversion, dietary n3-PUFA supplementation impacts the overall oxylipin profile resulting in a shift from predominantly pro-inflammatory, e.g. 2-series prostaglandins, towards n3-PUFA derived oxylipins with less potency or even anti-inflammatory properties [27].

Furthermore, in recent years activity of LOX with n3-PUFA have been related to the formation of multiple hydroxylated PUFA, e.g. resolvins, maresins and protectins which have been attributed to be actively involved in the resolution of inflammation [38], though several studies fail to detect them in biological samples [39, 40].

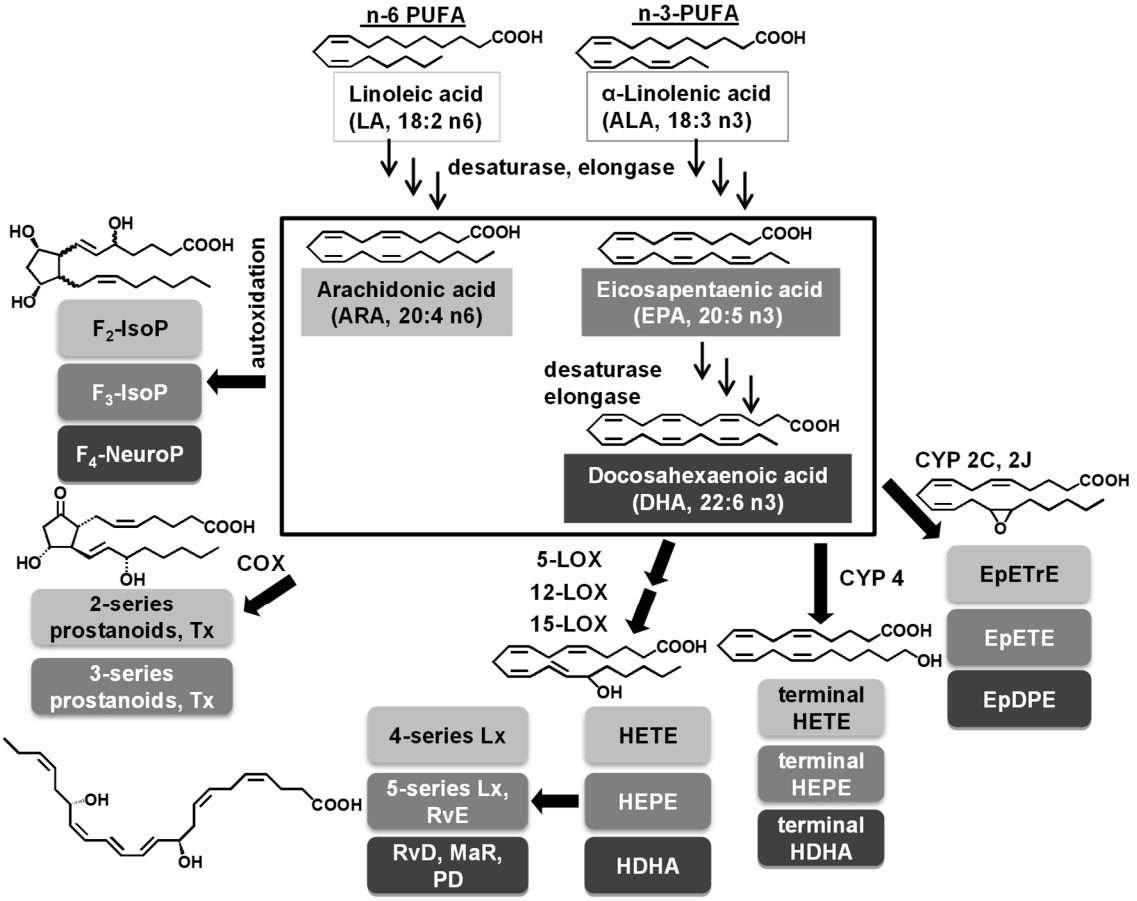

Fig. 5.1: Simplified overview of the biosynthesis of arachidonic acid (20:4 n6, ARA) from linoleic acid (18:2 n6, LA), and eicosapenatenoic acid (20:5 n3, EPA) and docosahexaenoic acid (20:6 n3, DHA) from α-linolenic acid (18:3 n3, ALA), and selected pathways for their oxygenation within the ARA cascade. COX – cyclooxygenase, LOX – lipoxygenase, CYP – cytochrome P450 monooxygenase, Tx – thromboxane; HETE – hydroxy eicosatetraenoic acid; HEPE – hydroxy eicosapentaenoic acid; HDHA – hydroxy docosahexaenoic acid; EpETrE – epoxy eicosatrienoic acid; EpETE – epoxy eicosatetraenoic acid; EpDPE – epoxy docosapentaenoic acid; IsoP – isoprostane; NeuroP – neuroprostane; Rv – resolvin; Lx – lipoxin; PD – protectin; MaR – maresin.

Changes in the oxylipin pattern in the context of kidney function in AKI have been sparsely investigated. Therefore, we used a well characterized model of ischemia induced AKI in mice [41, 42] to study the effect of dietary n3-PUFA (EPA and DHA) supplementation – based on a linoleic acid rich western-like

diet [43] for 14 days prior to surgery – on the fatty acid composition and oxylipin pattern in blood and tissue in comparison to renal damage and inflammation at 24 h after reperfusion injury.

5.2 Experimental

5.2.1 Chemicals and Biological Materials

Oxylipin and deuterated oxylipin standards were purchased from Cayman Chemicals (local distributor: Biomol, Hamburg, Germany). Methyl pentacosanoate (FAME C25:0) was obtained from Santa Cruz Biotechnology (Heidelberg, Germany). PD1 and isoprostane standards were included in the method based on in-house synthesis as described [40, 44]. HPLC grade and LC-MS grade methanol (MeOH), LC-MS grade acetonitrile (ACN), LC-MS grade isopropanol, LC-MS grade acetic acid and HPLC grade methyl *tert*-butyl ether (Acros Organics) were purchased from Fisher Scientific (Schwerte, Germany). Sodium hydrogen phosphate and *n*-hexane (HPLC grade) were obtained from Carl Roth (Karlsruhe, Germany). Ammonium acetate (p.a.) was obtained from Merck (Darmstadt, Germany) and potassium hydroxide (85%) from Gruessing GmbH (Filsum, Germany). Ethyl acetate, acetyl chloride and potassium carbonate (anhydrous) were purchased from Sigma Aldrich (Schnelldorf, Germany).

5.2.2 Feeding experiment and renal ischemia reperfusion injury in mice

C57BL/6J$^{ham\text{-}ztm}$ male mice (12–14 weeks of age) were obtained from the institute of laboratory animal science (Hannover Medical School, Germany). Mice were cared for in accordance with the institution's guidelines for experimental animal welfare and with the guidelines of the American Physiological Society. All experiments were approved by the animal protection committee of the local authorities (Lower Saxony State Department for Food

Safety and Animal Welfare, LAVES; approval 33.19-42502-04-14/1657). Mice were housed under conventional conditions with a 14/10 h light/dark cycle. Mice were divided into two feeding groups receiving either a sunflower oil based standard diet (STD) or the same diet enriched with n3-PUFA containing 1% eicosapentaenoic acid (EPA) and 1% docosahexaenoic acid (DHA) as ethyl esters (10% each in fat; STD+n3) based on a standard experimental diet (ssniff Spezialdiaeten GmbH, Soest, Germany). Both diets contained in total 10% fat. The fatty acid composition of the diets is shown in the appendix (Tab. 8.4). During the whole feeding period every 2–3 days fresh chow was provided and animals had free access to the food and domestic quality drinking water.

After 14 days of feeding, renal IRI was initiated in general isoflurane anesthesia (5% induction, 2% maintenance) combined with iv butorphanol as analgetic treatment. IRI was induced by transient bilateral renal pedicle clamping for 30 min using a non-traumatic vascular clamp [45]. Mice were sacrificed 24 h after reperfusion by deep general anesthesia and total body perfusion with ice cold PBS [45].

IRI experiments were conducted in three sets each with n = 7–8 animals in the STD and STD+n3 fed group. In one of these experiments additionally a sham group (n = 5) receiving STD chow was included which underwent midline laparotomy but without renal pedicle clamping.

Blood was collected at baseline (before starting the feeding) and at 24 h after reperfusion. An aliquot of 30 µL whole blood was diluted with 150 µL deionized water for fatty acid analysis and EDTA-plasma was generated by centrifugation (10 min, 4 °C, 4000 × *g*) and stored at −80 °C until analysis for clinical chemistry and oxylipins. Kidneys were collected at endpoint, dissected and immediately processed as follows: one piece was fixed in paraformaldehyde for histology, one piece was stored in RNAlater for qPCR and one piece was shock frozen in liquid nitrogen and stored at −80 °C for fatty acid and oxylipin analysis. Renal function (serum-creatinine and BUN) and liver enzymes (aspartate transaminase: AST, alanine transaminase: ALT) were measured in EDTA-

plasma by an Olympus analyzer (AU400) in an automated fashion according to the manufacturer's instruction.

5.2.3 Histology and immunohistochemistry

The middle part of the kidney was fixed in 4% paraformaldehyde (PFA) overnight and embedded in paraffin. Two µm paraffin sections were cut and PAS (Periodic Acid-Schiff) stain according to standard diagnostic protocols was done. For determination of AKI scores a semi-quantitative grading system was used: 0 = focal AKI with < 5% of tubuli of the cortex affected, 1 = mild AKI with 5–25% of tubuli affected, 2 = moderate AKI with 26–50% of tubuli affected, 3 = severe AKI with 51–75% of the tubuli affected, 4 = very severe AKI with > 75% of tubuli affected.

Immunohistochemistry for neutrophil infiltration (Gr-1 antibody, Biorad), the tubular function marker alpha-1 microglobulin (A1M; gift from Magnus Gram, Lund University) and heme oxygenase-1 (HO-1 antibody; Enzo Life Sciences, Switzerland) was done on paraffin sections. Sections were incubated with trypsin for 15 min at 37 °C for antigen retrieval. Nonspecific binding sites were blocked with 10% normal donkey serum (Jackson ImmunoResearch Lab, West Grove, USA) for 30 min and then primary antibodies (Invitrogen, California, USA) were incubated for 60 min at room temperature in the dark. Afterwards secondary antibodies (Invitrogen, California, USA) were incubated for additional 60 min in the dark. Analysis was performed in a blinded manner using a Leica imaging microscope. Gr-1 positive neutrophil infiltration was scored with a 0–4 grading system in 10 different view fields (VF) per section in 200-fold magnification: 0 = no infiltrates, 1 = mild infiltrates with < 5 cells/VF, 2 = moderate infiltrates with 6–10 cells/VF, 3 = severe infiltration with 11–25 cells/VF, 4 = very severe infiltration with > 25 cells/VF. Semiquantitative analysis of the percentage of A1M or HO-1 positive proximal tubuli in the cortex was done in 10 different VF per section.

5.2.4 Detection of pro-inflammatory cytokines by qPCR

For mRNA work-up one part of the kidneys was fixed in RNAlater immediately. For total RNA extraction the RNeasy mini kit system (Qiagen, Hilden, Germany) was used and RNA was transcribed with Qiagen mini kits. For quantitative PCR (qPCR) 1 µg of DNase-treated total RNA was reverse transcribed using Superscript II reverse transcriptase (Invitrogen) and qPCR was performed on a Lightcycler 420 II (Roche Diagnostics, Penzberg, Germany) using FastStart SYBR Green chemistry. Gene-specific primers for MCP-1 (QT00167832) and IL-6 (QT00098875) were used. For normalization HPRT (QT00166768) was used as housekeeping gene. Quantification was carried out using qgene software.

5.2.5 Extraction and quantification of fatty acids

The fatty acid composition was analyzed in diluted whole blood (15 µL blood + 75 µL water) and kidney tissue (15 ± 2 mg) as fatty acid methyl esters (FAME) using gas chromatography with flame ionization detection (GC-FID) as described with slight modifications [46]. Briefly, 10 µL internal standard (FAME C25:0, 750 µM) was added to diluted whole blood and kidney tissue samples. Kidney tissue was homogenized in 300 µL MeOH and 50 µL water using two stainless steel beads (3 mm, 5 min, 25 Hz) with a vibration ball mill (MM 400, Retsch, Haan, Germany). Lipids were extracted with MeOH/methyl *tert*-butyl ether and the lipid extract was trans-esterified to fatty acid methyl esters using methanolic hydrogen chloride. The calculation of the absolute fatty acid concentrations and relative pattern was based on response factors as described [46]. The LLOQ was 0.5 µg/mL for all FAME in the injected solution and the variability in quality control plasma was < 5% within batch.

5.2.6 Extraction and quantification of oxylipins

Oxylipins in plasma and kidney tissue were extracted using anion exchange Bond Elut Certify II SPE cartridges (Agilent, Waldbronn, Germany) as described with modifications [40, 44]. In the first step of oxylipin extraction 10 µL antioxidant solution and internal standards were added to each sample.

For the determination of free oxylipins in plasma (150–200 µL) the 2.8-fold volume of MeOH was added and the samples were stored at −80 °C for 30 min. After centrifugation the supernatant was diluted with 0.1 M disodium hydrogen phosphate buffer yielding a MeOH content ≤ 18% (pH 6.0) and loaded on the preconditioned SPE cartridge.

For analysis of free oxylipins in kidney tissue (50 ± 5 mg) samples were homogenized with 300 µL MeOH as described [47]. After centrifugation the supernatant was diluted with 2.7 mL 0.1 M disodium hydrogen phosphate buffer (pH 6.0) and loaded on the preconditioned SPE cartridge.

For quantification of total, i.e. free and esterified oxylipins in kidney tissue (20 ± 2 mg) samples were homogenized in 400 µL isopropanol and stored for 30 min at −80 °C. Samples were centrifuged and the supernatant was hydrolyzed (300 µL 1.5 M KOH (75/25, MeOH/water, *v/v*), immediately neutralized with acetic acid, diluted with 2 mL 0.1 M disodium hydrogen phosphate buffer (pH 5.5) and loaded on the preconditioned SPE cartridge.

The SPE procedure was carried out as described and samples were analyzed by LC-MS/MS (QTRAP, Sciex, Darmstadt, Germany) in scheduled selected reaction monitoring mode following negative electrospray ionization as described [40, 44]. The lower limit of quantification [40, 44] and the analytical variability [48] of the representative set of quantified oxylipins are summarized in the appendix (Tab. 8.5).

5.2.7 Data analysis

Data evaluation and statistical analyses were performed using GraphPad Prism software for Windows (version 5.0, La Jolla California USA). Data are presented as mean ± standard error of mean (SEM). For oxylipin and fatty acid analysis for the calculation of the mean ½ lower limit of quantification (LLOQ) was used if the concentration was below the LLOQ. The concentration was set to LLOQ if the analyte could not be quantified in more than 50% of the samples in one group. For comparison of two groups two-tailed unpaired student's t-test was used. For multiple comparisons ANOVA with post hoc Tukey correction was applied. Differences were considered significant at a p-value < 0.05 (* $p < 0.05$, ** $p < 0.01$, *** $p < 0.001$).

5.3 Results

Bodyweight and food intake of both feeding groups were not different between the STD and the STD+n3 diet.

5.3.1 Blood and tissue pattern of fatty acids and their oxidative metabolites

After 14 days of feeding an n3-PUFA enriched sunflower oil based diet (1% EPA and 1% DHA in the chow, STD+n3) absolute and relative levels of n3-PUFA in the kidney and in the circulation were significantly increased predominantly at the expense of n6-PUFA compared to mice on the STD diet (Fig. 5.2). Considering the very low levels of EPA in tissue and in the circulation of mice on the STD diet, especially relative levels of EPA were massively increased in response to the STD+n3 diet. Interestingly, in whole blood the STD+n3 diet led to an overall decrease in the absolute FA level. The relative concentration of the sum of EPA+DHA, reflecting the endogenous n3-PUFA status, increased 2.5- and 3.7-fold in the kidney and whole blood, respectively

(Fig. 5.2 B and D) indicating successful modulation of the n3-PUFA content by the supplementation.

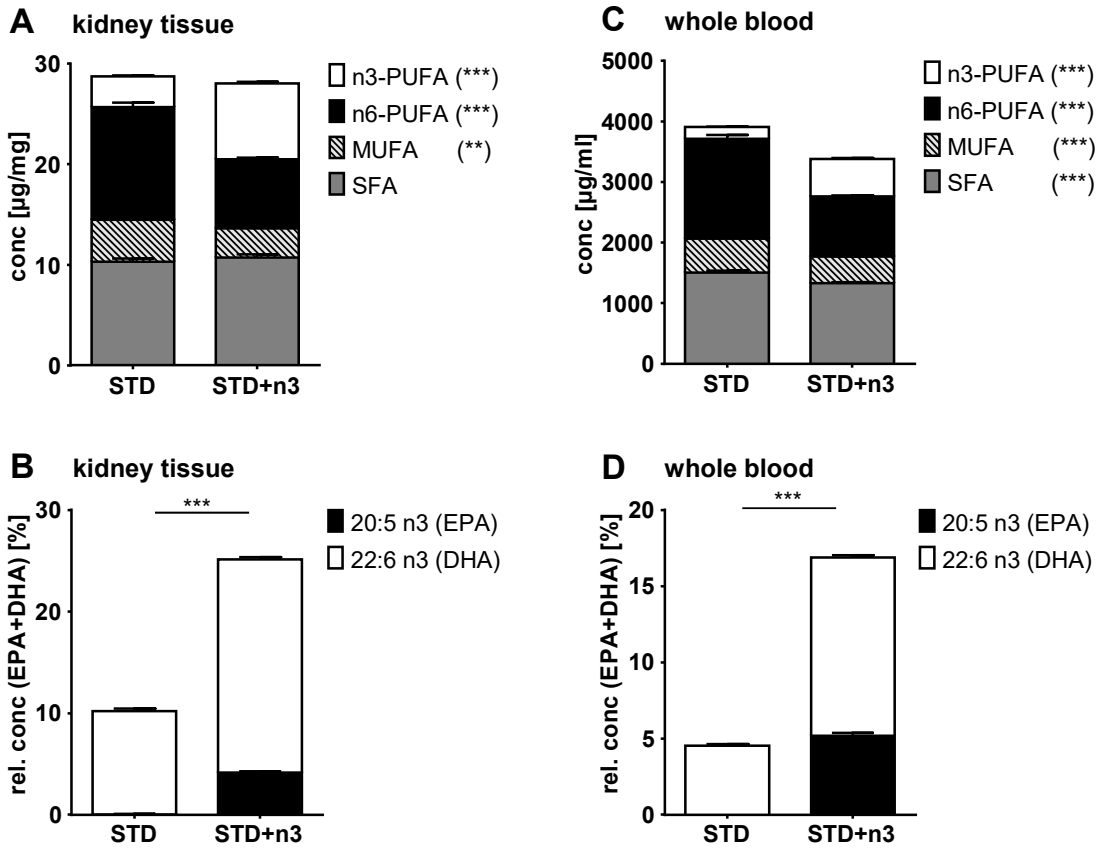

Fig. 5.2: Fatty acid composition in **(A)** kidney tissue and **(C)** whole blood 24 h after renal IRI in mice was shifted towards higher levels of n3-PUFA, while n6-PUFA decreased after 14 days of feeding a sunflower oil based diet enriched with EPA and DHA (STD+n3) compared to the same diet without EPA and DHA (STD). Consistently relative levels of EPA and DHA of all detected FA in **(B)** kidney tissue and **(D)** whole blood were significantly higher in mice on the STD+n3 diet. Shown are mean ± SEM, n = 14, ** $p < 0.01$, *** $p < 0.001$.

Consistent to the changes in the PUFA pattern, levels of eicosanoids and other oxylipins derived from ARA, EPA and DHA were massively altered in response to the STD+n3 diet, while concentrations of oxylipins in the plasma and kidney were almost similar in the IRI treated group compared to the sham group both fed with the STD diet (Fig. 5.3). Comparing levels of individual oxylipins 24 h after IRI a similar trend was observed for free metabolites in the plasma as well as for free and esterified oxylipins in kidney tissue, though levels of esterified oxylipins were massively higher than the respective free mediators: Overall STD+n3 diet led to a significant decrease of ARA derived metabolites from all

major formation pathways while EPA and DHA derived oxylipins were significantly elevated. Especially, regarding levels of free prostanoids in the kidney tissue, levels of ARA derived prostaglandins such as pro-inflammatory PGE_2 or the prostanoid TxB_2 were elevated following IRI compared to sham, while STD+n3 feeding caused their significant decrease and concomitant formation of the less potent EPA derived counterparts, i.e. PGE_3 and TxB_3 (Fig. 5.3 B). Amongst others in the circulation as well as in the kidney also a significant increase of 17-HDHA and 18-HEPE, precursors for the formation of specialized pro-resolving mediators (SPM), was observed in response to STD+n3. However, except for DHA derived protectin D1 (PD1) and its isomer PDX no signals above the lower limit of quantification (LLOQ), i.e. 0.25–2 nmol/kg in kidney tissue and 0.07–0.56 nM in plasma, were detected for all SPM. LC-MS/MS signals for PD1 indicated relevant apparent concentrations in plasma and kidney of STD+n3 fed mice (Fig. 5.6). However, the ratios between monitored transitions differed significantly between the authentic standard and the biological samples (Fig. 5.6).

Similar to enzymatically formed oxylipins, levels of prostaglandin-like autoxidation products formed esterified in phospholipids were massively altered by n3-PUFA feeding. Total levels of ARA derived 5(*R,S*)-5-F_{2t}-IsoP were decreased, while EPA and DHA derived 5(*R,S*)-5-F_{3t}-IsoP and 4(*R,S*)-4-F_{4t}-NeuroP were elevated in response to STD+n3. Interestingly, levels of these peroxidation products were lower following IRI compared to sham on the same STD diet (Fig. 5.7).

Fig. 5.3 (right, page 115): Concentration of free oxylipins in **(A)** plasma and **(B)** kidney tissue as well as **(C)** total, i.e. free and esterified oxylipins in kidney tissue. Shown are concentrations of selected (iso-)prostanoids, 5-LOX, 12/15-LOX, CYP2 and CYP4 products of ARA, EPA and DHA as well as 18-HEPE and PD1. Except for the sham group all patterns are determined in mice 24 h after renal IRI on a STD or STD+n3 diet. Feeding of the STD+n3 diet led to an increase of EPA and DHA derived lipid mediators while ARA derived oxylipins were decreased. Shown are mean ± SEM (sham n = 5, (A) STD: n = 19, STD+n3: n = 18; (B) STD: n = 13, STD+n3: n = 14; (C) STD: n = 7, STD+n3: n = 7). The lower limit of quantification (LLOQ) for those oxylipins is indicated by a dashed line in case it was not exceeded in > 50% of the samples per group. Statistical differences were determined between STD and STD+n3.

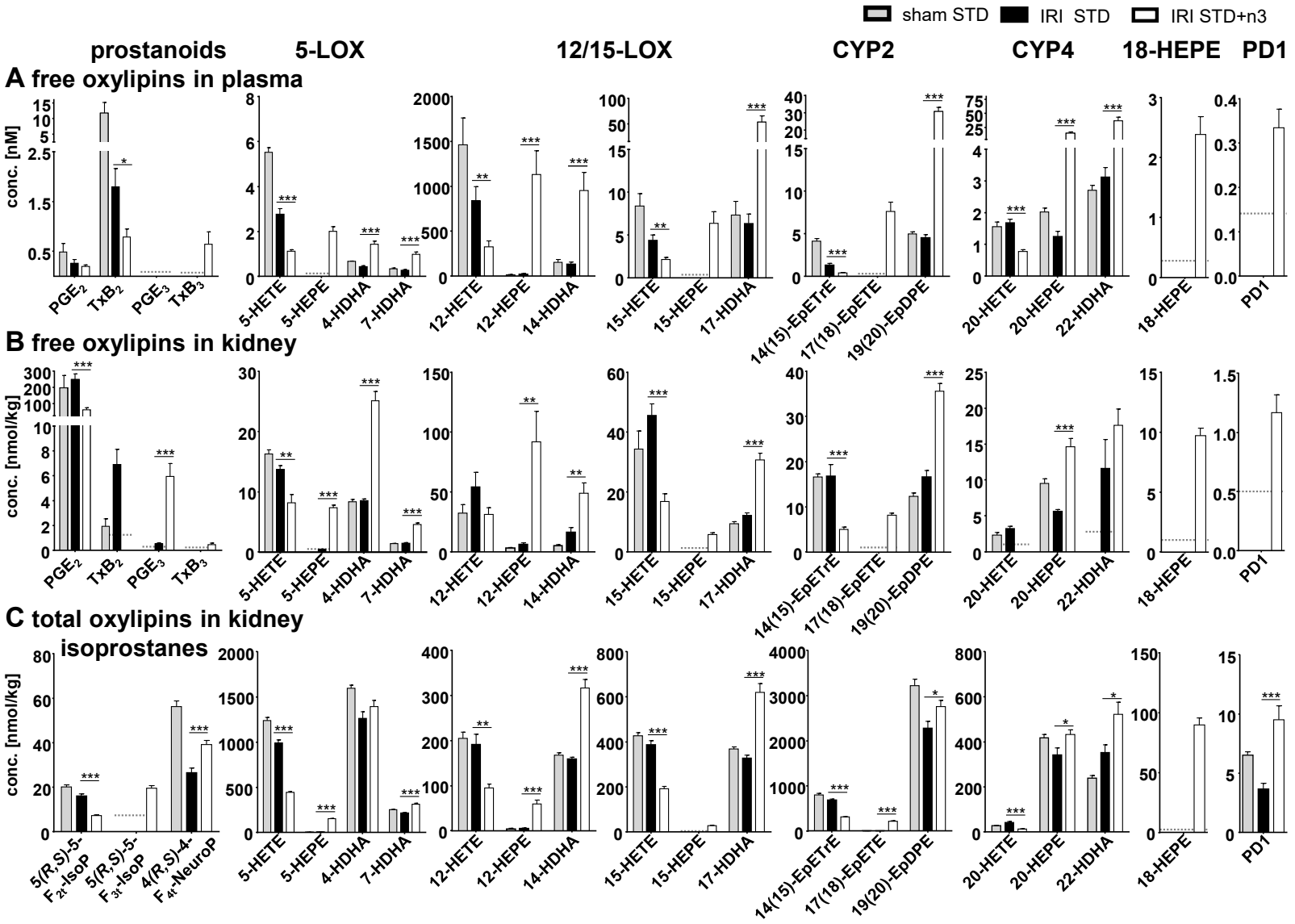
sham STD
IRI STD
IRI STD+n3
prostanoids
5-LOX
12/15-LOX
CYP2
CYP4
18-HEPE
PD1
A free oxylipins in plasma
B free oxylipins in kidney
C total oxylipins in kidney
isoprostanes
conc. [nM]
conc. [nmol/kg]
PGE2
TxB2
PGE3
TxB3
5-HETE
5-HEPE
4-HDHA
7-HDHA
12-HETE
12-HEPE
14-HDHA
15-HETE
15-HEPE
17-HDHA
14(15)-EpETrE
17(18)-EpETE
19(20)-EpDPE
20-HETE
20-HEPE
22-HDHA
18-HEPE
PD1
5(R,S)-5-F2t-IsoP
5(R,S)-5-F3t-IsoP
4(R,S)-4-F4t-NeuroP

5.3.2 Renal function, renal morphology and inflammation

Despite successful n3-PUFA supplementation indicated by the changes in PUFA and oxylipin patterns renal function impairment was similar in both groups. IRI caused a 6-fold elevation of serum creatinine (Fig. 5.4 I). In line with renal function deterioration, renal damage measured by AKI score was similar in both groups (Fig. 5.4 A, D and G). Furthermore, Gr-1 positive neutrophil infiltration showed moderate to severe leukocyte infiltration in both groups (Fig. 5.4 B, E and H). On mRNA-level the pro-inflammatory cytokines IL-6 and MCP-1 were elevated in both groups. The STD+n3 group even showed a trend towards higher values compared to the STD group (Fig. 5.4 C and F).

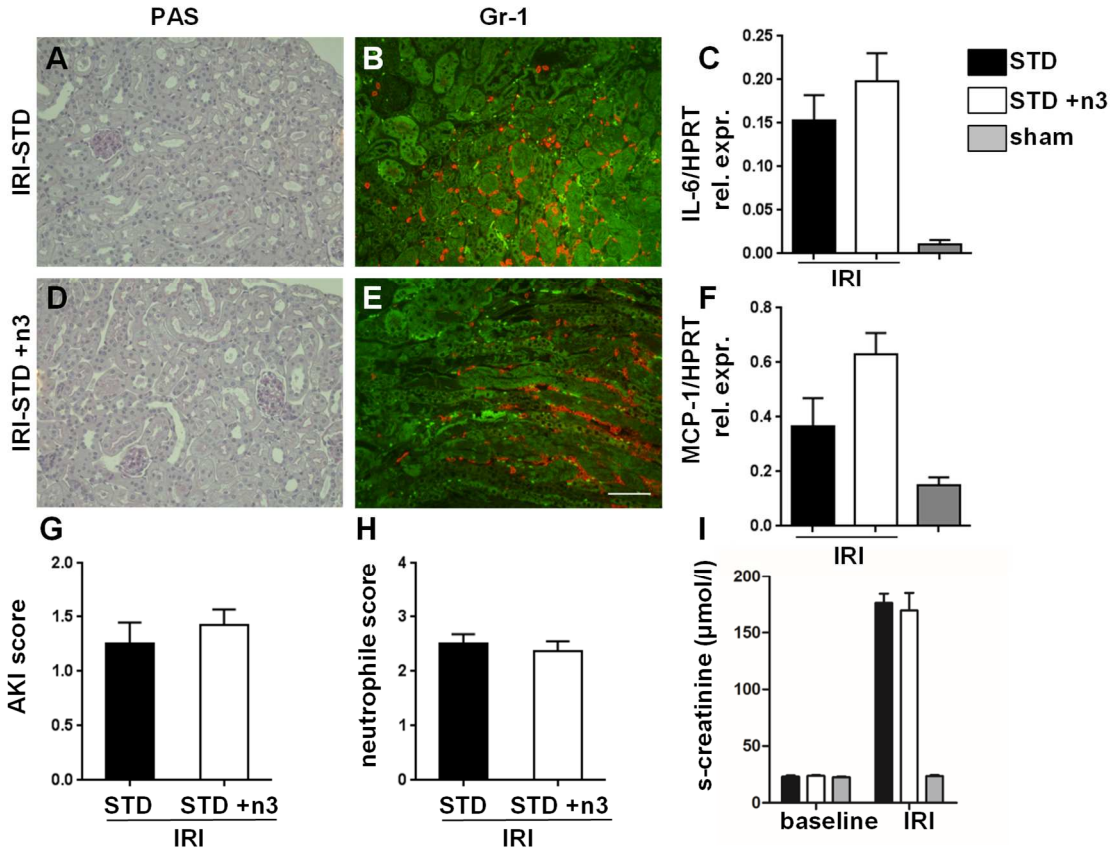

Fig. 5.4: Acute kidney injury and inflammation. Renal damage after IRI was comparable in STD and STD+n3 fed mice (**A, D, G**; STD: n = 18, STD+n3: n = 21). Neutrophil infiltration to the outer medulla was present in both groups without differences (**B, E, H**; STD: n = 18, STD+n3: n = 21). Renal function was significantly impaired after IRI in both groups (**I**; STD: n = 19, STD+n3: n = 21, sham n = 5). Relative expression of **(C)** IL-6 and **(F)** MCP-1 mRNA in kidney tissue was significantly up-regulated at 24 h after IRI in both groups without differences (STD: n = 7, STD+n3: n = 7). Shown are mean ± SEM.

5.3.3 Tubular function and heme oxygenase-1 expression

Alpha-1 microglobulin (A1M) is synthetized in the liver, filtered by the glomeruli and reabsorbed by proximal tubuli. In healthy kidneys A1M is present in vesicles in the cytoplasm of 60–70% of the tubuli. Upon AKI tubuli have a breakdown in energy metabolism and impaired transport function leading to lower cytoplasm concentration of A1M [49]. Due to IRI A1M expression decreased but was significantly higher in the STD+n3 group indicating better preservation of the tubular homeostasis and energy metabolism (Fig. 5.5 A, C and F). Heme oxygenase-1 (HO-1) is a renoprotective enzyme which is upregulated after AKI and mediates healing [50]. HO-1 expression was significantly higher in STD+n3 fed mice (Fig. 5.5 B, D and G).

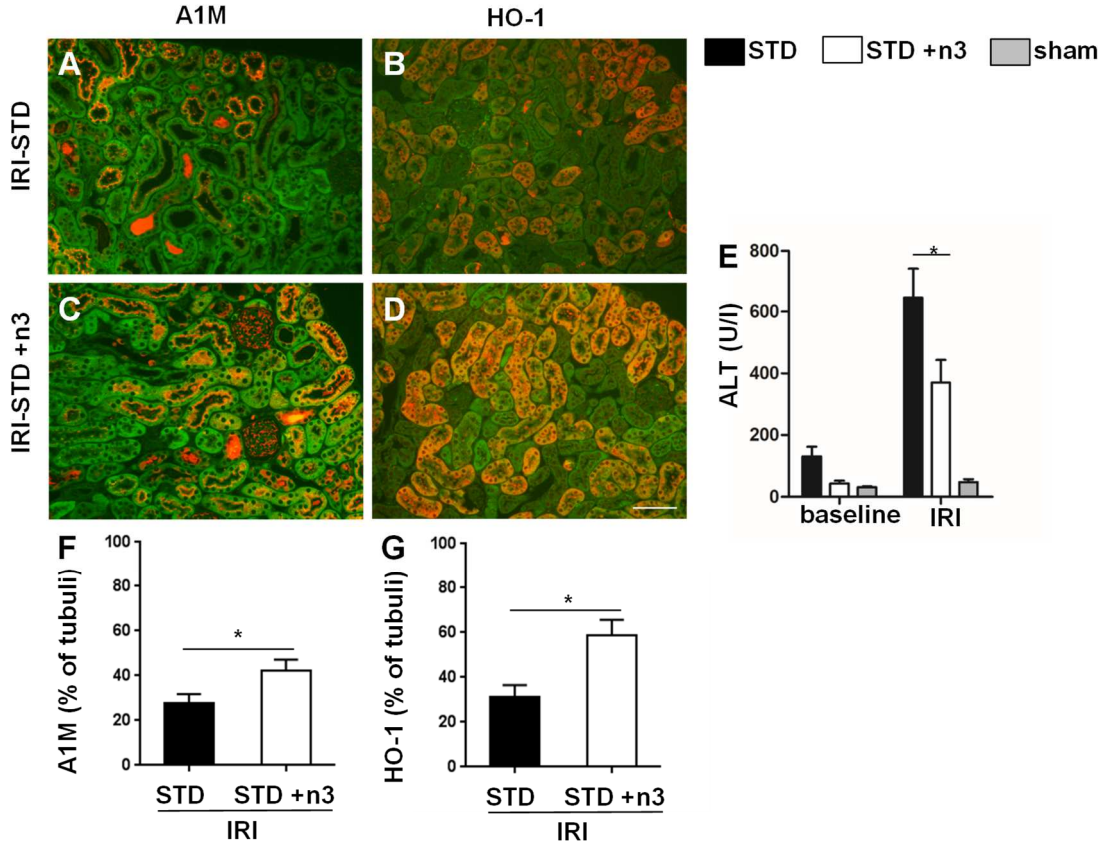

Fig. 5.5: Tubular transport and tubular regeneration. A1M expression was significantly higher after STD+n3 feeding which indicates preserved tubular transport function (**A, C, F**, STD: n = 18, STD+n3: n = 14). In addition, HO-1 expression was significantly upregulated in the STD+n3 fed group (**B, D, G**; STD: n = 7, STD+n3 n = 7) which correlates with tubular regeneration. Noteworthy, the elevation of the liver enzyme ALT was attenuated **(E)** by the STD+n3 diet and could point towards reduced distant organ injury (STD: n = 19, STD+n3 n = 21, sham n = 5). Shown are mean ± SEM, * $p < 0.05$.

Liver enzymes were elevated after IRI due to distant organ injury [51]. STD+n3 treatment caused less elevation of liver enzymes compared to the STD diet (Fig. 5.5 E). Overall, we observed some protective effects by the STD+n3 diet in the context of renal IRI (Fig. 5.5).

5.4 Discussion

Renal IRI is a common cause of AKI which is associated with high morbidity and mortality rates [7]. Particularly in the context of solid organ transplantations IRI is inevitable contributing to impaired allograft function [52]. Cardiac surgery in elderly patients with slightly decreased renal function has incidence rates of AKI of ~30% [53]. In the context of scheduled surgeries a dietary intervention would be possible, while the patients are waiting for the surgery. Beneficial effects of n3-PUFA supplementation have been reported, however in the context of kidney transplantation the outcome is inconsistent [26].

In the present study we investigated if dietary n3-PUFA supplementation improves renal function impairment in an ischemia induced AKI model following renal IRI in mice [42]. The control group received a chow, reflecting the omega-6 rich western diet [43] containing 10% linoleic acid rich sunflower oil (STD). For the investigation of potential beneficial effects of n3-PUFA supplementation on the base of a western diet, this chow was enriched with n3-PUFA (1% EPA and 1% DHA; STD+n3) as previously described [22]. In order to ensure a maximal modulation of the tissue fatty acid composition by the dietary PUFA supplementation a pre-feeding period of 14 days was included prior to induction of renal IRI. After 14 days of feeding the STD+n3 chow, the relative fatty acid pattern in the kidney, e.g. relative levels of the sum of saturated fatty acids, monounsaturated fatty acids, n6-PUFA and n3-PUFA (38.3%, 10.3%, 24.6% and 26.9% respectively), was comparable to the relative levels observed after 45 days of feeding the same diet to mice (38.1%, 13.0%, 25.2% and 23.9% respectively) [22] indicating that a steady-state in the modulation of the kidney fatty acid composition by the feeding was reached

after 14 days. This is also consistent with results from feeding fish oil to mice where a steady state of the PUFA status in heart and brain tissue was reached between 1 and 2 weeks [54]. Overall, feeding of the STD+n3 diet led to a massive elevation of absolute and relative levels of n3-PUFA (18:4 n3, 20:4 n3, 20:5 n3, 22:5 n3, 22:6 n3) with simultaneous decrease in n6-PUFA (18:3 n6, 20:2 n6, 20:3 n6, 20:4 n6, 22:4 n6, 22:5 n6) in the circulation and in the kidney. These changes are in line with previous reports showing extensive modulation of the PUFA composition in blood compartments and tissues by n3-PUFA feeding [22, 55-59] or by endogenous n3-PUFA accumulation in transgenic *fat-1* mice [22, 55, 60]. Compared to the STD chow, in response to the STD+n3 feeding the relative content of the main long-chain PUFA ARA, EPA and DHA in the kidney changed from 16.4% to 8.6% (0.5-fold), 0.04% to 4.1% (99-fold) and 10.1% to 21.0% (2-fold), respectively. Similar alterations in the renal fatty acid composition were also observed in mice and rats fed chow containing 1–3% each EPA and DHA (in each case in almost equal amount) [22, 56-58]. Relative levels in the kidney in response to STD+n3 are similar to earlier findings for n3-PUFA feeding in rodents ranging for EPA from 1–4.6% in mice and from 5.2–9.7% in rats and for DHA from 6.7–24.6% in mice and from 5.5–7.8% in rats depending primarily on the diet composition (e.g. ratio of n3/n6-PUFA). The differences in relative renal levels of EPA and DHA between mice and rats mainly originate from differing PUFA compositions under basal conditions (steady-state without n3-PUFA supplementation) [61]. The relative renal PUFA composition in response to STD+n3 was similar to the relative amount in murine renal phospholipids, especially phosphatidylcholines (9.0–12.4% ARA, 2.3–7.5% EPA and 10.0–18.1% DHA) observed after feeding fish oil supplemented chow [55, 59], reflecting that phospholipids as main membrane constituents are dominant lipids in the kidney [62, 63].

It should be noted, that the dietary supplementation by STD+n3 led to a more pronounced modulation of the n3-PUFA pattern compared to endogenous synthesis in transgenic *fat-1* mice [22, 55]: The relative levels in transgenic *fat-1* mice for ARA, EPA and DHA of 20.3%, 1.0% and 12.1% in the kidney [22] and

of 11.3%, 0.7% and 12.9% in kidney phospholipids, respectively [55] reveal that relative levels reached by STD+n3 feeding are around 4.1-fold and 1.7-fold higher for EPA and DHA, respectively.

The successful modulation of the endogenous n3-PUFA status by the feeding was also clearly indicated by the pronounced changes in %EPA+DHA levels in blood. In whole blood, which is dominated by the PUFA of erythrocytes, in response to the STD+n3 diet 3.7-fold higher levels of %EPA+DHA were observed compared to the STD diet (4.5 ± 0.1% in STD *vs*. 16.9 ± 0.3% in STD+n3). Extrapolating from mice to man, these concentrations reflect a very high endogenous n3-PUFA status, e.g. determined by the omega-3 index, i.e. the relative content of EPA+DHA in membranes of erythrocytes. With a value of 16.9% the endogenous n3-PUFA levels reached in response to the STD+n3 feeding are significantly higher than those which efficiently reduce overall mortality and the risk for cardiovascular diseases in men (i.e. an omega-3 index ≥ 8) [20, 21]. In contrast, the STD diet reflects the “western-diet” causing a low omega-3 index, even in mice, which more efficiently convert short-chain n3-PUFA to long-chain n3-PUFA than men [64]. Thus, it can be concluded that the n3-PUFA feeding strategy used in this study reflects the maximal shift in the PUFA pattern which can be reached. On a side note, a well-described clinical effect of n3-PUFA is the reduction of serum triglyceride (TG) concentration [65, 66]. Indeed, the total FA and thus TG concentration in whole blood was reduced in the animals receiving the STD+n3 compared to the STD diet (Fig. 5.2).

It is believed that a major portion of beneficial effects of n3-PUFA are mediated by changes in the pattern of oxygenated PUFA, i.e. eicosanoids and other oxylipins [27, 29]. As eicosanoids exert important functions in renal (patho)physiology including regulation of renal blood flow, glomerular filtration rate and tubular transport function [34-37], modulation of the oxylipin pattern by n3-PUFA may also impact kidney function in renal IRI.

Reflecting changes in the PUFA composition, the feeding strategy used in this study resulted in massive alterations of oxylipins in blood and renal tissue from

all major formation pathways (COX, LOX, CYP as well as non-enzymatic): ARA derived eicosanoids were significantly decreased while EPA and DHA derived oxylipins were significantly elevated in response to STD+n3 feeding (Fig. 5.3). Reduction of ARA derived eicosanoids was similar in plasma and kidney (free and total) for all investigated pathways with 40–75% lower levels after STD+n3 compared to STD feeding. Similarly, DHA derived oxylipins were 1.5–3-fold increased in the kidney, however a more pronounced elevation (7–12-fold) was observed for DHA derived products from 12/15-LOX as well as CYP in plasma. In contrast, EPA derived metabolites were increased to a greater extent (12–53-fold) and in several cases were below the LLOQ in STD while clearly elevated in STD+n3 fed mice. These changes are overall consistent with earlier studies after n3-PUFA (EPA and DHA) supplementation in mice [13, 22, 55, 67-70], rats [56, 67, 71-73] and humans [68, 74-76].

The strongest decrease was observed in kidney levels of ARA derived prostanoids, i.e. PGE_2 (250 *vs*. 62 nmol/kg) and TxB_2 (6.9 *vs* < 1.2 nmol/kg), and similar to earlier studies feeding EPA and DHA supplemented chow to mice [55, 67, 70]. Though respective EPA derived counterparts were simultaneously increased the resulting levels were considerably lower compared to their corresponding ARA derived prostanoids which is in line with their lower conversion rate by COX in addition to a simple PUFA competition [77]. Considering that EPA derived prostanoids are less bioactive, e.g. PGE_3 possesses less affinity towards EP receptors and exhibits lower potency regarding second messenger release [78] and also has been shown to cause less secretion of pro-inflammatory IL-6 [79] compared to PGE_2, this clear shift in the renal prostanoid pattern suggests that STD+n3 can contribute to a lower inflammatory status.

Regarding CYP derived metabolites a massive increase in levels of free terminal epoxy-PUFA derived from EPA and DHA, i.e. 17(18)-EpETE and 19(20)-EpDPE, was observed especially in plasma, concomitant with a relatively marked decrease in ARA derived 14(15)-EpETrE (16 *vs* 5 nmol/kg in

kidney and 1.3 *vs* 0.4 nM in plasma). Besides displacement of ARA by the n3-PUFA in response to the STD+n3 feeding this profound increase in n3-PUFA derived epoxy-PUFA can be explained by equal or higher conversion rates of DHA and EPA by several CYP isoforms in comparison to ARA [56, 80]. This marked elevation in n3-PUFA derived terminal epoxy-PUFA in plasma following STD+n3 feeding is similar to their clear increase observed in human plasma after fish oil supplementation [74, 81] supporting their ability to function as indicators for n3-PUFA supplementation as has been suggested [39]. Studies investigating the physiological role of epoxy-PUFA in the kidney are mainly focused on ARA derived EpETrE and comprise e.g. regulation of renal blood flow, inhibition of tubular sodium transport thereby promoting salt excretion, as well as anti-inflammatory effects [82]. Treatment of renal IRI in mice with an inhibitor of the soluble epoxide hydrolase have been shown to ameliorate kidney injury suggesting that epoxy-PUFA have beneficial effects on kidney function in renal IRI [83]. Similarly, n3-PUFA derived EpETE and EpDPE might impact renal physiology, e.g. owing to their higher potency regarding vasodilatory actions compared to EpETrE, as well as similar anti-inflammatory effects [82]. Regarding epoxy-PUFA, 19(20)-EpDPE reduced kidney fibrosis in a murine unilateral ureteral obstruction (UUO) model [84]. In contrast, in renal IRI administration of 19(20)-EpDPE led to aggravation of kidney damage while 14(15)-EpETrE as well as DHA itself alleviated kidney injury in mice [85].

In the past two decades, a class of multiple hydroxylated PUFA was proposed which actively terminate inflammation, so-called specialized pro-resolving mediators (SPM). From DHA, D-series resolvins as well as protectins and maresins are formed, while EPA gives rise to E-series resolvins [38]. Because of their low biological levels, these mediators are difficult to analyze [40]. Consistent with earlier reports [22, 67, 71] feeding of the n3-PUFA EPA and DHA led to a massive increase (2–9-fold) in the precursors of SPM, i.e. 17-HDHA, 14-HDHA and 18-HEPE. For example, the 18-HEPE content in the kidney in the STD+n3 group was 9.7 nmol/kg while in the control group it was below the LLOQ (1 nmol/kg). However, except for PD1 all signals for SPM were

below the LLOQ, i.e. in most cases below 2 nmol/kg kidney tissue. Thus, it has to be concluded that a 14-day feeding strategy with high n3-PUFA content (2%) does not increase the concentration of these mediators above 2 nmol/kg tissue or 0.56 nM blood. Either the SPM influence physiology in these picomolar, i.e. ppt (pg/g) concentrations or one has to conclude that they may not play a role in the physiological effects caused by n3-PUFA supplementation.

The signals for free PD1 in the kidney in response to STD+n3 feeding are in a similar range to a previous report detecting PD1 after fish oil supplementation in mice undergoing renal IRI [13]. Analysis of total oxylipins in the kidney suggested even higher levels of PD1 (Fig. 5.6). As internationally agreed for LC-MS compound identification (e.g. for pesticides [86]), we evaluated two mass transitions, i.e. *m/z* 359 → 153 [13, 87-89] and *m/z* 359 → 206 [87, 90, 91], which also have been previously used for PD1 detection. Particularly in the analysis of total PD1 in the kidney a massive divergence in the area ratio of these two transitions (compared to authentic PD1) was observed (Fig. 5.6). This clearly suggests that the signals result from isobaric interferences of the sample matrix and not from PD1 (Fig. 5.6). For free oxylipins in the kidney no signal was observed for *m/z* 359 → 206 and thus, it is even more clear that the signal of PD1 results from interfering matrix and not from the SPM. Isobaric interferences at the retention time of PD1 in reversed-phase HPLC at *m/z* 359 → 153 causing an apparent PD1 concentration also have been recently reported for plasma samples after storage [92]. By contrast, the relative intensities of the signals of the PD1-isomer PDX showed identical ratios for the authentic standard and biological samples (Fig. 5.6). Overall our data do not support the earlier described renal formation of PD1 in a mouse model of AKI following feeding a slightly lower dose of n3-PUFA (1.4% n3-PUFA in chow compared to 2% in this study) [13].

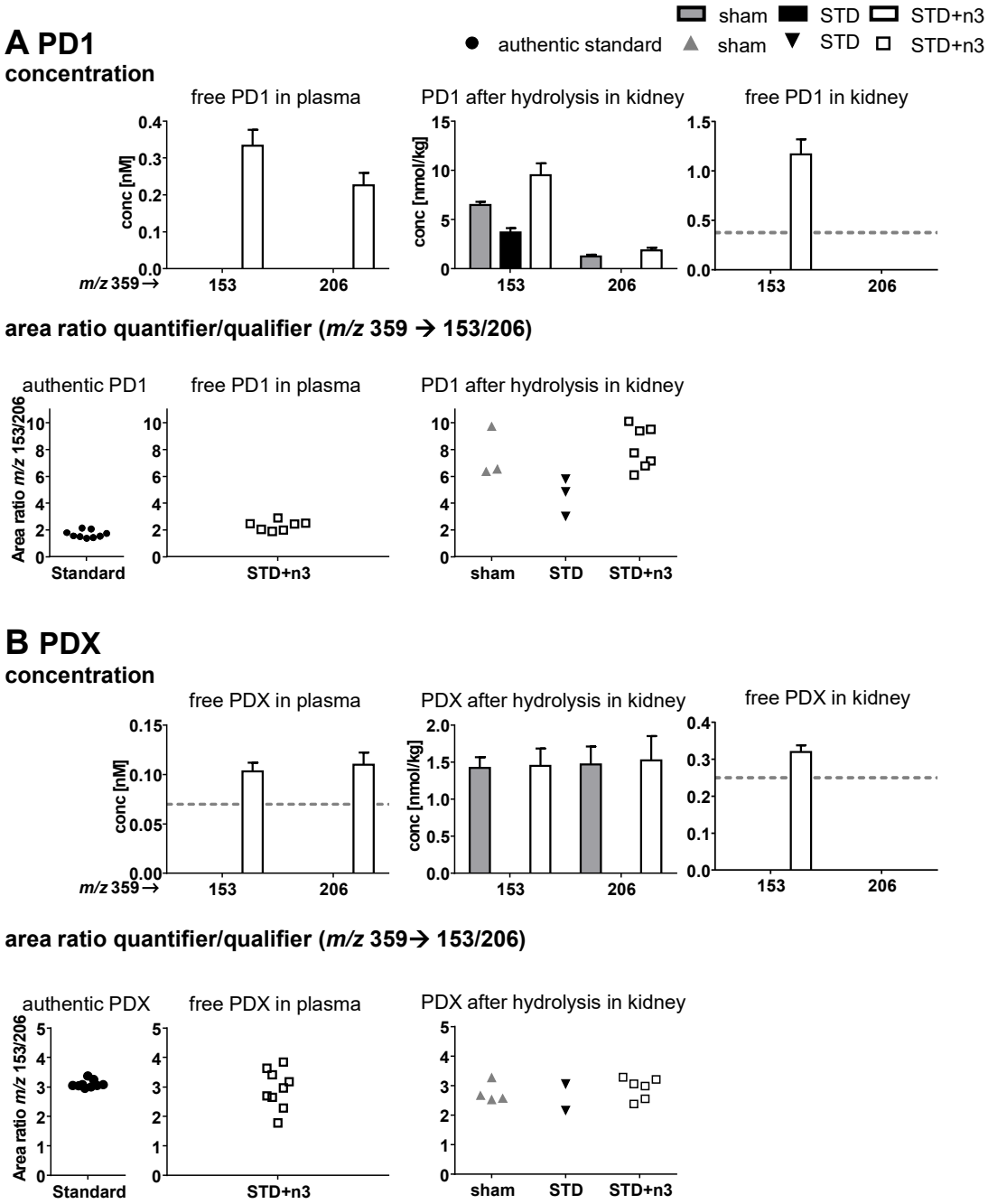

Fig. 5.6: Concentration of protectins **(A)** PD1 and **(B)** PDX quantified based on area analyte/area IS ratio on two different transitions for PD1 and PDX (*m/z* 359 → 153 and *m/z* 359 → 206) as free mediators in plasma and kidney as well as after alkaline hydrolysis in kidney. Shown are mean ± SEM. Means were only calculated when > 50% of the samples in the group were > LLOQ. The LLOQ is indicated as dashed line. For PD1 and PDX the area ratios resulting from both transitions were determined in authentic standard as well as in individual samples. Area ratios were calculated for every sample in which concentrations of both transitions were above LLOQ.

n3-PUFA are prone to oxidation and may lead to increased oxidative stress. Indeed, in humans receiving a very high dose of DHA (1.6 g/d) urinary 15-F_{2t}-IsoP, a marker of oxidative stress, was increased [93]. This could be even more important in ischemic injury were enhanced oxidative stress plays a key role in pathophysiology [6]. However, our data reveal, that the STD+n3 group did not show elevated IsoP levels in the kidney as well as in plasma following IRI compared to the STD fed mice (Fig. 5.3, Fig. 5.7). Similarly, lower levels of the autoxidation marker malondialdehyde were observed after renal IRI in the kidney tissue of rats treated with n3-PUFA [11, 12]. However, to comprehensively investigate oxidative stress caused by IRI and its modulation by n3-PUFA supplementation further autoxidation parameters, such as 8-hydroxyguanosine, glutathione, 4-hydroxy-nonenal and expression of (anti)oxidative stress response genes should be monitored in the future.

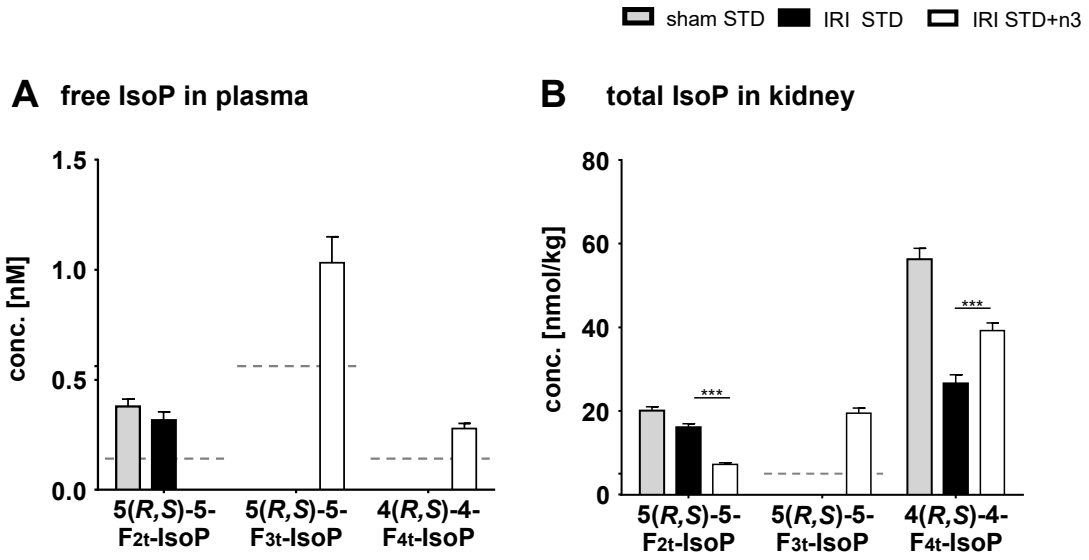

Fig. 5.7: Concentration of **(A)** free isoprostanes (IsoP) in plasma and **(B)** total IsoP following alkaline hydrolysis in kidney tissue. Shown are levels of selected IsoP derived from ARA, EPA and DHA, i.e. 5(*R,S*)-5-F_{2t}-IsoP, 5(*R,S*)-5-F_{3t}-IsoP and 4(*R,S*)-4-F_{4t}-NeuroP, respectively. The lower limit of quantification (LLOQ) is indicated by a dashed grey line in case it was not exceeded in > 50% of the samples per group. Statistical differences between STD and STD+n3 were determined by two-tailed t-test, * $p < 0.05$, ** $p < 0.01$, *** $p < 0.001$.

Altogether feeding of STD+n3 led to a maximal modulation of n3-PUFA and its lipid mediators dominated by n3-PUFA derived oxylipins. Thus, the feeding strategy allows to evaluate the effects of maximal dietary n3-PUFA modulation based on a western diet on acute kidney injury.

Despite the clear effects on oxylipins the STD+n3 diet did not result in an improvement of the overall renal function or reduction of pro-inflammatory cytokine production or leukocyte infiltration 24 h after IRI. However, there were measurable effects on protective molecular mechanisms such as up-regulation of HO-1. It has been shown that HO-1 fosters renal regeneration and healing in several models of renal injury [45, 94, 95]. In addition, the tubular transport function which depends on intact energy metabolism of the tubuli was preserved as shown by A1M staining. There was a direct correlation in previous studies between higher A1M expression and less tissue edema measured by functional MRI [49]. In the current study there was also less ALT elevation which is a marker for impaired liver function. It is well known that AKI causes distant organ injury *via* enhanced leukocyte infiltration into other organs such as liver, lung, brain, gut [51, 96]. Mechanisms are multifactorial such as release of cytokines and inflammatory mediators, increase in oxidative stress, activation of various immune cells, neutrophil extravasation, generalized endothelial injury, increased vascular permeability and tissue edema formation [97]. In a mouse model of liver IRI also beneficial effects with less tissue damage have been attributed to n3-PUFA treatment [98]. It is conceivable that the moderate beneficial effects could improve patient outcome in longer follow-up by reducing the general inflammatory status.

In a previous study on renal IRI beneficial effects of dietary n3-PUFA supplementation have been reported in mice [13]. However, the severity of AKI might differ between the studies. In the study by Hassan et al. creatinine elevation was only 2–3-fold which is less than in our study (6-fold) and might reflect a milder AKI model. In the clinical context interesting and relevant benefits from n3-PUFA diets were observed, e.g. they seemed to reduce

cardiovascular mortality in patients with chronic kidney disease [99]. In addition, another study showed that n3-PUFA reduced blood pressure and triglyceride levels in patients with CKD stage 3–4 in a placebo-controlled intervention study [100]. Since AKI has a high risk of progression to CKD there might be later beneficial effects on clinical outcome which are missed by the nature of the current study design with a 24-hour follow-up. Further investigations with in-depth analysis of oxylipin levels also at later time points of disease progression might be of interest and shall be addressed in the future.

5.5 Conclusion

In the present study supplementation of a western-style, i.e. linoleic acid rich diet with the long-chain n3-PUFA EPA and DHA led to a pronounced modulation of the PUFA and oxylipin pattern. However, in a murine model of moderate AKI pre-feeding of n3-PUFA did not attenuate renal function impairment, morphological renal damage and inflammation characterized by pro-inflammatory cytokine (IL-6 and MCP-1) mRNA up-regulation and neutrophil infiltration. However, also beneficial effects were seen such as preservation of tubular transport function indicated by enhanced alpha-1 microglobulin (A1M) expression in cortical proximal tubular epithelial cells and enhanced up-regulation of tubular heme oxygenase-1 (HO-1) expression which has been correlated to improved renal regeneration [45]. Thus n3-PUFA supplementation might lead to renal protection with respect to long-term damage.

Overall it is concluded that – despite a maximal elevation of endogenous n3-PUFA and n3-PUFA derived oxylipin levels – n3-PUFA supplementation did not result in attenuation of renal function impairment or acute kidney injury within 24 hours in this model.

5.6 References

1. Kidney Disease: Improving Global Outcomes (KDIGO) Acute Kidney Injury Work Group (2012) KDIGO Clinical Practice Guideline for Acute Kidney Injury. *Kidney Int Suppl*. 2(Supplement 1), pp. 1-138; doi: 10.1038/kisup.2011.32.
2. Sovik S., Isachsen M. S., Nordhuus K. M., Tveiten C. K., Eken T., Sunde K., Brurberg K. G. and Beitland S. (2019) Acute kidney injury in trauma patients admitted to the ICU: A systematic review and meta-analysis. *Intensive Care Med*. 45(4), pp. 407-419; doi: 10.1007/s00134-019-05535-y.
3. Chalikias G., Serif L., Kikas P., Thomaidis A., Stakos D., Makrygiannis D., Chatzikyriakou S., Papoulidis N., Voudris V., Lantzouraki A., Muller M., Arampatzis S., Konstantinides S. and Tziakas D. (2019) Long-term impact of acute kidney injury on prognosis in patients with acute myocardial infarction. *Int J Cardiol*. 283, pp. 48-54; doi: 10.1016/j.ijcard.2019.01.070.
4. Palant C. E., Amdur R. L. and Chawla L. S. (2017) Long-term consequences of acute kidney injury in the perioperative setting. *Curr Opin Anaesthesiol*. 30(1), pp. 100-104; doi: 10.1097/ACO.0000000000000428.
5. Chawla L. S., Eggers P. W., Star R. A. and Kimmel P. L. (2014) Acute kidney injury and chronic kidney disease as interconnected syndromes. *N Engl J Med*. 371(1), pp. 58-66; doi: 10.1056/NEJMra1214243.
6. Granger D. N. and Kvietys P. R. (2015) Reperfusion injury and reactive oxygen species: The evolution of a concept. *Redox Biol*. 6, pp. 524-551; doi: 10.1016/j.redox.2015.08.020.
7. Bonventre J. V. and Yang L. (2011) Cellular pathophysiology of ischemic acute kidney injury. *J Clin Invest*. 121(11), pp. 4210-4221; doi: 10.1172/JCI45161.
8. Eltzschig H. K. and Eckle T. (2011) Ischemia and reperfusion — from mechanism to translation. *Nat Med*. 17(11), pp. 1391-1401; doi: 10.1038/nm.2507.
9. Kinsey G. R., Li L. and Okusa M. D. (2008) Inflammation in acute kidney injury. *Nephron Exp Nephrol*. 109(4), pp. e102-e107; doi: 10.1159/000142934.
10. Gwon D. H., Hwang T. W., Ro J.-Y., Kang Y.-J., Jeong J. Y., Kim D.-K., Lim K., Kim D. W., Choi D. E. and Kim J.-J. (2017) High endogenous accumulation of ω-3 polyunsaturated fatty acids protect against ischemia-reperfusion renal injury through AMPK-mediated autophagy in fat-1 mice. *Int J Mol Sci*. 18(10):2081; doi: 10.3390/ijms18102081.
11. Ajami M., Davoodi S. H., Habibey R., Namazi N., Soleimani M. and Pazoki-Toroudi H. (2013) Effect of DHA+EPA on oxidative stress and apoptosis induced by ischemia-reperfusion in rat kidneys. *Fundam Clin Pharmacol*. 27(6), pp. 593-602; doi: 10.1111/j.1472-8206.2012.01066.x.
12. Ashtiyani S. C., Najafi H., Kabirinia K., Vahedi E. and Jamebozorky L. (2012) Oral omega-3 fatty acid for reduction of kidney dysfunction induced by reperfusion injury in rats. *Iran J Kidney Dis*. 6(4), pp. 275-283.
13. Hassan I. R. and Gronert K. (2009) Acute changes in dietary ω-3 and ω-6 polyunsaturated fatty acids have a pronounced impact on survival following ischemic renal injury and formation of renoprotective docosahexaenoic acid-derived protectin D1. *J Immunol*. 182(5), pp. 3223-3232; doi: 10.4049/jimmunol.0802064.
14. Kielar M. L., Jeyarajah D. R., Zhou X. J. and Lu C. Y. (2003) Docosahexaenoic acid ameliorates murine ischemic acute renal failure and prevents increases in mRNA abundance for both TNF-alpha and inducible nitric oxide synthase. *J Am Soc Nephrol*. 14(2), pp. 389-396; doi: 10.1097/01.ASN.0000045047.44107.0B

15. Torras J., Soto K., Riera M., Herrero I., Valles J., Cruzado J. M., Alsina J. and Grinyo J. M. (1996) Changes in renal hemodynamics and physiology after normothermic ischemia in animals supplemented with eicosapentaenoic acid. *Transpl Int*. 9 (Suppl 1), pp. S455-S459; doi: 10.1111/j.1432-2277.1996.tb01675.x.
16. Fassett R. G., Gobe G. C., Peake J. M. and Coombes J. S. (2010) Omega-3 polyunsaturated fatty acids in the treatment of kidney disease. *Am J Kidney Dis*. 56(4), pp. 728-742; doi: 10.1053/j.ajkd.2010.03.009.
17. Gopinath B., Harris D. C., Flood V. M., Burlutsky G. and Mitchell P. (2011) Consumption of long-chain n-3 PUFA, alpha-linolenic acid and fish is associated with the prevalence of chronic kidney disease. *Br J Nutr*. 105(9), pp. 1361-1368; doi: 10.1017/S0007114510005040.
18. Huang X., Lindholm B., Stenvinkel P. and Carrero J. J. (2013) Dietary fat modification in patients with chronic kidney disease: n-3 Fatty acids and beyond. *J Nephrol*. 26(6), pp. 960-974; doi: 10.5301/jn.5000284.
19. Hu J., Liu Z. and Zhang H. (2017) Omega-3 fatty acid supplementation as an adjunctive therapy in the treatment of chronic kidney disease: A meta-analysis. *Clinics (Sao Paulo)*. 72(1), pp. 58-64; doi: 10.6061/clinics/2017(01)10.
20. Harris W. S. and von Schacky C. (2004) The Omega-3 Index: A new risk factor for death from coronary heart disease? *Prev Med*. 39(1), pp. 212-220; doi: 10.1016/j.ypmed.2004.02.030.
21. von Schacky C. (2011) The Omega-3 Index as a risk factor for cardiovascular diseases. *Prostaglandins Other Lipid Mediat*. 96(1-4), pp. 94-98; doi: 10.1016/j.prostaglandins.2011.06.008.
22. Ostermann A. I., Waindok P., Schmidt M. J., Chiu C.-Y., Smyl C., Rohwer N., Weylandt K.-H. and Schebb N. H. (2017) Modulation of the endogenous omega-3 fatty acid and oxylipin profile in vivo — A comparison of the fat-1 transgenic mouse with C57BL/6 wildtype mice on an omega-3 fatty acid enriched diet. *PLoS One*. 12(9):e0184470; doi: 10.1371/journal.pone.0184470.
23. Harris W. S., Tintle N. L., Etherton M. R. and Vasan R. S. (2018) Erythrocyte long-chain omega-3 fatty acid levels are inversely associated with mortality and with incident cardiovascular disease: The Framingham Heart Study. *J Clin Lipidol*. 12(3), pp. 718-727.e716; doi: 10.1016/j.jacl.2018.02.010.
24. Abdelhamid A. S., Brown T. J., Brainard J. S., Biswas P., Thorpe G. C., Moore H. J., Deane K. H., AlAbdulghafoor F. K., Summerbell C. D., Worthington H. V., Song F. and Hooper L. (2018) Omega-3 fatty acids for the primary and secondary prevention of cardiovascular disease. *Cochrane Database Syst Rev*. 11:CD003177; doi: 10.1002/14651858.CD003177.pub4.
25. Aung T., Halsey J., Kromhout D., Gerstein H. C., Marchioli R., Tavazzi L., Geleijnse J. M., Rauch B., Ness A., Galan P., Chew E. Y., Bosch J., Collins R., Lewington S., Armitage J., Clarke R. and for the Omega-3 Treatment Trialists' C. (2018) Associations of omega-3 fatty acid supplement use with cardiovascular disease risks: Meta-analysis of 10 trials involving 77 917 individuals. *JAMA Cardiol*. 3(3), pp. 225-233; doi: 10.1001/jamacardio.2017.5205.
26. Tatsioni A., Chung M., Sun Y., Kupelnick B., Lichtenstein A. H., Perrone R., Chew P., Lau J. and Bonis P. A. (2005) Effects of fish oil supplementation on kidney transplantation: A systematic review and meta-analysis of randomized, controlled trials. *J Am Soc Nephrol*. 16(8), pp. 2462-2470; doi: 10.1681/ASN.2005020176.
27. Calder P. C. (2015) Marine omega-3 fatty acids and inflammatory processes: Effects, mechanisms and clinical relevance. *Biochim Biophys Acta*. 1851(4), pp. 469-484; doi: 10.1016/j.bbalip.2014.08.010.

28. Gabbs M., Leng S., Devassy J. G., Monirujjaman M. and Aukema H. M. (2015) Advances in our understanding of oxylipins derived from dietary PUFAs. *Adv Nutr*. 6(5), pp. 513-540; doi: 10.3945/an.114.007732.
29. Wang W., Zhu J., Lyu F., Panigrahy D., Ferrara K. W., Hammock B. and Zhang G. (2014) ω-3 Polyunsaturated fatty acids-derived lipid metabolites on angiogenesis, inflammation and cancer. *Prostaglandins Other Lipid Mediat*. 113-115, pp. 13-20; doi: 10.1016/j.prostaglandins.2014.07.002.
30. Gladine C., Ostermann A. I., Newman J. W. and Schebb N. H. (2019) MS-based targeted metabolomics of eicosanoids and other oxylipins: Analytical and inter-individual variabilities. *Free Radic Biol Med*. 144, pp. 72-89; doi: 10.1016/j.freeradbiomed.2019.05.012.
31. Buczynski M. W., Dumlao D. S. and Dennis E. A. (2009) Thematic review series: Proteomics - An integrated omics analysis of eicosanoid biology. *J Lipid Res*. 50(6), pp. 1015-1038; doi: 10.1194/jlr.R900004-JLR200.
32. Morrow J. D., Hill K. E., Burk R. F., Nammour T. M., Badr K. F. and Roberts II L. J. (1990) A series of prostaglandin F2-like compounds are produced in vivo in humans by a non-cyclooxygenase, free radical-catalyzed mechanism. *Proc Natl Acad Sci U S A*. 87(23), pp. 9383-9387; doi: 10.1073/pnas.87.23.9383.
33. Galano J.-M., Lee Y. Y., Oger C., Vigor C., Vercauteren J., Durand T., Giera M. and Lee J. C.-Y. (2017) Isoprostanes, neuroprostanes and phytoprostanes: An overview of 25 years of research in chemistry and biology. *Prog Lipid Res*. 68, pp. 83-108; doi: 10.1016/j.plipres.2017.09.004.
34. Imig J. D. (2000) Eicosanoid regulation of the renal vasculature. *Am J Physiol Renal Physiol*. 279(6), pp. F965-F981; doi: 10.1152/ajprenal.2000.279.6.F965.
35. Hao C. M. and Breyer M. D. (2007) Roles of lipid mediators in kidney injury. *Semin Nephrol*. 27(3), pp. 338-351; doi: 10.1016/j.semnephrol.2007.02.008.
36. Hao C. M. and Breyer M. D. (2008) Physiological regulation of prostaglandins in the kidney. *Annu Rev Physiol*. 70, pp. 357-377; doi: 10.1146/annurev.physiol.70.113006.100614.
37. Fan F. and Roman R. J. (2017) Effect of cytochrome P450 metabolites of arachidonic acid in nephrology. *J Am Soc Nephrol*. 28(10), pp. 2845-2855; doi: 10.1681/ASN.2017030252.
38. Serhan C. N. (2014) Pro-resolving lipid mediators are leads for resolution physiology. *Nature*. 510(7503), pp. 92-101; doi: 10.1038/nature13479.
39. Murphy R. C. (2015) Specialized pro-resolving mediators: Do they circulate in plasma? *J Lipid Res*. 56(9), pp. 1641-1642; doi: 10.1194/jlr.C062356.
40. Kutzner L., Rund K. M., Ostermann A. I., Hartung N. M., Galano J.-M., Balas L., Durand T., Balzer M. S., David S. and Schebb N. H. (2019) Development of an optimized LC-MS method for the detection of specialized pro-resolving mediators in biological samples. *Front Pharmacol*. 10:169; doi: 10.3389/fphar.2019.00169.
41. Hueper K., Gutberlet M., Rong S., Hartung D., Mengel M., Lu X., Haller H., Wacker F., Meier M. and Gueler F. (2014) Acute kidney injury: Arterial spin labeling to monitor renal perfusion impairment in mice - Comparison with histopathologic results and renal function. *Radiology*. 270(1), pp. 117-124; doi: 10.1148/radiol.13130367.
42. Gueler F., Shushakova N., Mengel M., Hueper K., Chen R., Liu X., Park J. K., Haller H., Wensvoort G. and Rong S. (2015) A novel therapy to attenuate acute kidney injury and ischemic allograft damage after allogenic kidney transplantation in mice. *PLoS One*. 10(1):e0115709; doi: 10.1371/journal.pone.0115709.
43. Blasbalg T. L., Hibbeln J. R., Ramsden C. E., Majchrzak S. F. and Rawlings R. R. (2011) Changes in consumption of omega-3 and omega-6 fatty acids in the United

States during the 20th century. *Am J Clin Nutr*. 93(5), pp. 950-962; doi: 10.3945/ajcn.110.006643.

44. Rund K. M., Ostermann A. I., Kutzner L., Galano J.-M., Oger C., Vigor C., Wecklein S., Seiwert N., Durand T. and Schebb N. H. (2018) Development of an LC-ESI(-)-MS/MS method for the simultaneous quantification of 35 isoprostanes and isofurans derived from the major n3- and n6-PUFAs. *Anal Chim Acta*. 1037, pp. 63-74; doi: 10.1016/j.aca.2017.11.002.
45. Thorenz A., Derlin K., Schröder C., Dressler L., Vijayan V., Pradhan P., Immenschuh S., Jörns A., Echtermeyer F., Herzog C., Chen R., Rong S., Bräsen J. H., van Kooten C., Kirsch T., Klemann C., Meier M., Klos A., Haller H., Hensen B. and Gueler F. (2018) Enhanced activation of interleukin-10, heme oxygenase-1, and AKT in C5aR2-deficient mice is associated with protection from ischemia reperfusion injury–induced inflammation and fibrosis. *Kidney Int*. 94(4), pp. 741-755; doi: 10.1016/j.kint.2018.04.005.
46. Ostermann A. I., Müller M., Willenberg I. and Schebb N. H. (2014) Determining the fatty acid composition in plasma and tissues as fatty acid methyl esters using gas chromatography – A comparison of different derivatization and extraction procedures. *Prostaglandins Leukot Essent Fatty Acids*. 91(6), pp. 235-241; doi: 10.1016/j.plefa.2014.10.002.
47. Gottschall H., Schmöcker C., Hartmann D., Rohwer N., Rund K., Kutzner L., Nolte F., Ostermann A. I., Schebb N. H. and Weylandt K. H. (2018) Aspirin alone and combined with a statin suppresses eicosanoid formation in human colon tissue. *J Lipid Res*. 59(5), pp. 864-871; doi: 10.1194/jlr.M078725.
48. Ostermann A. I., Greupner T., Kutzner L., Hartung N. M., Hahn A., Schuchardt J. P. and Schebb N. H. (2018) Intra-individual variance of the human plasma oxylipin pattern: Low inter-day variability in fasting blood samples versus high variability during the day. *Anal Methods*. 10(40), pp. 4935-4944; doi: 10.1039/C8AY01753K.
49. Hueper K., Gutberlet M., Brasen J. H., Jang M. S., Thorenz A., Chen R., Hertel B., Barrmeyer A., Schmidbauer M., Meier M., von Vietinghoff S., Khalifa A., Hartung D., Haller H., Wacker F., Rong S. and Gueler F. (2016) Multiparametric functional MRI: Non-invasive imaging of inflammation and edema formation after kidney transplantation in mice. *PLoS One*. 11(9):e0162705; doi: 10.1371/journal.pone.0162705.
50. Gueler F., Park J. K., Rong S., Kirsch T., Lindschau C., Zheng W., Elger M., Fiebeler A., Fliser D., Luft F. C. and Haller H. (2007) Statins attenuate ischemia-reperfusion injury by inducing heme oxygenase-1 in infiltrating macrophages. *Am J Pathol*. 170(4), pp. 1192-1199; doi: 10.2353/ajpath.2007.060782.
51. Doi K. and Rabb H. (2016) Impact of acute kidney injury on distant organ function: Recent findings and potential therapeutic targets. *Kidney Int*. 89(3), pp. 555-564; doi: 10.1016/j.kint.2015.11.019.
52. Salvadori M., Rosso G. and Bertoni E. (2015) Update on ischemia-reperfusion injury in kidney transplantation: Pathogenesis and treatment. *World J Transplant*. 5(2), pp. 52-67; doi: 10.5500/wjt.v5.i2.52.
53. Jiang W., Teng J., Xu J., Shen B., Wang Y., Fang Y., Zou Z., Jin J., Zhuang Y., Liu L., Luo Z., Wang C. and Ding X. (2016) Dynamic predictive scores for cardiac surgery-associated acute kidney injury. *J Am Heart Assoc*. 5(8):e003754; doi: 10.1161/JAHA.116.003754.
54. Swanson J. E., Mark Black J. and Kinsella J. E. (1988) Dietary menhaden oil: Effects on the rate and magnitude of modification of phospholipid fatty acid composition of mouse heart and brain. *Br J Nutr*. 59(3), pp. 535-545; doi: 10.1079/BJN19880062.

55. Kelton D., Lysecki C., Aukema H., Anderson B., Kang J. X. and Ma D. W. L. (2013) Endogenous synthesis of n−3 PUFA modifies fatty acid composition of kidney phospholipids and eicosanoid levels in the fat-1 mouse. *Prostaglandins Leukot Essent Fatty Acids*. 89(4), pp. 169-177; doi: 10.1016/j.plefa.2013.08.002.
56. Arnold C., Markovic M., Blossey K., Wallukat G., Fischer R., Dechend R., Konkel A., von Schacky C., Luft F. C., Muller D. N., Rothe M. and Schunck W. H. (2010) Arachidonic acid-metabolizing cytochrome P450 enzymes are targets of ω-3 fatty acids. *J Biol Chem*. 285(43), pp. 32720-32733; doi: 10.1074/jbc.M110.118406.
57. Ossani G. P., Denninghoff V. C., Uceda A. M., Diaz M. L., Uicich R. and Monserrat A. J. (2015) Short-term menhaden oil rich diet changes renal lipid profile in acute kidney injury. *J Oleo Sci*. 64(5), pp. 497-503; doi: 10.5650/jos.ess14186.
58. Gigliotti J. C., Benedito V. A., Livengood R., Oldaker C., Nanda N. and Tou J. C. (2013) Feeding different omega-3 polyunsaturated fatty acid sources influences renal fatty acid composition, inflammation, and occurrence of nephrocalcinosis in female Sprague-Dawley rats. *Food Nutr Sci*. 4(9A):36483, pp. 125-136; doi: 10.4236/fns.2013.49A1020.
59. Aukema H. M., Yamaguchi T., Takahashi H., Philbrick D. J. and Holub B. J. (1992) Effects of dietary fish oil on survival and renal fatty acid composition in murine polycystic kidney disease. *Nutr Res*. 12(11), pp. 1383-1392; doi: 10.1016/S0271-5317(05)80537-8.
60. Kang J. X., Wang J., Wu L. and Kang Z. B. (2004) Transgenic mice: Fat-1 mice convert n-6 to n-3 fatty acids. *Nature*. 427(6974), p 504; doi: 10.1038/427504a.
61. Couture P. and Hulbert A. J. (1995) Membrane fatty acid composition of tissues is related to body mass of mammals. *J Membr Biol*. 148(1), pp. 27-39; doi: 10.1007/bf00234153.
62. Druilhet R. E., Overturf M. L. and Kirkendall W. M. (1975) Structure of neutral glycerides and phosphoglycerides of human kidney. *Int J Biochem*. 6(12), pp. 893-901; doi: 10.1016/0020-711X(75)90010-5.
63. Rouser G., Simon G. and Kritchevsky G. (1969) Species variations in phospholipid class distribution of organs: I. Kidney, liver and spleen. *Lipids*. 4(6), pp. 599-606; doi: 10.1007/BF02531047.
64. Anderson B. M. and Ma D. W. L. (2009) Are all n-3 polyunsaturated fatty acids created equal? *Lipids Health Dis*. 8:33; doi: 10.1186/1476-511X-8-33.
65. Harris W. S. (2001) Omega-3 long-chain PUFA and triglyceride lowering: Minimum effective intakes. *Eur Heart J Suppl*. 3(Suppl D), pp. D59-D61; doi: 10.1016/S1520-765X(01)90121-X.
66. Sanders T. A. B. and Hochland M. C. (1983) A comparison of the influence on plasma lipids and platelet function of supplements of ω3 and ω6 polyunsaturated fatty acids. *Br J Nutr*. 50(3), pp. 521-529; doi: 10.1079/BJN19830123.
67. Devassy J. G., Yamaguchi T., Monirujjaman M., Gabbs M., Ravandi A., Zhou J. and Aukema H. M. (2017) Distinct effects of dietary flax compared to fish oil, soy protein compared to casein, and sex on the renal oxylipin profile in models of polycystic kidney disease. *Prostaglandins Leukot Essent Fatty Acids*. 123, pp. 1-13; doi: 10.1016/j.plefa.2017.07.002.
68. Zhang X., Yang N., Ai D. and Zhu Y. (2015) Systematic metabolomic analysis of eicosanoids after omega-3 polyunsaturated fatty acid supplementation by a highly specific liquid chromatography-tandem mass spectrometry-based method. *J Proteome Res*. 14(4), pp. 1843-1853; doi: 10.1021/pr501200u.
69. Balvers M. G., Verhoeckx K. C., Bijlsma S., Rubingh C. M., Meijerink J., Wortelboer H. M. and Witkamp R. F. (2012) Fish oil and inflammatory status alter the n-3 to n-6

balance of the endocannabinoid and oxylipin metabolomes in mouse plasma and tissues. *Metabolomics*. 8(6), pp. 1130-1147; doi: 10.1007/s11306-012-0421-9.

70. Gallon L. S. and Barcelli U. O. (1986) Measurement of prostaglandin E3 and other eicosanoids in biologic samples using high pressure liquid chromatography and radioimmunoassay. *Prostaglandins*. 31(2), pp. 217-225; doi: 10.1016/0090-6980(86)90048-1.
71. Leng S., Winter T. and Aukema H. M. (2018) Dietary ALA, EPA and DHA have distinct effects on oxylipin profiles in female and male rat kidney, liver and serum. *J Nutr Biochem*. 57, pp. 228-237; doi: 10.1016/j.jnutbio.2018.04.002.
72. Aukema H. M., Lu J., Borthwick F. and Proctor S. D. (2013) Dietary fish oil reduces glomerular injury and elevated renal hydroxyeicosatetraenoic acid levels in the JCR:LA-cp rat, a model of the metabolic syndrome. *Br J Nutr*. 110(1), pp. 11-19; doi: 10.1017/S0007114512004606.
73. Ibrahim N. H., Jia Y., Devassy J. G., Yamaguchi T. and Aukema H. M. (2014) Renal cyclooxygenase and lipoxygenase products are altered in polycystic kidneys and by dietary soy protein and fish oil treatment in the Han:SPRD-Cy rat. *Mol Nutr Food Res*. 58(4), pp. 768-781; doi: 10.1002/mnfr.201300332.
74. Fischer R., Konkel A., Mehling H., Blossey K., Gapelyuk A., Wessel N., von Schacky C., Dechend R., Muller D. N., Rothe M., Luft F. C., Weylandt K. and Schunck W. H. (2014) Dietary omega-3 fatty acids modulate the eicosanoid profile in man primarily via the CYP-epoxygenase pathway. *J Lipid Res*. 55(6), pp. 1150-1164; doi: 10.1194/jlr.M047357.
75. Zivkovic A. M., Yang J., Georgi K., Hegedus C., Nording M. L., O'Sullivan A., German J. B., Hogg R. J., Weiss R. H., Bay C. and Hammock B. D. (2012) Serum oxylipin profiles in IgA nephropathy patients reflect kidney functional alterations. *Metabolomics*. 8(6), pp. 1102-1113; doi: 10.1007/s11306-012-0417-5.
76. Schebb N. H., Ostermann A. I., Yang J., Hammock B. D., Hahn A. and Schuchardt J. P. (2014) Comparison of the effects of long-chain omega-3 fatty acid supplementation on plasma levels of free and esterified oxylipins. *Prostaglandins Other Lipid Mediat*. 113-115, pp. 21-29; doi: 10.1016/j.prostaglandins.2014.05.002.
77. Smith W. L., Urade Y. and Jakobsson P.-J. (2011) Enzymes of the cyclooxygenase pathways of prostanoid biosynthesis. *Chem Rev*. 111(10), pp. 5821-5865; doi: 10.1021/cr2002992.
78. Wada M., DeLong C. J., Hong Y. H., Rieke C. J., Song I., Sidhu R. S., Yuan C., Warnock M., Schmaier A. H., Yokoyama C., Smyth E. M., Wilson S. J., FitzGerald G. A., Garavito R. M., Sui D. X., Regan J. W. and Smith W. L. (2007) Enzymes and receptors of prostaglandin pathways with arachidonic acid-derived versus eicosapentaenoic acid-derived substrates and products. *J Biol Chem*. 282(31), pp. 22254-22266; doi: 10.1074/jbc.M703169200.
79. Bagga D., Wang L., Farias-Eisner R., Glaspy J. A. and Reddy S. T. (2003) Differential effects of prostaglandin derived from ω-6 and ω-3 polyunsaturated fatty acids on COX-2 expression and IL-6 secretion. *Proc Natl Acad Sci U S A*. 100(4), pp. 1751-1756; doi: 10.1073/pnas.0334211100.
80. Schuchardt J. P., Schmidt S., Kressel G., Willenberg I., Hammock B. D., Hahn A. and Schebb N. H. (2014) Modulation of blood oxylipin levels by long-chain omega-3 fatty acid supplementation in hyper- and normolipidemic men. *Prostaglandins Leukot Essent Fatty Acids*. 90(2-3), pp. 27-37; doi: 10.1016/j.plefa.2013.12.008.
81. Skarke C., Alamuddin N., Lawson J. A., Li X., Ferguson J. F., Reilly M. P. and FitzGerald G. A. (2015) Bioactive products formed in humans from fish oils. *J Lipid Res*. 56(9), pp. 1808-1820; doi: 10.1194/jlr.M060392.

82. Westphal C., Konkel A. and Schunck W.-H. (2015) Cytochrome P450 enzymes in the bioactivation of polyunsaturated fatty acids and their role in cardiovascular disease. In: *Monooxygenase, Peroxidase and Peroxygenase Properties and Mechanisms of Cytochrome P450*. E. G. Hrycay and S. M. Bandiera (eds.), Springer International Publishing, Cham, pp. 151-187; doi: 10.1007/978-3-319-16009-2_6.
83. Lee J. P., Yang S. H., Lee H. Y., Kim B., Cho J. Y., Paik J. H., Oh Y. J., Kim D. K., Lim C. S. and Kim Y. S. (2012) Soluble epoxide hydrolase activity determines the severity of ischemia-reperfusion injury in kidney. *PLoS One*. 7(5):e37075; doi: 10.1371/journal.pone.0037075.
84. Sharma A., Hye Khan M. A., Levick S. P., Lee K. S., Hammock B. D. and Imig J. D. (2016) Novel omega-3 fatty acid epoxygenase metabolite reduces kidney fibrosis. *Int J Mol Sci*. 17(5):751; doi: 10.3390/ijms17050751.
85. Deng B. Q., Luo Y., Kang X., Li C. B., Morisseau C., Yang J., Lee K. S. S., Huang J., Hu D. Y., Wu M. Y., Peng A., Hammock B. D. and Liu J. Y. (2017) Epoxide metabolites of arachidonate and docosahexaenoate function conversely in acute kidney injury involved in GSK3β signaling. *Proc Natl Acad Sci U S A*. 114(47), pp. 12608-12613; doi: 10.1073/pnas.1705615114.
86. European Commission (2017) Guidance document on analytical quality control and method validation procedures for pesticide residues and analysis in food and feed. SANTE/11813/2017. Directorate General for Health and Food Safety (SANTE), 21-22 November 2017.
87. Barden A., Mas E., Croft K. D., Phillips M. and Mori T. A. (2014) Short-term n-3 fatty acid supplementation but not aspirin increases plasma proresolving mediators of inflammation. *J Lipid Res*. 55(11), pp. 2401-2407; doi: 10.1194/jlr.M045583.
88. Toewe A., Balas L., Durand T., Geisslinger G. and Ferreirós N. (2018) Simultaneous determination of PUFA-derived pro-resolving metabolites and pathway markers using chiral chromatography and tandem mass spectrometry. *Anal Chim Acta*. 1031, pp. 185-194; doi: 10.1016/j.aca.2018.05.020.
89. English J. T., Norris P. C., Hodges R. R., Dartt D. A. and Serhan C. N. (2017) Identification and profiling of specialized pro-resolving mediators in human tears by lipid mediator metabolomics. *Prostaglandins Leukot Essent Fatty Acids*. 117, pp. 17-27; doi: 10.1016/j.plefa.2017.01.004.
90. Massey K. A. and Nicolaou A. (2013) Lipidomics of oxidized polyunsaturated fatty acids. *Free Radic Biol Med*. 59, pp. 45-55; doi: 10.1016/j.freeradbiomed.2012.08.565.
91. Masoodi M., Mir A. A., Petasis N. A., Serhan C. N. and Nicolaou A. (2008) Simultaneous lipidomic analysis of three families of bioactive lipid mediators leukotrienes, resolvins, protectins and related hydroxy-fatty acids by liquid chromatography/electrospray ionisation tandem mass spectrometry. *Rapid Commun Mass Spectrom*. 22(2), pp. 75-83; doi: 10.1002/rcm.3331.
92. Jonasdottir H. S., Brouwers H., Toes R. E. M., Ioan-Facsinay A. and Giera M. (2018) Effects of anticoagulants and storage conditions on clinical oxylipid levels in human plasma. *Biochim Biophys Acta*. 1863(12), pp. 1511-1522; doi: 10.1016/j.bbalip.2018.10.003.
93. Guillot N., Caillet E., Laville M., Calzada C., Lagarde M. and Vericel E. (2009) Increasing intakes of the long-chain ω-3 docosahexaenoic acid: Effects on platelet functions and redox status in healthy men. *FASEB J*. 23(9), pp. 2909-2916; doi: 10.1096/fj.09-133421.
94. Goncalves G. M., Cenedeze M. A., Feitoza C. Q., Wang P. M., Bertocchi A. P., Damiao M. J., Pinheiro H. S., Antunes Teixeira V. P., dos Reis M. A., Pacheco-Silva A. and Camara N. O. (2006) The role of heme oxygenase 1 in rapamycin-induced renal

dysfunction after ischemia and reperfusion injury. *Kidney Int*. 70(10), pp. 1742-1749; doi: 10.1038/sj.ki.5001893.

95. Ndisang J. F. and Tiwari S. (2014) Mechanisms by which heme oxygenase rescue renal dysfunction in obesity. *Redox Biol*. 2, pp. 1029-1037; doi: 10.1016/j.redox.2014.09.001.
96. Doyle J. F. and Forni L. G. (2016) Acute kidney injury: Short-term and long-term effects. *Crit Care*. 20(1):188; doi: 10.1186/s13054-016-1353-y.
97. Druml W. (2014) Systemic consequences of acute kidney injury. *Curr Opin Crit Care*. 20(6), pp. 613-619; doi: 10.1097/MCC.0000000000000150.
98. Raptis D. A., Limani P., Jang J. H., Ungethum U., Tschuor C., Graf R., Humar B. and Clavien P. A. (2014) GPR120 on Kupffer cells mediates hepatoprotective effects of ω3-fatty acids. *J Hepatol*. 60(3), pp. 625-632; doi: 10.1016/j.jhep.2013.11.006.
99. Saglimbene V. M., Wong G., van Zwieten A., Palmer S. C., Ruospo M., Natale P., Campbell K., Teixeira-Pinto A., Craig J. C. and Strippoli G. F. M. (2019) Effects of omega-3 polyunsaturated fatty acid intake in patients with chronic kidney disease: Systematic review and meta-analysis of randomized controlled trials. *Clin Nutr*. in press; doi: 10.1016/j.clnu.2019.02.041.
100. Mori T. A., Burke V., Puddey I., Irish A., Cowpland C. A., Beilin L., Dogra G. and Watts G. F. (2009) The effects of ω3 fatty acids and coenzyme Q10 on blood pressure and heart rate in chronic kidney disease: A randomized controlled trial. *J Hypertens*. 27(9), pp. 1863-1872; doi: 10.1097/HJH.0b013e32832e1bd9.

Chapter 6

Concluding Remarks and Future Perspectives

Within this thesis, the analytical and pre-analytical basis for a comprehensive analysis of oxylipins in biological samples has been established. The presented targeted LC-ESI(-)-MS/MS method is one of the most comprehensive methods for the analysis of oxylipins allowing the parallel quantification of a wide range of both, enzymatically and non-enzymatically formed oxylipins from the major biologically relevant n6- and n3-PUFA *(chapter 2)*. However, considering their endogenous origin and the interaction of their formation pathways, a multitude of structurally distinct oxylipins can be formed of which only a part is analytically covered. While some oxylipins are only short-lived and rather unstable, others will be unveiled in the future. Continuing adaption and extension of the instrumental analytical method, thus allowing to monitor effects on different formation pathways in parallel, is therefore essential to improve our understanding about the physiological roles of oxylipins. Analysis of potent unstable oxylipins which are rapidly transformed in the organism may be facilitated by determining their stable metabolites such as commonly carried out for thromboxane (Tx)B_2 used as a surrogate for the formation of unstable TxA_2. Particularly the multitude of possible regio- and stereoisomeric IsoP formed during autoxidation complicates their analysis as only a few ARA derived IsoP are commercially available. Thus, most of the IsoP und IsoF standards covered by the described LC-MS/MS method are only available through tight collaboration with organic chemists finding new synthetic pathways to generate authentic oxylipin standards. Analysis of samples related to oxidative stress may contribute to the discovery and elucidation of the structure of new autoxidation products and thus enable the identification of individual compounds or isomers which reflect oxidative stress best. Moreover, application of

innovative techniques such as untargeted oxylipin analysis in combination with chemical networking may facilitate the discovery of previously unknown oxylipins [1]. About 20 years ago a new class of autacoids, the so-called specialized pro-resolving mediators (SPM) was unveiled which are today controversially discussed with respect to their presence in biological samples. In order to contribute to the understanding of their physiological role the described targeted LC-MS/MS method (*chapter 2*) was further extended during the course of this thesis by a comprehensive set of SPMs comprising lipoxins, resolvins, protectins and maresins [2].

The multitude of stereoisomers, particularly of multiple hydroxylated PUFA, is a major challenge for their analysis. Parallel detection of two SRM transitions for the dihydroxy-DHA stereoisomers (N)PD1 and PDX (10*R*,17S-dihydroxy-*E,E,Z*-docosahexaenoic acid and 10*S*,17*S*-dihydroxy-*E,Z,E*-docosahexaenoic acid, respectively) revealed a clear deviation of the area ratio of both transitions for (N)PD1 in kidney tissue compared to the authentic (N)PD1 standard, even though the retention time matched with the authentic standard (*chapter 5*). Determination of multiple SRM transitions, or full MS/MS spectra and the ratios of the fragments is therefore indispensable to recognize isobaric interferences and to support the identification of individual oxylipins preventing misleading assignments. Moreover, use of orthogonal chromatographic techniques as well as application of chiral chromatography may allow to support the structural identification and additionally to gain information about their formation route.

Thus, the development of analytical methods in the field of oxylipins is an ongoing process and permanent challenge which requires on the one hand to constantly adapt and extend the covered analytes regarding the discovery of new oxylipins and on the other hand the awareness of potential isobaric interferences impeding reliable qualification and quantification.

A key aspect for the oxylipin analysis in biological samples is their pre-analytical (in)stability. The investigation of the free and the total (i.e. sum of free and esterified) oxylipin profile in plasma and serum generated from stored or

transported whole blood prior to processing provided important data for the characterization of the pre-analytical variability in clinical samples to evaluate their suitability in biomarker research *(chapter 3)*. Levels of total oxylipins in plasma were almost stable and only platelet derived oxylipins were susceptible to changes after prolonged storage or transport of whole blood emphasizing that the determined concentrations of these analytes need to be interpreted with caution. Based on this finding within this thesis, the total oxylipin pattern in plasma is currently analyzed in a large prospective cohort study to assess the role of oxylipins in the development and progression of the metabolic syndrome. However, the high analytical variance observed for total oxylipin levels in plasma suggests that a rather high number of subjects and samples (n) is necessary to deduce physiological features from the determined oxylipin pattern.

A central focus within this thesis is the investigation of *trans*-epoxy-PUFA formation in response to autoxidation and oxidative stress. Clear correlations of the *trans/cis*-epoxy-PUFA ratio with the autoxidatively formed IsoP in response to *tert*-butyl hydroperoxide as inducer of oxidative stress were found in multiple models ranging from different cell lines with various origin (colorectal, renal and hepatic carcinoma cells) to the model organism *Caenorhabditis elegans (chapter 4)*. This suggests the use of the *trans/cis*-epoxy-PUFA ratio as promising marker for autoxidation which warrants further investigation. Based on their separation in reversed-phase chromatography *trans*-epoxy-PUFA isomers can be easily analyzed in parallel with their respective *cis*-epoxy-PUFA isomers allowing their facile acquisition if the respective *cis*-epoxy-PUFA are already determined.

The absence of effects on the *trans/cis*-epoxy-PUFA ratio in the *in vivo* model of renal ischemia reperfusion injury might indicate that the used model is not associated with strong oxidative stress and lipid peroxidation. In order to obtain more insights in the role of epoxy-PUFA during oxidative stress further studies would be highly interesting, investigating different models and agents of

oxidative stress (e.g. CCl_4, paraquat) with respect to the mechanism by which they elicit (aut)oxidative effects. Furthermore, parallel analysis of additional oxidative stress markers other than those resulting from lipid peroxidation, e.g. GSH/GSSG, 8-hydroxyguanosine, may be valuable to support the role of epoxy-PUFA in oxidative stress. Moreover, the evaluation of lipoproteins, e.g. VLDL, for the presence of *trans*-epoxy-PUFA which could indicate oxidative stress in the liver based on plasma analysis would be of scientific interest.

The formation of epoxy-PUFA during autoxidative processes is also supported by our recent observations that apparent *cis*-epoxy-PUFA levels in hydrolyzed samples are clearly increased after SPE on silica-based material if cartridges are dried for longer time periods [3]. Here, massive amounts of free PUFA released after alkaline hydrolysis may attach on incompletely endcapped silica surfaces with their carboxy-terminus, thus maintaining the arrangement of their *cis*-oriented double bonds and enabling generation of *cis*-epoxy-isomers *via* nearby hydroperoxy-PUFA radicals particularly during drying processes [3, 4].

A main part of this thesis focused on the anti-inflammatory properties and physiological effects of n3-PUFA. Based on the analysis of PUFA and oxylipins in combination with functional and inflammatory parameters as well as (immuno)histology, the efficacy of n3-PUFA in an *in vivo* murine model of oxidative stress and inflammation was investigated *(chapter 5)*. Renal ischemia reperfusion injury (IRI), a common model for solid organ transplantation, is associated with renal function impairment. Moreover, it resembles the acute kidney injury which could occur during long surgeries such as cardiac surgery. Supplementation of long-chain n3-PUFA on a diet with a relatively high n6-PUFA background reflecting a typical western diet resulted only in minor effects on kidney function deterioration even though maximal modulation of n3-PUFA and their oxylipins were observed. However, n3-PUFA led to an improved tubular function 24 h after reperfusion. If this leads to an improved kidney function at later time points remains to be elucidated. Nevertheless, the increase of neutrophil infiltration and cytokines in spite of high n3-PUFA levels

suggest that shifting the fatty acid and oxylipin pattern seems not be sufficient to reduce IRI induced inflammation and preserve kidney function. Overall, translating these findings to humans suggests that dietary supplementation prior to surgery and clamping of the renal pedicle might only be little helpful in preventing renal function impairment.

Despite this on the first view disappointing finding, in cardiovascular diseases the dietary intake of long-chain n3-PUFA is clearly correlated with beneficial effects. Taken together, the results from the *in vivo* studies *(chapter 4+5)* indicate that the physiological effects and functions of PUFA and oxylipins in the organism are complex and far from being completely understood. Moreover, as observed for the acute formation of IsoP in the oxidative stress models (*chapter 4*), levels of oxylipins may show distinct time dependent changes. Thus, if only a single time point is chosen for analysis, this has to be carefully considered to ensure meaningful results.

Overall, based on the comprehensive determination of oxylipins combining their role as indicators of oxidative stress and the n3-PUFA status with their functional readout regarding biological activity, this thesis contributes to a better understanding of the role of oxylipins in (patho)physiology.

6.1 References

1. Watrous J. D., Niiranen T. J., Lagerborg K. A., Henglin M., Xu Y.-J., Rong J., Sharma S., Vasan R. S., Larson M. G., Armando A., Mora S., Quehenberger O., Dennis E. A., Cheng S. and Jain M. (2019) Directed non-targeted mass spectrometry and chemical networking for discovery of eicosanoids and related oxylipins. *Cell Chem Biol*. 26(3), pp. 433-442.e434; doi: 10.1016/j.chembiol.2018.11.015.
2. Kutzner L., Rund K. M., Ostermann A. I., Hartung N. M., Galano J.-M., Balas L., Durand T., Balzer M. S., David S. and Schebb N. H. (2019) Development of an optimized LC-MS method for the detection of specialized pro-resolving mediators in biological samples. *Front Pharmacol*. 10:169; doi: 10.3389/fphar.2019.00169.
3. Ostermann A. I., Koch E., Rund K. M., Kutzner L., Mainka M. and Schebb N. H. (2020) Targeting esterified oxylipins by LC-MS – Effect of sample preparation on oxylipin pattern. *Prostaglandins Other Lipid Mediat*. 146:106384; doi: 10.1016/j.prostaglandins.2019.106384.
4. Mead J. F. (1980) Membrane lipid peroxidation and its prevention. *Journal of the American Oil Chemists' Society*. 57(12), pp. 393-397; doi: 10.1007/BF02678922.

Summary

Oxidative metabolites of polyunsaturated fatty acids (PUFA) – oxylipins – are potent lipid mediators involved in the regulation of various physiological functions and dysregulation of oxylipin formation has been associated with the pathophysiology of multiple diseases. Although the physiological impact of the overall oxylipin pattern is still only poorly understood, this dual role of oxylipins being on the one hand formed in response to (patho)physiological stimuli and mediating on the other hand a wide range of biological processes represents a promising feature for their use as functional biomarkers. Thus, the present thesis aims to advance the understanding of this functional role of oxylipins

i. by improving the performance of their analysis in terms of expanding the analytical scope and characterizing the impact of clinical sample handling
ii. by investigating their formation under conditions of oxidative stress and inflammation

In the first part of this thesis analytical and preanalytical requirements for a comprehensive and reliable oxylipin quantification were established. For this purpose, the focus was set on the development of a reversed-phase LC-ESI(-)-MS/MS method for the determination of stable autoxidation products with prostaglandin-like structure considered as markers of oxidative stress, namely isoprostanes (IsoP) and isofurans (IsoF) *(chapter 2)*. Integration of a broad set of products from the major n6- and n3-PUFA (27 IsoP and 8 IsoF from 6 biologically relevant PUFA) offers the opportunity to analyze their formation during oxidative stress in samples with varying PUFA composition. Characteristic fragment ions resulting from α-fragmentation adjacent to the hydroxyl-group in the side chain were chosen to guarantee the selective determination of individual IsoP regioisomers in selected reaction monitoring

(SRM) mode. The implementation of a short isocratic step at the beginning of the gradient focusing the analytes at the front end of the column resulted in narrow peaks and thereby improved chromatographic resolution. In this way, the differentiation of most diastereomers, which show an identical fragmentation behavior, was achieved. Using mixed-mode C8 and anion-exchange solid phase extraction (SPE) material for sample preparation, extraction efficiency of internal standards from plasma, as well as intra- and inter-day accuracy and precision of IsoP and IsoF spiked in plasma samples were appropriate for their reliable quantification evaluated based on criteria for bioanalytical method validation. Through combination with an existing targeted oxylipin LC-MS/MS platform the developed method allows the sensitive and simultaneous quantification of a broad set of 164 enzymatically and non-enzymatically formed oxylipins from all formation branches and biologically relevant PUFA within 30.5 min. This analytical approach is currently one of the most comprehensive targeted methods for oxylipin analysis with comparable or even higher sensitivity, making oxylipin quantification in biological samples in subnanomolar concentrations possible.

However, (inappropriate) pre-analytical handling of biological samples could cause artificial alterations of endogenous oxylipin levels after sampling, thus affecting their reliable interpretation. In order to evaluate the suitability of clinical blood specimen for oxylipin analysis, the influence of typical procedures in clinical routine on the oxylipin profile, i.e. storage or pneumatic tube transport of whole blood prior to plasma or serum generation, was thoroughly characterized *(chapter 3)*. Analysis of free and total (i.e. sum of free and esterified) oxylipins in plasma and serum revealed that platelet derived (12-LOX and COX) metabolites, were most susceptible to artificial formation during storage or transport, while dihydroxy- and epoxy-PUFA as well as IsoP were almost stable under the investigated storage / transport conditions. Changes in serum were more pronounced with particularly platelet derived oxylipins showing high inter-individual variations. Notably, automated transport clearly increased levels of platelet derived oxylipins, with high variations in plasma and serum. Generally,

levels of total oxylipins were more stable than free oxylipins. Thus, for oxylipin analysis in clinical blood samples, the total plasma oxylipin profile, being almost stable after whole blood storage at 4 °C up to 24 h, seems to be most suitable.

In the second part of this thesis oxylipin formation in the context of oxidative stress as well as inflammation was investigated applying the analytical approach developed in chapter 2.

The presence of a second peak on the SRM transitions of epoxy-PUFA regioisomers – particularly in aged PUFA stocks – directed the attention towards the autoxidative formation of these tentatively identified *trans*-epoxy-PUFA isomers. The suitability of the *trans/cis*-epoxy-PUFA ratio as potential alternative oxidative stress marker was therefore characterized based on correlation with IsoP applying a tiered approach using (i) *tert*-butyl hydroperoxide (*t*-BOOH) as inducer of oxidative stress in three human carcinoma cell lines (from colorectal, hepatic and renal origin) as well as in (ii) the *in vivo* model organism *C. elegans* and (iii) renal ischemia reperfusion injury in mice *(chapter 4*). In all investigated cell lines as well as in *C. elegans*, *t*-BOOH treatment led to a dose dependent increase in IsoP and *trans*-epoxy-PUFA levels. Regarding incubation time, the different cell lines showed a distinct time dependent pattern which was consistent for these two oxylipin classes within each cell line. In murine kidney tissue after renal ischemia reperfusion injury no effects on epoxy-PUFA were observed. Nevertheless, clear and highly significant correlations of the *trans/cis*-epoxy-PUFA ratio with the IsoP levels in the investigated cell lines of different origin and in *C. elegans* suggest its potential use as marker of lipid peroxidation which can easily be assessed in parallel when enzymatically formed *cis*-epoxy-PUFA are already monitored by the RP-LC-MS/MS method and warrants further investigation.

Considering the described anti-inflammatory properties of long-chain n3-PUFA, the effectivity of dietary n3-PUFA supplementation of a western-like diet on preserving kidney function after renal ischemia reperfusion injury was evaluated in a murine model *(chapter 5)*. Renal ischemia reperfusion injury is

characterized by temporal occlusion and subsequent reperfusion of the renal blood flow and is a model for oxidative stress and inflammation. Moreover, this model also reflects processes occurring during solid organ transplantation. n3-PUFA pre-feeding resulted in maximal modulation of the PUFA and oxylipin pattern towards n3-PUFA and their oxylipins in blood and kidney, with particular increase in levels of terminal epoxy-PUFA and precursors of specialized pro-resolving mediators, e.g. 18-HEPE and 17-HDHA at the dispense of n6-PUFA and their oxylipins. However, the overall impaired kidney function, renal morphological damage and inflammation was similar to mice not receiving n3-PUFA. Nevertheless, n3-PUFA fed mice showed beneficial effects on tubular transport function which could contribute to renal protection in the long term.

Appendix

Chapter 2

Tab. 8.1: List of all internal standards used for the quantification of oxylipins with their LC-ESI(-)-MS/MS parameters. Shown are the mass transitions for quantification in scheduled SRM mode, electronical MS parameters (declustering potential (DP), entrance potential (EP), collision energy (CE), collision cell exit potential (CXP)), and retention time (t_R).

Analyte	Mass transition		MS parameters				t_R
	Q1	Q3	DP	EP	CE	CXP	[min]
C19-17-*epi*-17-F_{1t}-PhytoP	341.3	239.0	−70	−10	−35	−8	6.02
$^2H_4$-6-keto-$PGF_{1\alpha}$	373.3	167.1	−80	−10	−36	−8	6.10
$^2H_4$-15-F_{2t}-IsoP	357.2	196.8	−50	−6	−33	−8	7.54
$^2H_4$-TxB_2	373.3	173.2	−65	−10	−24	−8	7.64
$^2H_{11}$-5(*R,S*)-5-F_{2t}-IsoP	364.3	115.2	−40	−10	−29	−10	7.97
$^2H_4$-PGE_2	355.2	275.3	−60	−10	−25	−6	8.93
C21-15-F_{2t}-IsoP	367.2	193.1	−60	−10	−35	−8	9.18
$^2H_4$-PGD_2	355.2	275.3	−60	−10	−25	−6	9.43
$^2H_4$-LTB_4	339.2	197.2	−65	−10	−23	−9	14.00
$^2H_4$-9,10-DiHOME	317.2	203.4	−80	−10	−29	−8	15.13
$^2H_{11}$-14,15-DiHETrE	348.2	207.1	−65	−10	−25	−10	15.83
$^2H_6$-20-HETE	325.2	295.2	−70	−10	−24	−6	18.31
$^2H_4$-9-HODE	299.2	172.3	−80	−10	−26	−6	19.69
$^2H_8$-12-HETE	327.2	184.2	−65	−10	−22	−8	21.20
$^2H_8$-5-HETE	327.2	116.1	−60	−10	−21	−8	21.75
$^2H_{11}$-14(15)-EpETrE	330.2	219.3	−65	−10	−20	−4	22.48
$^2H_4$-9(10)-EpOME	299.2	172.2	−80	−10	−23	−8	22.54

Tab. 8.2 (right, page 149): Parameters of the combined LC-ESI(-)-MS/MS method for the quantification of non-enzymatically and enzymatically formed oxylipins. Shown are the mass transitions for quantification in scheduled SRM mode, electronical MS parameters (declustering potential (DP), entrance potential (EP), collision energy (CE), collision cell exit potential (CXP)), the assigned internal standards (IS), retention time (t_R), full peak width at half maximum (FWHM), limit of detection (LOD), the calibration range (lower limit of quantification (LLOQ), upper limit of quantification (ULOQ)) and the correlation coefficient (r) of the calibration curve.

Tab. 8.2: Continued. Parameters of the LC-ESI(-)-MS/MS method for oxylipin analysis.

Analyte	Mass transition		MS parameters				Internal standard	t_R [1] [min]	FWHM [2] [sec]	LOD [3] [nM]	LOD [3] [pg on column]	Calibration range LLOQ [4] [nM]	Calibration range ULOQ [5] [nM]	r [6]
	Q1	Q3	DP	EP	CE	CXP								
20-OH-PGE_2	367.2	189.1	-30	-10	-25	-8	$^2H_4$-PGE_2	3.68	3.4	0.10	0.18	0.25	500	0.9986
ent-16(*R,S*)-13-*epi*-ST-Δ^{14}-9-PhytoF 1	343.1	200.9	-80	-10	-33	-8	C19-17-*epi*-17-F_{1t}-PhytoP	4.19	3.4	0.12	0.20	0.24	235	0.9993
ent-16(*R,S*)-13-*epi*-ST-Δ^{14}-9-PhytoF 2	343.1	200.9	-80	-10	-33	-8	C19-17-*epi*-17-F_{1t}-PhytoP	4.30	3.4	0.13	0.23	0.26	265	0.9995
ent-16-*epi*-16-F_{1t}-PhytoP	327.3	225.0	-70	-10	-34	-8	C19-17-*epi*-17-F_{1t}-PhytoP	4.72	3.3	0.25	0.41	0.5	500	0.9983
ent-16-F_{1t}-PhytoP	327.3	225.0	-70	-10	-34	-8	C19-17-*epi*-17-F_{1t}-PhytoP	4.89	3.4	0.50	0.82	1.0	500	0.9997
ent-9-F_{1t}-PhytoP	327.3	170.9	-40	-10	-31	-8	C19-17-*epi*-17-F_{1t}-PhytoP	4.81	3.3	0.10	0.16	0.25	500	0.9991
ent-9-*epi*-9-F_{1t}-PhytoP	327.3	170.9	-40	-10	-31	-8	C19-17-*epi*-17-F_{1t}-PhytoP	4.98	3.3	0.25	0.41	0.5	500	0.9990
Δ^{17}-6-keto-$PGF_{1\alpha}$	367.2	163.2	-40	-10	-36	-10	$^2H_4$-6-keto-$PGF_{1\alpha}$	4.99	21	0.50	0.92	1.0	500	0.9938
2,3-dinor-TxB_1	343.0	142.9	-30	-10	-19	-8	$^2H_4$-TxB_2	5.11	4.1	2.0	3.4	5.0	500	0.9961
15(*R,S*)-2,3-dinor-15-F_{2t}-IsoP	325.2	237.0	-40	-10	-18	-8	C19-17-*epi*-17-F_{1t}-PhytoP	5.41	3.3	0.25	0.41	0.5	500	0.9995
2,3-dinor-TxB_2	341.2	167.0	-40	-10	-15	-8	$^2H_4$-TxB_2	5.59	3.8	0.50	0.86	1.0	500	0.9971
6-keto-$PGF_{1\alpha}$	369.3	163.2	-70	-10	-36	-6	$^2H_4$-6-keto-$PGF_{1\alpha}$	6.10	24	0.90	1.7	1.8	500	0.9937
8-F_{3t}-IsoP	351.1	155.0	-60	-10	-27	-8	C19-17-*epi*-17-F_{1t}-PhytoP	6.15	3.6	0.50	0.88	1.0	500	0.9980
8-*epi*-8-F_{3t}-IsoP	351.1	155.0	-60	-10	-27	-8	C19-17-*epi*-17-F_{1t}-PhytoP	6.51	3.3	0.50	0.88	1.0	500	0.9992
RvE1	349.3	195.0	-65	-10	-22	-10	$^2H_4$-TxB_2	6.21	3.5	0.60	1.1	1.2	480	0.9947
20-COOH-LTB_4	365.2	347.2	-80	-10	-25	-8	$^2H_4$-TxB_2	6.25	3.8	0.50	0.92	1.0	40	0.9619
TxB_3	367.3	169.3	-70	-10	-34	-8	$^2H_4$-TxB_2	6.51	3.5	0.10	0.18	0.25	100	0.9976
20-OH-LTB_4	351.2	195.2	-80	-10	-25	-8	$^2H_4$-PGD_2	6.52	3.3	0.10	0.18	0.25	40	0.9984
5(*R,S*)-5-F_{3t}-IsoP	351.2	114.9	-50	-10	-27	-8	C19-17-*epi*-17-F_{1t}-PhytoP	6.53	3.4	1.0	1.8	2.0	500	0.9962
13,14-dihydro-15-keto-tetranor-PGE_2	296.9	109.0	-30	-10	-19	-8	$^2H_4$-PGE_2	7.29	3.9	0.10	0.15	0.25	500	0.9992

Tab. 8.2: Continued. Parameters of the LC-ESI(-)-MS/MS method for oxylipin analysis.

Analyte	Mass transition		MS parameters				Internal standard	t_R [1] [min]	FWHM [2] [sec]	LOD [3]		Calibration range [nM]		r [6]
	Q1	Q3	DP	EP	CE	CXP				[nM]	[pg on column]	LLOQ [4]	ULOQ [5]	
TxB_1	371.3	171.2	-70	-10	-34	-10	$^2H_4$-TxB_2	7.36	3.9	0.25	0.47	0.5	100	0.9982
15-F_{2t}-IsoP (8-*iso*-$PGF_{2\alpha}$)	353.1	193.1	-70	-6	-33	-8	$^2H_4$-15-F_{2t}-IsoP	7.56	3.7	0.25	0.44	0.5	500	0.9989
TxB_2	369.2	169.1	-60	-10	-25	-7	$^2H_4$-TxB_2	7.68	3.8	0.25	0.46	1.3	500	0.9949
11-dehydro-TxB_3	365.3	161.2	-30	-10	-25	-8	$^2H_4$-TxB_2	7.75	3.6	0.50	0.92	1.0	100	0.9969
PGE_3	349.3	269.2	-60	-10	-22	-6	$^2H_4$-PGE_2	7.76	3.5	0.15	0.26	0.3	120	0.9995
11β-$PGF_{2\alpha}$	353.3	193.1	-30	-12	-36	-12	$^2H_4$-PGE_2	7.84	3.3	0.25	0.44	0.5	500	0.9952
10-F_{4t}-NeuroP	377.2	153.0	-40	-10	-25	-8	$^2H_4$-15-F_{2t}-IsoP	8.04	3.3	0.25	0.47	0.5	500	0.9989
10-*epi*-10-F_{4t}-NeuroP	377.2	153.0	-40	-10	-25	-8	$^2H_4$-15-F_{2t}-IsoP	8.37	3.5	0.50	0.95	1.0	500	0.9990
5(*R,S*)-5-F_{2t}-IsoP (5-i$PF_{2\alpha}$-VI)	353.2	114.8	-60	-10	-26	-8	$^2H_{11}$-5(*R,S*)-5-F_{2t}-IsoP	8.07	3.5	0.25	0.44	0.5	500	0.9959
PGD_3	349.3	269.2	-60	-10	-22	-6	$^2H_4$-PGD_2	8.15	3.4	0.50	0.88	1.0	40	0.9992
16-B_1-PhytoP	307.3	235.0	-60	-10	-27	-8	$^2H_{11}$-5(*R,S*)-5-F_{2t}-IsoP	8.26	3.7	0.10	0.15	0.25	500	0.9994
9-L_1-PhytoP	307.3	185.1	-60	-10	-27	-8	$^2H_{11}$-5(*R,S*)-5-F_{2t}-IsoP	8.33	3.7	0.10	0.15	0.25	500	0.9986
$PGF_{2\alpha}$	353.2	309.2	-80	-10	-26	-7	$^2H_4$-PGE_2	8.59	3.5	0.35	0.62	0.70	281	0.9991
14(*R,S*)-14-F_{4t}-NeuroP	377.2	205.1	-50	-10	-27	-8	C21-15-F_{2t}-IsoP	8.62	6.5	10	19	20	500	0.9998
$PGF_{1\alpha}$	355.4	293.2	-90	-12	-36	-6	$^2H_4$-PGE_2	8.63	3.5	0.10	0.18	0.25	500	0.9985
PGE_2	351.2	271.3	-60	-10	-24	-6	$^2H_4$-PGE_2	8.98	3.5	0.10	0.18	0.25	500	0.9982
11-dehydro-TxB_2	367.0	161.1	-50	-10	-27	-8	$^2H_4$-TxB_2	9.08	3.7	0.25	0.46	0.50	100	0.9988
PGE_1	353.3	317.2	-60	-10	-20	-6	$^2H_4$-PGE_2	9.27	3.6	0.13	0.23	0.33	260	0.9984
4(*R,S*)-4-F_{4t}-NeuroP	377.1	101.3	-60	-10	-26	-8	C21-15-F_{2t}-IsoP	9.35	3.8	0.50	0.95	1.0	500	0.9982
PGD_1	353.3	317.2	-60	-10	-20	-6	$^2H_4$-PGD_2	9.45	3.6	0.25	0.44	0.50	40	0.9956

Tab. 8.2: Continued. Parameters of the LC-ESI(-)-MS/MS method for oxylipin analysis.

Analyte	Mass transition		MS parameters				Internal standard	t_R [1] [min]	FWHM [2] [sec]	LOD [3] [nM]	LOD [3] [pg on column]	Calibration range LLOQ [4] [nM]	Calibration range ULOQ [5] [nM]	r [6]
	Q1	Q3	DP	EP	CE	CXP								
PGD_2	351.2	271.3	-60	-10	-24	-6	$^2H_4$-PGD_2	9.46	3.6	0.50	0.88	1.0	500	0.9960
15-keto-$PGF_{1\alpha}$	353.3	193.1	-40	-12	-38	-6	$^2H_4$-PGE_2	9.54	3.7	0.10	0.18	0.25	500	0.9970
4(*R,S*)-ST-Δ^5-8-NeuroF	393.3	187.2	-40	-10	-29	-8	C21-15-F_{2t}-IsoP	9.59	4.2	20	39	40	500	0.9941
17(*R,S*)-17-F_{2t}-dihomo-IsoP 1	381.3	263.2	-90	-10	-31	-8	C21-15-F_{2t}-IsoP	9.78	3.6	0.63	1.2	1.3	314	0.9967
17(*R,S*)-17-F_{2t}-dihomo-IsoP 2	381.3	263.2	-90	-10	-31	-8	C21-15-F_{2t}-IsoP	9.95	3.2	0.37	0.71	0.75	186	0.9980
7(*R,S*)-ST-Δ^8-11-dihomo-IsoF	397.3	245.1	-50	-10	-31	-8	C21-15-F_{2t}-IsoP	9.81	3.8	1.0	2.0	2.0	500	0.9993
ent-7(*R,S*)-7-F_{2t}-dihomo-IsoP	381.3	143.0	-50	-10	-31	-8	C21-15-F_{2t}-IsoP	9.86	5.7	0.25	0.48	0.50	500	0.9972
11,12,15-TriHETrE	353.2	167.1	-80	-10	-28	-10	$^2H_4$-PGE_2	10.20	3.4	0.25	0.44	0.50	100	0.9988
LXA_4	351.2	115.2	-60	-10	-21	-8	$^2H_4$-PGE_2	10.23	3.7	0.088	0.15	0.18	70	0.9985
RvD1	375.3	141.0	-50	-10	-20	-8	$^2H_4$-PGE_2	10.35	3.6	0.10	0.19	0.25	100	0.9993
13,14-dihydro-15-keto-$PGF_{2\alpha}$	353.3	183.3	-80	-10	-36	-10	$^2H_4$-PGE_2	10.41	3.6	0.25	0.44	0.50	500	0.9990
13,14-dihydro-15-keto-PGE_1	353.3	221.2	-40	-6	-30	-6	$^2H_4$-PGE_2	10.97	4.5	0.25	0.44	0.50	500	0.9989
dihomo-$PGF_{2\alpha}$	381.4	221.1	-60	-10	-38	-10	$^2H_4$-PGE_2	11.01	3.8	0.025	0.048	0.10	500	0.9977
4*(R,S)*-4-F_{3t}-$NeuroP_{n6}$	379.2	273.0	-50	-10	-27	-8	C21-15-F_{2t}-IsoP	11.03	4.1	0.50	0.95	1.0	500	0.9971
17(*R,S*)-10-*epi*-SC-Δ^{15}-11-dihomo-IsoF 1	397.1	221.0	-90	-10	-31	-8	C21-15-F_{2t}-IsoP	11.26	3.7	0.52	1.0	1.0	260	0.9992
17(*R,S*)-10-*epi*-SC-Δ^{15}-11-dihomo-IsoF 2	397.1	221.0	-90	-10	-31	-8	C21-15-F_{2t}-IsoP	11.44	3.7	0.48	0.96	0.96	240	0.9982
RvE2	333.2	253.3	-60	-10	-20	-9	$^2H_4$-PGE_2	11.42	3.7	1.0	1.7	2.0	100	0.9991
PGJ_2	333.3	189.2	-60	-10	-25	-8	$^2H_4$-PGE_2	12.02	3.8	0.80	1.3	1.6	160	0.9957
Δ^{12}-PGJ_2	333.1	189.0	-40	-10	-22	-8	$^2H_4$-PGE_2	12.09	4.0	0.50	0.84	1.0	500	0.9986
LTB_5	333.3	195.2	-65	-10	-22	-8	$^2H_4$-LTB_4	12.11	4.0	0.050	0.084	0.10	200	0.9992

Tab. 8.2: Continued. Parameters of the LC-ESI(-)-MS/MS method for oxylipin analysis.

Analyte	Mass transition		MS parameters				Internal standard	t_R [1] [min]	FWHM [2] [sec]	LOD [3]		Calibration range [nM]		r [6]
	Q1	Q3	DP	EP	CE	CXP				[nM]	[pg on column]	LLOQ [4]	ULOQ [5]	
PGB_2	333.3	175.1	-60	-10	-28	-8	$^2H_4$-PGE_2	12.13	4.0	0.20	0.33	0.40	800	0.9982
THF diol	353.2	127.1	-80	-10	-32	-8	$^2H_4$-LTB_4	12.27	4.0	0.13	0.22	0.25	100	0.9987
18(*S*)-RvE3	333.2	201.3	-60	-10	-20	-9	$^2H_4$-PGE_2	12.78	4.1	0.50	0.84	1.0	100	0.9976
12-OH-17(18)-EpETE	333.1	179.3	-65	-10	-20	-6	$^2H_4$-9,10-DiHOME	12.85	4.3	0.25	0.42	0.50	100	0.9992
15,16-DiHODE	311.2	223.2	-80	-10	-29	-10	$^2H_4$-9,10-DiHOME	12.99	4.3	0.50	0.78	1.0	80	0.9992
9,10-DiHODE	311.2	201.2	-65	-10	-27	-10	$^2H_4$-9,10-DiHOME	13.05	4.2	0.10	0.16	0.20	80	0.9998
12,13-DiHODE	311.2	183.1	-80	-10	-30	-8	$^2H_4$-9,10-DiHOME	13.15	4.3	0.50	0.78	1.0	80	0.9990
8,15-DiHETE	335.2	235.2	-65	-10	-22	-4	$^2H_{11}$-14,15-DiHETrE	13.17	4.0	0.40	0.67	0.80	80	0.9981
10(*S*),17(*S*)-diH n3 DPA	361.3	262.9	-40	-10	-23	-8	$^2H_4$-9,10-DiHOME	13.36	4.3	0.50	0.91	1.0	500	0.9991
18(*R*)-RvE3	333.2	201.3	-60	-10	-20	-9	$^2H_4$-PGE_2	13.45	4.2	0.25	0.42	0.50	100	0.9960
NPD1	359.0	153.0	-50	-10	-21	-8	$^2H_4$-9,10-DiHOME	13.49	4.2	0.25	0.45	0.50	500	0.9985
6-*trans*-LTB_4	335.2	195.1	-65	-10	-23	-9	$^2H_4$-LTB_4	13.58	4.2	0.25	0.42	0.50	200	0.9984
5,15-DiHETE	335.3	173.2	-60	-10	-21	-8	$^2H_{11}$-14,15-DiHETrE	13.60	4.0	0.13	0.21	0.25	100	0.9984
17,18-DiHETE	335.3	247.2	-65	-10	-24	-8	$^2H_{11}$-14,15-DiHETrE	13.71	4.3	0.13	0.21	0.25	100	0.9978
LTB_4	335.2	195.1	-65	-10	-23	-9	$^2H_4$-LTB_4	14.07	4.3	0.10	0.17	0.25	200	0.9996
7(*S*),17(*S*)-diH n3 DPA	361.5	263.3	-65	-10	-20	-4	$^2H_4$-9,10-DiHOME	14.29	3.8	0.30	0.54	0.75	500	0.9989
14,15-DiHETE	335.3	207.2	-65	-10	-25	-10	$^2H_{11}$-14,15-DiHETrE	14.34	4.5	0.13	0.21	0.25	100	0.9992
11,12-DiHETE	335.2	167.1	-65	-10	-26	-5	$^2H_{11}$-14,15-DiHETrE	14.57	4.6	0.13	0.21	0.25	100	0.9977
12,13-DiHOME	313.2	183.2	-80	-10	-30	-8	$^2H_4$-9,10-DiHOME	14.76	4.7	0.25	0.39	0.50	200	0.9986
8,9-DiHETE	335.2	127.1	-65	-10	-26	-5	$^2H_{11}$-14,15-DiHETrE	14.98	4.7	0.25	0.42	0.50	100	0.9962

Tab. 8.2: Continued. Parameters of the LC-ESI(-)-MS/MS method for oxylipin analysis.

Analyte	Mass transition		MS parameters				Internal standard	t_R [1] [min]	FWHM [2] [sec]	LOD [3]		Calibration range [nM]		r [6]
										[nM]	[pg on column]	LLOQ [4]	ULOQ [5]	
	Q1	Q3	DP	EP	CE	CXP								
10(*S*),17(*S*)-diH n6 DPA	361.2	153.1	-50	-10	-21	-8	$^2H_{11}$-14,15-DiHETrE	15.14	4.5	0.10	0.18	0.25	500	0.9987
9,10-DiHOME	313.2	201.2	-80	-10	-29	-8	$^2H_4$-9,10-DiHOME	15.24	4.7	0.25	0.39	0.50	200	0.9991
10(*S*),17(*S*)-diH AdA	363.4	263.2	-80	-10	-23	-8	$^2H_{11}$-14,15-DiHETrE	15.90	4.6	0.50	0.91	1.0	500	0.9993
12(*S*)-HHTrE	279.1	179.0	-50	-10	-17	-8	$^2H_{11}$-14,15-DiHETrE	15.96	4.9	0.25	0.35	0.50	500	0.9977
14,15-DiHETrE	337.2	207.1	-65	-10	-25	-10	$^2H_{11}$-14,15-DiHETrE	16.00	4.8	0.050	0.085	0.10	200	0.9985
19,20-DiHDPE	361.2	273.2	-65	-10	-24	-6	$^2H_{11}$-14,15-DiHETrE	16.05	4.8	0.25	0.45	0.50	100	0.9972
LTB_3	337.2	195.2	-65	-10	-22	-8	$^2H_4$-LTB_4	16.27	5.0	0.25	0.42	0.50	200	0.9995
9,10-diH-stearic acid	315.0	170.8	-60	-10	-36	-9	$^2H_4$-9,10-DiHOME	16.61	5.1	1.0	1.6	2.0	500	0.9994
16,17-DiHDPE	361.2	233.2	-65	-10	-24	-6	$^2H_{11}$-14,15-DiHETrE	16.69	4.7	0.25	0.45	0.50	100	0.9984
11,12-DiHETrE	337.2	167.1	-65	-10	-26	-8	$^2H_{11}$-14,15-DiHETrE	16.82	5.0	0.10	0.17	0.25	200	0.9980
19-HEPE	317.2	229.3	-50	-10	-18	-8	$^2H_8$-12-HETE	16.98	-	0.30	0.48	0.71		#
13,14-DiHDPE	361.2	193.2	-65	-10	-24	-6	$^2H_{11}$-14,15-DiHETrE	16.99	4.8	0.13	0.23	0.25	100	0.9985
20-HEPE	317.2	287.3	-50	-10	-20	-8	$^2H_8$-12-HETE	17.11	5.0	0.50	0.80	1.0	100	0.9985
9-HOTrE	293.2	171.2	-65	-10	-22	-8	$^2H_4$-9-HODE	17.23	5.2	0.25	0.37	0.50	500	0.9994
10,11-DiHDPE	361.2	153.2	-65	-10	-24	-6	$^2H_{11}$-14,15-DiHETrE	17.37	4.8	0.13	0.23	0.25	100	0.9987
8,9-DiHETrE	337.2	127.1	-70	-10	-30	-8	$^2H_{11}$-14,15-DiHETrE	17.48	5.1	0.25	0.42	0.50	200	0.9993
13-HOTrE	293.2	195.1	-70	-10	-24	-8	$^2H_4$-9-HODE	17.60	4.6	0.30	0.44	0.60	12	0.9961
18-HEPE	317.2	259.2	-55	-10	-17	-7	$^2H_8$-12-HETE	17.67	4.9	0.50	0.80	1.0	500	0.9972
15-deoxy-PGJ_2	315.2	271.2	-65	-10	-20	-6	$^2H_{11}$-14,15-DiHETrE	18.09	6.1	0.20	0.32	0.50	400	0.9989
19-HETE	319.3	230.9	-50	-10	-21	-6	$^2H_4$-9-HODE	18.15	5.3	5.0	8.0	10	500	0.9981

Tab. 8.2: Continued. Parameters of the LC-ESI(-)-MS/MS method for oxylipin analysis.

Analyte	Mass transition		MS parameters				Internal standard	t_R [1] [min]	FWHM [2] [sec]	LOD [3]		Calibration range [nM]		r [6]
										[nM]	[pg on column]	LLOQ [4]	ULOQ [5]	
	Q1	Q3	DP	EP	CE	CXP								
7,8-DiHDPE	361.2	113.1	-65	-10	-24	-6	$^2H_{11}$-14,15-DiHETrE	18.22	5.3	0.50	0.91	1.0	100	0.9988
20-HETE	319.2	289.1	-80	-10	-24	-6	$^2H_6$-20-HETE	18.40	5.1	0.50	0.80	1.0	500	0.9983
15-HEPE	317.2	219.2	-60	-10	-20	-10	$^2H_8$-12-HETE	18.43	5.1	0.63	0.99	1.3	500	0.9991
5,6-DiHETrE	337.2	145.1	-70	-10	-26	-10	$^2H_{11}$-14,15-DiHETrE	18.44	5.4	0.25	0.42	0.50	200	0.9989
11-HEPE	317.0	167.0	-40	-10	-21	-8	$^2H_8$-12-HETE	18.52	4.5	0.25	0.40	0.50	500	0.9962
8-HEPE	317.2	155.2	-60	-10	-20	-8	$^2H_8$-12-HETE	18.77	5.1	0.25	0.40	0.63	500	0.9986
12-HEPE	317.2	179.2	-65	-10	-20	-8	$^2H_8$-12-HETE	18.96	5.0	0.25	0.40	0.63	500	0.9989
9-HEPE	317.2	166.9	-40	-10	-19	-8	$^2H_8$-12-HETE	19.11	4.4	0.25	0.40	0.50	500	0.9970
21-HDHA	343.0	255.0	-60	-10	-18	-7	$^2H_8$-12-HETE	19.38	-	1.3	2.24	1.65		#
5-HEPE	317.2	115.1	-60	-10	-20	-6	$^2H_8$-12-HETE	19.49	5.2	0.20	0.32	0.50	500	0.9988
22-HDHA	343.2	313.2	-65	-10	-20	-7	$^2H_8$-12-HETE	19.49	-	1.40	2.41	2.80		#
4,5-DiHDPE	361.2	229.3	-65	-10	-24	-6	$^2H_{11}$-14,15-DiHETrE	19.51	4.7	1.0	1.8	2.0	100	0.9940
13-HODE	295.2	195.2	-80	-10	-26	-9	$^2H_4$-9-HODE	19.70	5.3	2.5	3.7	5.0	400	0.9985
9-HODE	295.2	171.1	-80	-10	-26	-7	$^2H_4$-9-HODE	19.81	5.2	2.5	3.7	5.0	400	0.9995
20-HDHA	343.2	241.2	-55	-10	-19	-7	$^2H_8$-12-HETE	20.07	4.9	0.25	0.43	0.50	20	0.9975
15(16)-EpODE	293.3	235.2	-65	-10	-20	-4	$^2H_4$-9(10)-EpOME	20.34	5.5	0.25	0.37	0.50	20	0.9973
15-HETE	319.2	219.2	-60	-10	-20	-8	$^2H_8$-12-HETE	20.45	5.0	0.50	0.80	1.3	500	0.9996
9(10)-EpODE	293.3	171.2	-65	-10	-20	-8	$^2H_4$-9(10)-EpOME	20.51	5.4	0.20	0.29	0.40	16	0.9953
17(18)-EpETE	317.2	215.2	-65	-10	-20	-6	$^2H_{11}$-14(15)-EpETrE	20.58	5.2	0.50	0.80	1.0	20	0.9994
16-HDHA	343.2	233.2	-55	-10	-19	-7	$^2H_8$-12-HETE	20.61	4.6	0.10	0.17	0.25	20	0.9993

Tab. 8.2: Continued. Parameters of the LC-ESI(-)-MS/MS method for oxylipin analysis.

Analyte	Mass transition		MS parameters				Internal standard	t_R [1] [min]	FWHM [2] [sec]	LOD [3]		Calibration range [nM]		r [6]
										[nM]	[pg on column]	LLOQ [4]	ULOQ [5]	
	Q1	Q3	DP	EP	CE	CXP								
17-HDHA	343.2	201.2	-60	-10	-20	-6	$^2H_8$-12-HETE	20.73	4.7	1.0	1.7	2.0	500	0.9990
13-HDHA	343.2	193.1	-55	-10	-19	-7	$^2H_8$-12-HETE	20.91	4.5	0.25	0.43	0.50	20	0.9985
12(13)-EpODE	293.2	183.1	-65	-10	-24	-8	$^2H_4$-9(10)-EpOME	20.93	5.1	0.25	0.37	0.50	20	0.9960
13-oxo-ODE	293.2	195.1	-75	-10	-20	-8	$^2H_4$-9-HODE	20.93	4.8	0.50	0.74	1.0	20	0.9966
11-HETE	319.2	167.2	-60	-10	-23	-7	$^2H_8$-12-HETE	20.98	4.7	0.25	0.40	0.50	500	0.9995
10-HDHA	343.2	153.2	-45	-10	-21	-7	$^2H_8$-12-HETE	21.14	4.4	0.25	0.43	0.50	20	0.9994
14-HDHA	343.2	205.2	-50	-10	-19	-7	$^2H_8$-12-HETE	21.14	4.2	0.50	0.86	1.0	500	0.9979
9-oxo-ODE	293.2	185.1	-90	-10	-28	-8	$^2H_4$-9-HODE	21.17	5.0	0.50	0.74	1.0	20	0.9934
15-oxo-ETE	317.2	113.1	-65	-10	-25	-8	$^2H_8$-5-HETE	21.18	4.3	0.25	0.40	0.50	100	0.9981
14(15)-EpETE	317.2	207.2	-65	-10	-20	-6	$^2H_{11}$-14(15)-EpETrE	21.25	4.8	0.25	0.40	0.50	20	0.9952
8-HETE	319.2	155.2	-60	-10	-22	-6	$^2H_8$-12-HETE	21.33	4.5	0.50	0.80	1.3	500	0.9989
12-HETE	319.2	179.2	-60	-10	-20	-8	$^2H_8$-12-HETE	21.36	4.4	0.25	0.40	0.50	500	0.9970
11(12)-EpETE	317.2	167.2	-65	-10	-20	-6	$^2H_{11}$-14(15)-EpETrE	21.40	4.3	0.25	0.40	0.50	20	0.9970
11-HDHA	343.2	121.1	-45	-10	-20	-7	$^2H_8$-5-HETE	21.41	4.0	0.10	0.17	0.25	20	0.9992
7-HDHA	343.2	141.2	-55	-10	-19	-7	$^2H_8$-5-HETE	21.54	4.2	0.50	0.86	1.0	500	0.9984
8(9)-EpETE	317.2	127.2	-65	-10	-20	-6	$^2H_{11}$-14(15)-EpETrE	21.55	4.9	0.50	0.80	1.0	20	0.9969
9-HETE	319.2	167.2	-60	-10	-23	-7	$^2H_8$-5-HETE	21.64	4.2	1.3	2.0	2.5	1000	0.9987
15(S)-HETrE	321.2	221.2	-70	-10	-23	-10	$^2H_8$-5-HETE	21.68	4.3	0.25	0.40	0.50	200	0.9984
8-HDHA	343.2	189.2	-50	-10	-19	-7	$^2H_8$-5-HETE	21.73	3.8	0.50	0.86	0.50	20	0.9976
5-HETE	319.2	115.2	-60	-10	-21	-7	$^2H_8$-5-HETE	21.88	4.1	0.25	0.40	0.50	1000	0.9990

Tab. 8.2: Continued. Parameters of the LC-ESI(-)-MS/MS method for oxylipin analysis.

Analyte	Mass transition		MS parameters				Internal standard	t_R [1] [min]	FWHM [2] [sec]	LOD [3] [nM]	LOD [3] [pg on column]	Calibration range LLOQ [4] [nM]	Calibration range ULOQ [5] [nM]	r [6]
	Q1	Q3	DP	EP	CE	CXP								
4-HDHA	343.2	101.1	-55	-10	-19	-7	$^2H_8$-5-HETE	22.31	3.7	0.25	0.43	0.25	500	0.9986
19(20)-EpDPE	343.2	241.2	-65	-10	-20	-7	$^2H_{11}$-14(15)-EpETrE	22.39	3.3	0.25	0.43	0.50	20	0.9994
12(13)-EpOME	295.3	195.2	-80	-10	-23	-8	$^2H_4$-9(10)-EpOME	22.45	3.8	0.10	0.15	0.25	40	0.9980
14(15)-EpETrE	319.2	219.3	-65	-10	-20	-4	$^2H_{11}$-14(15)-EpETrE	22.60	3.8	0.25	0.40	0.50	20	0.9985
9(10)-EpOME	295.3	171.1	-80	-10	-23	-8	$^2H_4$-9(10)-EpOME	22.64	3.8	0.10	0.15	0.25	40	0.9949
16(17)-EpDPE	343.2	233.2	-65	-10	-20	-7	$^2H_{11}$-14(15)-EpETrE	22.80	3.5	0.25	0.43	0.50	20	0.9978
13(14)-EpDPE	343.2	193.2	-65	-10	-20	-7	$^2H_{11}$-14(15)-EpETrE	22.88	3.4	0.25	0.43	0.50	20	0.9961
5-oxo-ETE	317.2	273.2	-65	-10	-22	-6	$^2H_4$-9(10)-EpOME	22.95	3.5	1.0	1.6	2.0	20	0.9998
10(11)-EpDPE	343.2	153.2	-65	-10	-20	-7	$^2H_{11}$-14(15)-EpETrE	22.98	3.4	0.13	0.22	0.25	20	0.9990
11(12)-EpETrE	319.3	167.2	-60	-10	-20	-7	$^2H_{11}$-14(15)-EpETrE	23.09	3.3	0.25	0.40	0.50	40	0.9965
8(9)-EpETrE	319.2	155.2	-65	-10	-20	-6	$^2H_{11}$-14(15)-EpETrE	23.24	3.3	0.50	0.80	1.0	20	0.9993
5(6)-EpETrE	319.2	191.1	-60	-10	-20	-7	$^2H_{11}$-14(15)-EpETrE	23.41	2.9	1.0	1.6	2.0	20	0.9974
5(S)-HETrE	321.2	115.1	-70	-10	-19	-9	$^2H_8$-5-HETE	23.55	3.0	0.1	0.2	0.2	500	0.9991
9(10)-ep-stearic acid	297.0	170.8	-100	-10	-28	-11	$^2H_4$-9(10)-EpOME	23.97	3.5	1.0	1.5	2.0	500	0.9953

1) Relative standard deviation for t_R within one batch was ≤ 0.18% (< 0.01 min).
2) Full peak width at half maximum (FWHM) was determined as mean width of standards, concentration 1–200 nM.
3) LOD was set to the lowest concentration yielding a signal to noise ratio ≥ 3.
4) LLOQ was set to the lowest calibration standard yielding a signal to noise ratio ≥ 5 and an accuracy within the calibration curve of ± 20%.
5) ULOQ concentration does not represent the end of the dynamic range, but is the highest calibration standard injected.
6) Calibration was performed as weighted regression using $1/x^2$ weighting.
#) 19-HEPE and 21- and 22-HDHA are quantified based on a response factor relative to 20-HEPE and 20-HDHA, respectively.

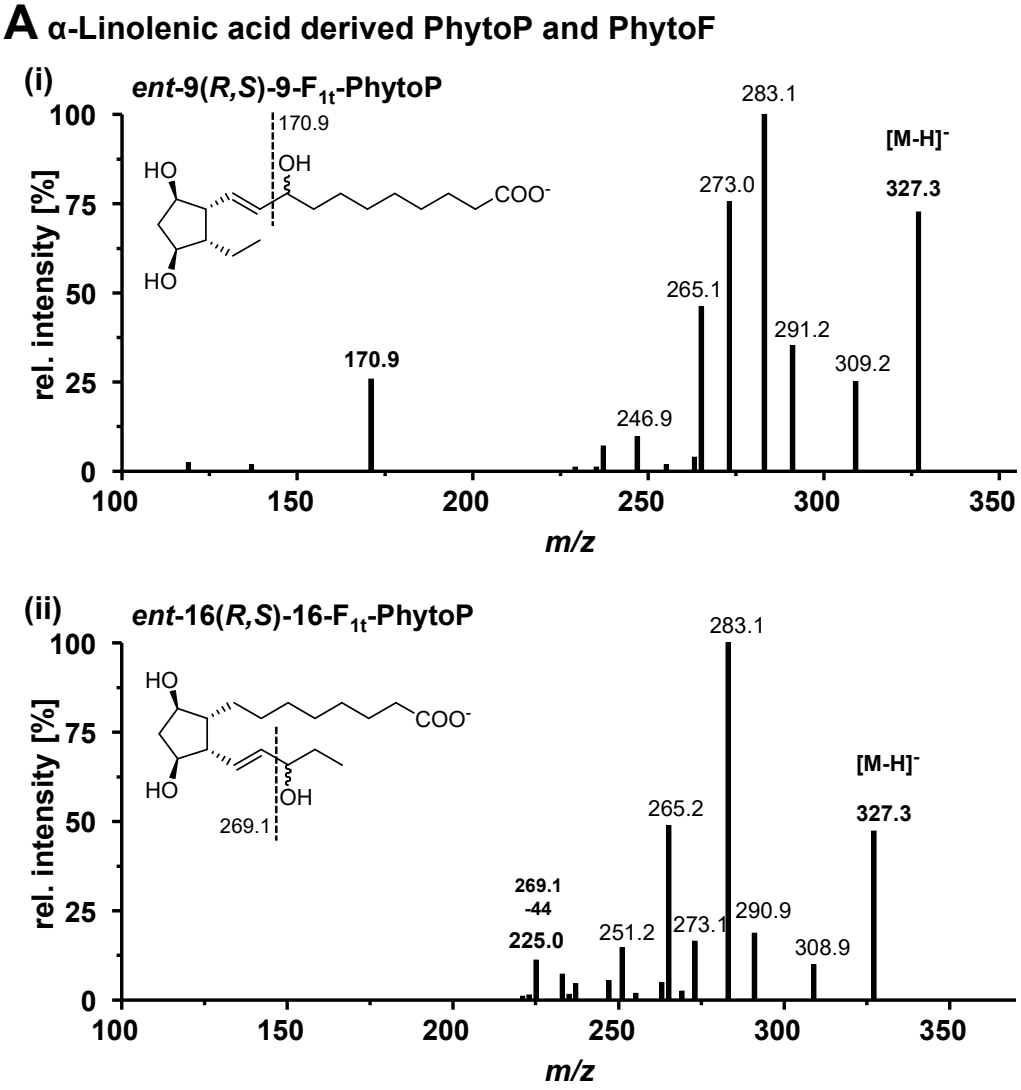

Fig. 8.1: Product ion spectra of isoprostanoids and isofurans derived from different PUFA. The spectra were aquired via CID of the ESI(-)-generated carboxylate-anion $[M-H]^-$ using a collision energy ramp from −17 to −30.
(A) (i)-(v) α-Linolenic acid derived PhytoP and PhytoF
(B) (i)-(iii) Arachidonic acid derived F_{2t}-IsoP
(C) (i)-(ii) Eicosapentaenoic acid derived F_{3t}-IsoP
(D) (i)-(iv) Docosahexaenoic acid derived F_{4t}-NeuroP and NeuroF
(E) (i)-(iv) Adrenic acid derived F_{2t}-dihomo-IsoP and dihomo-IsoF
(F) (i) Docosapentaenoic acid derived F_{3t}-$NeuroP_{n6}$
(G) (i)-(iv) Internal Standards

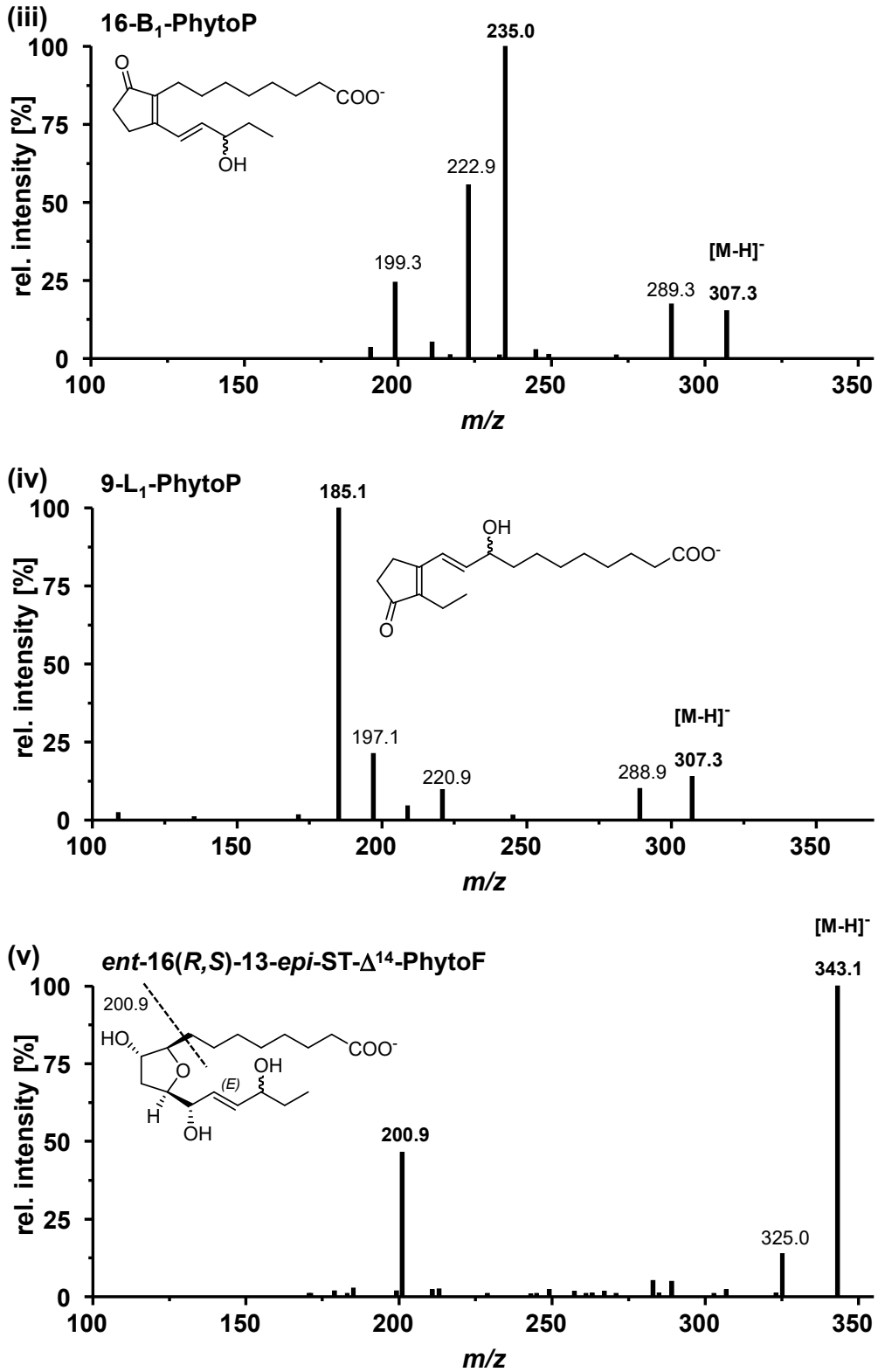

Fig. 8.1: Continued. (A) (i)-(v) α-Linolenic acid derived PhytoP and PhytoF.

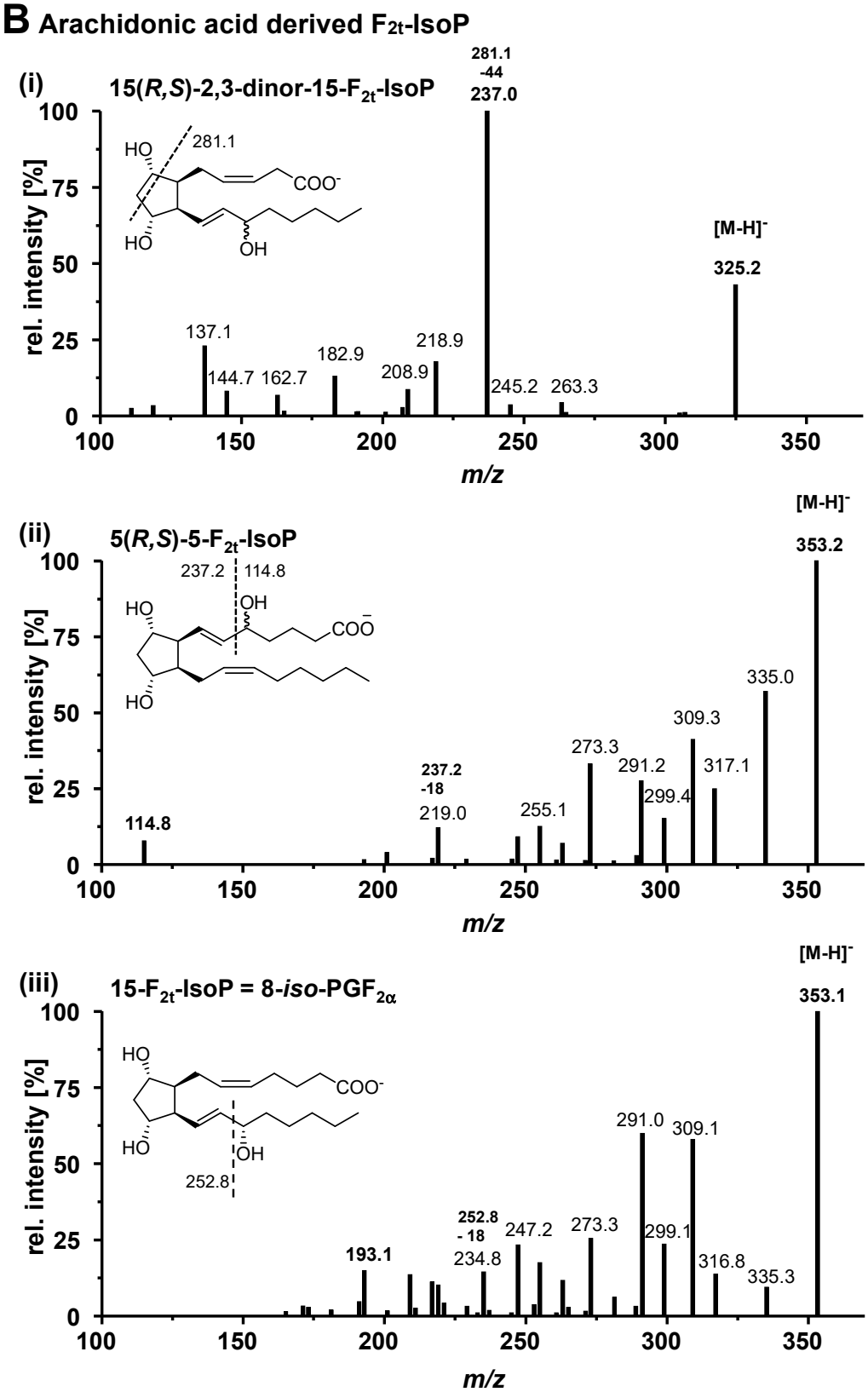

Fig. 8.1: Continued. (B) (i)-(iii) Arachidonic acid derived F_{2t}-IsoP.

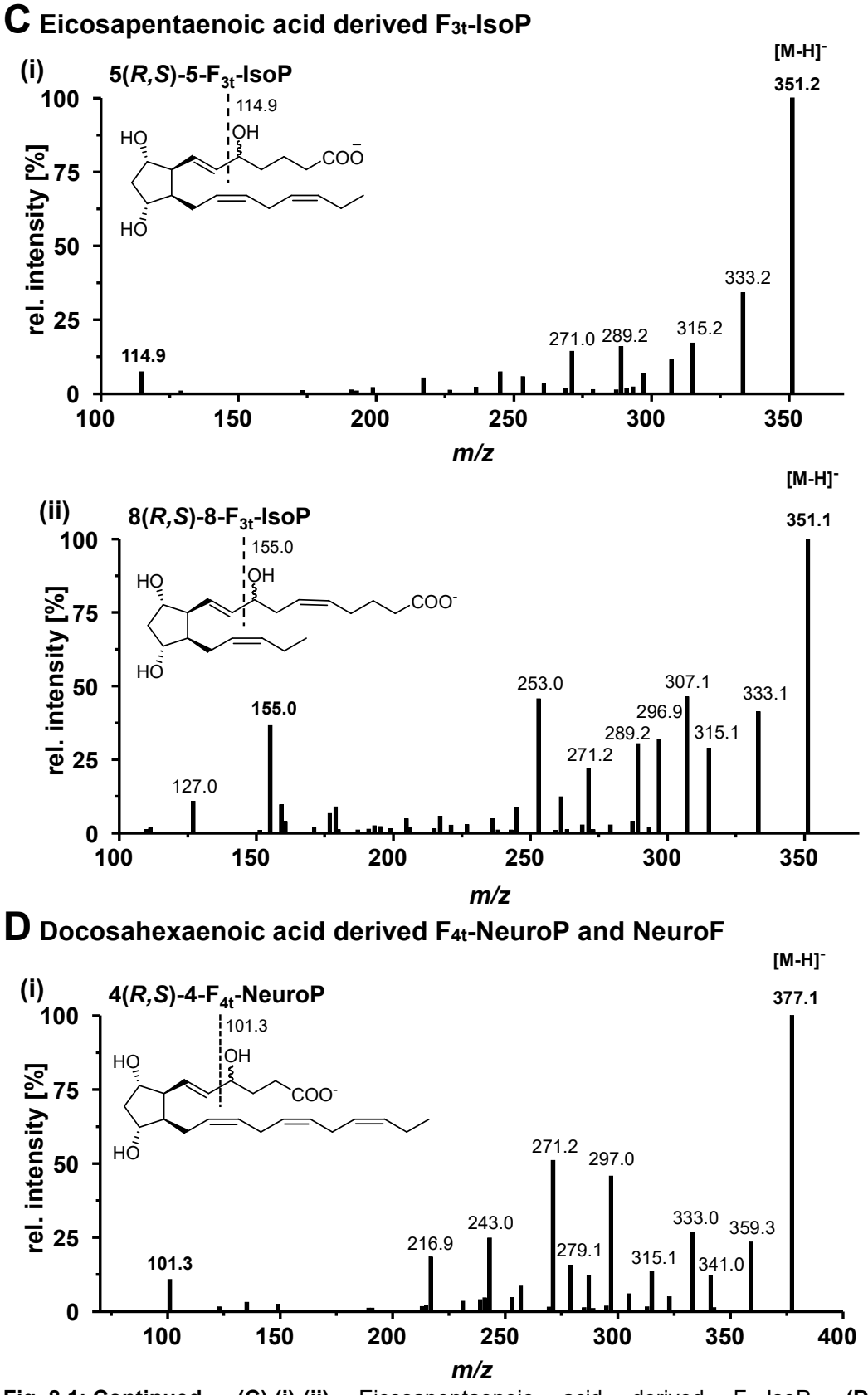

Fig. 8.1: Continued. **(C) (i)-(ii)** Eicosapentaenoic acid derived F_{3t}-IsoP, **(D) (i)-(iv)** Docosahexaenoic acid derived F_{4t}-NeuroP and NeuroF.

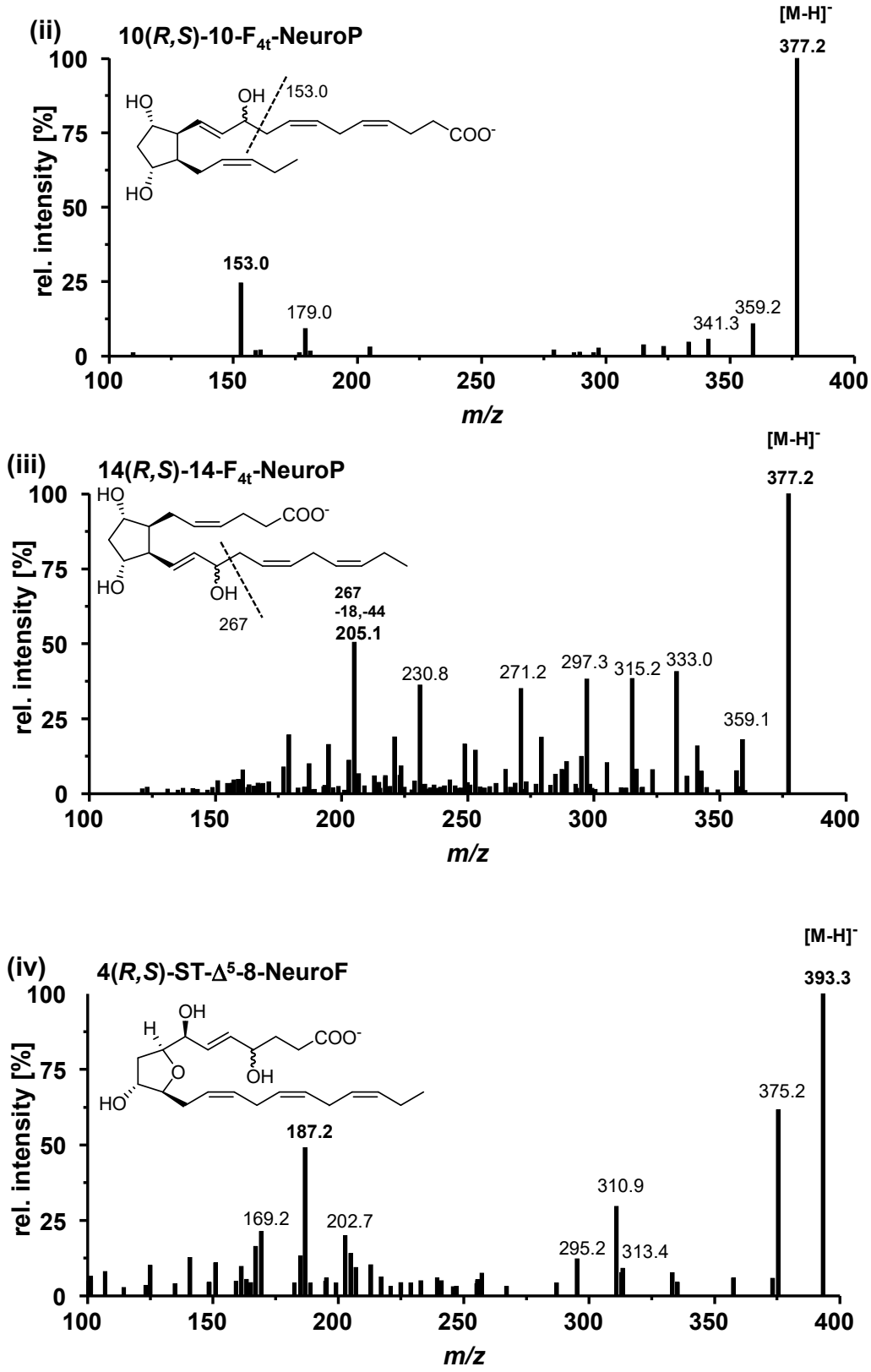

Fig. 8.1: Continued. (D) (i)-(iv) Docosahexaenoic acid derived F_{4t}-NeuroP and NeuroF.

E Adrenic acid derived F_{2t}-dihomo-IsoP and dihomo-IsoF

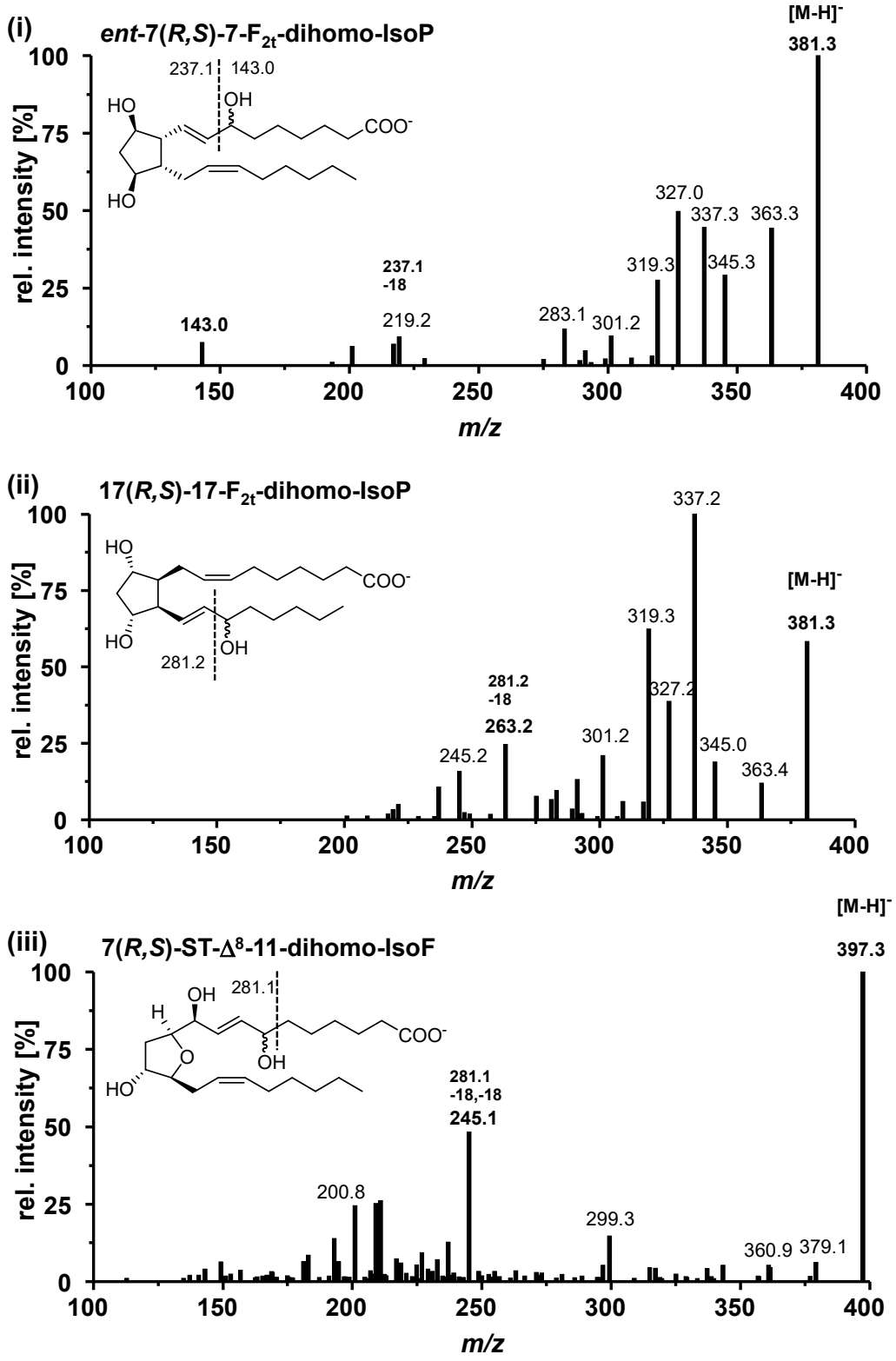

Fig. 8.1: Continued. (E) (i)-(iv) Adrenic acid derived F_{2t}-dihomo-IsoP and dihomo-IsoF.

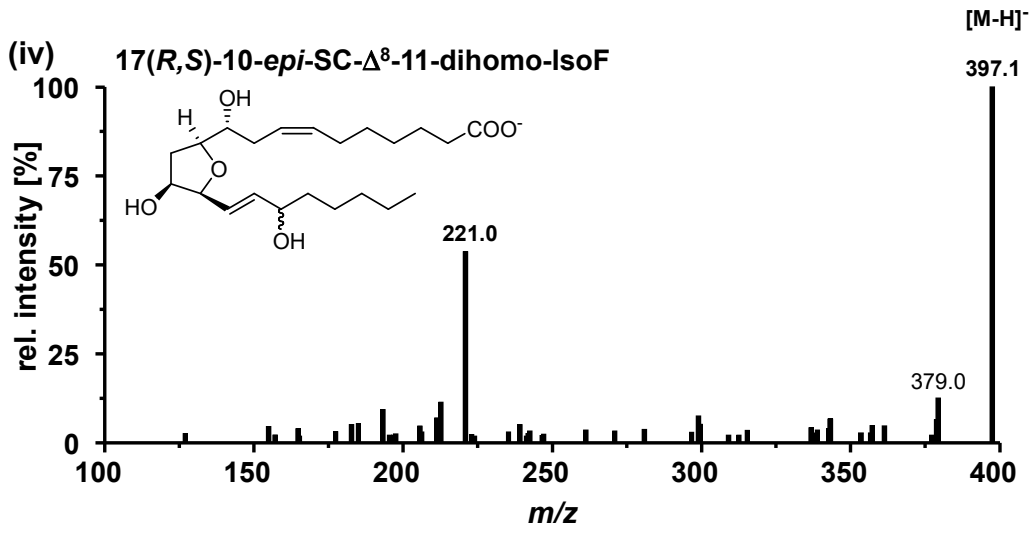

F Docosahexaenoic acid derived F_{3t}-$NeuroP_{n6}$

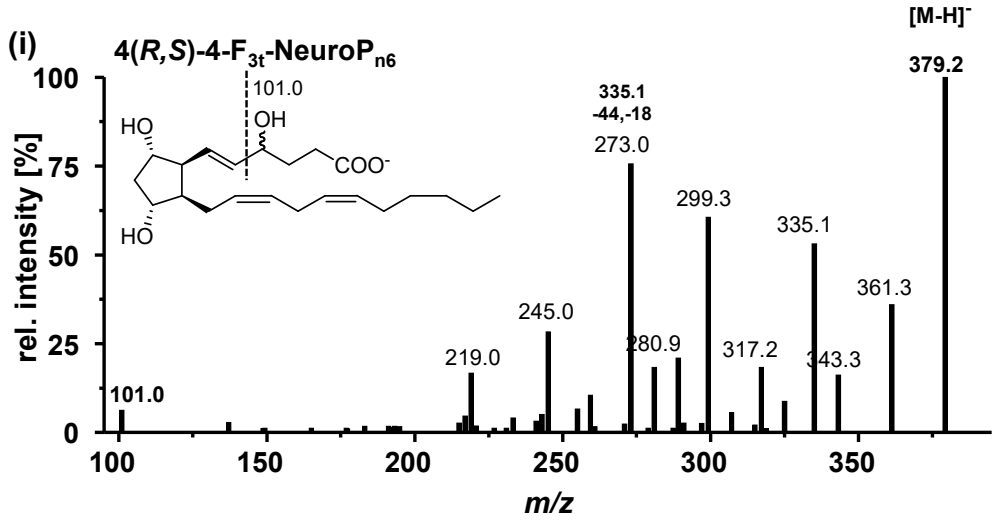

G Internal Standards

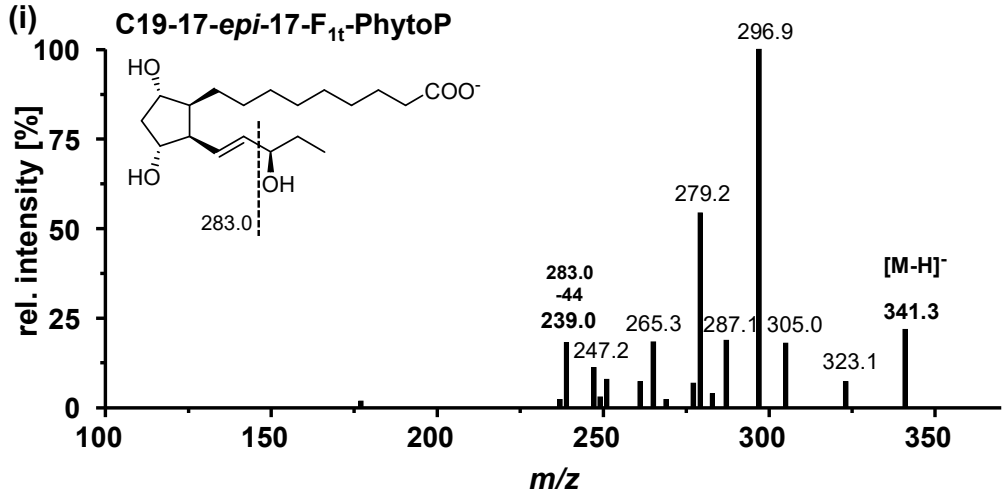

Fig. 8.1: Continued. (E) (i)-(iv) Adrenic acid derived F_{2t}-dihomo-IsoP and dihomo-IsoF, **(F) (i)** Docosapentaenoic acid derived F_{3t}-$NeuroP_{n6}$ **(G) (i)-(iv)** Internal Standards.

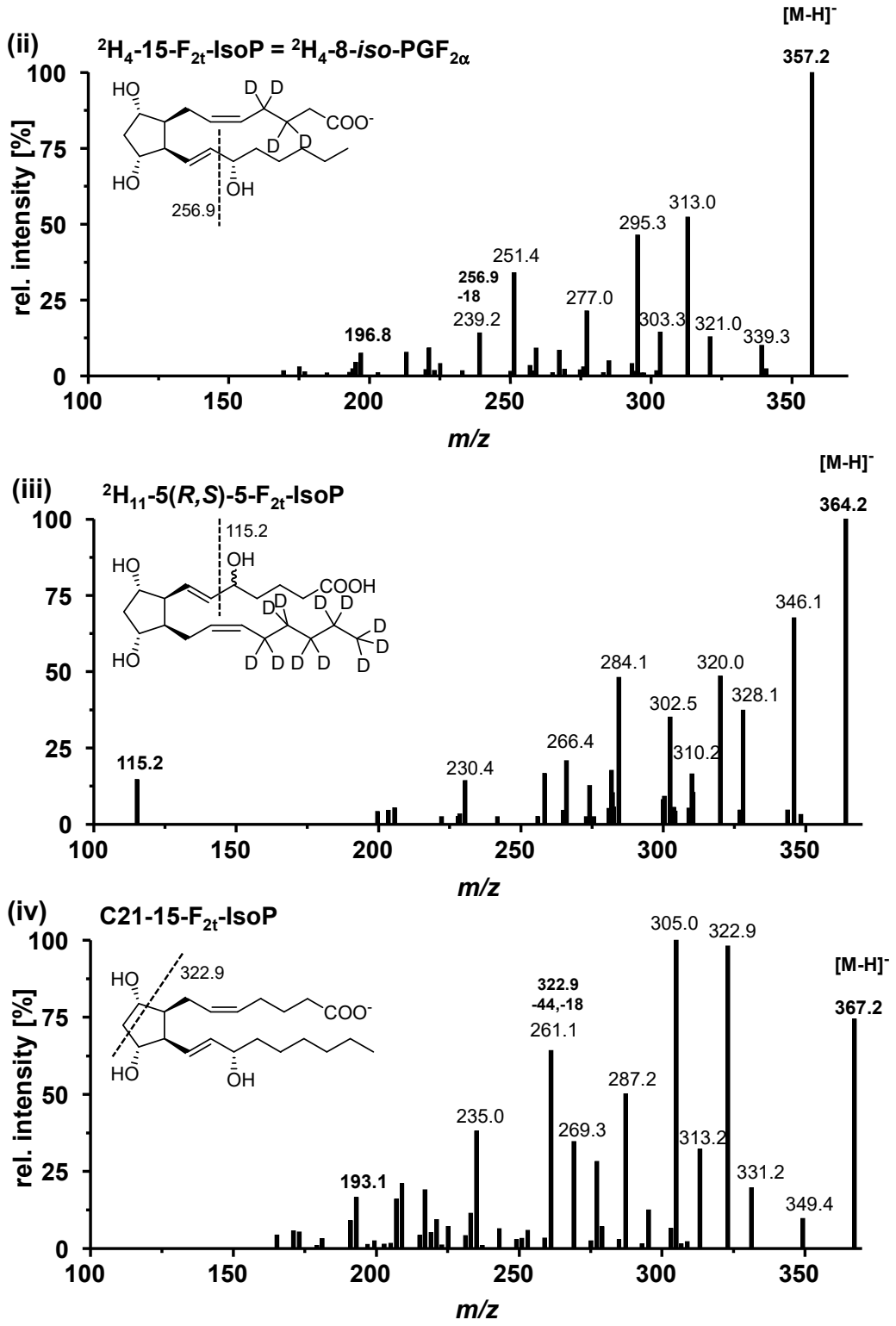

Fig. 8.1: Continued. (G) (i)-(iv) Internal Standards.

Chapter 3

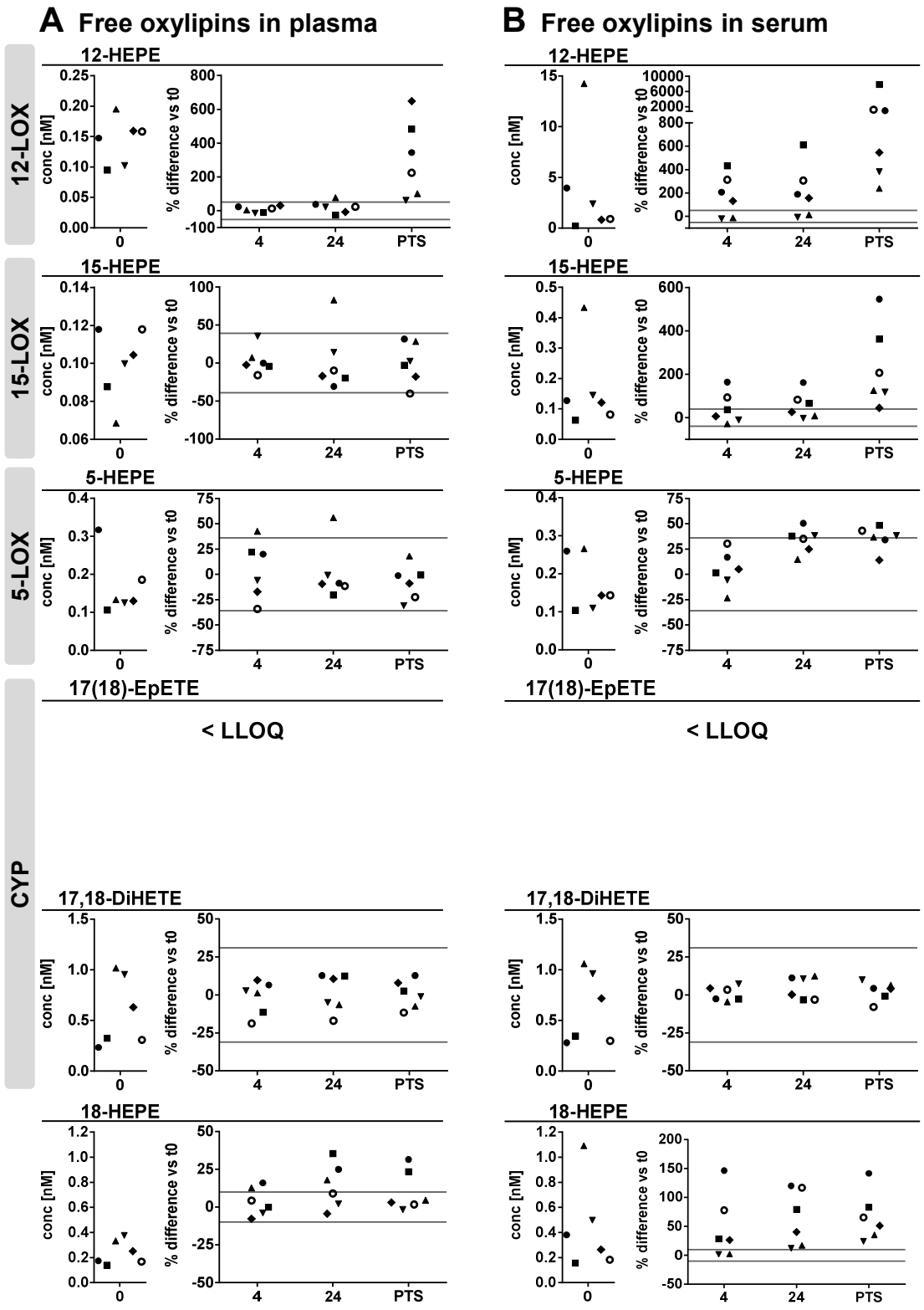

Fig. 8.2: EPA derived free oxylipins in **(A)** plasma and **(B)** serum. Shown are individual concentration (n = 6) of selected oxylipins from major formation pathways at t0 (immediate processing) and %difference *vs* t0 after storage for 4 hours and 24 hours at 4 °C or after pneumatic tube transport (PTS) before centrifugation to generate plasma or serum. The different symbols represent samples from different individual human subjects. The grey lines indicate acceptable change limits calculated based on relative standard deviation of quality control plasma (summarized in Tab. 3.1).

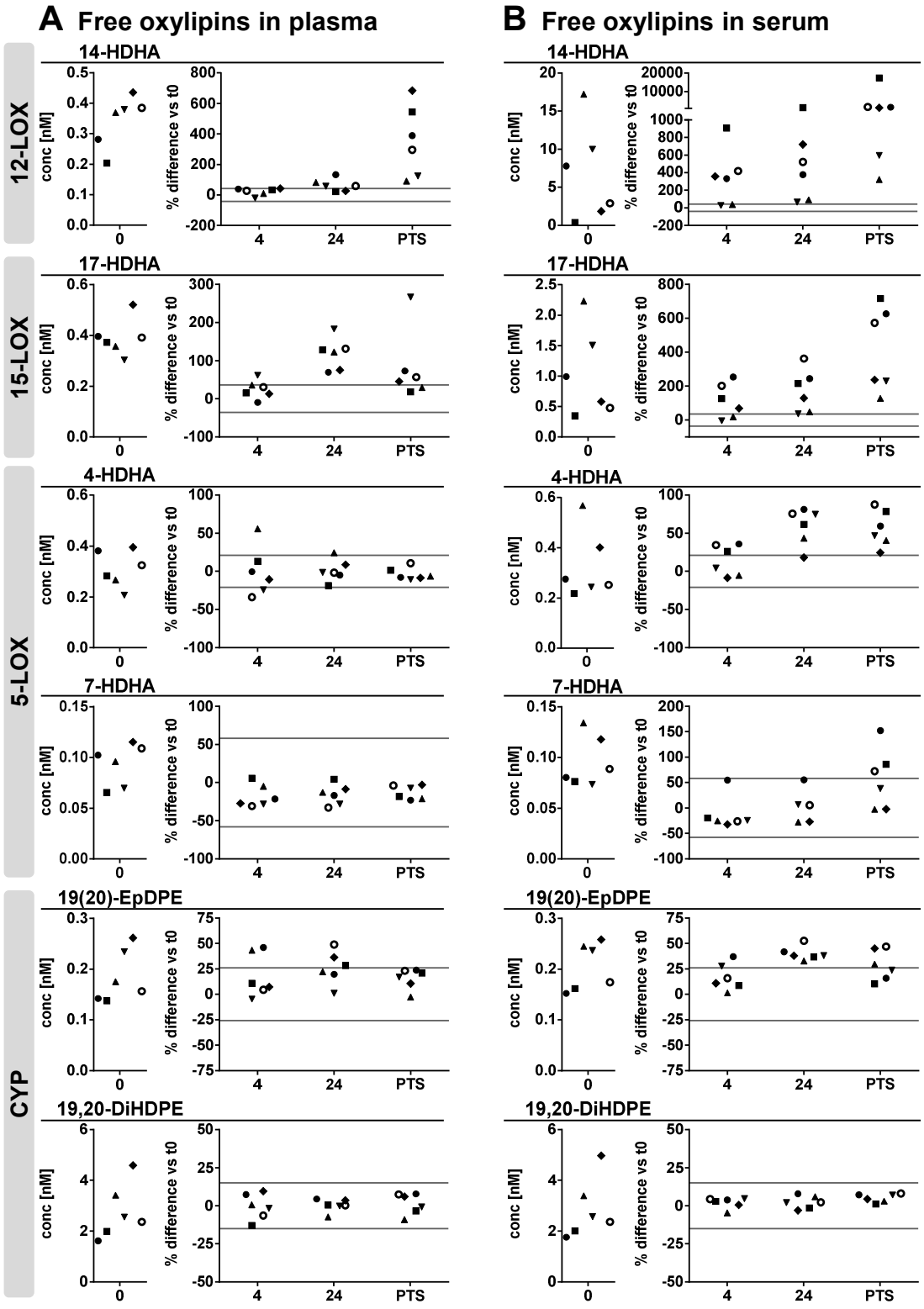

Fig. 8.3: DHA derived free oxylipins in **(A)** plasma and **(B)** serum. Shown are individual concentration (n = 6) of selected oxylipins from major formation pathways at t0 (immediate processing) and %difference *vs* t0 after storage for 4 hours and 24 hours at 4 °C or after pneumatic tube transport before centrifugation to generate plasma or serum. The different symbols represent samples from different individual human subjects. The grey lines indicate acceptable change limits calculated based on relative standard deviation of quality control plasma (summarized in Tab. 3.1).

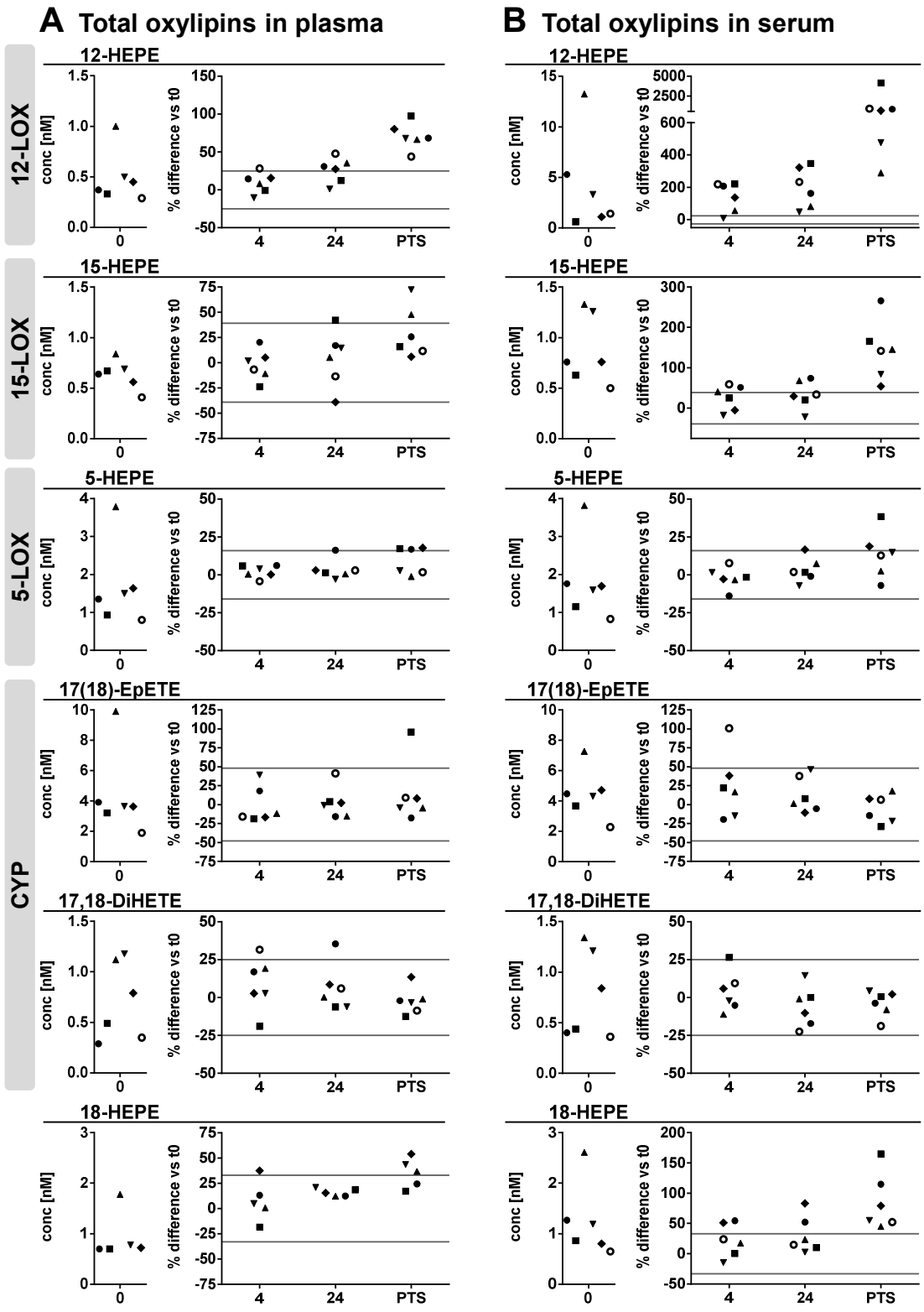

Fig. 8.4: EPA derived total (i.e. sum of free and esterified) oxylipins in **(A)** plasma and **(B)** serum. Shown are individual concentration (n = 6) of selected oxylipins from major formation pathways at t0 (immediate processing) and %difference *vs* t0 after storage for 4 hours and 24 hours at 4 °C or after pneumatic tube transport before centrifugation to generate plasma or serum. The different symbols represent samples from different individual human subjects. The grey lines indicate acceptable change limits calculated based on relative SD of quality control plasma (summarized in Tab. 3.1).

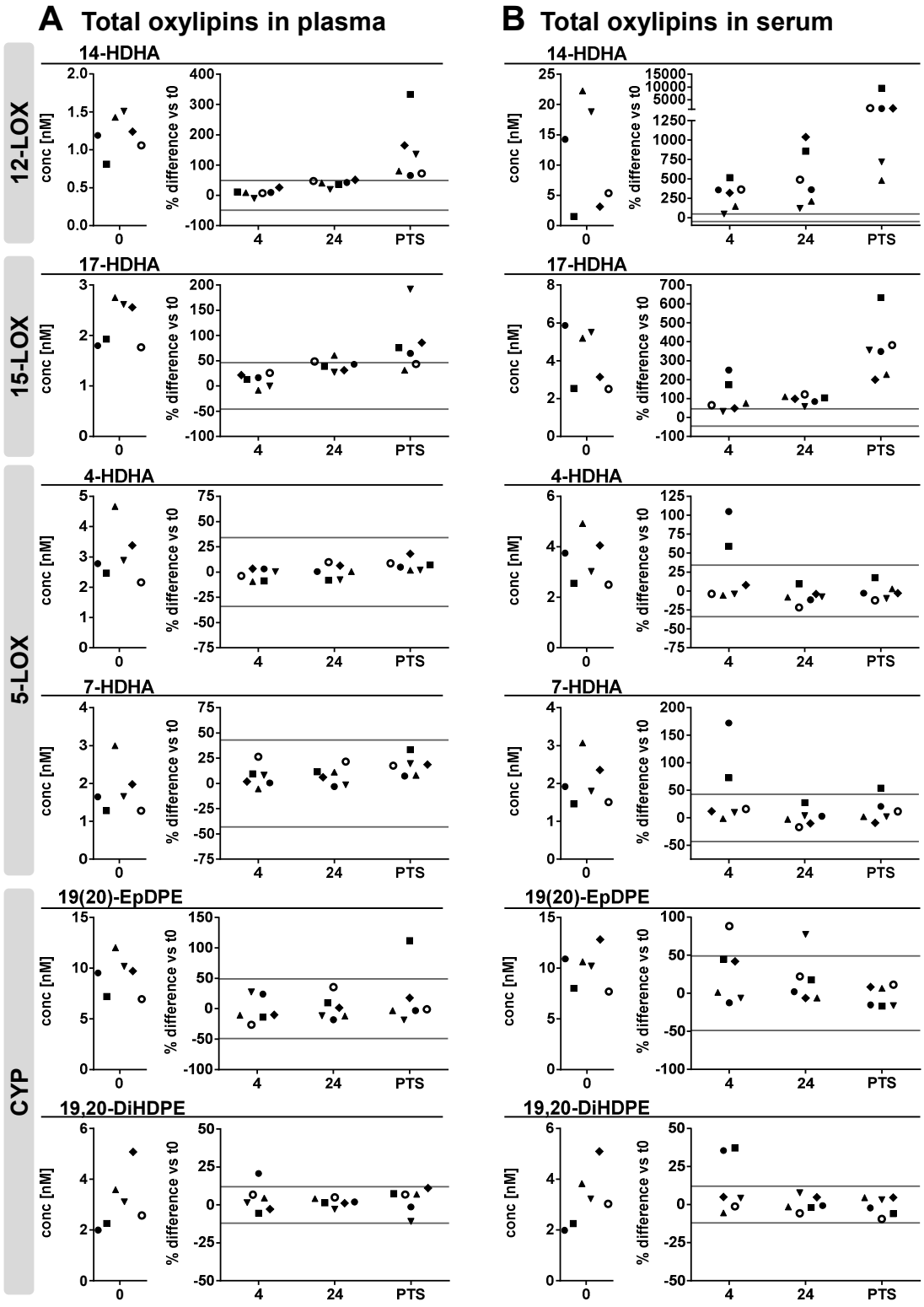

Fig. 8.5: DHA derived total (i.e. sum of free and esterified) oxylipins in **(A)** plasma and **(B)** serum. Shown are individual concentration (n = 6) of selected oxylipins from major formation pathways at t0 (immediate processing) and %difference *vs* t0 after storage for 4 hours and 24 hours at 4 °C or after pneumatic tube transport before centrifugation to generate plasma or serum. The different symbols represent samples from different individual human subjects. The grey lines indicate acceptable change limits calculated based on relative SD of quality control plasma (summarized in Tab. 3.1).

Chapter 4

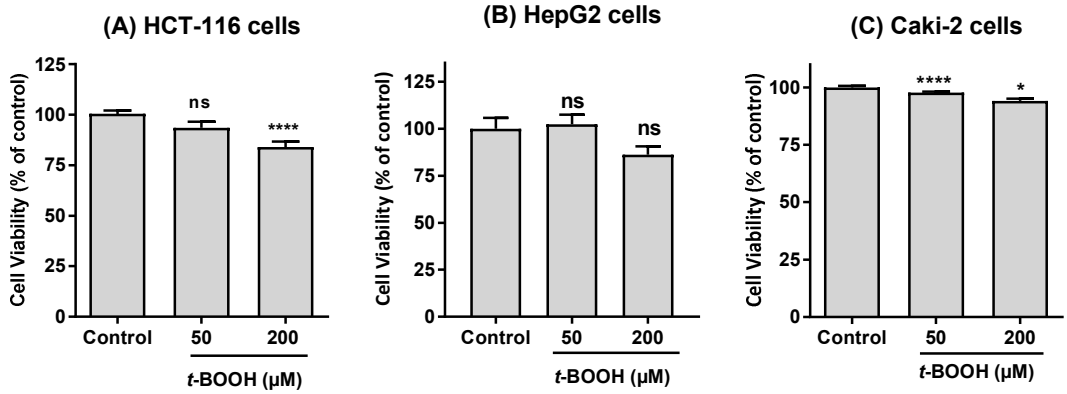

Fig. 8.6: Cell viability of **(A)** HCT-116, **(B)** HepG2 and **(C)** Caki-2 cells following treatment with 50 µM and 200 µM *tert*-butyl hydroperoxide (*t*-BOOH) for 2 h determined by MTS-assay.

Tab. 8.3: Statistical evaluation of the time dependent formation of IsoP and epoxy-PUFA in *C. elegans* following incubation with 6.5 mM *tert*-butyl hydroperoxide for 15, 30, 45 and 60 min. Statistical differences between control (C) and the different treatment time points were evaluated by one-way ANOVA followed by Tukey post-test (* $p < 0.05$, ** $p < 0.01$, *** $p < 0.001$). [a] analyte was below LLOQ in the control group.

			C *vs* 15	C *vs* 30	C *vs* 45	C *vs* 60	15 *vs* 30	15 *vs* 45	15 *vs* 60	30 *vs* 45	30 *vs* 60	45 *vs* 60
ARA	IsoP	5(*R,S*)-5-F_{2t}-IsoP[a]	-	-	-	-	ns	*	***	ns	**	ns
	EpETrE	14(15)-	ns	*	*	***	ns	ns	*	ns	ns	ns
		11(12)-	ns	*	**	***	ns	*	***	ns	ns	ns
		8(9)-	ns	***	***	***	***	***	***	ns	***	*
EPA	IsoP	5(*R,S*)-5-F_{3t}-IsoP	ns	**	***	***	ns	**	***	ns	**	ns
	EpETE	17(18)-	ns	ns	*	**	ns	ns	*	ns	ns	ns
		14(15)-	ns	ns	**	***	ns	ns	*	ns	ns	ns
		11(12)-	ns	*	**	***	ns	ns	*	ns	ns	ns
		8(9)-	ns	*	***	***	ns	*	**	ns	ns	ns

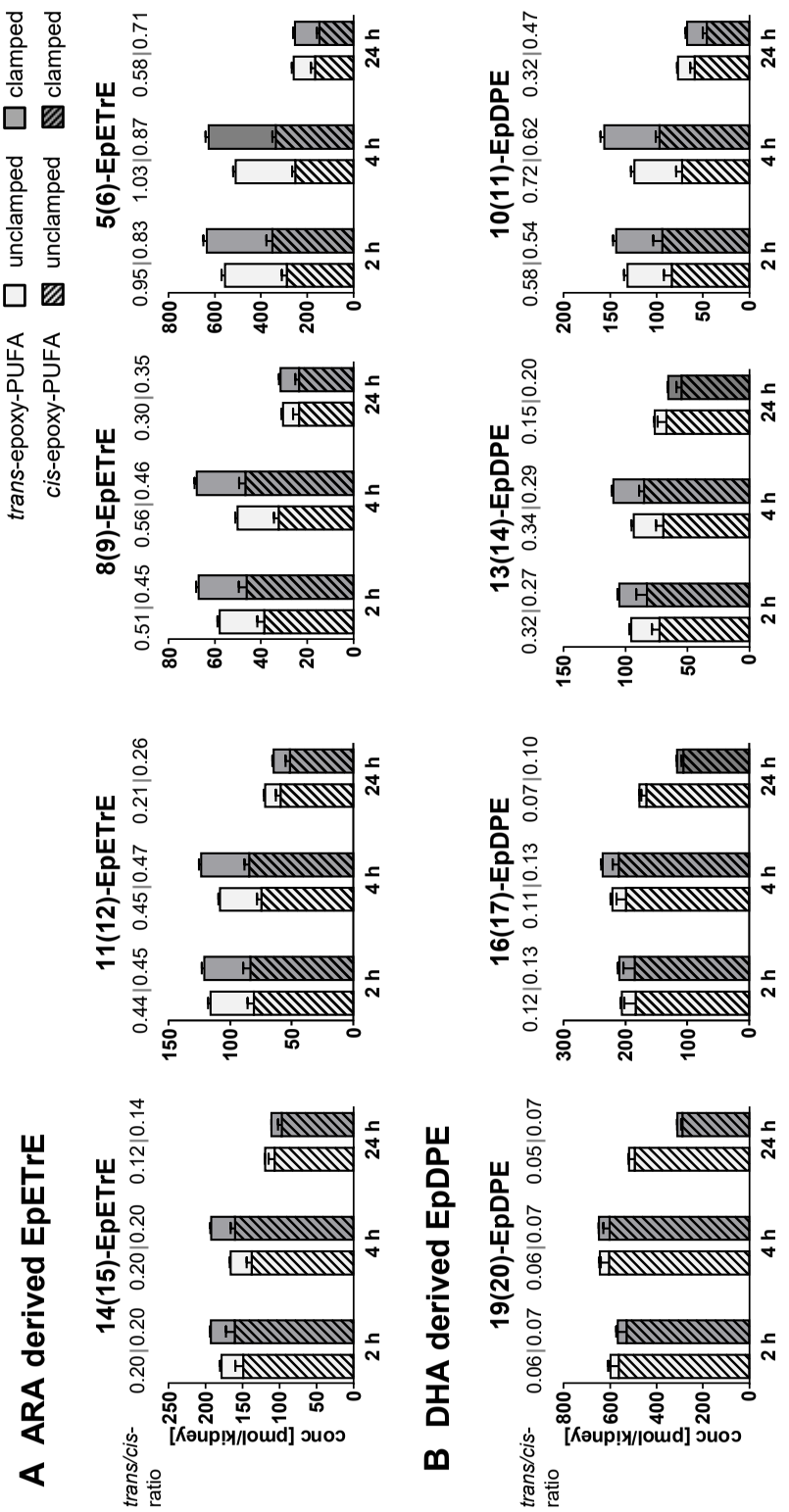

Fig. 8.7: Total levels of epoxy-PUFA derived from **(A)** ARA and **(B)** DHA in murine kidney tissue following unilateral IRI for 35 min. Shown are mean ± SEM (n = 6) in the unclamped and IRI kidneys 2 h, 4 h and 24 h after reperfusion. The *trans/cis*-epoxy-PUFA-ratio (*trans/cis*-ratio) is indicated above the corresponding bars.

Chapter 5

Tab. 8.4: Determined fat content and fatty acid composition of the experimental diets. Diets were based on a linoleic acid rich sunflower oil based standard diet from ssniff Spezialdiäten GmbH (product number: E15051; with 17.6% crude protein, 5.0% crude fiber, 5.3% crude ash, 31.4% starch, 11.0% sugar and 10.1% fat as specified by the manufacturer). All results are shown as mean ± deviation from the mean (n = 2).

	STD	**STD+n3**
Determined **fat content** in the diet [g/100 g]	9.7 ± 0.2	9.9 ± 0.2
[%] Fatty Acid in lipid extract		
C14:0	0.15 ± 0.05	0.19 ± 0.04
C15:0	0.07 ± 0.02	-
C16:0	7.995 ± 0.008	6.61 ± 0.05
C16:1n7	0.217 ± 0.008	0.24 ± 0.03
C17:0	0.071 ± 0.007	0.058 ± 0.007
C18:0	3.288 ± 0.001	2.64 ± 0.03
C18:1n9	27.064 ± 0.004	21.65 ± 0.06
C18:1n7	1.26 ± 0.04	1.047 ± 0.003
C18:2n6	58.306 ± 0.003	46.5 ± 0.1
C18:3n3	0.335 ± 0.005	0.287 ± 0.003
C20:0	0.218 ± 0.003	0.184 ± 0.004
C20:1n9	0.167 ± 0.002	0.14 ± 0.01
C20:4n6	-	0.303 ± 0.003
C20:5n3	-	8.91 ± 0.07
C22:0	0.653 ± 0.008	0.95 ± 0.03
C22:5n3	-	1.18 ± 0.05
C24:0	0.204 ± 0.008	-
C22:6n3	-	8.91 ± 0.09
C24:1n9	-	0.17 ± 0.02

For the determination of the fatty acid composition lipids were first extracted from the pellets according to the Weibull-Stoldt method, performed as rapid microextraction [1].

The fatty acid composition was determined after derivatization to fatty acid methyl esters by means of gas chromatography with flame ionization detection using response factors [2].

References

1. Schulte E. (2004) Vereinfachte Mikromethode zur gravimetrischen Bestimmung des Fettgehaltes von Lebensmitteln nach Säureaufschluss (Kurzmitteilung). *Deutsche Lebensmittelrundschau*. 100(5), pp. 188-189.
2. Ostermann A. I., Müller M., Willenberg I. and Schebb N. H. (2014) Determining the fatty acid composition in plasma and tissues as fatty acid methyl esters using gas chromatography – A comparison of different derivatization and extraction procedures. *Prostaglandins Leukot Essent Fatty Acids*. 91(6), pp. 235-241; doi: 10.1016/j.plefa.2014.10.002.

Tab. 8.5: Lower limit of quantification (LLOQ) and analytical variability of the LC-MS method expressed as relative 95% standard deviation (SD). The LLOQ corresponds to the lowest calibration standard injected yielding a signal to noise ratio ≥ 5 and an accuracy within ± 20% in the calibration curve [1, 2]. The rel. 95% SD was determined for free oxylipins in quality control samples (plasma, n = 15) according to [3]. # Analyte was < LLOQ in quality control plasma.

analyte	LLOQ [nM]	rel 95% SD (= 1.96 × RSD)
PGE_2	0.25	18
TxB_2	1.3	15
PGE_3	0.3	#
TxB_3	0.25	#
5(*R,S*)-5-F_{2t}-IsoP (5-i$PF_{2\alpha}$-VI)	0.5	22
5(*R,S*)-5-F_{3t}-IsoP	2.0	#
4(*R,S*)-4-F_{4t}-NeuroP	1.0	#
5-HETE	0.50	7.7
5-HEPE	0.50	13
4-HDHA	0.25	9.2
7-HDHA	1	#
12-HETE	0.50	15
12-HEPE	0.63	17
14-HDHA	1.0	22
15-HETE	1.3	10
15-HEPE	1.3	19
17-HDHA	2.0	17
14(15)-EpETrE	0.50	15
17(18)-EpETE	1.0	#
19(20)-EpDPE	0.50	12
20-HETE	1.0	7.7
20-HEPE	1.0	16
22-HDHA	2.80	8.2
18-HEPE	1.0	9.8
NPD1 (*m/z* 359 →153)	0.50	#
NPD1 (*m/z* 359 → 206	0.38	#
PDx (*m/z* 359 →153)	0.25	#
PDx (*m/z* 359 → 206)	0.25	#

References

1. Rund K. M., Ostermann A. I., Kutzner L., Galano J.-M., Oger C., Vigor C., Wecklein S., Seiwert N., Durand T. and Schebb N. H. (2018) Development of an LC-ESI(-)-MS/MS method for the simultaneous quantification of 35 isoprostanes and isofurans derived from the major n3- and n6-PUFAs. *Anal Chim Acta*. 1037, pp. 63-74; doi: 10.1016/j.aca.2017.11.002.
2. Kutzner L., Rund K. M., Ostermann A. I., Hartung N. M., Galano J.-M., Balas L., Durand T., Balzer M. S., David S. and Schebb N. H. (2019) Development of an optimized LC-MS method for the detection of specialized pro-resolving mediators in biological samples. *Front Pharmacol*. 10:169; doi: 10.3389/fphar.2019.00169.
3. Ostermann A. I., Greupner T., Kutzner L., Hartung N. M., Hahn A., Schuchardt J. P. and Schebb N. H. (2018) Intra-individual variance of the human plasma oxylipin pattern: Low inter-day variability in fasting blood samples versus high variability during the day. *Anal Methods*. 10(40), pp. 4935-4944; doi: 10.1039/C8AY01753K.

Abbreviations

A1M	alpha-1 microglobulin
ACL	acceptable change limit
ACN	acetonitrile
AdA	adrenic acid (C22:4 n6)
AKI	acute kidney injury
ALA	α-linolenic acid (C18:3 n3)
ALT	alanine transaminase
ANOVA	analysis of variance
ARA	arachidonic acid (C20:4 n6)
AST	aspartate transaminase
BHT	butylated hydroxytoluene
BUN	blood urea nitrogen
C. elegans	*Caenorhabditis elegans*
CE	collision energy
CID	collision-induced dissociation
CKD	chronic kidney disease
COX	cyclooxygenase
CXP	collision cell exit potential
CYP	cytochrome P450 monooxygenase
DHA	docosahexaenoic acid (C22:6 n3)
diH	dihydroxy
DiHDPE	dihydroxy docosapentaenoic acid
DiHETE	dihydroxy eicosatetraenoic acid
DiHETrE	dihydroxy eicosatrienoic acid
DiHODE	dihydroxy octadecadienoic acid

DiHOME	dihydroxy octadecenoic acid
dihomo-IsoF	dihomo-isofuran
dihomo-IsoP	dihomo-isoprostane
DP	declustering potential
n6-DPA	docosapentaenoic acid (C22:5 n6)
EDTA	ethylenediaminetetraacetic acid
ELISA	enzyme-linked immunosorbent assay
EP	entrance potential
EPA	eicosapentaenoic acid (C20:5 n3)
EpDPE	epoxy docosapentaenoic acid
EpETE	epoxy eicosatetraenoic acid
EpETrE	epoxy eicosatrienoic acid
EpODE	epoxy octadecadienoic acid
EpOME	epoxy octadecenoic acid
ESI	electrospray ionization
FAME	fatty acid methyl ester
FID	flame ionization detector
FWHM	full width at half maximum
GC	gas chromatography
GFR	glomerular filtration rate
GSH	gluathione (reduced form)
GSSG	glutathione disulfide (oxidized form)
HDHA	hydroxy docosahexaenoic acid
HEPE	hydroxy eicosapentaenoic acid
HETE	hydroxy eicosatetraenoic acid
HETrE	hydroxy eicosatrienoic acid
HHT/ HHTrE	hydroxy heptadecatrienoic acid
HO-1	heme oxygenase-1
HODE	hydroxy octadecadienoic acid
HOTrE	hydroxy octadecatrienoic acid
HpETE	hydroperoxy eicosatetraenoic acid; hydroperoxy-ARA

HPLC	high performance liquid chromatography
HPRT	hypoxanthine-guanine phosphoribosyltransferase
IL	interleukin
IRI	ischemia reperfusion injury
IS	internal standard
IsoF	isofuran
IsoP	isoprostane
iv	intravenous
KOH	potassium hydroxide
LC	liquid chromatography
LD50	lethal dose 50%
LLOQ	lower limit of quantification
LOD	limit of detection
LOX	lipoxygenase
LT	leukotriene
Lx	lipoxin
m/z	mass to charge ratio
MACE	major adverse cardiac event
MaR	maresin
MCP	monocyte chemoattractant protein
MDA	malondialdehyde
MeOH	methanol
MRI	magnetic resonance imaging
MRM	multiple reaction monitoring
mRNA	messenger ribonucleic acid
MS	mass spectrometry
MTBE	methyl *tert*-butyl ether
MTS	3-(4,5-dimethylthiazol-2-yl)-5-(3-carboxymethoxyphenyl)-2-(4-sulfophenyl)-2H-tetrazolium
NaClO	sodium hypochlorite
NaOH	sodium hydroxide
NeuroF	neurofuran

NeuroP	neuroprostane
NF-κB	nuclear factor κB
NGM	nematode growth medium
(N)PD1	(neuro)protectin D1
oxo-ETE	oxo eicosatetraenoic acid
oxo-ODE	oxo octadecadienoic acid
PAS	Periodic Acid-Schiff
PBS	phosphate buffered saline
PDX	protectin DX
PFA	paraformaldehyde
PG	prostaglandin
PhytoF	phytofuran
PhytoP	phytoprostane
PLA	phospholipase A
PMSF	phenyl methyl sulfonyl fluoride
PPAR	peroxisome proliferator activated receptor
PTS	pneumatic tube system transport
PUFA	polyunsaturated fatty acid
n3-PUFA	omega-3 polyunsaturated fatty acid
n6-PUFA	omega-6 polyunsaturated fatty acid
QC	quality control
qPCR	quantitative polymerase chain reaction
R	resolution
RBC	red blood cells
RONS	reactive oxygen and nitrogen species
ROS	reactive oxygen species
RP	reversed-phase
rpm	rounds per minute
RSD	relative standard deviation
RT	room temperature
Rv	resolvin

S/N	signal to noise ratio
SD	standard deviation
sEH	soluble epoxide hydrolase
SEM	standard error of the mean
SIM	single ion monitoring
SPE	solid phase extraction
SPM	specialized pro-resolving mediator
SRM	selected reaction monitoring
STD	standard diet (linoleic acid rich, sunflower oil based, 10% fat)
STD+n3	n3-PUFA enriched standard diet (1% EPA and 1% DHA ethyl ester in the diet)
t-AUCB	*trans*-4-[4-(3-adamantan-1-yl-ureido)-cyclohexyloxy]-benzoic acid
t-BOOH	*tert*-butyl hydroperoxide
2-TEDC	2-(1-thienyl)ethyl 3,4-dihydroxybenzylidenecyanoacetate
TG	triglyceride
t_R	retention time
Tx	thromboxane
ULOQ	upper limit of quantification
UUO	unilateral ureteral obstraction
VF	view field
VLDL	very low density lipoprotein

Acknowledgement

This thesis was carried out from July 2015 to September 2019 in the Institute for Food Toxicology (University of Veterinary Medicine Hannover) and at the Chair of Food Chemistry (University of Wuppertal) in the research group of Prof. Dr. Nils Helge Schebb.

Facing the completion of this thesis, I would deeply thank all people who supported, encouraged and accompanied me during this time filled with ups and downs (challenges ;-)) and who contributed to the successful termination of this thesis.

First of all, I would like to thank my supervisor Prof. Dr. Nils Helge Schebb for the opportunity to work in his group on an interesting topic which allowed me combining the work with analytical techniques with the investigation of biological questions. I thank him for the support and encouragement throughout the whole time of my thesis. And I am grateful for the chance to join so many national and international conferences for presenting my results and broadening my horizon.

I thank Prof. Dr. Julia Bornhorst not only for being a board member of the PhD examination committee, but also for the collaboration in the work with *C. elegans* and her kind support and advices since we are together in Wuppertal.

For the financial support in form of a Kekulé fellowship I would like to thank the Fonds der Chemischen Industrie (Frankfurt/Main, Germany).

I thank Judith Schäfer and Prof. Dr. Mirko Bunzel who awakened my interest and assisted my first steps in scientific work during my diploma thesis.

For giving me the opportunity to finish parts of my work in Hannover before moving to Wuppertal I gratefully acknowledge Prof. Dr. Kietzmann.

As it can be seen by the number of coauthors the work of this thesis is based on cooperations with many researchers whom I would like to thank for their help and support working with me on the different parts of this thesis.

I would like to thank Prof Dr. Faikah Gueler for the cooperation in the study of clinical sample handling allowing us to mimic “real” clinical routine blood handling. Furthermore, I thank her for our successful collaboration in the experiments with ischemia reperfusion injury. In our discussions between analytics, medicine and physiology I learned a lot about the interpretation of clinical results and design of *in vivo* experiments. Moreover, I want to thank Faikah’s team (Shu Peng, Rongjun Chen, Julian Doricic, Robert Greite, Herle Chlebusch and Martina Ackermann) for their uncomplicated and friendly collaboration.

Furthermore, I thank Prof. Dr. Jörg Fahrer and the members of his group (Nina Seiwert, Sabine Wecklein, Daniel Heylmann) for the fruitful collaboration with the cell culture experiments, laying the foundation for the work with oxidative stress.

I would like to thank Prof. Dr. Thierry Durand and his team of organic chemists (Jean-Marie Galano, Camille Oger, Claire Vigor, Laurence Balas) for synthesizing and providing the standard substances of isoprostanoids as well as protectin used in part for method development which were otherwise unavailable.

Moreover, I thank Cornelius Claaßen and Fabian Nolte for their valuable contributions to this work during their master thesis’ and also in part as research assistant.

A special thanks goes to all of my colleagues from the AG Schebb for sharing funny and stressful moments in the lab, on conferences and beyond:
Laura Kutzner (for her “Meinung” in any practical and scientific questions her critical “…ja, aber”, and for always having an ready ear) and Nicole Hartung (for her motivating “Inspiration” ;-) and excellent advices in every linguistic issues) who work with me in Hannover and shared the challenges of moving to Wuppertal; “Weg-werf”-Nadja Kampschulte (for sharing freezer sessions, nearly endless motivation and working together till deep in the night), Elisabeth Koch (for shared challenges with epoxy-PUFA and hydrolysis and always having “ne Frage”), Malwina Mainka and Ayah Alasmer (for the supply with sweets and keeping the good mood). In addition, I thank Patrick Waindok for his patience with me and the analytical device.

Moreover, I thank my former colleagues Ina Willenberg and Annika Ostermann for introducing me in the secrets and challenges of analyzing oxylipins and the wonderful time. Particularly Annika for always being ready to lend an ear, many helpful scientific advices and numerous motivating and enjoyable discussions.

Furthermore, I thank Dieter Riegel (for his helpfulness and always knowing whom to ask in the case of technical problems), Claudia Steinhage (for the reliable and pleasant working together in preparation of the upcoming practical courses) and Sabine Scalet (for taking caring about “Bürokratie”).

Let me also thank AG B(ornhorst), Vivien Michaelis and Merle Nicolai for coping with crazy PAL autosamplers ;-) and having fun with popcorn, cheese and pretzels.

For the pleasant atmosphere, I want to thank all members of the Institute for Food Toxicology of the University of Veterinary Medicine Hannover, especially Michael Empl (for endless discussions with ”… lange Rede, kurzer Sinn”), Tina Kostka and Maren Schenke (geb. Lück). Thank you for pizza dates and game evenings “escaping” from work.

I am grateful for old and new friends with whom I shared life and a wonderful time beyond work.

Mein letzter, aber zugleich wichtigster Dank richtet sich an meine Familie: meine Eltern, meine Brüder Julian und Martin, meine Großeltern. Danke, dass ihr mir alles ermöglicht, immer an mich geglaubt und mich in jeglicher Hinsicht unterstützt habt! Danke dem gesamten “Brüderle-Clan”, für die herzliche Aufnahme in die Familie.
Mein größter Dank gilt jedoch dir, Matthias! Danke für deine grenzenlose Unterstützung, deine unermüdliche gute Hoffnung (!), Geduld und Liebe!
Si deus pro nobis quis contra nos (Röm 8,31).

Ohne Euch alle hätte ich das nie geschafft! DANKE

Curriculum Vitae

Der Lebenslauf ist aus Gründen des Datenschutzes in der Online-Version nicht enthalten.

Der Lebenslauf ist aus Gründen des Datenschutzes in der Online-Version nicht enthalten.

List of Publications

Publications in peer-reviewed Journals

Within the Scope of this Thesis

K. M. Rund, F. Nolte, J. Doricic, R. Greite, S. Schott, R. Lichtinghagen, F. Gueler and N. H. Schebb **(2020)** Clinical blood sampling for oxylipin analysis – Effect of storage and pneumatic tube transport of blood on free and total oxylipin profile in human plasma and serum. *Analyst*. 145, pp. 2378-2388; doi: 10.1039/C9AN01880H.

K. M. Rund*, S. Peng*, R. Greite, C. Claaßen, F. Nolte, C. Oger, J.-M. Galano, L. Balas, T. Durand, R. Chen, F. Gueler* and N. H. Schebb* **(2020)** Dietary omega-3 PUFA improved tubular function after ischemia induced acute kidney injury in mice but did not attenuate impairment of renal function. *Prostaglandins Other Lipid Mediat.* 146:106386; doi: 10.1016/j.prostaglandins.2019.106386.
*Authors contributed equally to this work.

K. M. Rund, D. Heylmann, N. Seiwert, S. Wecklein, C. Oger, J.-M. Galano, T. Durand, R. Chen, F. Gueler, J. Fahrer, J. Bornhorst and N. H. Schebb **(2019)** Formation of *trans*-epoxy fatty acids correlates with formation of isoprostanes and could serve as biomarker of oxidative stress. *Prostaglandins Other Lipid Mediat*. 144:106334; doi: 10.1016/j.prostaglandins.2019.04.004.

K. M. Rund, A. I. Ostermann, L. Kutzner, J.-M. Galano, C. Oger, C. Vigor, S. Wecklein, N. Seiwert, T. Durand and N. H. Schebb **(2018)** Development of an LC-ESI(-)-MS/MS method for the simultaneous quantification of 35 isoprostanes and isofurans derived from the major n3- and n6-PUFAs. *Anal Chim Acta*. 1037, pp. 63-74; doi: 10.1016/j.aca.2017.11.002.

FURTHER PUBLICATIONS

A. I. Ostermann, E. Koch, K. M. Rund, L. Kutzner, M. Mainka and N. H. Schebb **(2020)** Targeting esterified oxylipins by LC-MS – Effect of sample preparation on oxylipin pattern, *Prostaglandins Other Lipid Mediat.* 146:106384; doi: 10.1016/j.prostaglandins.2019.106384.

P. Waindok, E. Janecek-Erfurth, D. Lindenwald, E. Wilk, K. Schughart, R. Geffers, L. Balas, T. Durand, K. M. Rund, N. H. Schebb and C. Strube **(2019)** Multiplex profiling of inflammation-related bioactive lipid mediators in Toxocara canis- and Toxocara cati-induced neurotoxocarosis. *PLoS Negl Trop Dis*. 13(9):e0007706; doi: 10.1371/journal.pntd.0007706.

N. M. Hartung, J. Fischer, A. I. Ostermann, I. Willenberg, K. M. Rund, N. H. Schebb and U. Garscha **(2019)** Impact of food polyphenols on oxylipin biosynthesis in human neutrophils. *Biochim Biophys Acta*. 1864(10), pp. 1536-1544; doi: 10.1016/j.bbalip.2019.05.002.

S. Hellms, F. Gueler, M. Gutberlet, N. H. Schebb, K. Rund, J. T. Kielstein, V. VoChieu, S. Rauhut, R. Greite, P. Martirosian, H. Haller, F. Wacker and K. Derlin **(2019)** Single-dose diclofenac in healthy volunteers can cause decrease in renal perfusion measured by functional magnetic resonance imaging. *J Pharm Pharmacol*. 71(8), pp. 1262-1270; doi: 10.1111/jphp.13105.

L. Kutzner, K. M. Rund, A. I. Ostermann, N. M. Hartung, J.-M. Galano, L. Balas, T. Durand, M. S. Balzer, S. David and N. H. Schebb **(2019)** Development of an optimized LC-MS method for the detection of specialized pro-resolving mediators in biological samples. *Front Pharmacol*. 10:169; doi: 10.3389/fphar.2019.00169.

H. Gottschall, C. Schmöcker, D. Hartmann, N. Rohwer, K. Rund, L. Kutzner, F. Nolte, A. I. Ostermann, N. H. Schebb and K. H. Weylandt **(2018)** Aspirin alone and combined with a statin suppresses eicosanoid formation in human colon tissue. *J Lipid Res*. 59(5), pp. 864-871; doi: 10.1194/jlr.M078725.

K. Möller, A. I. Ostermann, K. Rund, S. Thoms, C. Blume, F. Stahl, A. Hahn, N. H. Schebb and J. P. Schuchardt **(2016)** Influence of weight reduction on blood levels of C-reactive protein, tumor necrosis factor-α, interleukin-6, and oxylipins in obese

subjects. *Prostaglandins Leukot Essent Fatty Acids*. 106, pp. 39-49; doi: 10.1016/j.plefa.2015.12.001.

I. Willenberg, K. Rund, S. Rong, N. Shushakova, F. Gueler and N. H. Schebb **(2016)** Characterization of changes in plasma and tissue oxylipin levels in LPS and CLP induced murine sepsis. *Inflamm Res*. 65(2), pp. 133-142; doi: 10.1007/s00011-015-0897-7.

J. Schäfer, F. Urbat, K. Rund and M. Bunzel **(2015)** A stable-isotope dilution GC-MS approach for the analysis of DFRC (Derivatization Followed by Reductive Cleavage) monomers from low-lignin plant materials. *J Agric Food Chem*. 63(10), pp. 2668-2673; doi: 10.1021/jf506221p.

ORAL PRESENTATIONS

K. M. Rund **(2019)** Bildung von Oxidationsprodukten mehrfach ungesättigter Fettsäuren und deren Eignung als Marker für oxidativen Stress. Arbeitstagung 2019 des Regionalverbandes NRW der Lebensmittelchemischen Gesellschaft, 06.03.2019, Wuppertal, Germany.

K. Rund **(2017)** Oxidationsprodukte von ungesättigten Fettsäuren als funktionelle Marker für oxidativen Stress? Stipendiatentreffen 2017/2018 des Fonds der Chemischen Industrie, 30.11.2017, Berlin, Germany.

K. Rund **(2017)** Targeted LC-ESI(-)-MS/MS based metabolomics of prostaglandin-like autoxidation products. 27. Doktorandenseminar des Arbeitskreis Separation Science der Fachgruppe Analytische Chemie der GDCh, 08.–10.01.2017, Hohenroda, Germany.

POSTER PRESENTATIONS

C. Schmöcker, N. Rohwer, H. Gottschall, K. Rund, L. Kutzner, A. I. Ostermann, D. Hartmann, N. H. Schebb and K. H. Weylandt **(2019)** Aspirin treatment changes oxylipin levels in murine and human colon tissue. United European Gastroenterology (UEG) Week, 19.–23.10.2019, Barcelona, Spain.

K. M. Rund, S. Peng, S. Rong, R. Chen, F. Gueler and N. H. Schebb **(2019)** Dietary supplementation with long-chain omega-3 PUFA improved kidney function in a mouse model of renal ischemia reperfusion injury. 48. Deutscher Lebensmittelchemikertag, 16.–18.09.2019, Dresden, Germany.

K. M. Rund, S. Peng, S. Rong, R. Chen, F. Gueler and N. H. Schebb **(2019)** Feeding of a long-chain omega-3 PUFA enriched diet improved kidney function after renal ischemia reperfusion in mice. Summer School Neuruppin, 2. Symposium der Viszeralmedizinischen Abteilungen der Ruppiner Kliniken – Medizinische Hochschule Brandenburg, 24.–25.05.2019, Neuruppin, Germany.

C. Hidalgo-Shrestha, K. M. Rund, N. Rohwer, K. H. Weylandt, B. D. Hammock and N. H. Schebb **(2019)** Modulation of acute DSS-induced colitis by inhibition of soluble epoxide hydrolase in two rodent models. Summer School Neuruppin, 2. Symposium der Viszeralmedizinischen Abteilungen der Ruppiner Kliniken – Medizinische Hochschule Brandenburg, 24.–25.05.2019, Germany.

K. M. Rund, J.-M. Galano, C. Oger, T. Durand, J. Bornhorst and N. H. Schebb **(2019)** Characterizing oxidative stress by targeted LC-MS/MS based analysis of autoxidation products from polyunsaturated fatty acids. 8. Berliner LC-MS/MS Sciex Symposium, 02.04.2019, Berlin, Germany.

L. Kutzner, K. M. Rund and N. H. Schebb **(2019)** Detection of specialized pro-resolving mediators on a QTRAP 6500 system. 8. Berliner LC-MS/MS Sciex Symposium, 02.04.2019, Berlin, Germany.

K. M. Rund, D. Heylmann, N. Seiwert, J. Bornhorst, J. Fahrer and N. H. Schebb **(2018)** Combined evaluation of epoxy-fatty acid and isoprostane formation in response to oxidative stress. 47. Deutscher Lebensmittelchemikertag, 17.–19.09.2018, Berlin, Germany.

K. M. Rund, S. Peng, S. Rong, R. Chen, F. Gueler and N. H. Schebb **(2018)** Omega-3 PUFA moderately attenuate acute kidney injury in a murine model of renal ischemia reperfusion injury. 7th European Workshop on Lipid Mediators, 12.–14.09.2018, Brussels, Belgium.

K. M. Rund, D. Heylmann, N. Seiwert, J. Bornhorst, J. Fahrer and N. H. Schebb **(2018)** Correlation of the epoxy-fatty acid pattern with isoprostane formation during oxidative stress. 7th European Workshop on Lipid Mediators, 12.–14.09.2018, Brussels, Belgium.

C. Schmöcker, H. Gottschall, C. D. Hartmann, N. Rohwer, K. Rund, L. Kutzner, F. Nolte, A. I. Ostermann, N. H. Schebb and K. H. Weylandt **(2018)** Oxylipin formation in human colon tissue. 7th European Workshop on Lipid Mediators, 12.–14.09.2018, Brussels, Belgium.

K. M. Rund, D. Heylmann, N. Seiwert, J.-M. Galano, C. Oger, C. Vigor, T. Durand, F. Gueler, J. Fahrer and N. H. Schebb **(2018)** Exploiting isoprostanes and epoxy-fatty acids as markers of autoxidation. 17th International Winter Eicosanoid Conference, 11.–13.03.2018, Baltimore, USA.

M. Mainka, S. Schueler, T. Hecker, K. Rund and N. H. Schebb **(2018)** Comparison of the glucuronidation-rate of n3-and n6-polyunsaturated fatty acid derived dihydroxy-FA. 17th International Winter Eicosanoid Conference, 11.–13.03.2018, Baltimore, USA.

C. Schmöcker, H. Gottschall, N. Rohwer, K. M. Rund, L. Kutzner, A. I. Ostermann, N. H. Schebb and K. H. Weylandt **(2018)** Oxylipins in human colon mucosa, adenoma and carcinoma tissues. 17th International Winter Eicosanoid Conference, 11.–13.03.2018, Baltimore, USA.

P. Waindok, E. Janecek, K. M. Rund, N. H. Schebb and C. Strube **(2017)** Bioactive lipid mediator profiling of *Toxocara canis*- and *T. cati*-infected brains. 26th International Conference of the World Association for the Advancement of Veterinary Parasitology, 04.–08.09.2017, Kuala Lumpur, Malaysia.

K. Rund, A. I. Ostermann, S. Wecklein, J. Fahrer and N. H. Schebb **(2017)** Investigation of the formation of epoxy fatty acids by autoxidation. 46. Deutscher Lebensmittelchemikertag, 25.–27.09.2017, Würzburg, Germany.

K. Rund, A. I. Ostermann, F. Nolte, S. Wecklein, J. Fahrer, C. Oger, J.-M. Galano, T. Durand and N. H. Schebb **(2017)** Quantification of isoprostanes and isofurans from n3- and n6-PUFA by means of liquid chromatography mass spectrometry. 6th European Lipidomic Meeting, 10.–12.04 2017, Tolouse, France.

P. Waindok, E. Janecek, K. M. Rund, N. H. Schebb and C. Strube **(2016)** Profiling of bioactive lipid mediators during *Toxocara* brain infection. 9th Graduate School Day of Veterinary Pathobiology, Neuroinfectiology, and Translational Medicine, 25.–26.11.2016, Hannover, Germany.

H. Gottschall, C. Schmöcker, D. Hartmann, K. Rund, N. Rohwer, N. Schebb and K. Weyland **(2016)** 15-Lipoxygenase metabolites in human colon mucosa, adenoma and carcinoma tissues. 24th United European Gastroenterology (UEG) Week, 15.–19.10.2016, Vienna, Austria.

K. Rund, A. I. Ostermann, F. Nolte, S. Wecklein, J. Fahrer, J.-M. Galano, C. Oger, C. Vigor, T. Durand and N. H. Schebb **(2016)** Development of a targeted LC-ESI(-)-MS/MS method for the parallel quantification of 27 isoprostanes and 8 isofurans. 6th European Workshop on Lipid Mediators, 27.–30.09.2016, Frankfurt am Main, Germany.

M. Karber, K. Rund, M. Blum, M. Rothe, N. H. Schebb, U. F. Pape, K. H. Weylandt and W. H. Schunck **(2016)** Formation of 18-hydroxy-eicosapentaenoic acid by human cytochrome P450 isoforms. 6th European Workshop on Lipid Mediators, 27.–30.09.2016, Frankfurt am Main, Germany.

S. Schüler, T. Hecker, K. Rund and N. H. Schebb **(2016)** Comparison of the glucuronidation of n-3 and n-6 dihydroxylated polyunsaturated fatty acids. 6th European Workshop on Lipid Mediators, 27.–30.09.2016, Frankfurt am Main, Germany.

H. Gottschall, C. Schmöcker, D. Hartmann, K. Rund, N. Rohwer, N. H. Schebb and K. H. Weylandt **(2016)** Lipid metabolites in human colon mucosa, adenoma and carcinoma tissues. 6th European Workshop on Lipid Mediators, 27.–30.09.2016, Frankfurt am Main, Germany.

K. Rund, A. I. Ostermann, F. Nolte, S. Wecklein, J. Fahrer, T. Durand and N. H. Schebb **(2016)** Targeted metabolomics of prostaglandin-like autoxidation products of polyunsaturated fatty acids. 45. Deutscher Lebensmittelchemikertag, 12.–14.09.2016, Freising-Weihenstephan, Germany.

S. Schüler, T. Hecker, K. Rund and N. H. Schebb **(2016)** Investigation of the glucuronidation of dihydroxylated polyunsaturated fatty acids. 45. Deutscher Lebensmittelchemikertag, 12.–14.09.2016, Freising-Weihenstephan, Germany.

H. Gottschall, C. Schmöcker, D. Hartmann, K. Rund, L. Kutzner, F. Nolte, N. H Schebb and K. H. Weylandt **(2016)** Quantitative profiling of 15-lipoxygenase lipid metabolites in human colon tissue reveals distinct lipidomic profiles for human colon carcinoma and adenoma tissue. Wissenschaftliches Symposium der Gastroenterologischen Abteilungen der Charité – Universitätsmedizin Berlin, 15.–16.07.2016, Potsdam, Germany.

K. Rund, A. I. Ostermann, V. Beumler, B. D. Hammock, K. H. Weylandt and N. H. Schebb (**2016**) Modulation of acute DSS induced colitis in the rat by inhibition of soluble epoxide hydrolase. 16th International Winter Eicosanoid Conference, 13.–16.03.2016, Baltimore, USA.

A. I. Ostermann, K. Rund, M. Schmidt, C.-Y. Chiu, C. Smyl, K. H. Weylandt and N. H. Schebb (**2016**) Comparison of oxylipin pattern in FAT-1 mice and wildtype animals on a n3-polyunsaturated fatty acid rich diet. 16th International Winter Eicosanoid Conference, 13.–16.03.2016, Baltimore, USA.

N. Rohwer, A. Kühl, A. Ostermann, K. Rund, D. Zopf, F. M. McDonald, N. H. Schebb and K. H. Weylandt (**2016**) Low dose aspirin treatment inhibits mouse colon tumorigenesis and modifies the eicosanoid metabolome. 16th International Winter Eicosanoid Conference, 13.–16.03.2016, Baltimore, USA.

C. Smyl, N. Rohwer, H. Kühn, A. I. Ostermann, K. Rund, N. H. Schebb and K. H. Weylandt (**2016**) Knock-Out of 12/15-lipoxygenase in Fat-1 mice reduces protection from TNBS-induced colitis. 16th International Winter Eicosanoid Conference, 13.–16.03.2016 Baltimore, USA.

C. Claßen, K. Rund, L. Kutzner, V. Beumler, A. I. Ostermann, K. Weylandt and N.H. Schebb **(2016)** Modulation of the fatty acid- and oxylipin-pattern by an EPA/DHA-rich diet and its effects on DSS-induced acute colitis in Sprague-Dawley rats. Arbeitstagung des Regionalverbandes Nordrhein-Westfalen der Lebensmittelchemischen Gesellschaft der GDCh, 9.03.2016, Möchengladbach, Germany.

K. Rund, A. I. Ostermann, M. Schmidt, C.-Y. Chiu, C. Smyl, K. H. Weylandt and N. H. Schebb (**2016**) Monitoring the effects of n3-polyunsaturated fatty acids feeding of mice by means of targeted metabolomics of oxylipins and fatty acids. 53. Wissenschaftlicher Kongress der Deutschen Gesellschaft für Ernährung (DGE), 02.–04.03.2016, Fulda, Germany.

K. Rund, A. I. Ostermann, M. Schmidt, C.-Y. Chiu, C. Smyl, K. H. Weylandt and N. H. Schebb **(2015)** Oxylipin and fatty acid pattern following feeding of mice with n3-polyunsaturated fatty acids. Lipidomics Forum, 15.–17.11.2015, Borstel, Germany.

K. Rund, A. I. Ostermann, M. Schmidt, C.-Y. Chiu, C. Smyl, K. H. Weylandt and N. H. Schebb **(2015)** Effects of a n3-polyunsaturated fatty acid diet on the oxylipin and fatty acid pattern in mice. 44. Deutscher Lebensmittelchemikertag, 14.–16.09.2015, Karlsruhe, Germany.

K. Rund, A. I. Ostermann, M. Schmidt, C.-Y. Chiu, C. Smyl, K. H. Weylandt and N. H. Schebb **(2015)** 45 Day feeding of mice with a n3-polyunsaturated fatty acid diet: Effects on the oxylipin and fatty acid pattern. 14th International Conference on Bioactive Lipids in Cancer, Inflammation, and Related Diseases, 12.–15.07.2015, Budapest, Hungary.

K. H. Weylandt, K. Rund, C.-Y. Chiu, H. Kühn and N. H. Schebb **(2015)** Characterization of the oxylipin pattern in 12/15-lipoxygenase knock out (Alox15 (-/-)) mice. 14th International Conference on Bioactive Lipids in Cancer, Inflammation, and Related Diseases, 12.–15.07.2015, Budapest, Hungary.

V. Beumler, K. Rund, K. H. Weylandt, B. Hammock and N. H. Schebb **(2015)** Modulation of acute DSS induced colitis by inhibition of soluble epoxide hydrolase. 14th International Conference on Bioactive Lipids in Cancer, Inflammation, and Related Diseases, 12.–15.07.2015, Budapest, Hungary.

H. Gottschall, C. Schmöcker, D. Hartmann, K. Rund, N. H. Schebb and K. H. Weylandt **(2015)** Quantitative profiling of hydroxylated lipid metabolites in human colon tissue reveals distinct lipidomic profiles for human colon carcinoma and adenoma tissue. 14th International Conference on Bioactive Lipids in Cancer, Inflammation, and Related Diseases, 12.–15.07.2015, Budapest, Hungary.

J. P. Schuchardt, K. Möller, A.I. Ostermann, K. Rund, S. Thoms, F. Stahl, A. Hahn, N. H. Schebb **(2015)** Levels of free blood oxylipins in obese subjects before and after weight reduction. 14th International Conference on Bioactive Lipids in Cancer, Inflammation, and Related Diseases, 12.–15.07.2015, Budapest, Hungary.